



Programa de Doctorado en Tecnologías Industriales y de
Telecomunicación

**Interfaz cerebro-máquina multiparadigma para el
control de la marcha con un exoesqueleto de miembro
inferior**

Laura Ferrero Montes

Director de la tesis:

José María Azorín Poveda

Codirector de la tesis:

Mario Ortiz García

Universidad Miguel Hernández de Elche

La presente Tesis Doctoral, titulada “Interfaz cerebro-máquina multiparadigma para el control de la marcha con un exoesqueleto de miembro inferior”, se presenta bajo la modalidad de **tesis por compendio** de las siguientes **publicaciones**:

- *Sensory Integration in Human Movement: A New Brain-Machine Interface Based on Gamma Band and Attention Level for Controlling a Lower-Limb Exoskeleton.*
M. Ortiz, L. Ferrero, E. Iáñez, J. M. Azorín y J.L. Contreras-Vidal.
Frontiers in Bioengineering and Biotechnology. Vol 8(2020).
ISSN: 2296-4185 . Ed. FRONTIERS.
JCR-SCI Factor de impacto (2020): 5.89, Cuartil: **Q1**.
Fecha de publicación: 03 septiembre 2020.
DOI: <https://doi.org/10.3389/fbioe.2020.00735>
- *Improving Motor Imagery of Gait on a Brain-Computer Interface by Means of Virtual Reality: A Case of Study.*
L. Ferrero, M. Ortiz, V. Quiles, E. Iáñez y J.M. Azorín.
IEEE Access. Vol 9 (2021).
ISSN: 2169-3536. Ed. IEEE.
JCR-SCI Factor de impacto (2021): 3.476, Cuartil: **Q2**.
Fecha de publicación: 26 marzo 2021.
DOI: <https://doi.org/10.1109/ACCESS.2021.3068929>
- *A BMI Based on Motor Imagery and Attention for Commanding a Lower-Limb Robotic Exoskeleton. A Case Study.*
L. Ferrero, V. Quiles, M. Ortiz, E. Iáñez y J.M. Azorín.
Applied Sciences. Vol 11 (9).
ISSN: 2076-3417. Ed. MDPI.
JCR-SCI Factor de impacto (2021): 2.838, Cuartil: **Q2**.
Fecha de publicación: 30 abril 2021
DOI: <https://doi.org/10.3390/app11094106>

- *Brain Symmetry Analysis during the Use of a BCI Based on Motor Imagery for the Control of a Lower-Limb Exoskeleton.*
L. Ferrero, M. Ortiz, V. Quiles, E. Iáñez, J.A. Flores y J.M. Azorín.
Symmetry. Vol 13 (9).
ISSN: 2073-8994. Ed. MDPI.
JCR-SCI Factor de impacto (2021): 2.94, Cuartil: **Q2**.
Fecha de publicación: 19 septiembre 2021.
DOI: <https://doi.org/10.3390/sym13091746>

- *Brain-computer interface enhanced by virtual reality training for controlling a lower limb exoskeleton.*
L. Ferrero, V. Quiles, M. Ortiz, E. Iáñez, A. Gil-Agudo y J.M. Azorín.
iScience. Vol 26 (5).
ISSN: 2589-0042. Ed. Cell Press.
JCR-SCI Factor de impacto (2022): 5.8, Cuartil: **Q1**.
Fecha de publicación: 19 mayo 2023.
DOI: <https://doi.org/10.1016/j.isci.2023.106675>



El Dr. D. José María Azorín Poveda, director, y el Dr. D. Mario Ortiz García, codirector de la tesis doctoral titulada “Interfaz cerebro-máquina multiparadigma para el control de la marcha con un exoesqueleto de miembro inferior”.

INFORMA/N:

Que Dña. Laura Ferrero Montes ha realizado bajo nuestra supervisión el trabajo titulado “Interfaz cerebro-máquina multiparadigma para el control de la marcha con un exoesqueleto de miembro inferior” conforme a los términos y condiciones definidos en su Plan de Investigación y de acuerdo al Código de Buenas Prácticas de la Universidad Miguel Hernández de Elche, cumpliendo los objetivos previstos de forma satisfactoria para su defensa pública como tesis doctoral.

Lo que firmo/firmamos para los efectos oportunos, en a
de de 202....

Director de la tesis
Dr. D. José María Azorín Poveda

Codirector de la tesis
Dr. D. Mario Ortiz García



El Dr. D. Óscar Reinoso García, Coordinador del Programa de Doctorado en Tecnologías Industriales y de Telecomunicación

INFORMA:

Que D./Dña. Laura Ferrero Montes ha realizado bajo la supervisión de nuestro Programa de Doctorado el trabajo titulado “Interfaz cerebro-máquina multiparadigma para el control de la marcha con un exoesqueleto de miembro inferior” conforme a los términos y condiciones definidos en su Plan de Investigación y de acuerdo al Código de Buenas Prácticas de la Universidad Miguel Hernández de Elche, cumpliendo los objetivos previstos de forma satisfactoria para su defensa pública como tesis doctoral.

Lo que firmo para los efectos oportunos, en a de de 202....

Prof. Dr. D. Óscar Reinoso García

Coordinador/a del Programa de Doctorado en Tecnologías Industriales y de Telecomunicación

Esta tesis está dedicada a mi padre.

Agradecimientos

Hay mucha gente que me ha apoyado a seguir este camino y han sido un pilar fundamental desde el principio hasta el final de mi tesis doctoral, así que voy a intentar nombrarlos a todos. En primer lugar, me gustaría agradecer a los miembros de mi laboratorio, empezando por mi tutor José M. Azorín y mi co-tutor Mario Ortiz que me propusieron esta línea de investigación y han seguido todos mis avances tanto buenos como malos, siempre dándome ideas y sugerencias. También me gustaría agradecer a Eduardo Iáñez que aunque no me ha tutorizado la tesis, es como si también lo hubiera hecho, especialmente en lo que atañe a los problemas y desafíos de la famosa arquitectura. Siguiendo con los miembros del laboratorio, me gustaría dar las gracias a Vicente Quiles, my partner in crime, con quien empecé y terminé la tesis. No hay nadie que me haya comprendido como él porque ambos hemos experimentado la montaña rusa emocional que implica realizar una tesis doctoral. También me gustaría agradecer a Juan Marcos Bravo, quien me ha ayudado con todos los problemas de infraestructura y también ha colaborado en mis experimentos. Para Juan, la palabra ‘no’ no existe, ya que todo lo que le proponemos en el laboratorio lo ve viable por muy loco que sea. Finalmente, pero no menos importante, me gustaría agradecer a los demás compañeros del laboratorio que se han ido incorporando más tarde como Javi, Cristina, Paula y Desirée, que han hecho que Vicente y yo no estemos tan solos y que el laboratorio haya sido como una familia.

En estos agradecimientos no puede faltar mi familia, pero no solo por su apoyo durante mi investigación sino a lo largo de mi vida. Son ellos quienes me han dado la educación y las herramientas para elegir este camino y para querer SIEMPRE aprender más. Ellos son mis padres, mis grandes referentes en lo que debería ser una persona modelo, mi hermano que siempre será mi persona favorita, mis abuelos, tíos y primos, porque en mi familia todo lo hacemos y lo vivimos juntos.

Otro de los grandes pilares con quien tengo la suerte de compartir la vida es mi pareja. A él todo lo que le propongo le parece bien, desde estudiar una carrera poco conocida en Valencia, hacer un máster por medio mundo y por supuesto, empezar un doctorado. En cada uno de mis pasos ha estado a mi lado y no lo concibo de otra forma. Además, debo agradecerle su participación como sujeto de pruebas.

Por último, me gustaría agradecer a mis amigos, todos los que se han preocupado por

preguntarme cómo me iba, los que se han interesado por mi línea de investigación aunque lo que les contase les sonase a chino, los que también han participado en mis pruebas y con quienes lo celebraré cuando ponga fin a esta etapa.

Muchas gracias a todos.

Contenido

Agradecimientos	XI
Índice de figuras	XVIII
Índice de tablas	XXI
Resumen	XXII
Abstract	XXVI
Glosario	XXX
1. Introducción	1
1.1. Motivación	1
1.2. Hipótesis	2
1.3. Objetivos	3
1.4. Líneas de investigación	4
2. Estado del arte	9
2.1. Interfaces cerebro-máquina	9
2.1.1. Electroencefalografía	9
2.1.2. Paradigmas	15
2.1.3. Imaginación motora	16
2.1.4. Protocolos experimentales	17
2.1.5. Diagrama de flujo de una BMI	18
2.1.6. Tipos de dispositivos a controlar	22
2.2. Lesión de la médula espinal	23
2.2.1. Patología	23
2.2.2. Rehabilitación	23
2.3. Interfaces cerebro-máquina para neurorrehabilitación	26

2.3.1.	Interfaces cerebro-máquina basadas en imaginación motora del miembro inferior	26
2.3.2.	Desafíos	28
3.	Sensory integration in human movement: a new brain-machine interface based on gamma band and attention level for controlling a lower-limb exoskeleton (P1)	31
3.1.	Materiales	32
3.1.1.	Sujetos	32
3.1.2.	Equipo	32
3.2.	Métodos	32
3.3.	Resultados y discusión	36
3.3.1.	Lazo-abierto	37
3.3.2.	Lazo-cerrado	37
4.	Improving motor imagery of gait on a brain-computer interface by means of virtual reality: a case of study (P2)	41
4.1.	Materiales	42
4.1.1.	Sujetos	42
4.1.2.	Equipo	42
4.2.	Métodos	43
4.3.	Resultados y discusión	46
4.3.1.	Lazo-abierto	46
4.3.2.	Lazo-cerrado	46
5.	A BMI Based on motor imagery and attention for commanding a lower-limb robotic exoskeleton: a case study (P3)	51
5.1.	Materiales	52
5.1.1.	Sujetos	52
5.1.2.	Equipo	52
5.2.	Métodos	53
5.3.	Resultados y discusión	55
5.3.1.	Lazo-abierto	55
5.3.2.	Lazo-cerrado	56
6.	Brain symmetry analysis during the use of a BCI based on motor imagery for the control of a lower-limb exoskeleton (P4)	59
6.1.	Materiales	60
6.1.1.	Sujetos	60
6.1.2.	Equipo	60

6.2.	Métodos	60
6.3.	Resultados y discusión	61
6.3.1.	Influencia de la metodología	61
6.3.2.	Influencia del sujeto	61
6.3.3.	Evolución del entrenamiento y diferencias entre hemisferios cerebrales	62
7.	Brain-computer interface enhanced by virtual reality training for controlling a lower limb exoskeleton (P5)	65
7.1.	Materiales	66
7.1.1.	Sujetos	66
7.1.2.	Equipo	66
7.2.	Métodos	66
7.3.	Resultados y discusión	67
7.3.1.	Lazo-abierto	68
7.3.2.	Lazo-cerrado	70
7.3.3.	Pacientes con LME	70
8.	Discusión global	73
8.1.	Paradigmas de control: imaginación motora y/o atención	73
8.2.	Condiciones en estático y en movimiento	74
8.3.	Diferencias entre sujetos	74
8.4.	Evolución con las sesiones	75
8.5.	Entrenamiento previo con realidad virtual	75
8.6.	Pacientes con LME	75
8.7.	Limitaciones del estudio	76
9.	Contribuciones, conclusiones y líneas futuras	77
9.1.	Contribuciones	78
9.2.	Conclusiones	79
9.3.	Líneas futuras	80
	Bibliografía	97
	Anexo A. Compendio de publicaciones	99
	Contribución P1	100
	Contribución P2	117
	Contribución P3	127
	Contribución P4	141
	Contribución P5	155

Índice de figuras

1.1. Coherencia temática de las contribuciones. Esta figura muestra las líneas de investigación que se han seguido en esta tesis doctoral, así como las contribuciones asociadas a cada una. Imagen adaptada de [1, 2, 3, 4, 5] con licencia Creative Commons Attribution 4.0 International (CC 4.0) y licencia Creative Commons Attribution-NonCommercial-NoDerivatives 4.0 International (CC BY-NC-ND 4.0).	7
2.1. Potencial de acción. Durante el potencial de acción de una neurona participan los iones y canales iónicos de sodio (Na^+), potasio (K^+) y calcio (Ca^+). Este potencial viaja a través del axón hasta que alcanza el espacio sináptico donde se produce una liberación de neurotransmisores que cuando alcanzan la membrana de la otra neurona generarán una determinada respuesta. Imagen de [6] con permiso de Springer.	10
2.2. Dipolos generados por neuronas piramidales. Dipolos radiales (A) y dipolos tangenciales (B). Imagen de [7] con permiso de Psychophysiology.	11
2.3. Esquema del flujo de datos en una interfaz cerebro-máquina.	18
3.1. Distribución de electrodos escogida en las contribución P1 con 60 electrodos para el registro de la señal cerebral. Se buscaba cubrir la corteza motora primaria, el AMS, la PM y el lóbulo parietal superior.	33
3.2. Exoesqueleto REX y equipo de electroencefalografía brainAmp.	34
3.3. Metodología de procesado seguida en la contribución P1. Esta contribución utiliza dos paradigmas de control, por lo tanto, se procesan las señales cerebrales de dos formas distintas. Uno de los paradigmas consiste en discernir cuando los usuarios están realizando IM y cuando están relajados. El otro paradigma trata de diferenciar cuando los sujetos están prestando atención a tareas distintas.	35

3.4.	Secuencia de tareas seguida en los registros de lazo-abierto (A) y en los registros de lazo-cerrado (B). Los sujetos recibían indicaciones auditivas para cambiar de tarea mental. La duración de las tareas fue diferente en la contribución P1 con respecto a las contribuciones P3, P4 y P5. Los registros comenzaron con un período de 15 segundos en el que no se requería que los participantes realizaran ninguna tarea mental. Después de esto, debían permanecer relajados. A continuación, durante el periodo período de IM, los participantes debían concentrarse en imaginar el movimiento de sus piernas como si estuvieran caminando. Luego, durante la tarea de la cuenta regresiva debían realizar mentalmente una serie de sustracciones (por ejemplo, 900-7, 893, 886, 879, etc.), y finalmente otra vez en estado de relajación.	38
4.1.	Distribución de electrodos escogida en las contribución P2 con 31 electrodos para el registro de la señal cerebral. Se buscaba cubrir la corteza motora primaria, el AMS, la PM, el lóbulo parietal superior y el lóbulo occipital. .	42
4.2.	Equipo de realidad virtual y equipo de electroencefalografía actiCHamp. Imagen adaptada de [2] con licencia Creative Commons Attribution 4.0 International (CC 4.0).	43
4.3.	Metodología de procesado seguida en la contribución P2.	45
4.4.	Secuencia de tareas seguida en los registros de la contribución P2. Los sujetos recibían indicaciones auditivas para cambiar de tarea mental. Durante los periodos de relajación debían tratar de no pensar en nada y relajarse. Durante los periodos de IM, debían concentrarse en imaginar el movimiento de sus piernas como si estuvieran caminando. Y durante los periodos de libre, podían hacer lo que quisiesen.	48
5.1.	Distribución de electrodos escogida en las contribuciones P3,P4 y P5 con 27 electrodos para el registro de la señal cerebral. Se buscaba cubrir la corteza motora primaria, el AMS, la PM y el lóbulo parietal superior	52
5.2.	Exoesqueleto H3 y equipo de electroencefalografía actiCHamp. Imagen adaptada de [3] con licencia Creative Commons Attribution 4.0 International (CC 4.0).	53
5.3.	Metodología de procesado seguida en la contribución P3.	54

5.4.	Interfaz cerebro-máquina de doble estado. En el lazo-cerrado, en la condición estática, cuando los sujetos permanecían de pie con el exoesqueleto, el modelo(s) estático era el encargado de tomar decisiones. Este modelo decidía si mantener el exoesqueleto en una posición estática o iniciar la marcha basándose en los patrones cerebrales detectados en el sujeto. Por otro lado, en la condición de movimiento, cuando los sujetos caminaban asistidos por el exoesqueleto, el modelo(s) en movimiento supervisaba el control. Este modelo podía decidir si continuar con el movimiento o detenerlo.	56
6.1.	Evolución del entrenamiento para las pruebas en estático y movimiento con diferentes configuraciones de electrodos: todos los electrodos, sólo los electrodos ubicados en el hemisferio no dominante y los electrodos en el hemisferio dominante.	62
7.1.	Exoesqueleto REX, equipo de electroencefalografía Starstim R32 y equipo de realidad virtual.	67
7.2.	Resultados de lazo-abierto. %MI es la precisión del modelo que va de 0 a 100. S1-S5 son los sujetos del grupo de control y V1-V5 son los sujetos del grupo RV. Imagen de [5] con licencia Creative Commons Attribution-NonCommercial-NoDerivatives 4.0. International (CC BY-NC-ND 4.0) . . .	69

Índice de tablas

2.1. Estado del arte de las interfaces cerebro-máquina basadas en imaginación motora del miembro inferior.	28
3.1. Resultados de los registros en lazo-abierto y en pseudo-online. Tabla modificada de [1] con licencia Creative Commons Attribution 4.0 International (CC 4.0).	37
3.2. Resultados de los registros en lazo-cerrado. Tabla modificada de [1] con licencia Creative Commons Attribution 4.0 International (CC 4.0).	37
4.1. Resultados de los registros en lazo-abierto. Tabla de [2] con licencia Creative Commons Attribution 4.0 International (CC 4.0).	47
4.2. Resultados de los registros en lazo-cerrado. Tabla de [2] con licencia Creative Commons Attribution 4.0 International (CC 4.0).	49
5.1. Resultados de los registros en lazo-abierto de un sujeto. Stand son los resultados de los registros en estático y Gait son los resultados de los registros en movimiento. Tabla de [3] con licencia Creative Commons Attribution 4.0 International (CC 4.0).	55
5.2. Resultados de los registros en lazo-abierto de un sujeto. Stand son los resultados de los registros en estático y Gait son los resultados de los registros en movimiento. Tabla de [3] con licencia Creative Commons Attribution 4.0 International (CC 4.0).	57
5.3. Resultados de los registros en lazo-cerrado. Tabla modificada de [3] con licencia Creative Commons Attribution 4.0 International (CC 4.0).	58
6.1. Resultados de tres metodologías diferentes en todas las sesiones. Full-static son los resultados de los registros en estático y Full-motion son los resultados de los registros en movimiento. Tabla de [4] con licencia Creative Commons Attribution 4.0 International (CC 4.0).	61
7.1. Detalles de los pacientes	66

7.2.	Resultados de lazo-cerrado del grupo de control (Sham) y el grupo de realidad virtual (VR). Static son los resultados del modelo entrenado con los registros en estático y Motion son los resultados del modelo entrenado con los registros en movimiento. Tabla de [5] con licencia Creative Commons Attribution-NonCommercial-NoDerivatives 4.0. International (CC BY-NC-ND 4.0).	70
7.3.	Resultados de lazo-cerrado de los dos pacientes con lesión medular. Static son los resultados del modelo entrenado con los registros en estático y Motion son los resultados del modelo entrenado con los registros en movimiento. Tabla de [5] con licencia Creative Commons Attribution-NonCommercial-NoDerivatives 4.0. International (CC BY-NC-ND 4.0). . .	71
9.1.	Relación entre los objetivos e hipótesis y las publicaciones del compendio de la presente tesis doctoral.	78

Resumen

La lesión de la médula espinal (LME) ocurre como resultado de un daño en la médula que interrumpe las vías sensoriales y motoras, lo que puede llevar a una alteración temporal o permanente de la función motora y/o sensitiva. Cuando la lesión afecta a los miembros inferiores, repercute en la marcha, lo cual puede resultar en estigmatización y aumentar la susceptibilidad a nuevas lesiones. Además, la pérdida o deterioro de la capacidad para caminar de forma independiente impacta en la autonomía y la sensación de libertad, provocando así una disminución en la calidad de vida.

La mayoría de las lesiones de LME son incompletas, lo que significa que puede haber tejido espinal preservado que se pueda recuperar para restablecer la función motora. Las terapias convencionales se basan en actividades repetitivas específicas realizadas con la asistencia de fisioterapeutas. Existe evidencia que respalda la idea de que la cantidad y especificidad de la práctica son factores cruciales para promover la recuperación y el desarrollo de habilidades motoras. Los avances recientes en dispositivos robóticos han permitido su integración en los tratamientos como una alternativa a estas terapias convencionales, ya que requieren menos esfuerzo por parte de los fisioterapeutas y ofrecen una nueva forma de tratamiento con sesiones de entrenamiento más prolongadas y patrones de movimiento más reproducibles.

Existen diferentes formas de controlar los dispositivos robóticos, como aplicaciones móviles, joysticks y consolas de comandos. Sin embargo, las interfaces cerebro-máquina (BMIs, por sus siglas en inglés, Brain-Machine Interfaces) representan una alternativa que permite un control directo a partir de la decodificación de la actividad cerebral. Esta tecnología ofrece una oportunidad prometedora para el desarrollo de nuevas terapias de rehabilitación, ya que los usuarios pueden imaginar movimientos específicos, conocidos como imaginación motora (IM), para generar comandos que se traduzcan en el movimiento del exoesqueleto robótico. Desde una perspectiva de rehabilitación, la IM favorece el aprendizaje motor y, por lo tanto, la recuperación.

Esta tesis doctoral se centra en el diseño y evaluación de una BMI destinada a controlar el inicio y la detención de la marcha de un exoesqueleto de miembro inferior basándose en la actividad cerebral de los usuarios y concretamente en base a la detección de la IM de la marcha. El objetivo de este sistema es brindar asistencia a personas con movilidad

reducida y favorecer la rehabilitación. En base a este contexto, se han seguido tres líneas de investigación: el control de un exoesqueleto robótico de miembro inferior, el estudio de los patrones cerebrales de los sujetos y el entrenamiento en un entorno de realidad virtual.

La primera línea de investigación se centra en el control de un exoesqueleto robótico de miembro inferior. La BMI detecta en tiempo real los patrones cerebrales de los usuarios y toma decisiones cada 0.5 segundos. Se probaron dos enfoques de control diferentes. Uno combinaba la IM y la atención, donde los usuarios debían imaginar el movimiento de caminar para activar el exoesqueleto y relajarse para detenerlo, pero solo en situaciones en las que estuvieran altamente concentrados en la tarea. Esto permitía un control más seguro porque monitorizaba el nivel de atención de los usuarios durante las pruebas. El otro enfoque se basaba únicamente en la IM sin incorporar niveles adicionales de atención. Se decidió prescindir del uso del nivel de atención debido a las restricciones excesivas de la BMI, lo cual afectaba significativamente el rendimiento del sistema y generaba frustración en los sujetos. Además de la interfaz, se diseñaron protocolos de entrenamiento y evaluación del sistema. En este ámbito, se probaron dos alternativas. Un enfoque se basaba en que durante el entrenamiento, los usuarios practicaban tareas de IM mientras caminaban con la asistencia del exoesqueleto y practicaban la relajación mientras permanecían estáticos. Luego, para la evaluación, un modelo entrenado con estas dos tareas se utilizaba para controlar el sistema. Sin embargo, se observó que gran parte de las diferencias detectadas se debían a los artefactos generados por el movimiento, los cuales enmascaraban las señales cerebrales. Por lo tanto, se adoptó un segundo enfoque en el que los usuarios realizaban las tareas mentales en condiciones estáticas durante la mitad de los registros y, durante la otra mitad, realizaban las mismas tareas en condiciones de movimiento asistido por el exoesqueleto. Luego, en la evaluación del sistema, se utilizaron dos modelos, uno entrenado con registros estáticos y otro entrenado con registros en movimiento, y se utilizó uno u otro según el estado cinemático del exoesqueleto. Esta evaluación se condujo de manera integral, abarcando tanto a individuos sanos como a pacientes con lesión medular.

En la segunda línea de investigación, se estudiaron los patrones cerebrales generados en las señales electroencefalográficas durante la IM en comparación con los patrones generados durante la relajación. También se analizaron las diferencias en los patrones entre los participantes y a lo largo de las sesiones experimentales. Como resultado, se observaron diferencias significativas en la actividad cerebral entre los participantes y también a lo largo de las sesiones, lo cual sugiere la presencia de aprendizaje.

La tercera línea de investigación se centró en la inclusión de un entrenamiento con realidad virtual (RV) para reducir el tiempo de calibración de la BMI. Los participantes fueron sumergidos en un entorno virtual donde, al imaginar el acto de caminar, un avatar progresaba en consecuencia. Se llevó a cabo un entrenamiento en este entorno antes de asumir el control de un exoesqueleto mediante la BMI. Se analizaron tanto los cambios en el rendimiento como los patrones cerebrales de un grupo de participantes que recibió este

entrenamiento en comparación con un grupo de control que recibió un entrenamiento más prolongado en la BMI y no utilizó la RV. Los resultados mostraron que el grupo de RV logró un mayor rendimiento que el grupo de control.

En resumen, esta tesis doctoral se ha enfocado en el desarrollo y evaluación de una BMI para el control de un exoesqueleto de miembro inferior, destacando la importancia de utilizar la detección de la IM como un mecanismo de control fundamental. Durante esta investigación, se han identificado estrategias de control eficaces y se han observado diferencias cerebrales significativas cuando se compara la actividad cerebral durante la IM con estados de relajación. Además, se ha demostrado que la integración de la RV en el entrenamiento de la BMI conduce a mejoras en el rendimiento del usuario. Estos descubrimientos respaldan la relevancia y aplicabilidad de las BMIs en el ámbito de la rehabilitación para personas con movilidad reducida, y abren nuevas perspectivas para mejorar la calidad de vida de este grupo de individuos.

Abstract

Spinal cord injury (SCI) occurs when damage to the spinal cord disrupts sensory and motor pathways, resulting in temporary or permanent impairment of motor and/or sensory function. When the injury affects the lower limbs, it affects gait, leading to potential stigmatization and increased vulnerability to further injuries. Moreover, the loss or deterioration of the ability to walk independently impacts autonomy and the sense of freedom, ultimately diminishing the overall quality of life.

The majority of SCI injuries are incomplete, meaning that there may be preserved spinal tissue that can be rehabilitated and repaired to restore motor function. Conventional therapies typically involve repetitive specific activities performed with the assistance of physiotherapists. Evidence supports the notion that the quantity and specificity of practice play crucial roles in promoting recovery and the development of motor skills. Recent advancements in robotic devices have facilitated their integration into treatments as an alternative to conventional therapies, requiring less effort from physiotherapists and providing extended training sessions with more reproducible patterns of movement.

Various methods exist for controlling robotic devices, including mobile applications, joysticks, and command consoles. However, brain-machine interfaces (BMIs) present an alternative solution by enabling direct control through the mind. This technology holds promise for the development of innovative rehabilitation therapies, as users can mentally simulate specific movements, referred to as motor imagery (MI), to generate commands that translate into the movement of a robotic exoskeleton. From a rehabilitation perspective, MI promotes motor learning and, consequently, enhances the recovery process.

This doctoral thesis primarily focuses on the design and evaluation of a BMI system aimed at controlling the initiation and cessation of lower limb exoskeleton gait based on users' brain activity, specifically by detecting gait-related MI. The primary objective of this system is to provide assistance to individuals with reduced mobility and promote their rehabilitation progress. Within this context, three main lines of research have been pursued: the control of a lower limb robotic exoskeleton, the study of subjects' brain patterns, and training within a virtual reality (VR) environment.

The first line of research centers on the control of a lower limb robotic exoskeleton. The BMI system monitors users' brain patterns in real-time, making decisions at regular 0.5-

second intervals. Two distinct control approaches were tested. The first approach combined MI and attention, requiring users to imagine the act of walking to activate the exoskeleton and relax their mind to halt the movement, but only when they were highly focused on the task. This approach ensured safer control by monitoring users' attention levels during testing. The second approach relied solely on MI without incorporating additional attention-related factors. The use of attention levels was disregarded due to the excessive constraints imposed by the BMI system, significantly impacting performance and causing frustration among the subjects. In addition to the interface design, training and evaluation protocols for the system were developed. Two alternatives were explored in this regard. The initial approach involved users practicing MI tasks while walking with the assistance of the exoskeleton and practicing relaxation while remaining stationary. Afterwards, for evaluation, a model trained with these two tasks was used to control the system. However, it was observed that many of the differences detected were a result of artifacts generated by movement, which masked the true brain signals. Consequently, a second approach was adopted, where users performed mental tasks under static conditions for half of the trials and, for the remaining half, performed the same tasks while the exoskeleton facilitated movement. Subsequently, during the system evaluation, two models were utilized: one trained with static trials and another trained with trials during movement, based on the kinematic state of the exoskeleton. This evaluation was conducted comprehensively, encompassing both healthy individuals and patients with spinal cord injuries.

In the second line of research, patterns of brain activity generated in the electroencephalographic signals during MI were studied in comparison to patterns generated during relaxation. Differences in these patterns among participants and across experimental sessions were also analyzed. As a result, significant differences in brain activity were observed both among participants and across sessions, suggesting the presence of learning.

The third line of research incorporated training with VR to reduce BMI calibration time. Participants were immersed in a virtual environment where their imagined walking actions corresponded to the progression of an avatar. Training in this environment preceded assuming control of the exoskeleton via the BMI. Performance improvements and brain pattern analyses were conducted for a group that received VR training, comparing it to a control that received more extensive BMI training without VR. The results indicated superior performance by the VR group compared to the control group.

In summary, this doctoral thesis has focused on the development and evaluation of a BMI for controlling a lower limb exoskeleton, emphasizing the importance of using MI as a fundamental control mechanism. Throughout this research, effective control strategies have been identified, and significant brain differences have been observed when comparing brain activity during MI with states of relaxation. Furthermore, it has been demonstrated that integrating VR into BMI training leads to improvements in user performance. These findings support the relevance and applicability of BMIs in the field of rehabilitation for

individuals with reduced mobility, opening new perspectives to enhance their quality of life.

Glosario

Acrónimo	Descripción en castellano	Descripción en inglés
Acc	Precisión	Accuracy
AMS	Área Motora Suplementaria	
ASIA	Asociación Estadounidense de Lesiones de la Médula Espinal	American Spinal Injury Association
ASR	Reconstrucción del Subespacio de Artefactos	Artifact Subspace Reconstruction
BCI	Interfaz Cerebro-Computadora	Brain-Computer Interface
BMI	Interfaz Cerebro-Máquina	Brain-Machine Interface
CAR	Referencia de Promedio Común	Common Average Reference
CPCA	Análisis de Componentes Principales de la Multitud	Crowd Principal Component Analysis
CSP	Patrones Espaciales Comunes	Common Spatial Patterns
CWT	Transformada Continua Wavelet	Continuous Wavelet Transform
ECG	Electrocardiografía, electrocardiograma	
EEG	Electroencefalografía, electroencefalograma	
EMD	Descomposición Modal Empírica	Empirical Mode Decomposition
EOG	Electrooculografía, electrooculograma	
ERD	Desincronización Relacionada con Evento	Event Related Desynchronization
ERP	Potential Relacionado con Evento	Event Related Potential
ERS	Sincronización Relacionada con Evento	Event Related Synchronization

Acrónimo	Descripción en castellano	Descripción en inglés
FFT	Transformada Rápida de Fourier	Fast Fourier Transform
FP	Falsos Positivos	False Positives
FP/min	Falsos Positivos por minuto	False Positives per minute
FPR	Ratio de Falsos Positivos	False Positive Rate
ICA	Análisis de Componentes Independientes	Independent Component Analysis
IM	Imaginación motora	
JCR	Informe de Citas de Revistas	Journal Citation Reports
LDA	Análisis Discriminante Lineal	Linear Discriminant Analysis
LFDA	Análisis Discriminante de Fisher Local	Local Fisher Discriminant Analysis
LME	Lesión de Médula Espinal	
MEM	Método de Máxima Entropía	Maximum Entropy Method
MRCP	Potencial Cortical Asociado con el Movimiento	Movement Related Cortical Potential
PCA	Análisis de Componentes Principales	Principal Component Analysis
PM	Corteza Premotora	Premotor Cortex
PSD	Densidad Espectral de Potencia	Power Spectral Density
RV	Realidad Virtual	
SMR	Ritmos sensorimotores	Sensorimotor Rhythms
SSVEP	Potencial Visual Evocado de Estado Estable	Steady-State Visual Evoked Potential
ST	Transformada de Stockwell	Stockwell Transform
TPR	Ratio de Verdaderos Positivos	True Positive Rate
UMV	Umbral Máximo Visual	
VEP	Potencial Visual Evocado	Visual Evoked Potential
WD	Discriminador Ponderado	Weighted Discriminator
WOS	Web de la Ciencia	Web of Science

Capítulo 1

Introducción

1.1. Motivación

La lesión de la médula espinal (LME) se produce por un daño en la médula que interrumpe las vías sensoriales y motoras y que resulta en la alteración temporal o permanente de la función motora y/o sensitiva. La afección de la movilidad puede ser por parálisis, es decir, pérdida total de movimiento o por la presencia de patrones de movimiento patológicos. Estas alteraciones suelen manifestarse por debajo del nivel de la lesión.

La incidencia anual de lesiones de la médula espinal es de aproximadamente 54 casos por millón de habitantes en los Estados Unidos. Los gastos anuales promedio para todos los grupos de pacientes con LME son de \$676000. Por lo tanto, las LME representan una carga financiera tanto para el paciente individual como para su familia y la sociedad en general [8].

En España, la incidencia de la LME es de 30 casos por millón de habitantes. Se estima que cada año se registran alrededor de 1000 nuevos casos de lesiones traumáticas, siendo la mitad de ellos causados por accidentes de tráfico, mientras que el resto se debe a caídas, golpes, accidentes deportivos y otros tipos de traumatismos. Además, se suma aproximadamente un 30 % adicional de lesiones de origen médico, relacionadas con diversas enfermedades como la esclerosis múltiple y causas congénitas, como el mielomeningocele. Es importante destacar que el grupo de edad más afectado por estas lesiones se encuentra entre los 16 y los 30 años [9].

La rehabilitación es un tratamiento no invasivo que permite al paciente participar de manera pasiva o activa en actividades físicas repetitivas, brindando frecuentemente una estimulación rítmica a las regiones afectadas de la médula espinal. Se ha demostrado que el ejercicio preserva la masa muscular, restablece la función motora y sensorial, induce plasticidad sináptica y reduce la inflamación alrededor del sitio de la lesión [10].

Esta rehabilitación es asistida generalmente por fisioterapeutas. Sin embargo, los recientes avances en tecnologías robóticas ofrecen una oportunidad para el desarrollo de nuevas estrategias de rehabilitación en las que el paciente no esté limitado por el fisioterapeuta, pudiendo hacer ejercicio de formas previamente inaccesibles e incluso desde casa [11, 12].

La presente investigación se centra en la LME que afecta al movimiento de la marcha. Caminar incorrectamente crea un estigma y hace que los pacientes sean más susceptibles a lesiones. Además, la pérdida o deterioro de la deambulación independiente afecta a la autonomía y sensación de libertad. En conjunto, estos cambios producen un detrimento de la calidad de vida.

En esta tesis se aborda el diseño de un sistema tanto de rehabilitación como de asistencia basado en un exoesqueleto de miembro inferior para que los pacientes lo puedan controlar directamente con su actividad mental, mediante una interfaz cerebro-máquina (BMI, por sus siglas en inglés, Brain-Machine Interface).

1.2. Hipótesis

La hipótesis planteada en esta tesis doctoral sostiene que un sistema basado en una BMI, utilizado para controlar un exoesqueleto robótico de miembro inferior, puede ser empleado como una herramienta de rehabilitación y asistencia para pacientes que hayan experimentado una lesión medular incompleta. A partir de esta hipótesis principal, se derivan las siguientes hipótesis secundarias:

H1: Es posible distinguir las señales cerebrales que indican cuando los sujetos están realizando imaginación motora (IM) de la marcha, en comparación con un estado de relajación.

H2: Las señales cerebrales permiten identificar el nivel de atención del sujeto a la tarea mental de realización de la acción motora.

H3: La detección de la IM, junto con un nivel alto de atención, permite enviar comandos de control del arranque al exoesqueleto que se corresponden con la intención del sujeto.

H4: La práctica de la IM en un entorno de realidad virtual facilita que los usuarios alcancen niveles de desempeño superiores, lo que a su vez permite una mejor identificación de los patrones de IM a nivel cerebral.

H5: Las sesiones realizadas con este sistema por pacientes con LME incompletas no representan una carga física y/o cognitiva excesiva, y los pacientes pueden completarlas sin dificultad.

1.3. Objetivos

El objetivo de la presente investigación es el análisis, diseño y evaluación de un sistema de control del arranque y paro de un exoesqueleto de miembro inferior. Este control se basa en la detección del patrón de IM y del nivel de atención a la marcha en señales electroencefalográficas. De esta forma, se pretende desarrollar un sistema de asistencia y rehabilitación para personas con movilidad reducida que pueda ser controlado de forma directa y voluntaria mediante la actividad cerebral. El sistema se ha evaluado con una serie de pruebas, inicialmente con sujetos sanos y posteriormente con pacientes con LME incompleta y escala ASIA B y C (esta escala se detalla en el siguiente capítulo). Además, se estudia la reducción del número de sesiones necesarias para ajustar el sistema mediante el uso de sesiones previas de un entorno de realidad virtual. Más específicamente, los objetivos de esta investigación son:

01: Estudio y caracterización de las señales electroencefalográficas para discernir el patrón de IM y el nivel de atención a la marcha.

02: Selección del método análisis de la señal cerebral que maximice las diferencias entre el patrón a detectar y otros estados cerebrales.

03: Diseño de un sistema de control del arranque y paro de un exoesqueleto de miembro inferior con altas tasas de desempeño.

04: Definición y desarrollo de una serie de pruebas con sujetos sanos para recopilar información suficiente para el desarrollo y ajuste del sistema.

05: Desarrollo de esquemas de entrenamiento basados en realidad virtual para reducir la cantidad de sesiones de entrenamiento requeridas con la BMI y el exoesqueleto, manteniendo o mejorando el nivel de desempeño.

06: Definición y desarrollo de pruebas de usabilidad con pacientes con lesión de médula espinal para estudiar la viabilidad de la incorporación del sistema a terapias de rehabilitación.

Esta tesis doctoral se ha desarrollado en el contexto del proyecto WALK- Control de exoesqueletos de miembro inferior mediante interfaces cerebro-máquina para asistir a personas con problemas de marcha, con referencia RTI2018-096677-B-I00. Dicho proyecto ha sido financiado por el Ministerio de Ciencia, Innovación y Universidades (MCIN/AEI/10.13039/501100011033) y por la Unión Europea a través del Fondo Europeo de Desarrollo Regional - FEDER Una manera de hacer Europa. Además, esta investigación también ha recibido financiación del Ministerio de Ciencia, Innovación y Universidades mediante las Ayudas para la formación de profesorado universitario (FPU19/03165).

1.4. Líneas de investigación

La presente tesis doctoral tiene como objetivo desarrollar una BMI para controlar un exoesqueleto de miembro inferior. Esta investigación ha llevado a la publicación de cinco artículos en revistas indexadas en el JCR de WOS. Específicamente, se publicaron entre 2020 y 2023. Como consecuencia de la productividad científica mencionada anteriormente, esta tesis se presenta como un compendio de publicaciones. La Figura 1.1 muestra un esquema de la coherencia temática en base a tres líneas de investigación: el control de un exoesqueleto robótico de miembro inferior, el estudio de los patrones cerebrales de los sujetos y el entrenamiento en un entorno de realidad virtual.

La primera fila de la Figura 1.1 representa la línea de investigación enfocada en el control de un exoesqueleto robótico de miembro inferior utilizando una BMI. Esta línea de investigación trata de abordar las hipótesis **H3** y **H5** presentadas anteriormente, a través de los objetivos **O3**, **O4** y **O6**. Las tres contribuciones relacionadas con este tema se presentan en orden cronológico de izquierda a derecha: P1 [1], P3 [3] y P5 [5]. En P1, se empleó un paradigma que combinaba la IM de la marcha con la atención para establecer el control del exoesqueleto. La idea subyacente en este enfoque es que los usuarios deben imaginar el movimiento de caminar para enviar una señal de inicio al exoesqueleto y conseguir mantener la marcha, y relajarse para enviar una señal de detención y permanecer parados. Además, para aumentar la seguridad del sistema, se monitorizó el nivel de atención de los sujetos a la IM. Por lo tanto, solo se envió una señal de inicio cuando este nivel superó un umbral predefinido. La IM se caracterizó en la banda de frecuencia gamma. Sin embargo, en el estado del arte, las bandas más utilizadas son las bandas alfa y beta, debido a que, aunque las tres están asociadas con la planificación motora, estas últimas presentan una menor presencia de artefactos de movimiento. Por lo tanto, en el siguiente trabajo, P3, el estudio de la IM se llevó a cabo en las bandas alfa y beta. Otra diferencia entre P3 y P1 radica en que, en el segundo estudio, se utilizaron patrones espaciales de la señal cerebral para caracterizar la IM, los cuales ofrecieron mejores resultados y se consideran el estado del arte, mientras que en P1 se utilizaron patrones espectrales.

La última diferencia entre estas contribuciones se basa en el esquema de control del dispositivo y el protocolo de entrenamiento. En P3, este control se realizó mediante una máquina de estados. Se empleó un esquema de control diferente dependiendo del estado del exoesqueleto. Si el exoesqueleto estaba en reposo, es decir, para enviar un comando de arranque o permanecer en reposo, se utilizaba un control específico. Por otro lado, si el exoesqueleto estaba en movimiento, es decir, para enviar un comando de parada o mantenerse en movimiento, se empleaba otro esquema de control. Esta modificación se realizó debido a que en la contribución P1 se tomaban las mismas decisiones sin considerar el estado cinemático del exoesqueleto, es decir, se utilizaba un único esquema de control en el que se enviaban dos comandos: un comando de parada que servía para detenerse o

permanecer en reposo, y un comando de movimiento que permitía iniciar o mantener el movimiento. No obstante, se observó que la actividad cerebral se ve afectada por el estado del exoesqueleto por el propio movimiento. En P3 para conseguir este control, se diseñó un protocolo de entrenamiento en el que se realizaron dos tipos de pruebas, durante la mitad de los registros los usuarios realizaban las tareas mentales en condiciones estáticas y durante la otra mitad, realizaban las mismas tareas en condiciones de movimiento asistido por el exoesqueleto. Se crearon dos tipos de modelos, uno que se entrenaba con los registros de estático y otro con los registros en movimiento y durante la evaluación, el control de la BMI dependía de uno u otro en función del estado cinemático del exoesqueleto.

En último término, en P5 se mantuvieron los cambios introducidos en P3, pero se optó por prescindir del control basado en el nivel de atención. Aunque este enfoque proporcionaba una mayor seguridad en la emisión de comandos, se observó una reducción considerable en la eficacia del sistema y un impacto negativo en la motivación de los participantes. Además, se evaluó la viabilidad y usabilidad del sistema diseñado en relación a la hipótesis **H5** y el objetivo **O6**, mediante su implementación y evaluación con pacientes que presentaban una lesión medular incompleta.

La línea de investigación correspondiente a la segunda fila de la Figura 1.1 se enfoca en el estudio de los patrones cerebrales generados durante la IM en comparación con el período de relajación. Los objetivos de esta línea, identificados como **O1** y **O2**, tienen como propósito abordar las hipótesis **H1** y **H2**, respectivamente. En todas las contribuciones realizadas, se extraen características que permiten discernir entre los distintos estados mentales. No obstante, en las contribuciones P3, P4 [4] y P5 se llevó a cabo un estudio adicional para determinar los electrodos y las bandas de frecuencia que experimentaron cambios más significativos. En P3, se analizaron los patrones cerebrales generados durante cada tarea mental mediante la correlación entre electrodos, lo que permitió identificar las áreas cerebrales que colaboraban conjuntamente en cada tarea. En P4 se realizó un análisis similar al de P3, pero se profundizó en el papel de cada hemisferio cerebral, el desempeño de distintos métodos de análisis, se investigaron las diferencias entre los participantes y se evaluó la evolución de los patrones cerebrales a lo largo de las sesiones experimentales para identificar posibles cambios relacionados con el aprendizaje y el entrenamiento. Finalmente, en P5, se analizaron los patrones cerebrales en ambas tareas, comparando dos grupos de sujetos: un grupo de control y otro grupo que recibió entrenamiento de IM utilizando un entorno de realidad virtual. Este enfoque permitió examinar las diferencias entre los grupos y evaluar los efectos del entrenamiento.

La tercera fila de la Figura 1.1 hace referencia al uso de un entorno de realidad virtual para practicar la IM. Esta línea de investigación trata de abordar la hipótesis **H4** en consonancia con el objetivo **O5**. Las contribuciones relacionadas con esta línea de investigación, presentadas en orden cronológico, son P2 [2] y P5. No todos los individuos tienen la misma facilidad para modular su actividad cerebral y controlar una BMI. Por tanto, en

los estudios mencionados, los participantes fueron sumergidos en un entorno virtual donde, al imaginar el acto de caminar, un avatar progresaba en consecuencia. El trabajo P2 se centró exclusivamente en este entorno virtual, mientras que en P5 se introdujo un entrenamiento previo mediante este entorno de realidad virtual antes de asumir el control de un exoesqueleto mediante una BMI. Se analizaron tanto los cambios en el rendimiento como en los patrones cerebrales de un grupo de participantes que recibió dicho entrenamiento, en comparación con un grupo de control.

Dado que la presente tesis doctoral está organizada como un compendio de publicaciones, resulta fundamental consultar cada artículo por separado para comprender en su totalidad este documento. Los manuscritos mencionados anteriormente se encuentran disponibles en Anexo A.

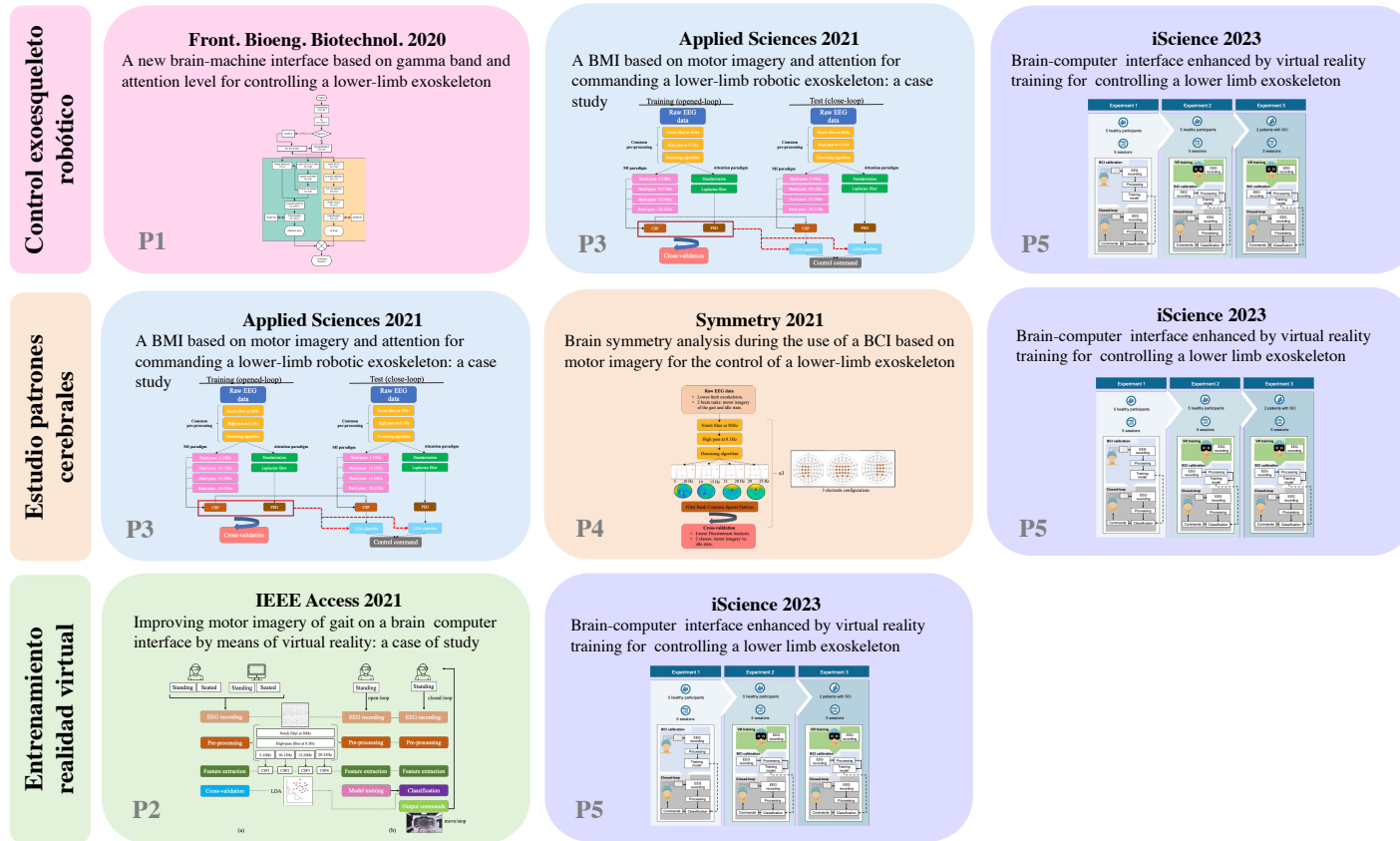


Figura 1.1: Coherencia temática de las contribuciones. Esta figura muestra las líneas de investigación que se han seguido en esta tesis doctoral, así como las contribuciones asociadas a cada una. Imagen adaptada de [1, 2, 3, 4, 5] con licencia Creative Commons Attribution 4.0 International (CC 4.0) y licencia Creative Commons Attribution-NonCommercial-NoDerivatives 4.0. International (CC BY-NC-ND 4.0).

Capítulo 2

Estado del arte

En este capítulo se presenta un contexto informativo sobre el campo de las interfaces cerebro-máquina, las terapias de rehabilitación para la lesión de la médula espinal y el estado actual de estos sistemas en la neurorrehabilitación.

2.1. Interfaces cerebro-máquina

Las interfaces cerebro-computadora (BCIs, por sus siglas en inglés, Brain-Computer Interfaces) son sistemas que adquieren señales cerebrales, las analizan y las traducen en comandos que se envían a un dispositivo externo para llevar a cabo una determinada acción. Dentro de las BCI, están las llamadas interfaces cerebro-máquina (BMIs, por sus siglas en inglés, Brain-Machine Interfaces) que son como las primeras, pero la acción deseada se realiza a nivel de hardware, por ejemplo, para controlar un robot. Sin embargo, en la literatura estos dos términos se utilizan de forma intercambiable [13].

2.1.1. Electroencefalografía

Existen diversas técnicas para medir la actividad cerebral, siendo la electroencefalografía (EEG) la más utilizada para las BMIs [14]. Entre las ventajas de esta técnica se destaca su portabilidad, que los registros de la actividad se realizan de forma no invasiva y que tiene una elevada resolución temporal [15].

Un electroencefalograma mide la actividad eléctrica de un conjunto de neuronas. Las neuronas tienen una polaridad negativa, es decir el potencial del medio intracelular es más negativo que el del medio extracelular. Esta diferencia de potencial se debe a la diferente concentración de iones entre ambos medios. Un estímulo externo puede cambiar la polaridad de la membrana celular desencadenando un potencial de acción. En el potencial de acción primero se abren los canales de sodio de la neurona y este entre de forma masiva

a la célula. Esto provoca la despolarización de la neurona, es decir el potencial intracelular cambia y se hace cada vez más positivo. Cuando se alcanza cierto umbral de potencial, los canales de sodio se cierran y se abren los de potasio que sale masivamente de la célula, provocando la repolarización. El potencial de acción se va desplazando a lo largo de la célula hasta alcanzar el final del axón. En este punto, se abren unos canales por los que entra calcio. El calcio produce que unas vesículas que contienen los neurotransmisores se desplacen a la membrana pre-sináptica y liberen los neurotransmisores en el espacio post-sináptico. Esta liberación puede provocar que se desencadene un potencial de acción en la siguiente neurona, lo que se conoce como potencial post-sináptico excitatorio o todo lo contrario, que se conoce como potencial inhibitorio [7]. La Figura 2.1 muestra el proceso de un potencial de acción.

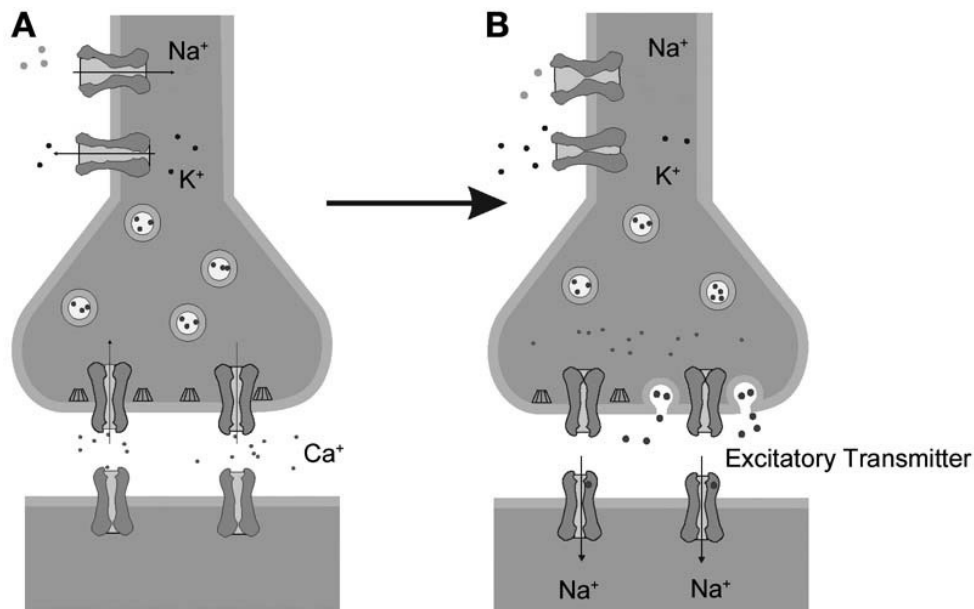


Figura 2.1: Potencial de acción. Durante el potencial de acción de una neurona participan los iones y canales iónicos de sodio (Na^+), potasio (K^+) y calcio (Ca^+). Este potencial viaja a través del axón hasta que alcanza el espacio sináptico donde se produce una liberación de neurotransmisores que cuando alcanzan la membrana de la otra neurona generarán una determinada respuesta. Imagen de [6] con permiso de Springer.

El EEG mide las diferencias de potencial entre dos puntos. Generalmente mide la diferencia entre cada electrodo y un electrodo de referencia. La actividad eléctrica registrada en cada electrodo es una medida atenuada del flujo de corriente extracelular que surge de la actividad sumada de muchas neuronas y amplificado por los tejidos de sostén. El EEG refleja predominantemente la actividad de neuronas corticales cercanas a los electrodos de

registro y concretamente de las neuronas piramidales. Los patrones oscilatorios del EEG surgen debido a las células marcapasos, en las que el voltaje de la membrana fluctúa espontáneamente, o debido a la interacción recíproca de neuronas excitatorias e inhibitorias en circuitos cerrados. El EEG humano muestra actividad en el rango de 1 a 30 Hz, con amplitudes en el rango de 20 a 300 μV .

Las fuentes de EEG se pueden aproximar mediante dipolos. Los dipolos están compuestos por dos cargas iguales y opuestas separadas por una pequeña distancia [7]. La Figura 2.2 muestra el dipolo que produce una única neurona en dos orientaciones y su proyección en la corteza cerebral.

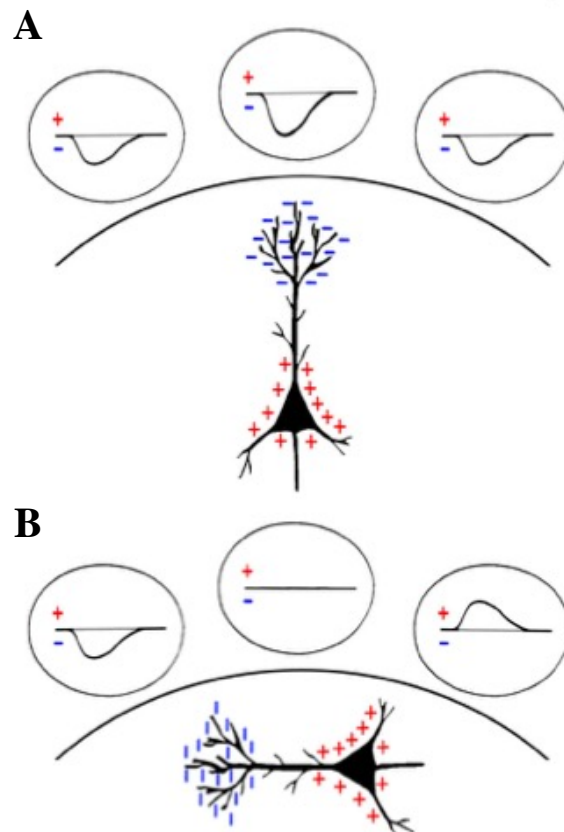


Figura 2.2: Dipolos generados por neuronas piramidales. Dipolos radiales (A) y dipolos tangenciales (B). Imagen de [7] con permiso de Psychophysiology.

La magnitud de las señales eléctricas medidas durante el registro está influenciada por diversos factores, tales como la actividad post-sináptica en las neuronas, la extensión de la corteza cerebral implicada en la actividad, la sincronización de los potenciales, la orien-

tación de los dipolos generados y la atenuación de la señal por los tejidos interpuestos. La función del equipo de electroencefalografía es aumentar la amplitud de la señal registrada para su posterior análisis [16, 17].

Una de las principales limitaciones del EEG es su no estacionariedad, lo que implica que las propiedades de las señales cambian con el tiempo, lo que dificulta la creación de modelos de análisis genéricos [18].

El EEG proporciona medidas no invasivas de la función cerebral en seres humanos. Independientemente de si un individuo recibe información sensorial o realiza procesos cognitivos superiores, las regiones cerebrales involucradas muestran una actividad eléctrica medible, y mediante el registro de esta actividad se puede determinar cuándo y dónde se produce el procesamiento de la información en el cerebro. Se pueden utilizar dos enfoques generales para registrar estos fenómenos neuroeléctricos: los potenciales relacionados con evento (ERP, por sus siglas en inglés, Event-Related Potentials) y las oscilaciones cerebrales [19].

Potencial relacionado con evento

Los ERP son voltajes pequeños generados en las estructuras cerebrales en respuesta a estímulos sensoriales, motores o cognitivos. Estos potenciales, como su nombre indica, se producen de manera sincronizada en el tiempo y ocurren en un momento determinado después de la presentación del estímulo. Para obtener los ERP, se segmenta el EEG desde la presentación del estímulo hasta un período posterior, y luego se promedian estos segmentos en múltiples señales para formar una forma de onda estable. Al comparar la amplitud, la topografía y el tiempo de estas ondas entre diferentes condiciones, es posible inferir diferencias en el procesamiento de la información [20].

En humanos, los ERP se pueden dividir en dos categorías. Las ondas tempranas, o componentes que alcanzan su máximo aproximadamente en los primeros 100 milisegundos después del estímulo se denominan sensoriales o exógenas, ya que dependen en gran medida de los parámetros físicos del estímulo. Por otro lado, los ERP generados de forma posterior reflejan la forma en que el sujeto evalúa el estímulo y se denominan cognitivos o endógenos, ya que examinan el procesamiento de la información. Un ejemplo de ERP del primer tipo sería el potencial evocado visual (VEP, por sus siglas en inglés, Visual Evoked Potential), mientras que un ejemplo del segundo sería la componente P50. VEP es una medida de la señal eléctrica generada en la corteza visual en respuesta a un estímulo visual. Este potencial depende de la integridad de la vía visual, que incluye el ojo, el nervio óptico, el quiasma óptico, el tracto óptico, la radiación óptica y la corteza cerebral, por lo que se utiliza como una herramienta de diagnóstico. Por otro lado, la componente P50 es un potencial relacionado con eventos que ocurre aproximadamente 50 ms después de la presentación de un estímulo, generalmente un sonido o click auditivo. La respuesta P50

se utiliza para medir el filtrado sensorial, es decir, la reducción de la respuesta neurofisiológica a estímulos redundantes. Este componente del potencial evocado es importante para comprender cómo el cerebro procesa y filtra la información sensorial para evitar una sobrecarga de estímulos irrelevantes [21].

Los ERP son potenciales evocados por un evento o un estímulo. El término potenciales evocados se utiliza comúnmente para referirse a aquellos potenciales que se generan en respuesta a estímulos sensoriales específicos, es decir, aquellos que dependen de la presentación de estímulos externos. Por otro lado, el término ERP se suele utilizar únicamente para hacer referencia a los procesos cerebrales de orden superior que se desencadenan en relación con actividades mentales como la memoria, la expectativa, la atención o los cambios en el estado mental [21]. Sin embargo, es importante señalar que, en la literatura, estos dos términos a menudo se utilizan indistintamente, sin hacer una distinción clara entre ellos [22].

En el contexto de la generación de los ERP, las teorías tradicionales sostienen que las formas de onda obtenidas mediante el promedio de señales individuales representan activaciones aditivas a la actividad de fondo del EEG, independiente del estímulo. Sin embargo, investigaciones recientes han propuesto una perspectiva teórica contraria a esta visión tradicional. En particular, se plantea que los componentes de los ERP pueden surgir de cambios en la dinámica de las oscilaciones del EEG de fondo en diferentes bandas de frecuencia, lo cual refleja la participación de procesos sensoriales, motores y/o cognitivos en curso [23, 19].

Oscilaciones cerebrales

Las oscilaciones cerebrales se refieren a la actividad eléctrica rítmica y/o repetitiva generada de manera espontánea y/o en respuesta a estímulos por el sistema nervioso central [24].

Procesos mentales complejos como la percepción, el lenguaje, el afecto y la memoria dependen de la actividad conjunta de una serie de áreas cerebrales que se coordinan de forma transitoria formando lo que se conoce como redes funcionales. Estas redes procesan información de manera colectiva y la coordinación de las áreas involucradas se realiza a través de oscilaciones neuronales sincronizadas [25].

Dependiendo de la frecuencia de esta actividad síncrona, se distinguen diferentes ondas cerebrales llamadas ritmos [26]:

- Ondas delta ($\sim 0,5 - 4$ Hz): Estas ondas están asociadas principalmente con el sueño profundo y reparador. Se caracterizan por tener una amplitud alta y reflejan una actividad cerebral lenta y sincronizada.
- Ondas theta ($\sim 4 - 8$ Hz): Estas ondas se relacionan con estados de relajación

profunda y concentración interna. Se han asociado con la meditación, la creatividad y la imaginación.

- Ondas alfa ($\sim 8 - 14$ Hz): Las ondas alfa se observan en estados de relajación y atención pasiva. Son más prominentes cuando los ojos están cerrados y se asocian con un estado de calma y relajación mental.
- Ondas beta ($\sim 14 - 30$ Hz): Estas ondas se relacionan con estados de activación mental, atención externa y actividad cognitiva. La amplitud de las ondas beta puede aumentar en situaciones de estrés, ansiedad o concentración intensa. También están presentes durante la vigilia y el procesamiento de información activo.
- Ondas gamma ($\sim 30+$ Hz): Las ondas gamma están asociadas con la integración sensorial, la atención selectiva y la actividad cognitiva de alto nivel.

Las variaciones en los patrones de estas ondas cerebrales pueden indicar el nivel de conciencia, el estado psicológico o la presencia de trastornos neurológicos.

Existen tres tipos de oscilaciones neuronales en función de su origen: las oscilaciones neuronales evocadas, las cuales están generadas por un estímulo y están sincronizadas con el inicio de este; las oscilaciones neuronales inducidas, que no están estrictamente sincronizadas con el inicio del estímulo, pero están relacionadas con él; y las oscilaciones espontáneas o en estado de reposo, que se refieren a la actividad oscilatoria espontánea del cerebro en ausencia de estimulación [27, 25, 20].

Las oscilaciones evocadas son un tipo de respuesta a estímulos que están sincronizadas en fase y tiempo con el inicio del estímulo. Al promediar las señales EEG que se producen después del estímulo, se cancelan las oscilaciones no sincronizadas en fase dejando intacta la respuesta evocada. De hecho, estas oscilaciones evocadas son equivalentes a los ERP descritos anteriormente, pero las características que se analizan son temporales y espectrales [25].

Las oscilaciones inducidas o no sincronizadas en fase ocurren en fases o latencias variables con respecto al inicio del estímulo, especialmente durante tareas perceptuales y cognitivas. Estas respuestas no sincronizadas en tiempo se disminuyen considerablemente o desaparecen por completo al promediar las señales. Por lo tanto, el análisis de las oscilaciones inducidas requiere un análisis en tiempo y frecuencia de cada señal [25].

Por último, en cuanto a las oscilaciones espontáneas, el cerebro exhibe fluctuaciones organizadas de la actividad neural, incluso en ausencia de tareas o estímulos sensoriales. El EEG en estado de reposo está dominado por las oscilaciones alfa y theta [28].

2.1.2. Paradigmas

Las BMIs se basan en la distinción entre cambios en el EEG generados por algún tipo de evento sensorial, motor o cognitivo y la señal EEG espontánea. A continuación, se muestran los fenómenos neuroeléctricos que más se utilizan en BMIs agrupados por tipo:

Potencial relacionado con evento

Dentro de los ERP cabría hacer otra distinción en base al tipo de evento que genera el potencial: sensorial, motor o cognitivo [29]. Los potenciales sensoriales son generados como respuestas del EEG a estímulos externos. Un ejemplo es el trabajo de [30], en el que utilizaron una luz láser para simular la aparición de un obstáculo cuando los sujetos andaban asistidos por un exoesqueleto. Cuando aparecía el potencial derivado de esta luz en la señal EEG de los participantes, se enviaba un comando de parada al exoesqueleto.

Los potenciales motores reflejan actividad cortical asociada con movimientos voluntarios (MRCP, por sus siglas en inglés, Movement Related Cortical Potential). Los cambios en la actividad cerebral se producen por la planificación y ejecución del movimiento. Las interfaces que utilizan el paradigma MRCP se basan en identificar los ritmos asociados con el pre-movimiento para poder detectar la intención de moverse del usuario [31, 32].

Los potenciales cognitivos son respuestas a eventos internos que implican procesamiento cerebral de alto nivel relacionado con actividades mentales como expectación, memoria, atención y cambios en el estado mental [33]. Un ejemplo muy utilizado sería la onda P300, esta forma de onda aparece 300ms después de que se presente el estímulo [34, 35]. La onda P300 se produce tras reconocer un estímulo de baja probabilidad que se presenta mezclado con una serie de estímulos irrelevantes. Los estímulos pueden ser visuales o auditivos y la onda P300 se genera como resultado del proceso de toma de decisión.

Oscilaciones cerebrales evocadas

Un ejemplo de este tipo que se ha empleado en BMI es el potencial visual evocado de estado estable (SSVEP, por sus siglas en inglés, Steady-State Visual Evoked Potentials) que se manifiesta tras una estimulación luminosa a frecuencias específicas. Cuando la retina se excita por un estímulo visual a frecuencias entre 3.5Hz y 7Hz, la respuesta cerebral se genera a la misma frecuencia (o múltiplo de estas). En [36], emplearon distintos estímulos visuales y cada uno de ellos se correspondía con una acción a realizar por el usuario. De esta forma cuando la BMI detectaba uno de estos potenciales, lo diferenciaba del resto y enviaba el correspondiente comando a un exoesqueleto [37].

Oscilaciones cerebrales inducidas

En cuanto a las oscilaciones inducidas, un paradigma que se ha empleado para las BMIs es la sincronización y desincronización relacionada con evento (ERD, por sus siglas en inglés, Event Related Desynchronization) y (ERS, por sus siglas en inglés, Event Related Synchronization). Las redes neuronales pueden tener distintos grados de sincronía con oscilaciones a distintas frecuencias. La ERD que se produce en las bandas de frecuencia alfa (8-14 Hz) y beta (14-30 Hz) es característica de áreas corticales activadas que están preparadas para procesar información o preparar un movimiento. En contraposición, cuando se produce el fenómeno ERS en las mismas bandas de frecuencia, se asocia con una correlación electrofisiológica de las áreas corticales en un estado de reposo [38]. Este paradigma también se ha utilizado para detectar la intención de movimiento [31] o la IM.

2.1.3. Imaginación motora

La IM se define como un proceso cognitivo en el cual una persona simula mentalmente la ejecución de movimientos sin realizarlos físicamente. Se ha demostrado que los procesos neuronales involucrados en la realización de IM emulan en espectro y espacio los procesos que se producen cuando realmente se produce una ejecución motora [39]. Como consecuencia, son diversos los autores que han diseñado BMIs basadas en IM con el empleo del paradigma ERD/ERS para discernir cuando el usuario está imaginando un movimiento y cuando está en un estado de relajación o cuando está imaginando dos movimientos distintos [40, 41, 14, 42, 43, 44].

Investigaciones previas han descrito las similitudes entre la ejecución motora y la IM, centrándose específicamente en la corteza motora primaria. La corteza motora primaria está subdividida en múltiples secciones, cada una responsable del control de un área del cuerpo, en una disposición a menudo referida como el homúnculo cortical [45].

Otras áreas de interés para la detección de la IM son el área motora suplementaria (AMS) y la corteza premotora (PM), ubicadas anteriormente a la corteza motora primaria y también involucradas en la red motora. Las neuronas en el AMS están involucradas en la preparación de los movimientos, por lo que es razonable suponer que los aspectos preparatorios de un movimiento pueden estar estrechamente relacionados con la IM. En cuanto a la PM, diferentes estrategias de imaginación involucran diferentes partes de activación: mientras que la imaginación somatosensorial implica la PM dorsal, las estrategias visuales involucran partes más ventrales [46].

También se han hallado activaciones en el lóbulo parietal superior durante la IM que involucra aspectos espaciales superiores. El lóbulo parietal superior está estrechamente conectado con el AMS posterior, pero también con la PM [46].

El proceso de la imaginación no depende de la capacidad de ejecutar un movimiento, sino más bien de mecanismos de procesamiento central. En comparación con individuos

sanos, los pacientes con lesiones en la corteza motora y los pacientes con enfermedad de Parkinson muestran una disminución en la velocidad del movimiento durante la ejecución motora y la IM, mientras que los pacientes con lesiones espinales solo muestran una duración prolongada de la ejecución motora pero la misma duración de la IM [46].

Considerando la presente tesis doctoral, el enfoque se realiza en la IM del movimiento de caminar. En la corteza motora primaria, la ubicación de la región responsable del movimiento de las piernas está en la fisura interhemisférica. Por ello, otra limitación de esta investigación es la dificultad de medir mediante EEG la actividad generada por esta región. Esto se produce porque los dipolos generados por las neuronas en las dos paredes del surco apuntan en direcciones opuestas lo que resulta en una cancelación significativa de las señales extracraneales [47]. Además, la señal captada en la corteza incluye también los dipolos generados por otras neuronas más superficiales, enmascarando la señal de interés [6].

Los paradigmas BMI basados en potenciales y oscilaciones evocados tienen una alta tasa de acierto en la detección de la acción a realizar por el usuario y su precisión es mayor que en los basados en IM. Sin embargo, las interfaces que utilizan este último paradigma son más prometedoras desde el punto de vista de fomentar la rehabilitación de la función motora al implicar al paciente cognitivamente en el movimiento a repetir [48].

2.1.4. Protocolos experimentales

En las BMIs, los sujetos deben generar patrones específicos de actividad cerebral para lograr acciones concretas en los dispositivos externos. La calibración de una BMI es un proceso crítico para su correcto funcionamiento. Durante la calibración, el sujeto realiza una serie de tareas mentales mientras la BMI registra la actividad cerebral asociada a ellas. Estos datos se utilizan para entrenar la BMI y que pueda reconocer estos patrones específicos.

Para llevar a cabo la calibración, se definen protocolos que indican las tareas mentales a realizar y su duración [49]. Durante esta fase, el dispositivo externo no está controlado por la BMI, sino que se utiliza mediante comandos predefinidos, lo que se conoce como control en lazo-abierto.

Es importante mencionar que la calibración se realiza típicamente al inicio de cada sesión experimental debido a la naturaleza no estacionaria de los datos de EEG. De esta forma, se registra la señal EEG y se entrena el sistema antes de su uso. Posteriormente, se realizan pruebas de lazo-cerrado, en las que los comandos que controlan el dispositivo se generan a partir de la salida de la BMI en función de la señal EEG. La calidad de la calibración y la estabilidad de los patrones de actividad cerebral son fundamentales para el correcto funcionamiento de una BMI [13].

La prueba que se realiza a un sujeto en una fecha se define como sesión y dentro de

una sesión cada vez que se repite el protocolo se define como un registro.

2.1.5. Diagrama de flujo de una BMI

Los distintos pasos de una BMI, desde que se adquieren los datos del sujeto hasta que el sistema toma una decisión que se envía al dispositivo externo, se pueden ver en la Figura 2.3. .

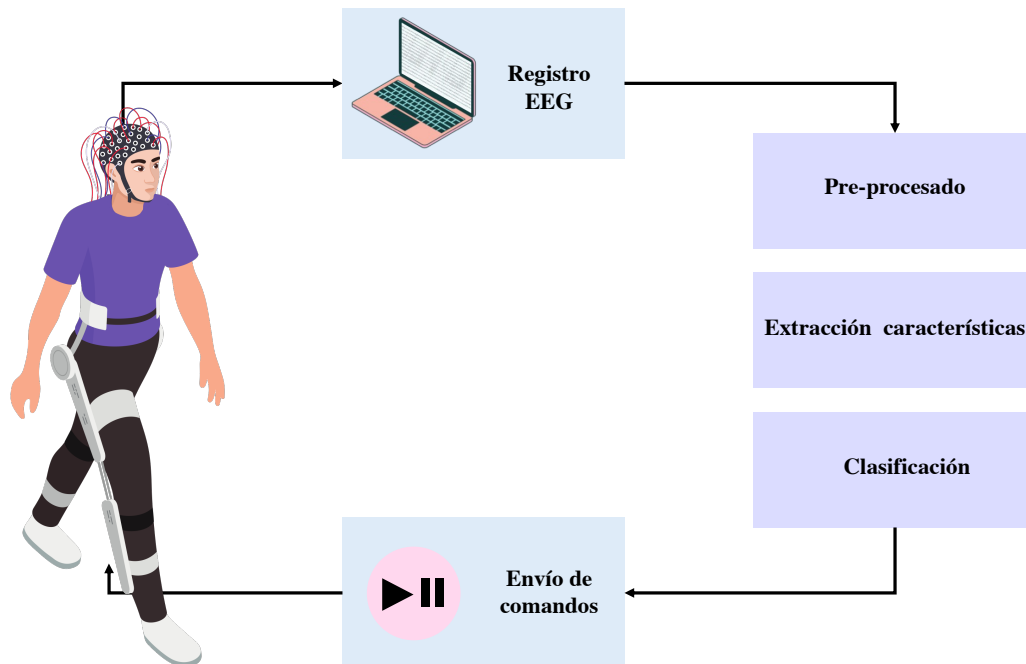


Figura 2.3: Esquema del flujo de datos en una interfaz cerebro-máquina.

Adquisición

Las señales EEG se registran mediante electrodos que se sitúan alrededor del cráneo. Originalmente, el posicionamiento se definió para 21 electrodos siguiendo un sistema 10-20 [50]. Estos valores representan la distancia de los electrodos adyacentes como el porcentaje de la distancia que hay entre el hueso frontal y occipital y la distancia entre los huesos temporales respectivamente [51]. Un mayor número de electrodos de registro implica un aumento de la resolución espacial de la señal. Es por ello, que el sistema original de referencia mencionado anteriormente se ha incrementado a un sistema 10-5 que permite la utilización de 345 electrodos [52]. Uno de los electrodos del montaje se utiliza de puesta a tierra y normalmente se posiciona en el lóbulo de la oreja [53].

Pre-procesado

El propósito de este paso es el de mejorar la calidad de la señal que se utilizará para interpretar la voluntad del usuario. Durante la adquisición, hay oscilaciones en el EEG que pueden haber sido generadas por artefactos o ruido y pueden ocultar las oscilaciones que el sistema quiere detectar. Los artefactos son debidos a actividad fisiológica como fluctuaciones de impedancias, electrooculograma (EOG), parpadeos, electrocardiograma (ECG), movimientos faciales o del cuerpo y respiración. En cuanto al ruido, este se puede producir por la degradación del instrumental o la interferencia de ondas electromagnéticas de distintas fuentes como móviles u ordenadores [54]. En la literatura se han identificado distintos métodos de pre-procesado.

Por un lado, están los filtros en frecuencia que discriminan una determinada frecuencia o gama de frecuencias. Los filtros Notch se utilizan para eliminar los artefactos generados por la red eléctrica [37]. Los filtros paso bajo se utilizan para eliminar artefactos que pueden producirse por el movimiento a altas frecuencias [55]. Y finalmente, los filtros paso banda se emplean para seleccionar las bandas de frecuencia que son de interés para el análisis.

Los filtros espaciales tienen como objetivo eliminar la contribución que realiza el resto de los electrodos a un electrodo en concreto. Una solución física consiste en el empleo de un electrodo de referencia [53]. De esta forma, la medida de cada electrodo se calcula como la diferencia entre este y el de referencia. Sin embargo, este método presenta como limitación que la información de un electrodo no se puede utilizar para la BMI y además, si el área donde se sitúa este electrodo de referencia no es neutra, se puede producir una distorsión topográfica de las señales del resto de electrodos. Como alternativa, existen los métodos denominados reference-free (del inglés) que no necesitan un electrodo de referencia [56]. El filtro espacial que más se ha utilizado en la literatura es el CAR (del inglés Common Average Reference) [57, 58], este filtro consiste en calcular el potencial de cada electrodo como la diferencia entre este y la media de todos los electrodos [40, 41, 14, 42, 43, 49, 59, 60]. Otro método ampliamente empleado es el filtro Laplaciano que se basa en el cálculo del potencial de cada electrodo como la diferencia entre este y la media ponderada de los potenciales de los electrodos adyacentes [61, 62]. De esta forma se consigue eliminar la influencia de las señales cercanas [44]. Por último, también existe la posibilidad de combinar montajes con electrodos de referencia con pasos adicionales de filtrado espacial [53].

Para la eliminación de artefactos existen una serie de métodos que se centran en artefactos concretos. El método ASR (por sus siglas en inglés, Artifact Subspace Reconstruction) [63] realiza una descomposición PCA (por sus siglas en inglés, Principal Component Analysis) [64] en cada ventana de tiempo de la señal y la compara con un segmento de la señal que se haya establecido como libre de artefactos. Aquellas componentes cuya desviación estándar supere un determinado umbral son eliminadas y luego se reconstruye la señal

[49, 53, 65]. ASR no se especializa en ningún tipo de artefacto, sino que trata de eliminar cualquier elemento que no se encuentre en la señal definida como libre de artefactos. Por otro lado, el algoritmo presentado por [53] se centra en eliminar artefactos de movimiento ocular, parpadeo y cambios de amplitud que pueden ser causados por cambios en las impedancias de los electrodos o en las características del amplificador. Este método tiene como objetivo estimar la contribución del EOG, medido con cuatro electrodos situados alrededor de los ojos, a los cambios de amplitud a la señal EEG. Una vez se ha estimado la contribución, se resta de la señal original. ICA (por sus siglas en inglés, Independent Component Analysis) [66, 67, 68] es otra técnica que descompone las señales EEG en distintas fuentes de origen, como por ejemplo los movimientos oculares o la actividad muscular, que pueden contaminar la señal de interés. Una vez que se separan estas fuentes, se pueden identificar y eliminar aquellas que no son relevantes para el estudio, y así limpiar la señal EEG para que contenga principalmente la actividad cerebral que se quiere analizar [69].

Otro método de pre-procesado consiste en la estandarización de las señales. En [70] propusieron un algoritmo para estandarizar las señales de los distintos canales y así poder comparar entre distintos individuos sin perder información.

Como alternativa para reducir el ruido en las señales EEG, algunos estudios han utilizado métodos que consisten en eliminar canales o registros considerados ruidosos [40, 42, 43]. Estos métodos se basan en una inspección visual de las señales o en la utilización de umbrales de voltaje para detectar valores anormales.

Es difícil establecer qué metodología de pre-procesado proporciona mejores resultados para cada tipo de BMI porque son pocos los estudios que comparan las distintas alternativas o proporcionan razones de su elección [53, 56].

Extracción de características

Una vez las señales están pre-procesadas, se obtienen características temporales, espaciales o espectrales. Las características se pueden obtener en tiempo real de forma síncrona con su registro, lo que se denomina online, o de forma offline. En el caso online, como no es posible un análisis continuo de los datos es necesario discretizar su análisis mediante el uso de pequeñas ventanas temporales. De esta forma primero se registra una ventana de la señal, se pre-procesa y se extraen sus características. El análisis online limita los métodos que se pueden utilizar, ya que todo el proceso debe realizarse antes de que se actualice la siguiente ventana temporal. Por otro lado, en el análisis offline, primero se registra toda la señal, se pre-procesa y luego se extraen características de los fragmentos que se corresponden con cada tarea. El análisis offline, aunque no tiene las limitaciones de tiempo que tiene un análisis online, generalmente se emplea para estudiar la señal y seleccionar las características más discriminantes, ya que no se puede utilizar para controlar un dispositivo externo en tiempo real. Las características se pueden agrupar en tres

bloques: temporales, espectrales y espaciales [71].

Las características temporales se utilizan en su mayoría en los paradigmas ERP. En un análisis offline lo más común es promediar distintos registros para encontrar la forma de la señal y luego comparar las características temporales del promedio en una ventana de tiempo alrededor del estímulo con el resto de las ventanas de tiempo de la señal [38]. En un análisis online las características se extraen de cada ventana temporal antes de que la siguiente ventana de señal EEG llene el buffer de actualización del registro [31, 32, 59, 65].

Las características del espectro de frecuencia se suelen utilizar en los paradigmas ERD/ERS. Hay distintas formas de caracterizar el espectro de una señal. Una característica que se ha usado ampliamente es la densidad espectral de potencia (PSD, por sus siglas en inglés, Power Spectral Density) [72] que proporciona información de cómo está distribuida la potencia (o energía) de una señal en las distintas frecuencias que la componen. El método tradicional para la estimación de la PSD se basa en la transformada de Fourier [73, 74]. Es una buena aproximación para señales estacionarias y en el caso de señales no estacionarias, como el EEG, se emplea mediante ventanas. El uso de ventanas no supone una limitación, ya que es la base del análisis online [36, 75]. Otra forma de calcular la PSD es mediante el método de Welch [76, 77] que descompone la señal (o en el caso online, la ventana de señal) en segmentos más pequeños y calcula el espectro promedio de estos segmentos [41, 78]. Otras métricas se basan en la estimación de la frecuencia y amplitud instantáneas como la transformada Stockwell (ST) [79] y la transformada Hilbert-Huang [80, 81, 82], que emplea una descomposición empírica en modos de frecuencia (EMD, por sus siglas en inglés, Empirical Mode Decomposition) [83, 84, 75].

Los dos ejemplos más utilizados en la literatura de BMIs basadas en características espaciales son los patrones espaciales comunes (CSP, por sus siglas en inglés, Common Spatial Patterns) [85] y la geometría de Riemann [86]. Los CSP se basan en que a veces la varianza de un patrón de actividad cerebral es mayor en un canal o conjunto de canales que en el resto. Estas diferencias se producen porque diferentes patrones de actividad producen cambios del EEG en distintas áreas cerebrales. El método CSP realiza una proyección del EEG multi-canal en un nuevo espacio buscando maximizar las diferencias en varianza entre los distintos patrones a detectar. Las características espaciales se obtienen al aplicar esta transformación, usada en la proyección, a la señal. En el caso de la geometría de Riemann, el enfoque es similar. Se calculan las matrices de covarianza de las señales EEG que, por definición, pertenecen al espacio Riemann. Después se calcula el centro de todas estas matrices de EEG que pertenecen a cada clase. Finalmente, se calcula la distancia en este espacio de una nueva matriz a cada centro o se proyecta al espacio tangencial, que es Euclidiano, y se pueden utilizar clasificadores tradicionales para su análisis.

Por último, en la extracción de características, las redes neuronales han demostrado resultados prometedores en otros campos como técnicas que no requieren un cálculo manual de métricas, y ahora están siendo utilizadas en sistemas BMI [87]. La mayoría de los

trabajos utilizaron señales EEG en crudo o normalizadas como entrada a la red. Además, en algunos casos estas señales se filtraron por bandas de frecuencia de interés, como alfa o beta [88]. También existen alternativas que aplicaron la transformada de Wavelet [89, 90, 91] o CSP antes de utilizar la red neuronal [92]. En cuanto a la arquitectura de la red, los estudios que trabajaron con IM como estrategia mental, prefirieron las capas convolucionales para capturar las relaciones espaciales entre diferentes áreas cerebrales [87].

Selección de características

Debido al gran número de características que se extraen, puede surgir un problema de gran dimensionalidad en las aplicaciones BMI. Por ello, se han empleado distintos métodos para seleccionar un subconjunto de características relevantes: PCA e ICA que también se utilizan como técnicas de pre-procesado y se han definido en el apartado anterior, LFDA (por sus siglas en inglés, Local Fisher Discriminant Analysis) [32, 42] y CPCA (por sus siglas en inglés, Crowd Principal Component Analysis) [40].

Clasificación

Una vez se han extraído y en su caso, seleccionado las características, estas se utilizan para la clasificación. En el análisis online son las distintas ventanas, también llamadas épocas, las que clasifican entre las distintas tareas. En el análisis offline los trozos de la señal que se corresponden a cada tarea son los que se clasifican. Primero el clasificador se entrena con datos cuya clase sea conocida y posteriormente se emplea para predecir la clase de nueva señal. Como última etapa de la BMI, las predicciones de los modelos son enviadas como comandos a los dispositivos a controlar.

2.1.6. Tipos de dispositivos a controlar

Las BCIs se pueden utilizar para controlar diversos dispositivos. Desde el punto de vista del software, se pueden utilizar para controlar el cursor de una pantalla, un juego o un avatar en un entorno de realidad virtual [18, 93, 94].

Considerando el caso concreto de las BMIs, los dispositivos a controlar van desde una silla de ruedas en la que se controla el avance y la parada, o un exoesqueleto robótico que sirva de apoyo o potencie las capacidades físicas de los usuarios que lo lleven [49].

2.2. Lesión de la médula espinal

2.2.1. Patología

La lesión de médula espinal se refiere al daño en la médula espinal que puede ser causado por una lesión directa o por el daño en los tejidos que la rodean. La médula espinal actúa como canal de comunicación entre el cerebro y los órganos del cuerpo, por lo que una lesión en la médula espinal puede afectar diferentes funcionalidades corporales. Como consecuencia, puede dar lugar a una variedad de síntomas, incluyendo la parálisis o reducción de la movilidad, la afectación de la sensibilidad y la pérdida del control sobre los esfínteres. Estos síntomas pueden tener un impacto significativo en la calidad de vida de los pacientes y su capacidad para llevar a cabo actividades cotidianas [95].

El daño de la médula espinal se produce por dos procesos: el mecanismo primario y el mecanismo secundario. El proceso primario es causado por la contusión y la compresión directa de la médula, lo que desencadena una respuesta inflamatoria. Esta respuesta inicia procesos bioquímicos y celulares que generan la lesión secundaria y resultan en la muerte neuronal [95].

Las LME se clasifican según la escala de la American Spinal Injury Association (ASIA) [96]. Esta escala se basa en la gravedad de la lesión y mide el nivel de afectación de la movilidad, los reflejos y el nivel sensitivo. Los grados de ASIA son los siguientes:

A: Lesión completa. Sin función motora o sensitiva en segmentos sacros.

B: Lesión incompleta sensitiva. Preservación de la sensibilidad, pero función motora no conservada por debajo de la lesión, incluyendo niveles sacros.

C: Lesión incompleta motora. Preservación de la función motora por debajo de la lesión y al menos, la mitad de los músculos clave tiene un balance muscular menor de 3.

D: Lesión incompleta motora. Preservación de la función motora por debajo de la lesión y al menos, la mitad de los músculos clave tiene un balance muscular de 3 o más.

E: Función sensitiva y motora conservada.

La recuperación después de una LME puede verse afectada por diferentes factores, como la completitud de la lesión, su localización en la médula espinal, el nivel de actividad física y las terapias de rehabilitación, y el desarrollo de complicaciones secundarias [97].

2.2.2. Rehabilitación

La mayoría de las lesiones de LME son incompletas, e incluso en casos de lesiones completas, es posible que exista tejido espinal preservado que pueda ser rescatado y reparado para restablecer la función motora. El objetivo de los tratamientos es fomentar el paso de señales de control descendente a través de la región de la lesión y hacia tejido espinal más funcional [98].

Neuroplasticidad

La neuroplasticidad se define como el potencial del sistema nervioso de producir cambios funcionales y anatómicos en respuesta a estímulos durante el aprendizaje o en respuesta a lesiones. Estos procesos son responsables del aprendizaje, la memoria y el ajuste fino del control motor. Se ha encontrado evidencia de neuroplasticidad tanto en la médula espinal como en el cerebro [99, 98, 100].

Un elemento clave en la neuroplasticidad, especialmente en adultos, es la plasticidad de las sinapsis, que consiste en cambios en la fuerza de las sinapsis excitatorias e inhibitorias. La potenciación de larga duración ocurre cuando las sinapsis se fortalecen y requieren menos estimulación para propagar un potencial de acción. Por el contrario, la depresión de larga duración ocurre cuando la fuerza sináptica se reduce y se requiere más estimulación para propagar un potencial de acción [99, 100].

El brote y poda sináptica son dos de los principales resultados de la potenciación y depresión sináptica. El brote sináptico, o sinaptogénesis, a menudo sigue a la potenciación sináptica. Básicamente, las sinapsis que experimentan una fuerza suficiente se dividen, creando dos sinapsis. Este cambio físico permite una mayor probabilidad de que los potenciales postsinápticos excitatorios se sumen en potenciales de acción. Por otro lado, la depresión resulta en la poda de sinapsis, y las sinapsis inactivas eventualmente se eliminan [99].

Después de un daño en el tejido nervioso, como una lesión de médula espinal, puede iniciarse una plasticidad espontánea. Esta plasticidad espontánea puede ser mal adaptativa, tomando la forma de sinaptogénesis, ya que las neuronas intentan compensar las conexiones perdidas o regenerarse a través del sitio de la lesión en respuesta a la inflamación. Esta formación de nuevas conexiones conlleva hiperexcitabilidad e ineficiencia, lo que dificulta la restauración de la función normal [99].

Dos mecanismos clave que afectan el control del movimiento poco después de la lesión son la pérdida de proyecciones descendentes y la reducción de la excitabilidad de los circuitos motores de la médula espinal parcialmente denervados caudales a la lesión. Por lo tanto, las terapias de rehabilitación buscan aumentar o detener la pérdida de proyecciones descendentes y aumentar la excitabilidad de la médula. Estas terapias se basan en la combinación de dos enfoques, la neuromodulación utilizando estimulación espinal o cortical y la rehabilitación física mediante entrenamiento de tareas específicas [99, 100].

Entrenamiento de tareas específicas

Las terapias convencionales se fundamentan en la realización de actividades específicas altamente repetitivas, las cuales son asistidas por profesionales de la fisioterapia. La evidencia respalda la idea de que la cantidad y especificidad de la práctica son factores cruciales para fomentar la recuperación y el desarrollo de habilidades motoras. La pro-

visión de una cantidad considerable de práctica específica de tareas conduce a mayores mejoras en la función motora en comparación con una práctica limitada o la práctica de tareas alternativas [101].

Los recientes avances en dispositivos robóticos han permitido su incorporación en los tratamientos como alternativa a estas terapias, pero no de forma sustitutiva. La terapia con exoesqueletos robóticos requiere menos esfuerzo por parte de los fisioterapeutas, y ofrece una nueva forma de tratamiento con sesiones de entrenamiento más largas y patrones de movimiento más reproducibles pudiendo graduar los niveles de esfuerzo o el rango de movimiento, permitiendo una mayor continuidad entre sesiones. Un ejemplo de estas terapias es el entrenamiento en cinta de correr con soporte de peso corporal, que ha sido un método establecido en rehabilitación y ha mostrado una mejora significativa en pacientes con lesiones incompletas de LME [95].

Aprendizaje motor con imaginación motora

El aprendizaje del movimiento implica varios componentes interconectados: el procesamiento y la recopilación de entradas sensoriales relevantes para la acción, la aplicación de una serie de estrategias de toma de decisiones que definen los parámetros del movimiento y la activación de procesos de control de avance durante la ejecución motora [102].

Si bien la práctica física es vital para la adquisición y consolidación de nuevas habilidades motoras, la observación de la acción y la IM son dos métodos complementarios que también promueven el aprendizaje motor. A pesar de que existe una amplia evidencia que demuestra los efectos positivos del entrenamiento mental en el rendimiento motor, se sabe poco sobre los orígenes neurales de este beneficio. Esta falta de información puede deberse a la complejidad de las tareas motoras [103, 102].

La disminución de la información aferente enviada al cerebro, como consecuencia de una lesión, induce una reducción en el tamaño de la representación topográfica muscular en la corteza somatosensorial y motora. Esta reducción resalta el impacto de las interacciones sensoriomotoras en la organización cortical [102].

Durante el entrenamiento de la IM, se producen adaptaciones sensoriomotoras que revelan la integración de información del entorno para construir y modular en tiempo real el programa motor, incluso en ausencia de movimiento voluntario. Esto sugiere que la IM involucra mecanismos neurales relacionados con el control y la coordinación motora [103].

2.3. Interfaces cerebro-máquina para neurorrehabilitación

Es posible ejercer el control sobre los dispositivos robóticos a través de diversos medios, tales como aplicaciones móviles, joysticks y consolas de comandos. No obstante, las BMIs constituyen una alternativa que permite establecer un control directo a través de la mente humana. Este tipo de tecnología representa una oportunidad prometedora para el desarrollo de nuevas terapias de rehabilitación [49].

Como se ha mencionado anteriormente, existen diversos enfoques de control que pueden aplicarse con el fin de generar una acción específica en el exoesqueleto robótico. Entre los paradigmas más exitosos destacan aquellos que se basan en respuestas evocadas, como el SSVEP, cuya clasificación ha sido objeto de estudio en diversas investigaciones [36, 104]. Sin embargo, a diferencia de estos estímulos externos, la IM permite inducir cambios en los patrones cerebrales de forma voluntaria e interna por parte del usuario, lo que le otorga un mayor control sobre la tarea a realizar [105].

Desde el punto de vista de la rehabilitación, la IM favorece el aprendizaje motor y por ello, la recuperación. La decodificación de esta señal cerebral permite generar una salida específica en la BMI, que puede traducirse en el movimiento del exoesqueleto o en algún otro tipo de modificación en un dispositivo externo. Esta retroalimentación en tiempo real contribuye a que el usuario intente modular su actividad cerebral para mejorar el rendimiento del sistema. Además, la realización de una tarea de movimiento real en la extremidad afectada es la base de la rehabilitación física que también fomenta la recuperación de la funcionalidad perdida. Los elementos clave para un entrenamiento neurorrehabilitativo son las intenciones voluntarias de movimiento y una retroalimentación sensorial y propioceptiva sincronizada con las acciones motoras de las extremidades [106].

2.3.1. Interfaces cerebro-máquina basadas en imaginación motora del miembro inferior

El estado del arte en la literatura revela que hay más trabajos que han diseñado interfaces cerebro-máquina basadas en la IM de la mano para el control de prótesis robóticas [85, 14, 78, 107, 108, 109], en comparación con los trabajos basados en IM de las piernas [110]. Una limitación importante de esta última línea de investigación es que la representación de las piernas en la corteza motora está a una profundidad de 1-4 cm de la superficie, lo que dificulta la captación de la activación de esta zona mediante EEG [111]. Para abordar esta problemática, la presente tesis se enfoca en el diseño de una BMI basada en la IM del miembro inferior para controlar un exoesqueleto robótico. La Tabla 2.1 detalla las últimas contribuciones presentes en la literatura basadas en IM de las piernas/pies y contribuciones basadas en la intención de movimiento. Las últimas tres contribuciones se

corresponden con las publicaciones P1, P3 y P5 del compendio de esta tesis doctoral.

Algunos autores han intentado combinar IM de las piernas con otros tipos de IM y así facilitar la tarea de discriminación, por ejemplo, con cuatro tareas mentales como IM de las piernas, mano derecha, mano izquierda y lengua. A pesar de que los resultados son prometedores [112], desde el punto de vista de la neurorrehabilitación es necesario realizar una tarea mental que esté estrictamente ligada al movimiento a realizar. Por ello, otros estudios previos han combinado la IM de las piernas con un estado de no-intención [113, 60, 44, 114, 40, 115]. Durante este estado, los usuarios deben estar relajados y para el control de un dispositivo robótico, la IM actuaría como condición activa y la no-intención como condición pasiva. Sin embargo, los resultados de este tipo de sistema son menores que los que incluyen otro tipo de IM.

Por otro lado, en lugar de trabajar con tareas de IM, algunos autores han diseñado enfoques experimentales basado en la intención de movimiento. Como se ha mencionado en sección paradigmas, la intención de movimiento es un potencial cortical producido por la corteza motora justo antes de que se realice un movimiento. En [32, 53], un paciente con lesión de médula espinal caminó asistido por un exoesqueleto que fue activado por un operador externo mientras se registraba su EEG. Luego, la intención de movimiento fue decodificada y utilizada para iniciar/detener el exoesqueleto. Además, en [42, 43], cuatro pacientes con lesión de médula espinal recibieron instrucciones para intentar iniciar un movimiento mientras estaban de pie y usando un exoesqueleto con las piernas bloqueadas. Luego, para el control real, se les pidió a los pacientes que realizaran el mismo intento cuando quisieran iniciar la marcha. Para garantizar la seguridad durante el experimento, se permitió a los participantes tener control completo sobre el exoesqueleto solo durante intervalos de tiempo específicos, mientras que el resto del tiempo, el exoesqueleto estaba bloqueado. Sin embargo, el principal beneficio de IM en comparación con la intención de movimiento es que requiere que los sujetos repitan mentalmente un cierto movimiento y deben estar cognitivamente involucrados durante la duración de la tarea, lo que promueve la recuperación motora [116]. [113] combinaron IM con retroalimentación visual y/o háptica para mejorar el rendimiento del modelo, mientras que [114] incluyeron el parpadeo de los ojos para el control. [40] desarrollaron una BMI basada puramente en IM de las piernas para controlar una ortesis de marcha robótica suspendida en una cinta de correr y fue evaluada con un individuo sano y un paciente con lesión de médula espinal. En [60], ocho pacientes con lesión de médula espinal participaron en tareas de IM para lograr caminar, ponerse de pie o chutar una pelota. Sin embargo, no se proporcionaron detalles técnicos precisos acerca de la BMI utilizada. [44] presentaron un diseño experimental para controlar el inicio de la marcha de un exoesqueleto robótico basado en MI de la marcha durante intervalos de tiempo determinados. Emplearon estimulación transcraneal de corriente continua (tDCS) para mejorar la práctica de IM y se evaluó con 12 sujetos sanos. En el trabajo de [115], se desarrolló una BMI en la que los participantes debían realizar IM

o relajarse durante intervalos de 4 s para conseguir la emisión de un comando específico.

Tabla 2.1: Estado del arte de las interfaces cerebro-máquina basadas en imaginación motora del miembro inferior.

Publicación	Método extracción características	Participantes	Retroalimentación	Exoesqueleto de miembro inferior
Do 2013 [40]	PSD	1 sano / 1 paciente con LME	Andar/Parar	ROGO
Kilicarslan 2013 [32] ^a	Ventana temporal (electrodos x muestras)	1 paciente con LME	Andar/Parar	REX
Donati 2016 [60]	CSP	8 pacientes con LME	Andar/Parar/Chutar una pelota	Lokomat y exoesqueleto personalizado
Kilicarslan 2016 [53] ^a	Ventana temporal (electrodos x muestras)	6 sanos/ 1 paciente con LME	Andar/Parar	REX
López-Larraz 2016 [42]	PSD con modelo autorregresivo	3 sanos/ 4 pacientes con LME	Andar/Parar	H2
Rajasekaran 2018 [43] ^a	Paradigmas de ERD y MRCP pero sin detalles	4 pacientes con LME	Andar (sin parada)	H1
Rodríguez-Ugarte 2018 [44] ^a	PSD	4 sujetos sanos	Andar (sin parada)	H2
Wang 2018[112]	CSP	4 sanos	Andar/ Parar/ Sentarse	SIAT
Gordleeva 2020 [115]	CSP	8 sanos	Andar (sin parada)	MADIN
Choi 2020 [114]	CSP	10 sanos	WALK/STAND/SIT	RoboWear
Barria 2021 [113]	PSD	5 pacientes con accidente cerebrovascular	Extensión/ Flexión de tobillo	FLEX
Ortiz 2019[117] ^b	Transformada de Stockwell	5 sanos	Andar/Parar	REX
Ferrero 2021 [3] ^b	CSP	2 sanos	Andar/Parar	H3
Ferrero 2023 [5] ^b	CSP	10 sanos /2 pacientes con LME	Andar/Parar	H3

^a Estas contribuciones utilizaron la intención de movimiento para el control y no la imaginación motora.

^b Las tres contribuciones marcadas se presentan en esta tesis por compendio de publicaciones.

2.3.2. Desafíos

Uno de los principales desafíos que enfrentan las BMIs es su calibración. Como se ha mencionado en la sección 2.1.4, la calibración es crucial para el correcto funcionamiento de la BMI y que ésta se adapte a la actividad cerebral de cada usuario. Por ello, se requiere una determinada cantidad de registros de actividad cerebral del usuario antes de poder utilizar el sistema para el control de un exoesqueleto robótico. Este proceso de registro puede ser largo y fatigante para los sujetos, especialmente para aquellos con limitaciones motoras que pueden requerir sesiones más cortas [118, 119].

Normalmente, la calibración se realiza al comienzo de cada sesión experimental debido a la naturaleza no estacionaria de los datos EEG. Algunos estudios han explorado enfoques sin calibración utilizando técnicas independientes del sujeto o transferencia de aprendizaje para reducir o eliminar por completo el proceso de calibración [118, 120]. Sin embargo, la efectividad de estos enfoques puede variar entre individuos [120, 121].

Otra alternativa para reducir la carga de la calibración es mejorar la calidad de las tareas mentales realizadas. En un estudio reciente, los participantes realizaron tareas de IM mientras observaban una barra acumulativa que se mostraba en una pantalla. La barra aumentaba a medida que el BCI decodificaba las tareas mentales correctamente y los sujetos no podían comenzar el control del exoesqueleto hasta alcanzar un cierto nivel de precisión [114].

Otro desafío en las aplicaciones de BMI basadas en IM es la variación en la forma en que los sujetos realizan las tareas mentales, lo que resulta en una alta variabilidad en las tasas de éxito [122]. En concreto, hay sujetos que no son capaces de controlar una BMI ya que no consiguen modular su actividad cerebral para generar ciertas acciones. Este fenómeno se conoce como BCI illiteracy [123, 124].

En el ámbito de las BMIs basadas en IM para el control de exoesqueletos de miembro inferior, resulta difícil realizar comparaciones entre los diversos estudios presentes en la literatura o con nuevos diseños, debido a que cada investigación presenta su propio protocolo experimental y utiliza métricas específicas. Esta dificultad se traduce en la falta de estándares comunes para evaluar y comparar el rendimiento de las BMIs [49].

Capítulo 3

Sensory integration in human movement: a new brain-machine interface based on gamma band and attention level for controlling a lower-limb exoskeleton (P1)

Esta contribución buscaba introducir una nueva BMI enfocada en decodificar la IM en la banda de frecuencia gamma y el nivel de atención de los sujetos para asegurar una correlación efectiva entre la tarea mental del usuario y la acción motora deseada, particularmente en contextos de la marcha. El estudio tenía como objetivo explorar el potencial de esta BMI para el control en tiempo real de un exoesqueleto REX, con implicaciones prometedoras en neurorrehabilitación. A continuación, se muestra información más detallada de la contribución:

Título: Sensory Integration in Human Movement: A New Brain-Machine Interface Based on Gamma Band and Attention Level for Controlling a Lower-Limb Exoskeleton.

Autores: M. Ortiz, L. Ferrero, E. Iáñez, J. M. Azorín y J.L. Contreras-Vidal.

Revista: Frontiers in Bioengineering and Biotechnology. Vol 8(2020).

ISSN: 2296-4185 . Ed. FRONTIERS.

JCR-SCI Factor de impacto (2020): 5.89, Cuartil: Q1.

Fecha de publicación: 03 septiembre 2020.

DOI: <https://doi.org/10.3389/fbioe.2020.00735>

3.1. Materiales

3.1.1. Sujetos

En esta contribución participaron cuatro participantes. No presentaban ninguna limitación de movimiento ni ninguna enfermedad conocida. Se les informó sobre los experimentos y firmaron el consentimiento informado. Todos los procedimientos fueron aprobados por Institutional Review Board of the University of Houston, Texas (Estados Unidos).

3.1.2. Equipo

La adquisición de datos se realizó mediante dos conjuntos de 32 electrodos sobre una unidad actiCAP (Brain Products GmbH, Alemania). Cuatro de los electrodos del primer conjunto se colocaron alrededor de los ojos en una configuración bipolar para medir la señal EOG. Los electrodos de referencia y tierra se colocaron en las orejas. Los datos se transmitieron mediante comunicación inalámbrica utilizando un transmisor Move y se amplificaron posteriormente mediante dos unidades brainAmp (Brain Products GmbH, Alemania). El EEG se registró a 1 kHz y se remuestreó a 200 Hz.

La Figura 3.1 muestra la distribución de electrodos escogida.

Los sujetos utilizaron el exoesqueleto REX (Rex Bionics, Nueva Zelanda). Entre sus características destaca que puede mover a personas con lesiones completas de la médula espinal, ya que puede sostenerse de forma independiente y soportar el peso del usuario. Durante los experimentos, se controlaba mediante comandos de alto nivel enviados por Bluetooth, para iniciar o detener la marcha. También proporcionaba retroalimentación en tiempo real sobre su estado.

La Figura 3.2 muestra todo el equipamiento utilizado en este estudio.

3.2. Métodos

En todas las contribuciones presentadas, se envía un comando de control cada 0.5 s, lo que se conoce como época. Por lo tanto, este proceso de “traducción” debe realizarse en tiempo real, es decir, cuando se han registrado 0.5 s de señal, deben ser pre-procesados, se extraen características, se clasifican en un patrón cerebral y se envía un comando de control al dispositivo externo. Todos estos pasos deben llevarse a cabo antes de que los siguientes 0.5 s de señal se hayan registrado. Como consecuencia, este tiempo es crucial

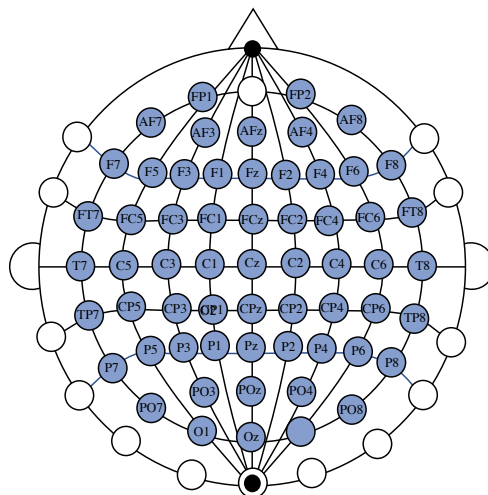


Figura 3.1: Distribución de electrodos escogida en las contribución P1 con 60 electrodos para el registro de la señal cerebral. Se buscaba cubrir la corteza motora primaria, el AMS, la PM y el lóbulo parietal superior.

para la elección de los métodos a utilizar. Por otro lado, la ventana de análisis puede ser mayor a 0.5s cogiendo instantes de tiempo anteriores. En este estudio, las ventanas de análisis fueron de 1 s.

En esta contribución se aplicaron dos paradigmas, uno que detectaba cuando el usuario realizaba IM de la marcha versus cuando estaba en un estado de relajación. Y un segundo paradigma que consistió en medir el nivel de atención del usuario durante la prueba. Por consiguiente, se siguieron dos metodologías distintas. La Figura 3.3 muestra un esquema de la metodología utilizada en cada paradigma.

Para el paradigma de IM, se aplicó inicialmente un algoritmo presentado en [53], con el fin de mitigar la presencia de artefactos oculares. Este algoritmo consiste en un esquema de cancelación de ruido adaptativo utilizando un filtrado para la eliminación simultánea de parpadeos, movimientos oculares, cambios de amplitud y sesgos de registro. Cada electrodo se trata como un subsistema separado, y así, el filtrado se ajusta a los artefactos presentes en cada uno.

Posteriormente, las señales de EEG de cada canal se estandarizaron siguiendo el proceso presentado en [70]. Para cada canal, se calculó el umbral máximo visual (UMV) como el promedio de los 6 valores más altos de la señal de cada electrodo. Este valor se actualizó de manera iterativa para cada época y se utilizó para estandarizar los datos según la siguiente fórmula:



Figura 3.2: Exoesqueleto REX y equipo de electroencefalografía brainAmp.

$$EV(t)_{ch} = \frac{V(t)_{ch}}{\frac{1}{Ch} \sum_{j=1}^{Ch} UMV_j}, \quad (3.1)$$

donde la señal de cada canal, $V(t)_{ch}$, se normalizó teniendo en cuenta el UMV de todos los canales.

A continuación, se utilizó el filtro de Laplaciano de superficie para reducir el ruido espacial y mejorar la actividad local de cada electrodo. Luego, se aplicó un filtro Notch a 60 Hz para eliminar la contribución de la red eléctrica. A continuación, se aplicó la transformada de Stockwell a la señal de sólo 8 electrodos: Fz, FC1, FCz, FC2, C1, Cz, C2, CP1, CPz y CP2.

La transformada de Stockwell realiza una descomposición tiempo-frecuencia. Es una modificación de la transformada de Wavelet continua (CWT, por sus siglas en inglés, Continuous Wavelet Transform) [125, 126] basada en una función Gaussiana corregida mediante un factor de fase. De esta forma, la ventana es ancha para bajas frecuencias

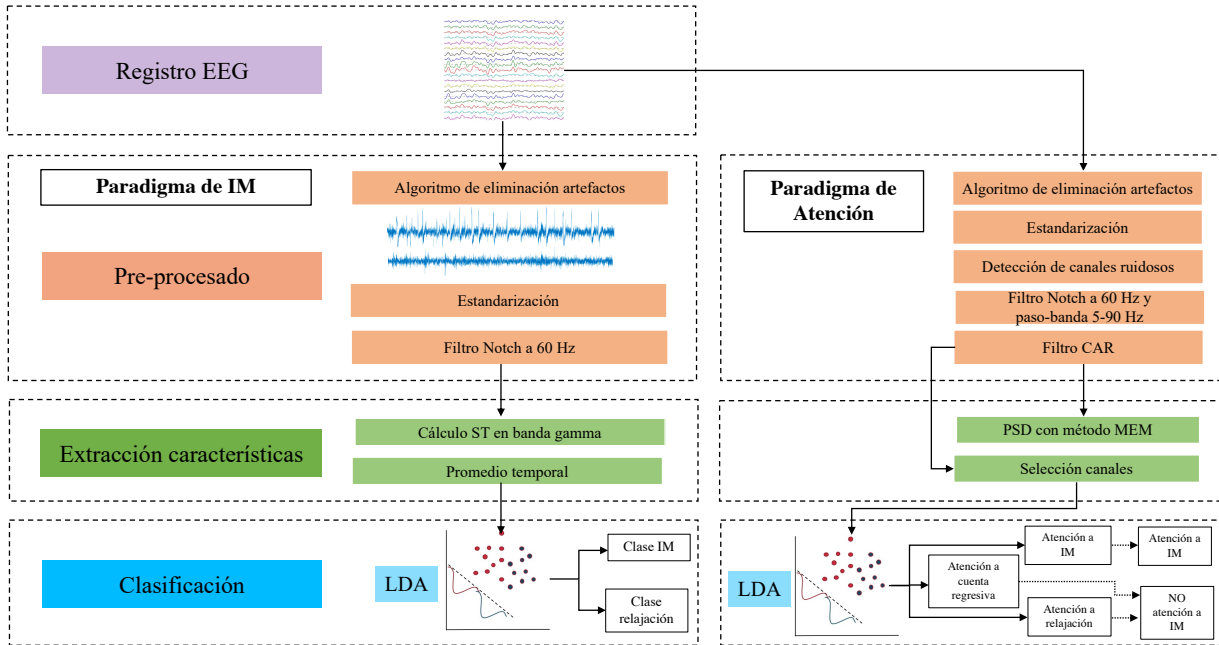


Figura 3.3: Metodología de procesado seguida en la contribución P1. Esta contribución utiliza dos paradigmas de control, por lo tanto, se procesan las señales cerebrales de dos formas distintas. Uno de los paradigmas consiste en discernir cuando los usuarios están realizando IM y cuando están relajados. El otro paradigma trata de diferenciar cuando los sujetos están prestando atención a tareas distintas.

y estrecha para altas frecuencias. La transformada permite definir señales ortogonales a distintos valores de frecuencia denominadas voces. Este carácter ortogonal le permite definir el contenido frecuencial en el tiempo y definir la amplitud y frecuencia instantáneas de la señal.

Finalmente, se computó el espectro marginal en el rango de frecuencia de 30-55 Hz promediándolo para cada época y electrodo considerado. El siguiente paso consistió en la clasificación de estas características mediante el análisis discriminante lineal (LDA, por sus siglas en inglés, Linear Discriminant Analysis) [127] para clasificar los datos en dos clases, IM de la marcha y relajación.

En cuanto al paradigma de atención, se aplicó el mismo algoritmo mencionado anteriormente para mitigar la presencia de artefactos oculares en las señales de EEG. A continuación, se estandarizaron las señales de EEG de cada canal siguiendo también el mismo proceso que para el paradigma de IM. El siguiente paso fue detectar la presencia de cualquier ruido residual en la señal. Se consideró que una época era ruidosa si el UMV superaba los $150 \mu\text{V}$, su curtosis instantánea era superior a $15 \mu\text{V}$ y su potencia espec-

tral obtenida mediante el método de máxima entropía, MEM (por sus siglas en inglés, Maximum Entropy Method), no superaba los $14\mu V^2$. Los siguientes pasos fueron un filtro Notch a 60 Hz y un filtro paso banda Butterworth de cuarto orden (5-90 Hz) a la época, seguido de un filtro de CAR. Después de eso, se calculó la densidad espectral de potencia mediante el método MEM en las bandas 30- 55 Hz y 65- 90 Hz [128].

En el método MEM, la señal de cada electrodo se estima como un modelo autorregresivo en el cual se calculan los coeficientes de autocorrelación conocidos y se estiman los coeficientes desconocidos maximizando la entropía espectral. Posteriormente, los coeficientes de autocorrelación se utilizan para calcular el espectro de potencia que es compatible con el fragmento de la señal analizada y generalista ante datos no vistos.

Finalmente se utilizó LDA para clasificar en tres niveles de atención: atención a la IM de la marcha, atención a la relajación y atención a la cuenta regresiva. Estos niveles se convirtieron en dos, atención a la IM de la marcha y NO atención a la IM de la marcha.

3.3. Resultados y discusión

Cada participante completó una o dos sesiones, las cuales se dividieron en entrenamiento (lazo-abierto) y test (lazo-cerrado). Durante el lazo-cerrado, se probaron dos mecanismos de control. Uno de ellos utilizó únicamente el paradigma de IM, mientras que el otro combinó el paradigma de IM con el paradigma de atención. Además, en las pruebas en lazo-abierto se realizó una simulación de los comandos que se hubiesen enviado al exoesqueleto en el caso de un control real, lo que se conoce como pseudo-online.

Para evaluar la BMI se utilizaron las siguientes métricas. Se utilizan términos en inglés porque son los que se presentaron en las publicaciones.

- %MI y %Att: porcentaje de épocas de datos clasificados correctamente para cada paradigma.
- %Commands: porcentaje de épocas de datos con comandos de control correctos.
- Accuracy (Acc): porcentaje de comandos correctos emitidos.
- True Positive Ratio (TPR): porcentaje de períodos de IM en los que se ejecuta un evento de caminata. Solo hay un evento de IM por prueba, por lo que este valor solo puede ser 0 o 100 %.
- False Positives (FP) y False Positives per minute (FP/min): número de comandos de movimiento emitidos durante períodos de relajación.
- %EXO: porcentaje de épocas con retroalimentación correcta del exoesqueleto.

3.3.1. Lazo-abierto

En la fase de entrenamiento (lazo-abierto), se realizaron tres tareas mentales, como se muestra en la Figura 3.4A. Los participantes llevaron a cabo un total de 10 registros en los que el movimiento del exoesqueleto no dependía de la tarea mental realizada, sino que se controlaba mediante comandos preestablecidos. Durante la IM y la cuenta regresiva, se enviaba un comando de inicio para activar el movimiento del exoesqueleto, mientras que durante el estado de relajación se enviaba un comando de detención para detener el movimiento.

En la Tabla 3.1 se presentan los resultados obtenidos para cada tipo de control en el caso de utilizar las señales EEG para enviar comandos al exoesqueleto, es decir, en pseudo-online.

Tabla 3.1: Resultados de los registros en lazo-abierto y en pseudo-online. Tabla modificada de [1] con licencia Creative Commons Attribution 4.0 International (CC 4.0).

Control	TPR	Acc	FP	FP/min	%MI	%Att	%Command
MI+Att	75±42.9	70.9±34.8	0.3±0.65	0.49±1.13	71.2±13.3	71.1±7	70±10.3
MI	90±30.4	69.5±26.8	0.85±1	1.5±1.77	71.2±13.3		69.1±13.2

3.3.2. Lazo-cerrado

Los registros utilizados para evaluar la BMI en lazo-cerrado fueron similares a los de entrenamiento, pero sin el evento de cuenta regresiva, como se muestra en la Figura 3.4B. Durante estos registros, el exoesqueleto funcionó en un control en lazo-cerrado. Por lo tanto, el comando para iniciar o detener el exoesqueleto se emitió solo cuando la BMI generó un comando de decisión. La Tabla 3.2 muestra los resultados obtenidos en el control en lazo-cerrado.

Tabla 3.2: Resultados de los registros en lazo-cerrado. Tabla modificada de [1] con licencia Creative Commons Attribution 4.0 International (CC 4.0).

Subject	Control	TPR	Acc	FP	FP/min	%MI	%Att	%Command	%EXO
S2	MI	100	95	0	0	74.4	64.4	67.6	56.3
	MI+Att	40	66.7	0.4	0.71	57.6	60	55.1	47.8
S3	MI	20	37.5	0.8	1.04	48.3	48.1	48.1	44.4
	MI+Att	0	0	0.2	0.26	51.7	53.9	56.6	57.5
S4	MI	80	55.8	1.4	1.83	54.9	60	54.9	51.2
	MI+Att	50	66.7	0.4	0.52	56.2	58	58.6	52.9

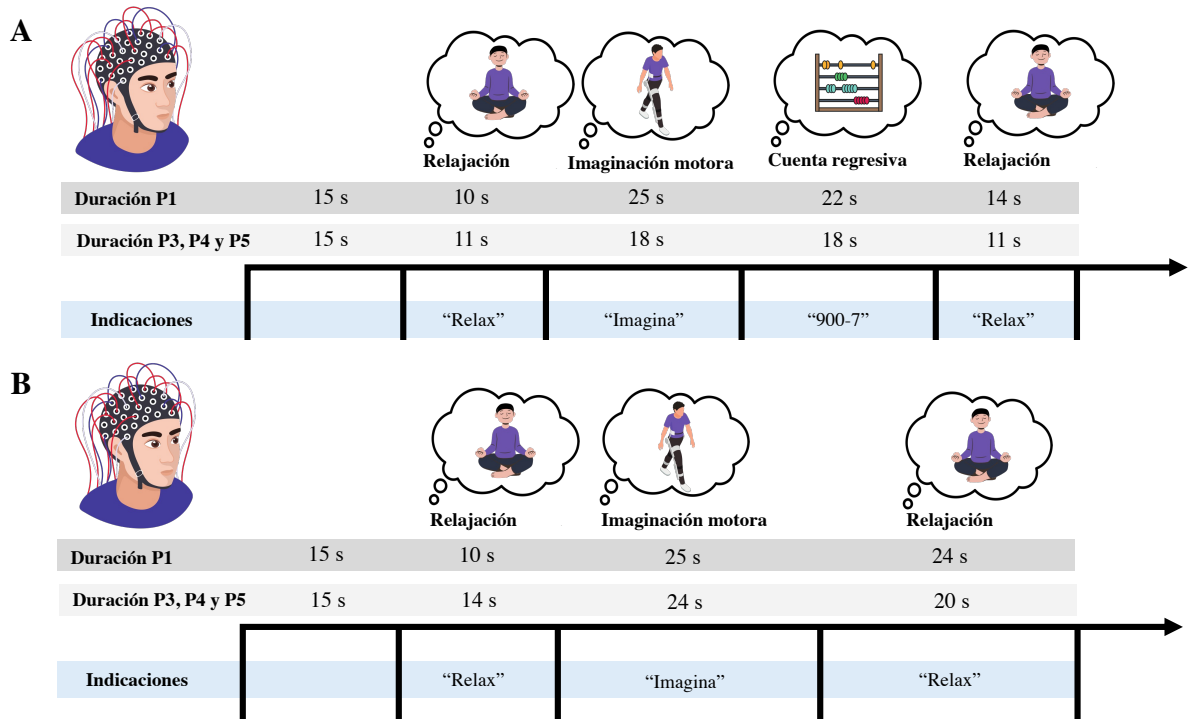


Figura 3.4: Secuencia de tareas seguida en los registros de lazo-abierto (A) y en los registros de lazo-cerrado (B). Los sujetos recibían indicaciones auditivas para cambiar de tarea mental. La duración de las tareas fue diferente en la contribución P1 con respecto a las contribuciones P3, P4 y P5. Los registros comenzaron con un período de 15 segundos en el que no se requería que los participantes realizaran ninguna tarea mental. Después de esto, debían permanecer relajados. A continuación, durante el periodo período de IM, los participantes debían concentrarse en imaginar el movimiento de sus piernas como si estuvieran caminando. Luego, durante la tarea de la cuenta regresiva debían realizar mentalmente una serie de sustracciones (por ejemplo, 900-7, 893, 886, 879, etc.), y finalmente otra vez en estado de relajación.

Los resultados obtenidos en el control en lazo-cerrado fueron inferiores en comparación con los obtenidos en el lazo-abierto y pseudo-online. Esta diferencia podría deberse al estado de los sujetos. Durante los experimentos de control real, entran en juego diversos factores que pueden afectar el rendimiento y que estuvieron ausentes durante la fase de lazo-abierto. En primer lugar, el estado mental de los sujetos difiere a medida que anticipan la recepción de retroalimentación, lo que genera un estado de expectativa. Además, su estado emocional puede verse influenciado por los resultados obtenidos, lo que puede generar sentimientos de emoción o frustración. Sin embargo, durante la fase de calibración, los sujetos desconocían el desempeño de su tarea [129, 18].

Por otro lado, la combinación de la interfaz cerebro-máquina y la atención mostró una eficacia menor, pero se observó una considerable reducción en el número de falsos positivos.

Capítulo 4

Improving motor imagery of gait on a brain-computer interface by means of virtual reality: a case of study (P2)

El propósito principal de esta contribución era investigar si la mejora de la IM de la marcha era posible al proporcionar retroalimentación visual a través de un entorno de RV, en contraste con la retroalimentación visual tradicional de pantalla. Además, se presentó un detallado estudio de caso que examinó el control en lazo-cerrado de la BMI en un entorno de RV.

Título: Improving Motor Imagery of Gait on a Brain–Computer Interface by Means of Virtual Reality: A Case of Study.

Autores: L. Ferrero, M. Ortiz, V. Quiles, E. Iáñez y J.M. Azorín.

Revista: IEEE Access. Vol 9 (2021).

ISSN: 2169-3536. Ed. IEEE.

JCR-SCI Factor de impacto (2020): 3.476, Cuartil: Q2.

Fecha de publicación: 26 marzo 2021.

DOI: <https://doi.org/10.1109/ACCESS.2021.3068929>

4.1. Materiales

4.1.1. Sujetos

En esta contribución, cinco sujetos sanos participaron en la investigación. La edad media de los sujetos fue de 29.8 ± 6.46 años. Todos los participantes firmaron el consentimiento informado de acuerdo con los principios éticos establecidos en la Declaración de Helsinki. Además, todos los procedimientos llevados a cabo en este estudio fueron aprobados por la Oficina de Investigación Responsable de la Universidad Miguel Hernández de Elche, España, bajo el número de protocolo DIS.JAP.03.18, con fecha de aprobación el 22/01/2019.

4.1.2. Equipo

En esta contribución se registró la actividad cerebral con un sistema de 32 electrodos. Los electrodos se colocaron en una unidad actiCAP (Brain Products GmbH, Alemania) y con la distribución presentada en la Figura 4.1. Los electrodos de tierra y referencia se ubicaron en los lóbulos derecho e izquierdo de la oreja, respectivamente. La señal de cada canal se amplificó con el amplificador actiCHamp (Brain Products GmbH, Alemania) y se transmitió de forma inalámbrica al software de grabación PyCorder con el transmisor Move (Brain Products GmbH, Alemania). El registro se realizó a 500 Hz.

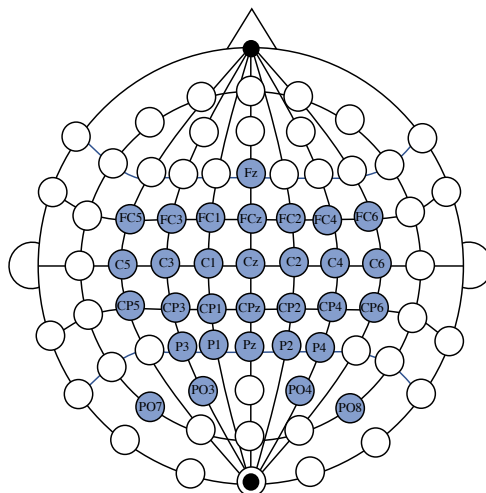


Figura 4.1: Distribución de electrodos escogida en las contribución P2 con 31 electrodos para el registro de la señal cerebral. Se buscaba cubrir la corteza motora primaria, el AMS, la PM, el lóbulo parietal superior y el lóbulo occipital.

También se incluyó un entorno de realidad virtual. El equipo incluía un casco HTC VIVE (HTC, Taiwán) con una resolución de 2160 x 1200 (1080 x 1200 por ojo) y una frecuencia de actualización de 90 Hz, dos estaciones base para rastrear la ubicación del casco, el software Steam (Valve, Estados Unidos) y un entorno desarrollado por nosotros creado con el motor Unity (Unity Technologies, Estados Unidos). La Figura 4.2 muestra el montaje para el entorno de realidad virtual y el equipo de EEG.

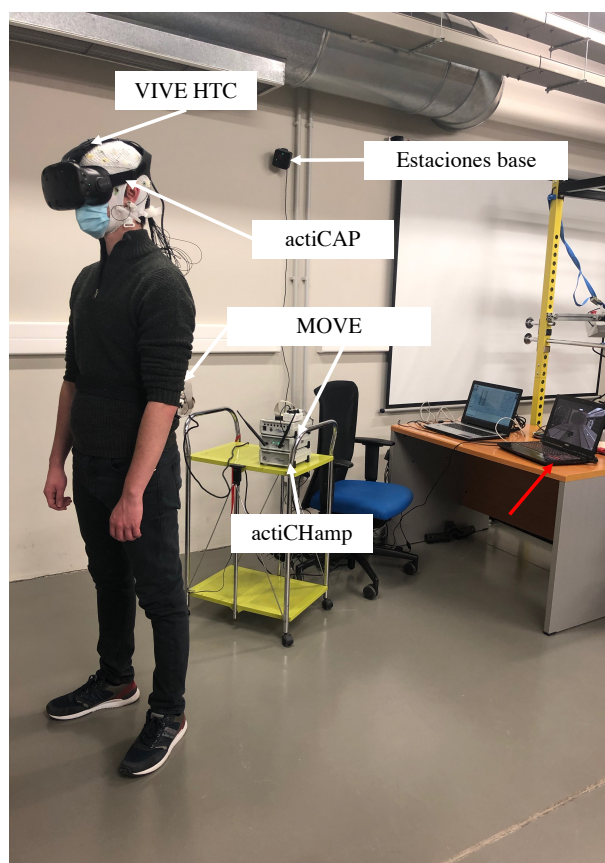


Figura 4.2: Equipo de realidad virtual y equipo de electroencefalografía actiCHamp. Imagen adaptada de [2] con licencia Creative Commons Attribution 4.0 International (CC 4.0).

4.2. Métodos

En esta contribución las ventanas de análisis fueron también de 1 s. El primer paso de pre-procesamiento consistió en aplicar un filtro Notch a 50 Hz para eliminar la contribución

de la red eléctrica. A continuación, se aplicó un filtro pasa alto a 0.1 Hz para eliminar la componente continua de la señal. Considerando el proceso mental de IM, se aplicaron cuatro filtros paso banda para obtener las ondas alfa y beta: 5-10 Hz, 10-15 Hz, 15-20 Hz, 20-25 Hz. Para la extracción de características, se utilizó el algoritmo CSP para obtener características espaciales asociadas a cada banda de frecuencia.

El algoritmo CSP estima una transformación espacial que maximiza la discriminabilidad entre dos patrones cerebrales. Si X es la señal de EEG con dimensiones $N * T$, donde N es el número de canales y T es el número de muestras, el algoritmo CSP estima una matriz de filtros espaciales W que discrimina entre dos clases: X_1 y X_2 . En primer lugar, se calculan las matrices de covarianza normalizadas para cada clase de la siguiente manera:

$$C_1 = \frac{X_1 X_1^T}{\text{trace}(X_1 X_1^T)}, C_2 = \frac{X_2 X_2^T}{\text{trace}(X_2 X_2^T)}. \quad (4.1)$$

Estas matrices se calculan para cada registro y se calcula \overline{C}_1 y \overline{C}_2 promediando todos los registros de la misma clase. Las matrices de covarianza promediadas se combinan para obtener la matriz de covarianza espacial compuesta que puede ser factorizada como:

$$C = \overline{C}_1 + \overline{C}_2 = U_0 \Sigma U_0^T. \quad (4.2)$$

U_0 es una matriz de autovectores y Σ es la matriz diagonal de autovalores. Las matrices de covarianza promediadas se transforman de la siguiente manera:

$$P = \Sigma^{1/2} U_0^T, \quad (4.3)$$

$$S_1 = P \overline{C}_1 P^T, S_2 = P \overline{C}_2 P^T. \quad (4.4)$$

S_1 y S_2 tienen autovectores comunes, y la suma de ambas matrices de autovalores es la matriz identidad.

$$S_1 = U \Sigma_1 U^T, S_2 = U \Sigma_2 U^T \text{ and } \Sigma_1 + \Sigma_2 = I. \quad (4.5)$$

La matriz de proyección se obtiene como

$$W = U^T P. \quad (4.6)$$

Z es la proyección de la señal EEG original X en otro espacio. Las columnas de W^{-1} representan los patrones espaciales.

$$Z = W X. \quad (4.7)$$

Aunque Z tiene $N * T$ dimensiones, las primeras y últimas filas son los componentes que pueden ser mejor discriminados en términos de su varianza. Por lo tanto, para la

extracción de características, solo se consideran los m primeros y últimos componentes de Z . Z_p es el subconjunto de Z y se calculan las varianzas de cada componente y se normalizan mediante el logaritmo como:

$$f_p = \log \frac{\text{var}(Z_p)}{\sum_{i=1}^{2m} Z_p}. \quad (4.8)$$

f_p es el vector de características y tiene una dimensión de $(fbands \cdot 2m)T$. Se estableció m en 4 y en la fase de preprocesamiento se emplearon 4 filtros pasa banda, por lo que la dimensión es de $32T$.

Finalmente, se procedió a la clasificación de estas características utilizando el análisis LDA para distinguir entre el estado de IM de la marcha y estado de relajación.

La Figura 4.3 muestra el esquema de esta metodología. A diferencia de la contribución anterior, en este trabajo se prescindió del paradigma de atención.

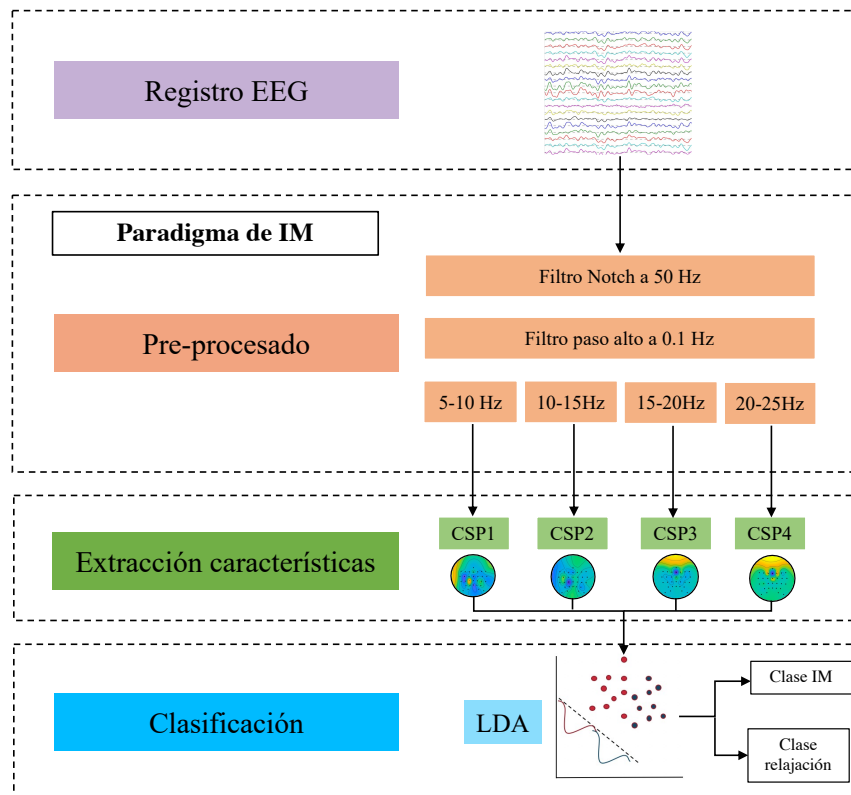


Figura 4.3: Metodología de procesado seguida en la contribución P2.

4.3. Resultados y discusión

Se llevaron a cabo dos experimentos diferentes. El objetivo del primer experimento fue investigar si era posible diferenciar entre los períodos en los que los sujetos realizaban IM de la marcha y los periodos en los que estaban relajados mientras recibían retroalimentación visual. Para ello, se compararon diferentes enfoques para la retroalimentación visual; por un lado, mediante una pantalla o un entorno de realidad virtual y por otro, estando sentados o de pie. En el segundo experimento, se utilizó el enfoque que mostró el rendimiento más alto que fue en el que los sujetos estaban de pie y utilizaban la realidad virtual. Por ello, fue el que se usó para la sesión experimental del segundo experimento. La primera parte de la sesión consistió en el lazo-abierto y la segunda parte consistió en el lazo-cerrado.

Se utilizaron las mismas métricas presentadas en P1 (3.3). Sin embargo, en este trabajo %MI se refiere únicamente a la tarea de imaginación motora y no al paradigma de IM; %Relax se refiere únicamente a los periodos de relajación y %Total se correspondería con la métrica %MI de la contribución anterior

4.3.1. Lazo-abierto

En la primera parte de la sesión, cada sujeto realizó 10 registros de entrenamiento. En cada uno, se les pidió a los usuarios que realizaran la secuencia de tareas mentales que se muestra en la Figura 4.4. Además, en el entorno de realidad virtual, había un avatar que caminaba por un pasillo y se programó para iniciar y finalizar la marcha en función de comandos preestablecidos, según si los sujetos estaban realizando IM o se encontraban en un estado de reposo respectivamente.

Estos registros se evaluaron mediante validación cruzada. Cada registro se utilizó una vez como test y los registros restantes conformaron el grupo de entrenamiento. Luego, las métricas se promediaron para todas las iteraciones. Los resultados se calcularon en función del número de épocas clasificadas correctamente para cada tarea mental. Estos resultados se muestran en la Tabla 4.1.

4.3.2. Lazo-cerrado

A continuación, cada sujeto realizó cinco registros de lazo-cerrado. En esta parte del experimento, el movimiento del avatar dependía de la salida de la BMI y, por lo tanto, de la actividad mental del usuario.

La Tabla 4.2 resume el rendimiento del lazo-cerrado. A partir de los resultados, se puede señalar que %Commands siempre es mayor que la Accuracy. Por otro lado, TPR es del 100% en todos los registros, lo que significa que hay una activación en todos los

Tabla 4.1: Resultados de los registros en lazo-abierto. Tabla de [2] con licencia Creative Commons Attribution 4.0 International (CC 4.0).

Subject	N	% Total	%MI	%Relax
S21	1	77.08	100.00	54.17
	2	76.04	89.58	62.50
	3	78.13	83.33	72.92
	4	79.17	93.75	64.58
	5	82.29	91.67	72.92
	6	95.83	97.92	93.75
	7	83.33	75.00	91.67
	8	83.33	87.50	79.17
	9	79.17	75.00	83.33
	10	88.54	87.50	89.58
	avg.	82.3±6.0	88.1±13.4	76.5±13.4
S22	1	82.29	97.92	66.67
	2	91.67	97.92	85.42
	3	82.29	70.83	93.75
	4	94.79	91.67	97.92
	5	79.17	68.75	89.58
	6	87.50	83.33	91.67
	7	88.54	85.42	91.67
	8	86.46	85.42	87.50
	9	73.96	62.50	85.42
	10	79.17	79.17	79.17
	avg.	84.6±6.4	82.3±8.8	86.9±8.8

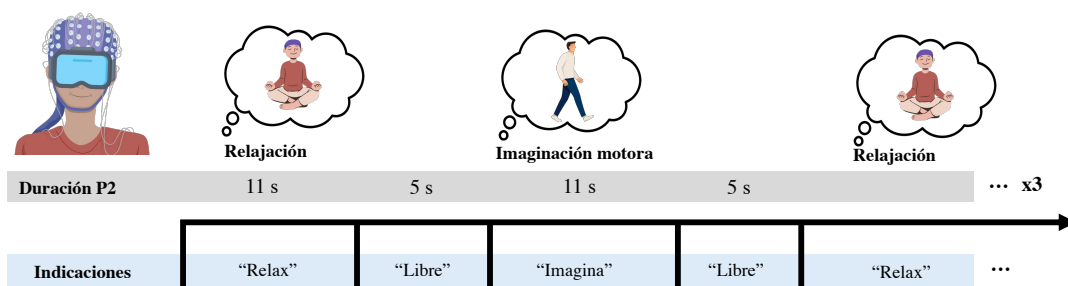


Figura 4.4: Secuencia de tareas seguida en los registros de la contribución P2. Los sujetos recibían indicaciones auditivas para cambiar de tarea mental. Durante los periodos de relajación debían tratar de no pensar en nada y relajarse. Durante los periodos de IM, debían concentrarse en imaginar el movimiento de sus piernas como si estuvieran caminando. Y durante los periodos de libre, podían hacer lo que quisiesen.

eventos de IM. En cuanto a FP/min, S22 tuvo una tasa de falsos positivos más baja que S12. Se obtuvo un patrón similar de resultados en los registros de lazo-abierto, donde S22 tuvo una mayor precisión en los eventos de relajación.

En consonancia con la contribución P1(3.3), se observaron diferencias significativas en el rendimiento entre los registros en lazo-abierto y los registros en lazo-cerrado. Sin embargo, se encontró que estas diferencias son menores cuando se utiliza el entorno de RV y no un exoesqueleto como en P1 3.3.

Tabla 4.2: Resultados de los registros en lazo-cerrado. Tabla de [2] con licencia Creative Commons Attribution 4.0 International (CC 4.0).

Subject	N	Accuracy	%Commands	TPR	FP	FP/min
S21	1	71.9	88.5	100.0	2.0	5.0
	2	70.8	97.9	100.0	3.0	7.5
	3	69.8	95.8	100.0	2.0	5.0
	4	60.4	82.3	100.0	2.0	5.0
	5	85.4	92.7	100.0	1.0	2.5
	avg.	71.7±8.9	91.5±6.2	100.0±0.0	2.0±0.7	5.0±1.8
S22	1	78.1	93.8	100.0	0.0	0.0
	2	63.5	100.0	100.0	3.0	7.5
	3	79.2	86.5	100.0	0.0	0.0
	4	87.5	90.6	100.0	0.0	0.0
	5	78.1	81.3	100.0	1.0	2.5
	avg.	77.3±8.6	90.4±7.1	100.0±0.0	0.8±1.3	2.0±3.3

Capítulo 5

A BMI Based on motor imagery and attention for commanding a lower-limb robotic exoskeleton: a case study (P3)

El objetivo central de esta contribución fue diseñar y evaluar una BMI basada en la IM para el control de la marcha de un exoesqueleto de miembro inferior. El sistema de control propuesto operaba como una máquina de estados, utilizando algoritmos de decodificación distintos para iniciar y detener la marcha. Además, la BMI combinaba dos paradigmas para reducir las falsas activaciones, uno basado en la IM y otro en la atención del usuario a la marcha.

Título: A BMI Based on Motor Imagery and Attention for Commanding a Lower-Limb Robotic Exoskeleton. A Case Study.

Autores: L. Ferrero, V. Quiles, M. Ortiz, E. Iáñez y J.M. Azorín.

Revista: Applied Sciences. Vol 11 (9).

ISSN: 2076-3417. Ed. MDPI.

JCR-SCI Factor de impacto (2020): 2.838, Cuartil: Q2.

Fecha de publicación: 30 abril 2021.

DOI: <https://doi.org/10.3390/app11094106>

5.1. Materiales

5.1.1. Sujetos

Dos sujetos sanos participaron en este estudio, un hombre y una mujer con edad media de 23.5 ± 3.5 . Es importante destacar que ninguno de los participantes tenía experiencia previa en el uso de una BMI ni en el uso de un exoesqueleto de miembro inferior.

Ambos participantes proporcionaron su consentimiento informado, en cumplimiento de los principios éticos establecidos en la Declaración de Helsinki. Además, todos los procedimientos llevados a cabo en este estudio fueron aprobados por la Oficina de Investigación Responsable de la Universidad Miguel Hernández de Elche, España, bajo el número de protocolo DIS.JAP.03.18, con fecha de aprobación el 22/01/2019.

5.1.2. Equipo

En esta contribución se utilizó el mismo equipo de electroencefalografía que en la contribución P2 (4.1.2), pero la adquisición se realizó a una frecuencia de muestreo de 200 Hz y con la distribución de electrodos que se muestra en la Figura 5.1.

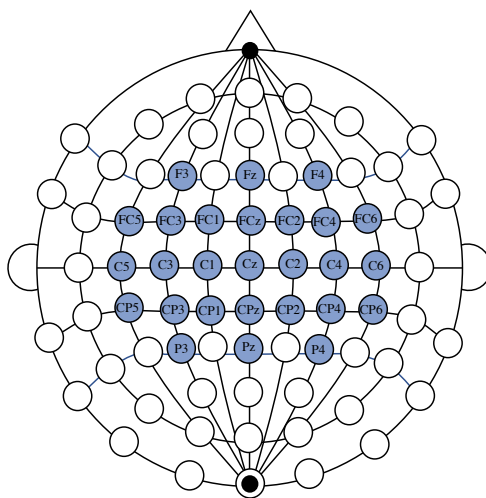


Figura 5.1: Distribución de electrodos escogida en las contribuciones P3,P4 y P5 con 27 electrodos para el registro de la señal cerebral. Se buscaba cubrir la corteza motora primaria, el AMS, la PM y el lóbulo parietal superior

Todos los participantes usaron el exoesqueleto H3 (Tecnhaid, España). Es un exoesqueleto activo de cadera-rodilla-tobillo que emula la marcha humana. A los participantes se les proporcionaron muletas o un carrito para garantizar su estabilidad. Los comandos de

control de alto nivel se transmitían mediante Bluetooth para iniciar y detener la marcha a una velocidad constante. Este dispositivo también proporcionaba información en tiempo real sobre su estado. La Figura 5.2 muestra todo el equipo utilizado en esta contribución.

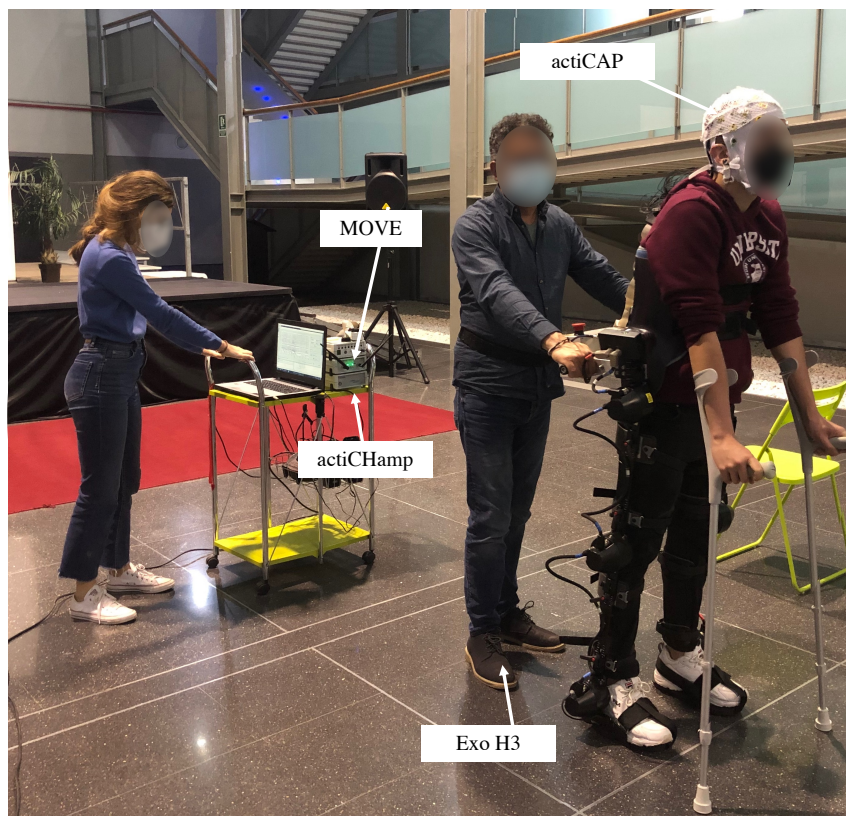


Figura 5.2: Exoesqueleto H3 y equipo de electroencefalografía actiCHamp. Imagen adaptada de [3] con licencia Creative Commons Attribution 4.0 International (CC 4.0).

5.2. Métodos

En esta contribución, al igual que en la contribución P1 (3.2), se utilizaron dos paradigmas: la detección de IM y la medición del nivel de atención. La Figura 5.3 muestra el esquema de esta metodología. Los primeros pasos de pre-procesamiento fueron idénticos para ambos paradigmas, pero luego se siguieron dos enfoques de pre-procesamiento distintos. Las ventanas de análisis fueron de 1 s. La etapa de pre-procesamiento comenzó con dos filtros de frecuencia, un filtro Notch a 50 Hz para eliminar la contribución de la línea

eléctrica y un filtro paso alto a 0.1 Hz. A continuación, se aplicó el algoritmo [53] como en P1 (3.2) para mitigar la presencia de artefactos oculares y desviaciones de la señal.

Para el paradigma de IM, se siguió el mismo proceso que en la la contribución P2(4.2). Primero, se aplicó un banco de filtros paso banda: 5-10 Hz, 10-15 Hz, 15-20 Hz, 20-25 Hz. Luego, se obtuvieron características CSP para cada banda de frecuencia y se utilizó el LDA como clasificador para discriminar entre la IM y el estado de relajación.

En cuanto al paradigma de atención, las señales de EEG de cada canal se estandarizaron siguiendo el proceso presentado en P1(3.2). Posteriormente, se utilizó el filtro Laplaciano para reducir el ruido espacial. Finalmente, como se hizo en la contribución P1, se calculó el espectro de frecuencia utilizando el método MEM en la banda de 30-45 Hz. La principal diferencia con la contribución P1 es la frecuencia de la red eléctrica. Las pruebas experimentales de P1 se realizaron en Estados Unidos, por lo que la señal se analizó en el rango de 30 a 55 Hz, mientras que las pruebas de P3 se llevaron a cabo en España, por lo que se estudió la banda gamma de 30 a 45 Hz. Como último paso, se utilizó el análisis LDA para realizar una clasificación binaria: alto nivel de atención a la marcha o bajo nivel de atención. Hubo un cambio en comparación con P1, ya que se pasó de predecir tres niveles de atención a dos, con el objetivo de lograr mayores porcentajes de acierto.

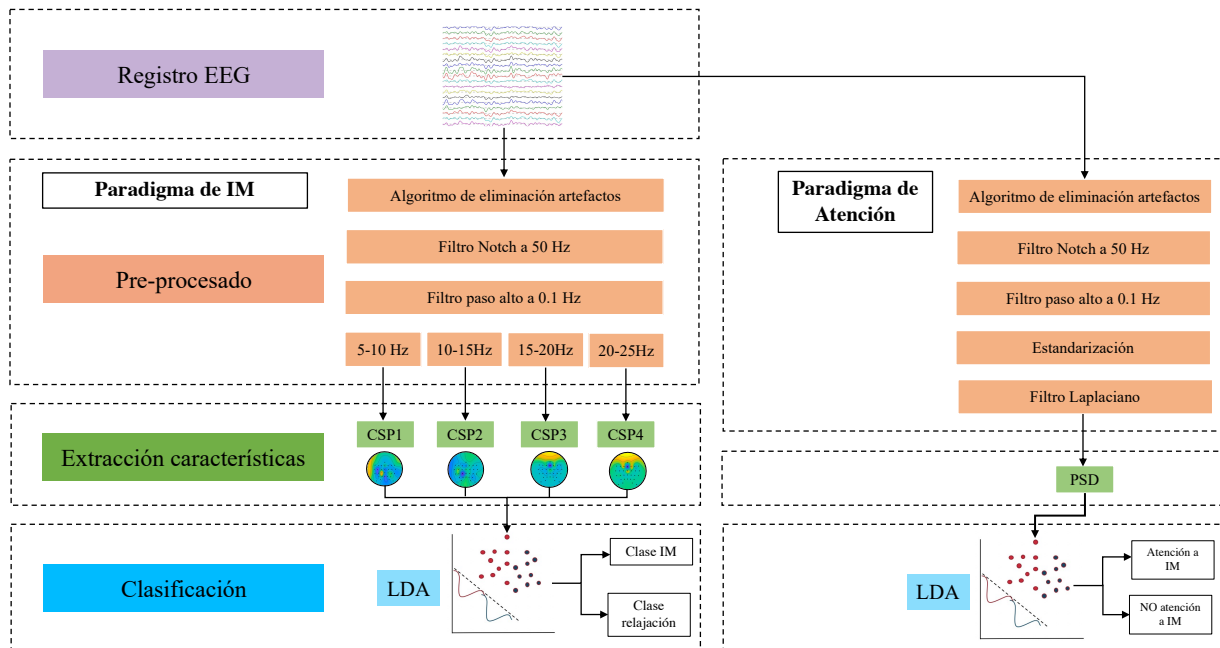


Figura 5.3: Metodología de procesamiento seguida en la contribución P3.

Tabla 5.1: Resultados de los registros en lazo-abierto de un sujeto. Stand son los resultados de los registros en estático y Gait son los resultados de los registros en movimiento. Tabla de [3] con licencia Creative Commons Attribution 4.0 International (CC 4.0).

		Session 1	Session 2
Stand	%MI	59.29±10.51	69.64±7.62
	% Att	57.38±9.27	60.83±7.58
Gait	%MI	58.93±11.60	75.89±5.41
	% Att	65.83±8.57	69.29±5.04

5.3. Resultados y discusión

Esta contribución se basó en la combinación del paradigma de IM y el paradigma de atención como la contribución P1. Cada participante completó varias sesiones, y cada sesión se dividió en entrenamiento (lazo-abierto) y test (lazo-cerrado).

Se utilizaron las mismas métricas presentadas en P1 (3.3).

5.3.1. Lazo-abierto

En el entrenamiento en lazo-abierto, se empleó un enfoque diferente al utilizado en las dos contribuciones anteriores. Los participantes realizaron 20 registros siguiendo las tareas mentales indicadas en la Figura 3.4A, pero el movimiento del exoesqueleto no se correspondía con la tarea mental que estaban realizando. Es decir, el exoesqueleto no se movía únicamente durante los periodos de IM o cuenta regresiva. De los 20 registros, 10 se realizaron en una condición de completa inmovilidad y los otros 10 en una condición de movimiento asistido por el exoesqueleto. El exoesqueleto estaba programado para iniciar y finalizar la marcha en función de comandos preestablecidos, dependiendo de si el registro iba a ser en estado estático o en movimiento. Cabe destacar que la secuencia de tareas fue idéntica para todos los registros, con el fin de facilitar la creación de una interfaz cerebro-máquina de doble estado (ilustrada en la Figura 5.4), la cual se utilizó posteriormente en la fase de control en lazo-cerrado.

Se realizó una validación cruzada para evaluar los registros. Este proceso se realizó de forma independiente para los registros en los que los sujetos estaban estáticos de pie y los registros en los que estaban en movimiento. Para su uso posterior en lazo-cerrado, se entrenaron cuatro clasificadores, por un lado, dependiendo del estado del sujeto, de pie o en movimiento; y por otro, en función del paradigma de decodificación, IM o atención.

Los resultados de los sujetos S1 y S2 se muestran en las Tablas 5.1 y 5.2, respectivamente. Cabe destacar que no tuvieron la misma cantidad de práctica, ya que participaron en un número diferente de sesiones.

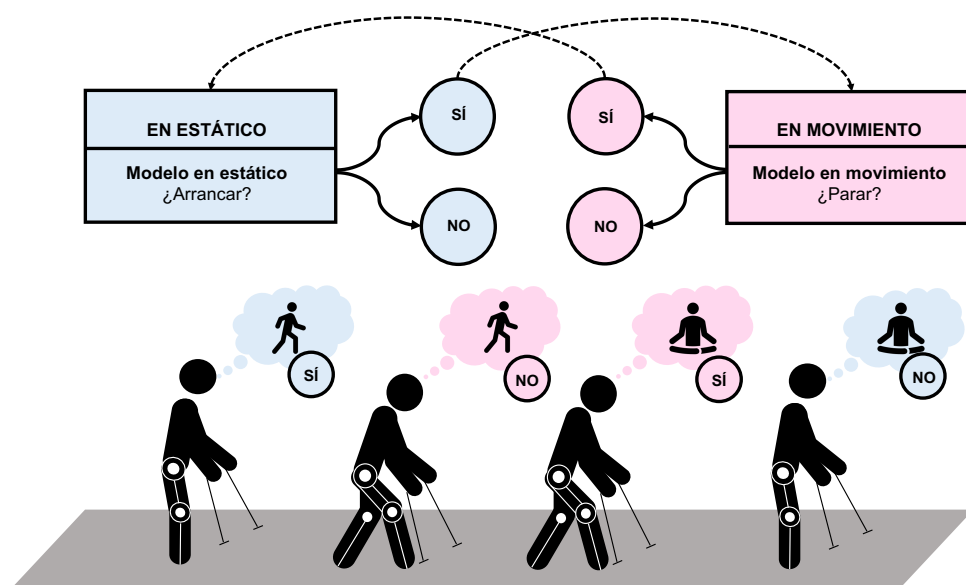


Figura 5.4: Interfaz cerebro-máquina de doble estado. En el lazo-cerrado, en la condición estática, cuando los sujetos permanecían de pie con el exoesqueleto, el modelo(s) estático era el encargado de tomar decisiones. Este modelo decidía si mantener el exoesqueleto en una posición estática o iniciar la marcha basándose en los patrones cerebrales detectados en el sujeto. Por otro lado, en la condición de movimiento, cuando los sujetos caminaban asistidos por el exoesqueleto, el modelo(s) en movimiento supervisaba el control. Este modelo podía decidir si continuar con el movimiento o detenerlo.

La precisión promedio obtenida mediante el uso del paradigma de IM, $68.44 \pm 8.46\%$, fue superior a la del paradigma de atención, $65.45 \pm 5.53\%$. Al considerar los registros tanto en estado estático como en movimiento, se observó que los resultados obtenidos en estado estático fueron superiores. Esta diferencia en el rendimiento podría estar relacionada con la complejidad del movimiento realizado con el exoesqueleto, ya que requiere de coordinación motora del tren superior.

5.3.2. Lazo-cerrado

En la fase de control en lazo-cerrado, la iniciación y finalización de la marcha del exoesqueleto fueron controladas por las prácticas mentales del sujeto a través de la BMI de doble estado. Durante esta fase, los sujetos realizaron cinco registros como se describe en la Figura 3.4B. Como una máquina de doble estado, los dos modelos entrenados con registros en estático se utilizaron para mantener el exoesqueleto inmóvil y detectar el inicio de la marcha. Sin embargo, una vez que el exoesqueleto inició la marcha, el control

Tabla 5.2: Resultados de los registros en lazo-abierto de un sujeto. Stand son los resultados de los registros en estático y Gait son los resultados de los registros en movimiento. Tabla de [3] con licencia Creative Commons Attribution 4.0 International (CC 4.0).

		Session 1	Session 2	Session 3	Session 4	Session 5
Stand	%MI	53.32±8.59	69.64±8.70	65.54±5.12	64.2±11.45	74.11±6.14
	% Att	63.95±4.44	62.57±8.77	58.21±8.76	59.52±8.44	60.83±5.48
Gait	%MI	50.26±7.54	54.17±8.75	62.50±8.91	59.82±10.11	54.11±12.71
	% Att	61.05±5.13	63.36±2.84	61.55±7.21	65.71±6.82	70.83±3.04

pasó a los dos modelos entrenados con registros en movimiento, que se utilizaron para mantener el exoesqueleto en movimiento hasta que se detectara el deseo de detenerse. Esto provocaría un cambio del modelo nuevamente a los modelos estáticos. La Figura 5.4 muestra el funcionamiento de esta máquina de estados. Se recopilaron las clases utilizadas en cada modelo en las mismas condiciones de ruido causado por movimiento, asegurando así que las diferencias entre las clases se basaran exclusivamente en las tareas mentales realizadas.

La Tabla 5.3 resume los resultados. El TPR es del 100 % en la mayoría de los casos, lo que significa que el exoesqueleto se activó al menos una vez durante el evento de IM. En cuanto al %Commands, mejoró en un 13 % desde la primera hasta la última sesión de S2, aunque su rendimiento en cada sesión no siempre fue superior al anterior.

Tabla 5.3: Resultados de los registros en lazo-cerrado. Tabla modificada de [3] con licencia Creative Commons Attribution 4.0 International (CC 4.0).

		Session 1	Session 2	Session 3	Session 4	Session 5
S1	%MI	56.3±6.13	56.52±4.71			
	%Att	53.26±3.7	58.26±6.13			
	%Commands	69.2±9.41	61.2±4.49			
	Acc	40±20	68.33±9.72			
	TPR	80±40	100±0			
	FP	0.4±0.49	1±0			
	FP/min	0.92±1.13	2.31±0			
S2	%MI	44.78±3.02	52.61±5.47	51.52±6.81	56.09±6.99	59.56±1.95
	%Att	52.17±3.35	58.04±8.98	49.56±4.52	63.48±9.18	65±6.49
	%Commands	54.4±2.61	58.6±14.91	69.8±7.95	64.2±8.58	67.8±14.39
	Acc	0±0	53.33±50.55	57±13.04	45±44.72	68±31.76
	TPR	100±0	80±44.72	100±0	100±0	100±0
	FP	1±0	0.6±0.55	1.6±0.55	0.8±0.45	1±1
	FP/min	2.31±0	1.38±1.26	3.69±1.26	1.85±1.03	2.31±2.31

Capítulo 6

Brain symmetry analysis during the use of a BCI based on motor imagery for the control of a lower-limb exoskeleton (P4)

En esta contribución, se planteó evaluar la lateralidad de la función cortical durante la IM del miembro inferior utilizando una BMI. Se analizaron las señales cerebrales de cinco sujetos con tres configuraciones de electrodos de EEG diferentes: abarcando ambos hemisferios cerebrales, solo el izquierdo y solo el derecho. También se evaluó la evolución del rendimiento y la lateralidad de la actividad cerebral a lo largo de las sesiones experimentales.

Título: Brain Symmetry Analysis during the Use of a BCI Based on Motor Imagery for the Control of a Lower-Limb Exoskeleton.

Autores: L. Ferrero, M. Ortiz, V. Quiles, E. Iáñez, J.A. Flores y J.M. Azorín.

Revista: Symmetry. Vol 13 (9).

ISSN: 2073-8994. Ed. MDPI.

JCR-SCI Factor de impacto (2020): 2.94, Cuartil: Q2.

Fecha de publicación: 19 septiembre 2021.

DOI: <https://doi.org/10.3390/sym13091746>

6.1. Materiales

6.1.1. Sujetos

Cinco sujetos sanos participaron en este estudio, con edad media de 23.2 ± 1.3 . Cuatro de los participantes eran hombres y el quinto era mujer. Ninguno de los sujetos tenía experiencia en el uso de BMI ni el control de un exoesqueleto.

Se les informó sobre los experimentos y firmaron el consentimiento informado de acuerdo con la declaración de Helsinki y todos los procedimientos fueron aprobados por la Oficina de Investigación Responsable de la Universidad Miguel Hernández de Elche, España (DIS.JAP.03.18, 22/01/2019).

6.1.2. Equipo

Al igual que en la contribución P3, se empleó el mismo equipo de electroencefalografía descrito en la contribución P2 (4.2), con la diferencia de que en esta ocasión la adquisición se realizó a una frecuencia de muestreo de 200 Hz y con la distribución de electrodos que se muestra en la Figura 5.1.

Asimismo, se utilizó el mismo exoesqueleto presentado en la contribución P3 (4.2).

6.2. Métodos

La metodología seguida en esta contribución es idéntica a la línea de IM de la contribución P3(5.2), Figura 5.3, pero con ventanas de análisis de 1.5 s. Sin embargo, además de extraer características con el algoritmo CSP, se aplicó la transformada de Stockwell y se estimó la PSD mediante el método de Welch [130].

Antes de utilizar estos dos últimos métodos, se aplicó un filtro Laplaciano. La transformada de ST se utilizó para realizar una descomposición tiempo-frecuencia, considerando las frecuencias de ritmos alfa y beta alta (8-14 y 20-30 Hz), y se calculó una suma de la amplitud de todas ellas. El método de Welch se empleó para estimar la densidad espectral de potencia. Se dividió la señal en segmentos superpuestos y en cada segmento se aplicó la transformada de Fourier (FFT) por ventanas. Finalmente, la PSD se calculó promediando el cuadrado de la FFT de cada segmento. Siguiendo el mismo procedimiento que en la transformada de ST, se sumó la potencia de las frecuencias en las bandas alfa y beta. Únicamente se utilizó información de 18 electrodos: FC3, FC1, FCz, FC2, FC4, C3, C1, Cz, C2, C4, CP3, CP1, CPz, CP2, CP4, P3, Pz, P4. Estos electrodos cubrían el área PM y ASM.

Al igual que en los otros experimentos, se utilizó LDA para clasificar las características obtenidas por cada método en dos clases, IM y estado de relajación.

6.3. Resultados y discusión

Esta investigación se llevó a cabo con el mismo protocolo experimental utilizado en el lazo-abierto de la contribución P3 5.3. Para el entrenamiento, cada sujeto realizó 22 registros con la secuencia mostrada en la Figura 3.4A. En esta investigación, no se analizó la tarea mental de atención, por lo que solo se consideraron los datos de IM y los del estado de reposo.

El objetivo de este estudio era evaluar si existe una especialización hemisférica durante la IM de la marcha. Además, también se estudió la evolución del rendimiento con la práctica; las diferencias entre sujetos; y el uso de tres metodologías de procesamiento.

Se utilizaron las mismas métricas de lazo-abierto que P2 (4.3).

6.3.1. Influencia de la metodología

Como se indica en la sección anterior, se utilizaron varias metodologías para extraer los patrones cerebrales de la IM. La Tabla 6.1 muestra la precisión promedio obtenida con cada una de ellas: CSP, ST y el método de Welch. Dado que CSP mostró la mayor precisión global, esta fue la metodología elegida para el resto de la investigación.

Tabla 6.1: Resultados de tres metodologías diferentes en todas las sesiones. Full-static son los resultados de los registros en estático y Full-motion son los resultados de los registros en movimiento. Tabla de [4] con licencia Creative Commons Attribution 4.0 International (CC 4.0).

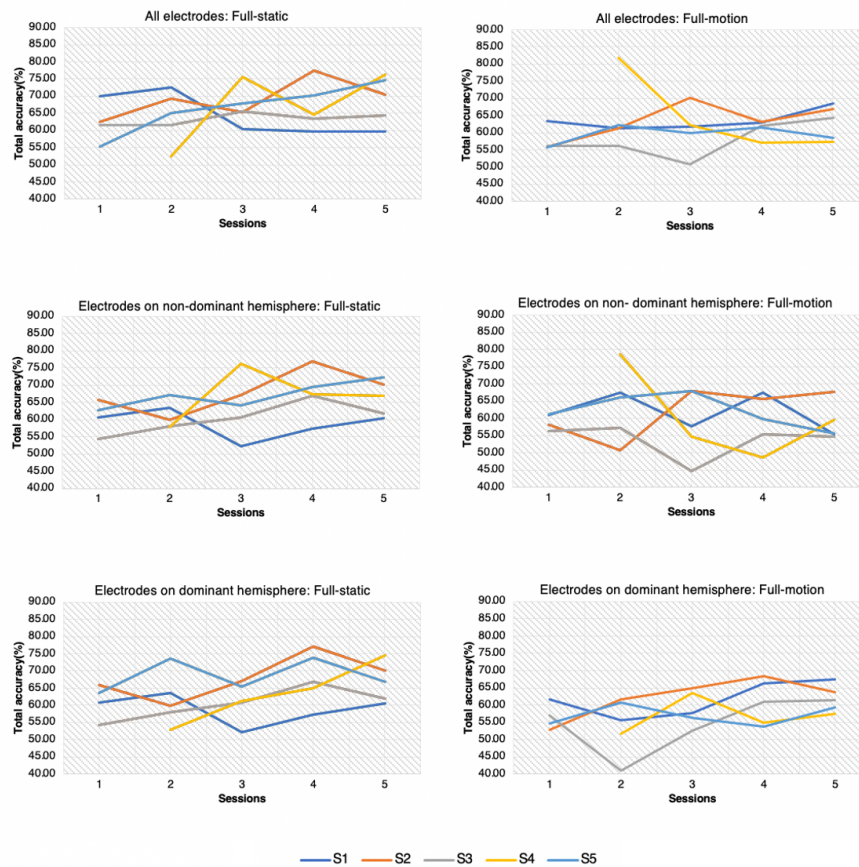
		FBCSP	ST	Welch's PSD
Full-static	%MI	64,7 ± 6,5	58,0 ± 6,4	62,6 ± 7,6
	% Relax	67,5 ± 8,9	62,5 ± 8,0	65,1 ± 6,1
	%Total	66,1 ± 6,6	60,2 ± 5,1	63,8 ± 4,6
Full-motion	%MI	61,0 ± 8,5	56,8 ± 8,6	60,0 ± 10,0
	% Relax	62,5 ± 8,0	55,5 ± 12,4	58,8 ± 11,0
	%Total	61,7 ± 6,2	56,1 ± 7,3	59,4 ± 8,3

6.3.2. Influencia del sujeto

Estudios previos han identificado diferencias entre sujetos en el uso de las interfaces cerebro-máquina [131], por lo que se evaluaron las diferencias entre sujetos en términos de precisión. Las diferencias se analizaron con una prueba de ANOVA para los registros en estático y otra para los registros en movimiento y solo se hallaron diferencias estadísticamente significativas entre sujetos en estático.

6.3.3. Evolución del entrenamiento y diferencias entre hemisferios cerebrales

Dado que hubo dependencia del sujeto, se analizó la lateralidad individualmente por sujeto. Para el análisis de lateralidad, se evaluó el rendimiento utilizando la información de todos los electrodos, solo los ubicados en el hemisferio dominante y solo los ubicados en el hemisferio no dominante. También se evaluó la evolución del rendimiento con las sesiones, como se puede observar en las diferentes imágenes de la Figura 6.1. Además, se determinó si la mejor configuración de electrodos cambió con el entrenamiento en términos de rendimiento.



1

Figura 6.1: Evolución del entrenamiento para las pruebas en estático y movimiento con diferentes configuraciones de electrodos: todos los electrodos, sólo los electrodos ubicados en el hemisferio no dominante y los electrodos en el hemisferio dominante.

Se lograron resultados ligeramente superiores con los electrodos que cubren ambos hemisferios. Sin embargo, no se encontraron diferencias estadísticamente significativas entre las tres configuraciones de electrodos. Por otro lado, la precisión evolucionó de manera positiva con más entrenamiento, pero el crecimiento no fue completamente lineal. De hecho, en algunos casos, la precisión disminuyó después de la cuarta sesión. Este patrón de evolución también se observó en la contribución P3(5.3)

Capítulo 7

Brain-computer interface enhanced by virtual reality training for controlling a lower limb exoskeleton (P5)

En esta contribución, el objetivo central consistió en analizar si la práctica de la IM en un entorno de RV mejoraba la eficacia de un sistema BMI basado en IM para el control de un exoesqueleto de miembro inferior. Este enfoque se diseñó con el propósito de facilitar la recuperación motora después de una lesión medular.

Título: Brain-computer interface enhanced by virtual reality training for controlling a lower limb exoskeleton.

Autores: L. Ferrero, V. Quiles, M. Ortiz, E. Iáñez, A. Gil-Agudo y J.M. Azorín.

Revista: iScience. Vol 26 (5).

ISSN: 2589-0042. Ed. Cell Press.

JCR-SCI Factor de impacto (2020): 5.8, Cuartil: Q1.

Fecha de publicación: 19 septiembre 2021.

DOI: <https://doi.org/10.1016/j.isci.2023.106675>

7.1. Materiales

7.1.1. Sujetos

Diez sujetos sanos participaron en el estudio, con edad media de 23.5 ± 2.0 . Cinco mujeres y cinco hombres. Firmaron el consentimiento informado de acuerdo con la declaración de Helsinki y todos los procedimientos fueron aprobados por la Oficina de Investigación Responsable de la Universidad Miguel Hernández de Elche, España (DIS.JAP.03.18, 22/01/2019).

Además, se reclutaron dos pacientes con lesión de la médula espinal del Hospital Nacional de Paraplégicos en Toledo. También firmaron un formulario de consentimiento informado de acuerdo con la Declaración de Helsinki y no tenían experiencia previa con la tecnología BMI. La Tabla 7.1 muestra información más detallada.

Tabla 7.1: Detalles de los pacientes

Sujeto	Paciente 1	Paciente 2
Género	Hombre	Hombre
Edad	51	62
Peso	75 kg	71 kg
Nivel de lesión	T4	L3
Nivel ASIA	C	B
Tipo lesión	Incompleta	Incompleta

7.1.2. Equipo

Las señales de EEG se registraron con el sistema Starstim R32 (Neuroelectrics, España). Las señales se registraron a 500 Hz y se remuestrearon a 200 Hz. Los electrodos de tierra y referencia se colocaron en el lóbulo derecho de la oreja y el resto se distribuyó como en la Figura 5.1. Se utilizó el software de registro NIC v2.0.5c (Neuroelectrics, España).

Se utilizó el mismo exoesqueleto utilizado en las contribuciones P3 y P4 (5.1.2). Y también se utilizó el mismo sistema de realidad virtual presentado en P2 (4.1.2).

La Figura 7.1 muestra todo el equipamiento utilizado en este estudio.

7.2. Métodos

La BMI utilizada en esta contribución es idéntica a la de la contribución P2 (4.2) como se muestra en la Figura 4.3 pero con ventanas de análisis de 1.5 s y como el paradigma



Figura 7.1: Exoesqueleto REX, equipo de electroencefalografía Starstim R32 y equipo de realidad virtual.

de IM de las contribuciones P3 (5.2) y P4 (6.2) sin incluir el algoritmo de filtrado de artefactos oculares. Este algoritmo no se pudo utilizar en este estudio porque el equipo de EEG no permitía el registro de la señal EOG.

7.3. Resultados y discusión

En esta investigación participaron tres grupos de sujetos: un grupo de control, un grupo de realidad virtual y dos pacientes con LME incompleta.

Todos los sujetos participaron en cinco sesiones, divididas en entrenamiento (lazo-abierto) y test (lazo-cerrado). Sin embargo, el entrenamiento de los sujetos del grupo de RV fue diferente al del grupo de control, ya que se redujo a la mitad. Esto se produjo porque antes del lazo-abierto, los participantes practicaron estrategias de IM para la marcha mientras recibían retroalimentación visual. Luego, utilizaron estas tareas para calibrar una BMI y controlar un exoesqueleto robótico. Dado que los participantes ya habían practicado

en RV, se necesitaba menos información para que la BMI lograra una alta precisión, reduciendo así el tiempo de entrenamiento y el esfuerzo físico. Finalmente, los pacientes realizaron las mismas sesiones que el grupo de RV, pero con una duración reducida de la inmersión en RV.

Se utilizaron algunas de las métricas presentadas en P1 (3.3), pero algunas se modificaron y se incluyeron otras nuevas:

- %Feedback EXO: porcentaje de épocas con retroalimentación correcta del exoesqueleto. Idéntica a %EXO de la contribución P1 (3.3).
- Missing trials: porcentaje de registros en los que el exoesqueleto nunca se activó durante el período de IM.

Por otro lado, a diferencia de P1 (3.3) y P3 (5.3), los valores de TPR, Acc y FP se calcularon por separado para el modelo estático (de arranque) y el modelo en movimiento (de parada). Asimismo, se incluyeron dos métricas nuevas para cada modelo:

- False Positive Ratio (FPR): para el modelo estático es relación entre la cantidad de comandos de activación emitidos durante el estado de reposo y la cantidad de veces que los sujetos estaban estáticos; para el modelo en movimiento es la relación entre la cantidad de comandos de parada emitidos durante el período de IM y la cantidad de veces que los sujetos estaban en movimiento.
- Weighted Discriminator (WD): esta métrica se introdujo en [132] y varía de -1 a 1. Se calcula de la siguiente manera:

$$WD = 0,4 \frac{TPR}{100} + 0,6 \frac{Acc}{100} - \frac{FPR}{100}. \quad (7.1)$$

7.3.1. Lazo-abierto

Siguiendo el protocolo definido en la contribución P35.3, los participantes del grupo de control realizaron 22 registros con la secuencia de tareas mentales mostrada en la Figura 3.4A: 11 estando de pie sin moverse con el exoesqueleto y 11 caminando. Por otro lado, el grupo de RV realizó una fase de lazo-abierto más corta con solo 12 registros (6 estáticos y 6 en movimiento). Se entrenaron dos modelos, uno con datos estáticos y otro con datos en movimiento para cada grupo como en las contribuciones P35.3 y P46.3.

Durante la fase de inmersión en RV, los participantes del grupo de RV fueron colocados en un corredor virtual dentro de una nave espacial, con vista en primera persona, el mismo que en la contribución P2. Completaron 10 registros en condiciones similares a la fase de calibración. En cinco de estos registros, el avatar del participante caminaba por el corredor, mientras que, en los otros cinco, permanecía quieto. Es importante destacar que

el movimiento del avatar estaba predefinido y no dependía de las prácticas mentales de los participantes.

La Figura 7.2 muestra la precisión promedio para cada sesión y sujeto. La Figura 7.2A muestra los resultados de validación cruzada con registros en estático. S1-S5 representan a los participantes del grupo de control, mientras que los sujetos V1-V5 representan a los participantes del grupo de RV. En cuanto a los registros en movimiento, la Figura 7.2B presenta sus resultados.

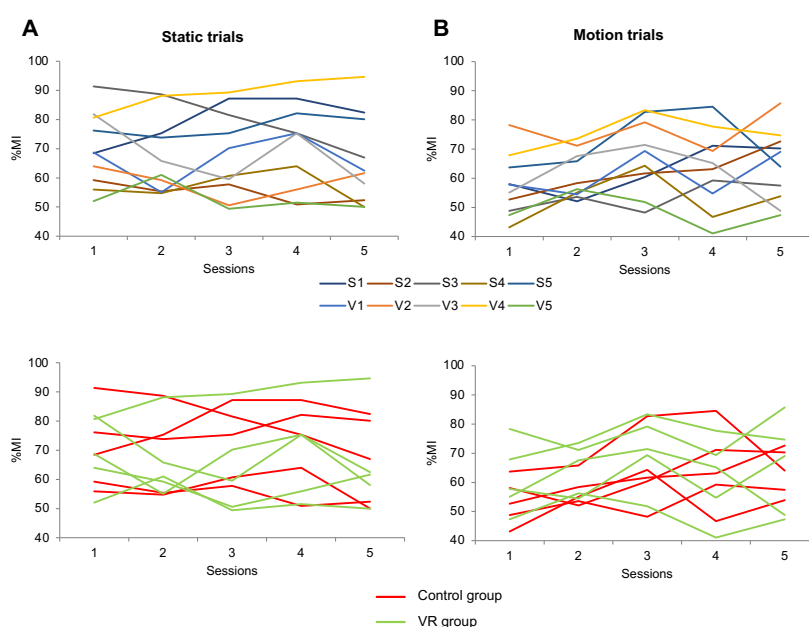


Figura 7.2: Resultados de lazo-abierto. %MI es la precisión del modelo que va de 0 a 100. S1-S5 son los sujetos del grupo de control y V1-V5 son los sujetos del grupo RV. Imagen de [5] con licencia Creative Commons Attribution-NonCommercial-NoDerivatives 4.0. International (CC BY-NC-ND 4.0)

Al examinar los registros estáticos, no se encontraron diferencias significativas entre las sesiones ni entre los grupos. Sin embargo, para los registros en movimiento, la prueba estadística reveló resultados significativamente superiores para el grupo de RV. Estos resultados son contrarios a la contribución P4 (6.3) en la que sí se hallaron diferencias con las sesiones que podrían estar relacionadas con el aprendizaje.

En consonancia con los resultados de la contribución P3(5.3) , los registros en estático mostraron mejores resultados que los registros en movimiento.

7.3.2. Lazo-cerrado

En la fase de control en lazo-cerrado, se siguió el mismo protocolo que se describe en la contribución P3(5.3). Se realizaron cinco registros con las secuencias de tareas mostrada en Figura 3.4B y con la máquina de estados como mecanismo de control (Figura 5.4).

La Tabla 7.2 presenta una comparación detallada de los resultados promedio para ambos grupos. En ambos casos, el modelo de movimiento demostró un rendimiento superior en comparación con el modelo estático, lo que indica que el modelo que controla el caminar o detenerse fue más efectivo. Al analizar los resultados de los experimentos realizados con %MI, %Feedback EXO y %Commands, ambos grupos mostraron un patrón de comportamiento similar. Sin embargo, siguiendo la tendencia observada en los registros de calibración, el rendimiento del modelo de movimiento en el grupo de RV superó ampliamente al del grupo de control.

Tabla 7.2: Resultados de lazo-cerrado del grupo de control (Sham) y el grupo de realidad virtual (VR). Static son los resultados del modelo entrenado con los registros en estático y Motion son los resultados del modelo entrenado con los registros en movimiento. Tabla de [5] con licencia Creative Commons Attribution-NonCommercial-NoDerivatives 4.0. International (CC BY-NC-ND 4.0).

	Sham	VR
%MI	55.83±14.68	55.69±6.73
%Commands	57.62±15.18	57.3±7.22
%Feedback EXO	51.87±16.62	54.91±6.43
Missing trials	0.12±0.12	0.02±0.02
Static model: TPR	58.61±31.05	84±11.79
Static model: FPR	44.93±25.41	58.53±16.42
Static model: Acc	42.35±23.96	45.16±11.91
Static model: WD	0.04±0.35	0.02±0.23
Motion model: TPR	46.67±28.06	64.2±10.8
Motion model: FPR	41.67±33.49	40.93±20.87
Motion model: Acc	49.86±32.13	66.8±14.98
Motion model: WD	0.07±0.48	0.25±0.3

7.3.3. Pacientes con LME

Una vez que la configuración experimental fue evaluada con sujetos sanos, se procedió a probarla con LME. La única diferencia con respecto a los participantes sanos fue que

las sesiones de RV fueron más cortas. Los pacientes realizaron 6 registros en el entorno de RV. Luego, realizaron 12 registros para la calibración.

Para el control en lazo-cerrado, los participantes realizaron siete registros. Sin embargo, solo cinco fueron en control real y se consideraron para la evaluación de métricas de la BMI, en los otros dos la BMI fue forzada manualmente a funcionar perfectamente. Esta estrategia se empleó para evitar su frustración. Además, en esta investigación, se evaluó la aceptación y usabilidad del sistema. El paciente P1 mostró mayor satisfacción en general que el paciente P2. Además, los pacientes percibieron que debían realizar un esfuerzo físico y mental considerable para obtener los resultados deseados, pero estaban satisfechos con su rendimiento. Aunque el nivel de esfuerzo aumentó progresivamente en cada sesión, los pacientes nunca alcanzaron valores de esfuerzo cercanos a su máximo.

El rendimiento de los dos pacientes durante el lazo-abierto se encuentra dentro del rango de los individuos sanos. Debido a las diferencias significativas entre los sujetos, es difícil decir si el rendimiento de los pacientes es en promedio inferior o superior al de los individuos sanos. La Tabla 7.3 muestra los resultados obtenidos en lazo-cerrado.

Tabla 7.3: Resultados de lazo-cerrado de los dos pacientes con lesión medular. Static son los resultados del modelo entrenado con los registros en estático y Motion son los resultados del modelo entrenado con los registros en movimiento. Tabla de [5] con licencia Creative Commons Attribution-NonCommercial-NoDerivatives 4.0. International (CC BY-NC-ND 4.0).

	P1	P2
%MI	50.26±3.03	48.53±5.98
%Commands	53.38±5.54	49.96±5.64
%Feedback EXO	53.55±4.75	49.27±4.56
Missing trials	0±0	0.05±0.1
Static model: TPR	77.71±7.74	76.67±14.14
Static model: FPR	56.67±17.43	64.58±8.32
Static model: Acc	45.33±12.28	37.92±4.59
Static model: WD	0.04±0.2	-0.11±0.12
Motion model: TPR	69.17±9.95	65.5±5.12
Motion model: FPR	66.67±19.44	67.92±11.97
Motion model: Acc	57.08±13.63	60±2.72
Motion model: WD	-0.05±0.29	-0.08±0.13

Capítulo 8

Discusión global

A lo largo de la presente tesis doctoral, se han investigado y analizado una serie de cuestiones fundamentales en tres líneas de investigación, cada una de las cuales ha aportado conocimientos significativos. A continuación, se resumirán y relacionarán estos hallazgos para ofrecer una visión completa de la investigación y su relevancia en un contexto más amplio.

8.1. Paradigmas de control: imaginación motora y/o atención

En las contribuciones P1 y P3, al considerar cada paradigma por separado, se observó que el paradigma de atención mostró un rendimiento inferior al paradigma de IM en pruebas de lazo-abierto. Si bien los resultados del paradigma de IM mostraron una tendencia creciente a lo largo de las sesiones, este patrón no es tan evidente para el paradigma de atención. Estos resultados concuerdan con las conclusiones de [133]. La realización de IM no es una actividad intuitiva para participantes nuevos y la práctica podría promover la modulación y la mejora de los patrones de actividad cerebral. Sin embargo, en cuanto a la atención del usuario a la marcha, el rendimiento no parece mejorar con la práctica. La atención es algo que las personas entrenamos a diario, por lo que unas pocas sesiones puede que no mejoren en mayor medida el rendimiento. No obstante, esta diferencia no es tan evidente en pruebas de lazo-cerrado. La combinación de atención e IM como paradigma de control requiere mantener un nivel de atención alto, lo que dificulta la activación del exoesqueleto, pero proporciona un menor número de FP. Esto hace que la BMI sea más conservadora. Por la misma razón, cuando se utilizan ambos paradigmas, los retrasos para comenzar la marcha con el exoesqueleto fueron más largos y para detenerse fueron más cortos. Por lo tanto, se podría decir que la combinación hace que el control sea más seguro,

pero con menor grado de reacción.

8.2. Condiciones en estático y en movimiento

Mientras que en nuestra investigación anterior de una BMI basada en la IM de la marcha para controlar una cinta de correr, [134] no se hallaron diferencias entre las pruebas en estático y las pruebas en movimiento, la presente investigación ha hallado cierta variación, concretamente las contribuciones P3 y P5. Es importante destacar que caminar con muletas asistido por un exoesqueleto es una tarea más compleja que caminar en una cinta de correr, por lo que los sujetos deben estar concentrados. En consecuencia, les resulta más difícil realizar otras tareas cerebrales como la IM o el conteo regresivo. Asimismo, los participantes informaron de una mayor percepción de complejidad en las tareas realizadas durante la marcha con el exoesqueleto en comparación con las tareas realizadas en posición estática.

8.3. Diferencias entre sujetos

Los resultados de esta investigación proporcionan evidencia de que el rendimiento de la BMI presenta diferencias estadísticamente significativas entre los sujetos. Las diferencias interindividuales en cuanto al rendimiento y los mecanismos neurales subyacentes aún no están claras. Estudios como el de [135], estudiaron qué características de la red de atención frontoparietal podrían desempeñar un papel relevante en la predicción del rendimiento de la BMI. Observaron ciertas características estructurales y funcionales que podrían estar asociadas con el rendimiento. Además, la presencia de ciertos estados cognitivos durante el estado de reposo también parece estar asociada con el rendimiento [136]. Siguiendo estudios anteriores, el presente trabajo abordó la variabilidad interindividual mediante la modelización específica del sujeto en la BMI. Se adaptaron los modelos a cada sujeto y sesión.

Dado que se ha demostrado que algunos usuarios encuentran más difícil modular los ritmos cerebrales de manera voluntaria, investigaciones futuras podrían centrarse en enfoques de entrenamiento adaptativo. Por ejemplo, algunos sujetos podrían necesitar más sesiones de entrenamiento o más ensayos en control de lazo-abierto antes de comenzar con el control de lazo-cerrado. En la literatura existen algunas metodologías que han demostrado predecir el rendimiento de la BMI de un sujeto [129]. Por lo tanto, estos predictores neurológicos podrían utilizarse para identificar qué individuos necesitarían más entrenamiento y más ayuda por parte de los investigadores antes de comenzar el experimento.

8.4. Evolución con las sesiones

En general, la evolución del rendimiento a lo largo de las sesiones fue positiva, y la precisión de la BMI en la última sesión fue mayor que en la primera. Estos resultados son consistentes con investigaciones previas [133].

En la contribución P4, esta tendencia positiva fue estadísticamente significativa tanto para las pruebas estáticas como en movimiento, pero fue más evidente en las pruebas estáticas. Esta diferencia puede atribuirse a la dificultad de realizar tareas mentales durante la marcha asistida por robots. Sin embargo, en la contribución P5, la evolución del rendimiento a lo largo de las sesiones solo fue significativa en las pruebas en movimiento. Este crecimiento fue significativamente diferente entre los sujetos en realidad virtual y los controles. La tendencia global fue similar para las primeras tres sesiones, pero en la cuarta, los sujetos de RV obtuvieron una precisión más baja que en la sesión anterior. Dado que la contribución P4 contaba solo con 5 participantes y la P5 con 10 participantes, es difícil llegar a una conclusión. Puede depender del sujeto, ya que algunos encontraron más fácil caminar asistidos por el dispositivo que otros.

8.5. Entrenamiento previo con realidad virtual

Se observaron diferencias significativas entre los sujetos en lazo-abierto, siendo el grupo de RV el que mostró un rendimiento superior en los registros en movimiento. Sin embargo, no se observaron diferencias significativas en los registros en estático. Es importante destacar que, aunque el rendimiento de los dos grupos fue similar, el enfoque de RV podría ofrecer un método alternativo de entrenamiento que requiere menos esfuerzo físico. Además, cuando el entrenamiento se dividió en fases de RV y calibración, se percibió como menos monótono, lo cual puede ser ventajoso para mantener a los sujetos motivados y concentrados. En cuanto al control en lazo-cerrado, se evaluó la eficiencia de la BMI en su conjunto, considerando el rendimiento del modelo tanto en registros estáticos como en registros en movimiento. En este sentido, ambos grupos mostraron un comportamiento similar. Al analizar el rendimiento de cada modelo de forma individual, se utilizó la métrica WD. Aunque el rendimiento del modelo en estático fue similar en ambos grupos, el modelo en movimiento del grupo de RV superó al del grupo de control. Estos hallazgos son consistentes con los observados en la fase de calibración.

8.6. Pacientes con LME

En la contribución P5, los resultados de la fase de calibración del primer paciente mostraron una tendencia positiva a lo largo de las sesiones. Sin embargo, el segundo

paciente no mostró el mismo efecto de aprendizaje. Es importante destacar que, aunque ambos pacientes sufrieron una lesión medular incompleta, la lesión del segundo afectó en mayor medida su función motora. Por lo tanto, este paciente podría necesitar más práctica con el sistema antes de alcanzar un nivel de rendimiento aceptable. En general, se demostró que la BMI propuesta es al menos tan efectiva como enfoques anteriores presentados en la literatura y presenta métricas de evaluación más restrictivas [113, 40, 32, 53, 43, 42].

Además, la BMI implementada en este estudio proporcionó un control completo e incondicional para que los pacientes pudiesen iniciar la marcha, mantenerla, detenerse y mantenerse de pie sin limitaciones de tiempo impuestas por el protocolo experimental.

8.7. Limitaciones del estudio

Esta investigación presenta diversas limitaciones. En primer lugar, las limitaciones se relacionan con los datos recopilados. A pesar de que todos los participantes carecían de experiencia previa en el uso de una interfaz cerebro-máquina, se observaron diferencias significativas en la eficiencia de la BMI para el control del exoesqueleto. Estas diferencias dificultan la obtención de resultados concluyentes. Además, la limitación en el tamaño del conjunto de datos también influye debido a la gran dependencia de los sujetos. Aunque este estudio contó con una cantidad considerable de sujetos en comparación con otros estudios de aplicaciones de BMI, el conjunto de datos no fue lo suficientemente grande como para representar todas las posibles situaciones de uso.

Otra limitación reside en el hecho de que realizar de forma mantenida la IM de la marcha mientras se usa un exoesqueleto puede resultar difícil. Los participantes experimentaron fatiga, lo que dificulta la concentración en las tareas mentales y, en última instancia, reduce la precisión de la BMI.

Por otro lado, en relación con el entrenamiento en un entorno de realidad virtual, los sujetos utilizaron el exoesqueleto y se mantuvieron en posición erguida y estática. Si bien esto implicó menos esfuerzo físico que caminar con el exoesqueleto, todavía requirió cierto esfuerzo, especialmente para los pacientes. En futuros intentos, sería beneficioso evaluar una fase de entrenamiento con dispositivos de RV en la que los participantes permanezcan sentados.

Además, es importante destacar que la precisión de las pruebas es menor en lazo-cerrado que en lazo-abierto. Esto podría deberse al hecho de que, durante las pruebas en lazo-cerrado, los sujetos son conscientes de su desempeño y esto puede afectar su enfoque en la tarea mental. Resultados similares se han reportado en estudios anteriores, como el realizado por [72], en el que se evaluó la IM de la mano y el pie, y el estudio de [48], donde se investigó la IM de la mano para controlar un exoesqueleto de miembro inferior.

Capítulo 9

Contribuciones, conclusiones y líneas futuras

En esta tesis doctoral se ha realizado un exhaustivo análisis, diseño y evaluación de un sistema de control basado en la decodificación de la actividad cerebral para el arranque y paro de un exoesqueleto de miembro inferior. El objetivo principal de este sistema es proporcionar asistencia y apoyo en la rehabilitación a personas que han sufrido una lesión medular. El control del exoesqueleto se lleva a cabo de manera directa y voluntaria a través de la imaginación motora de la marcha.

Las publicaciones presentadas en esta tesis se han organizado en tres líneas de investigación. La primera línea se centra en el control de un exoesqueleto robótico de miembro inferior. Se han probado dos enfoques de control diferentes, uno que combina la imaginación motora y la atención, donde los usuarios deben imaginar el movimiento de caminar para activar el exoesqueleto y relajarse para detenerlo, pero sólo en situaciones en las que tengan un alto nivel de atención a la tarea. El otro enfoque se basa únicamente en la imaginación motora, sin incluir niveles de atención adicionales. Además, se han diseñado dos mecanismos de control. El primero se basa en un único modelo que envía dos comandos, un comando de parada que sirve para detenerse o permanecer en reposo, y un comando de movimiento que permite iniciar o mantener el movimiento. El otro mecanismo de control funciona como una máquina de estados que depende del estado cinemático del exoesqueleto, de esta forma se utilizan dos modelos, uno para enviar un comando de arranque o permanecer en reposo, y otro para enviar un comando de parada o mantenerse en movimiento.

En la segunda línea de investigación, se ha estudiado la generación de patrones cerebrales en EEG durante la imaginación motora, en comparación con estados de relajación. Se han analizado las diferencias en los patrones cerebrales entre distintas tareas mentales, entre participantes y a lo largo de las sesiones experimentales.

La tercera línea de investigación se ha centrado en la inclusión de un entrenamiento con realidad virtual para reducir el tiempo de calibración de la interfaz cerebro-máquina. Se ha explorado la inmersión de los usuarios en un entorno de realidad virtual, donde un avatar avanza en función de las tareas mentales realizadas.

En esta sección, se presentan las principales contribuciones de todas las investigaciones realizadas y se resumen las conclusiones obtenidas. Además, se proponen posibles líneas futuras de investigación para continuar avanzando en este campo.

9.1. Contribuciones

La Tabla 9.1 muestra la relación entre los objetivos y las hipótesis planteadas al inicio de la investigación y las publicaciones del compendio en las que se han abordado. Entre las principales contribuciones destacan las siguientes:

Tabla 9.1: Relación entre los objetivos e hipótesis y las publicaciones del compendio de la presente tesis doctoral.

Objetivos	Hipótesis	Publicaciones en las que se han abordado
O1	H1, H2	P1, P3, P4, P5
O2	H1, H2	P4
O3	H3	P1, P3, P5
O4	H3	P1, P3, P5
O5	H4	P2, P5
O6	H5	P5

1. En base al objetivo O1, se han estudiado las señales de electroencefalografía en tres condiciones mentales, en un estado de relajación, durante la imaginación motora de la marcha y durante el cálculo de una cuenta regresiva. De esta forma se ha trabajado con dos paradigmas, el de imaginación motora y el de atención. En el paradigma de imaginación motora se ha discernido el patrón cerebral de la imaginación motora en comparación con un estado de relajación y se ha verificado la hipótesis H1. En el caso del paradigma de atención, se ha enfocado como tres o dos niveles de atención. En el primer caso se ha definido una atención distinta para la imaginación motora, otra para la cuenta regresiva y otra para la relajación. En el segundo caso, solo se han definido dos niveles de atención, el nivel de atención a la imaginación de la marcha y la atención a cualquier otra tarea mental y así se ha verificado la hipótesis H2.

2. En cuanto al objetivo O2, se han analizado distintos métodos de procesado de las señales cerebrales basados en características espectrales y espaciales y se han comparado los resultados obtenidos para seleccionar el método con mayores desempeños y así poder abordar las hipótesis H1 y H2.
3. Cumpliendo con el objetivo O3, se ha diseñado una interfaz de control tanto para un entorno de realidad virtual como para un exoesqueleto de miembro inferior basada en la imaginación motora de la marcha. Esta interfaz no incluye otros paradigmas de control que han demostrado ser más eficientes en la literatura como los potenciales evocados visuales o auditivos, pero que carecen de aplicación desde el punto de vista de la neurorrehabilitación. Además, en esta interfaz se ha prescindido del uso del nivel de atención en el sistema de control y por lo tanto, se ha rechazado la hipótesis H3.
4. Continuando con el objetivo O3, se ha definido un protocolo de control del dispositivo en el que los sujetos pueden empezar la marcha, mantenerla, pararla o mantenerse parados. Durante toda la duración de la prueba, los sujetos pueden producir un cambio en el exoesqueleto sin restricciones de tiempo.
5. El objetivo O4 se ha llevado a cabo mediante la evaluación del sistema con 26 sujetos sin limitaciones motoras y en 100 sesiones experimentales. Se han obtenido resultados superiores o en línea con el estado del arte, pero con menores restricciones de control y sin la inclusión de otros paradigmas de control.
6. La hipótesis H4 se ha verificado mediante el diseño de un protocolo para la práctica de la imaginación motora mediante un entorno de realidad virtual, cumpliendo con el objetivo O5, y así se ha reducido el tiempo de entrenamiento necesario para calibrar la BMI a la mitad.
7. La hipótesis H5 se ha probado mediante el estudio de la usabilidad de la interfaz cerebro-máquina para el control de un exoesqueleto de miembro inferior con dos pacientes con lesión de médula espinal y cinco sesiones experimentales y la adaptación de las sesiones en base a las limitaciones de cada paciente. De esta forma, se ha cumplido con el objetivo O6. Además, se ha incluido el entorno de realidad virtual como práctica previa al uso del sistema.

9.2. Conclusiones

Las conclusiones extraídas de las publicaciones incluidas en este compendio son las siguientes:

1. Considerando los paradigmas de control, se han obtenido mejores resultados sin incluir el paradigma de atención, solo mediante el paradigma de IM. De esta forma se consigue una mayor reacción del exoesqueleto despertando la motivación de los participantes.
2. Se han hallado diferencias significativas entre los usuarios, por lo que sería interesante adaptar los entrenamientos a cada uno de ellos, tanto en tiempo como en las tareas a realizar.
3. Varias sesiones son necesarias para percibir una evolución positiva en la capacidad del sistema para discernir entre tareas mentales. Por lo tanto, los sujetos necesitan práctica para conseguir modular su actividad cerebral. Sería de interés ampliar a más de cinco sesiones experimentales y estudiar la viabilidad de espaciarlas en el tiempo para ver si se percibe también una evolución positiva.
4. La inclusión de la realidad virtual consigue los mismos y/o mayores niveles de eficacia del sistema reduciendo el periodo de calibración a la mitad. Por lo tanto, su uso debería ser crucial en las BMIs basadas en imaginación motora y cuyos usuarios no tengan experiencia previa.
5. El sistema se puede utilizar en pacientes que hayan sufrido una lesión medular y su eficacia no es significativamente inferior a la eficacia de este en sujetos sin limitaciones motoras.

9.3. Líneas futuras

En cuanto a las líneas futuras de investigación, se proponen las siguientes mejoras y enfoques.

En primer lugar, sería de interés ampliar la base de datos con registros de EEG durante la imaginación motora y los estados de relajación. Esto permitiría identificar diferencias significativas y establecer hallazgos que sean aplicables al conjunto de participantes, evitando que los resultados sean específicos de cada individuo.

Por otro lado, se sugieren dos mejoras para el sistema de control que ya han sido implementadas durante el periodo de esta tesis doctoral, aunque los resultados están pendientes de publicación. En las investigaciones presentadas, se utilizaba la imaginación motora de forma continua, es decir, los sujetos debían imaginar el movimiento de la marcha durante todo el tiempo que deseaban que el exoesqueleto estuviera en movimiento. Como mejora, se ha propuesto utilizar la imaginación motora únicamente para producir un cambio, es decir, para iniciar o detener el movimiento. De esta manera, los sujetos realizarían una imaginación motora momentánea hasta lograr que el dispositivo comience la marcha, y

luego podrían descansar mentalmente mientras caminan y lo mismo para la parada. Otra mejora consiste en aplicar lo que se conoce como transferencia de aprendizaje (o transfer learning en inglés). Esta técnica se basa en utilizar una BMI que haya sido entrenada con datos de otros usuarios, lo que permitiría reducir aún más el tiempo de calibración. Para implementar esta transferencia de aprendizaje, se propone el uso de redes neuronales, ya que han demostrado ofrecer los mejores resultados. Además, estas redes tienen unos pesos que pueden adaptarse a los datos de cada usuario individualmente y a cada sesión experimental. Por lo tanto, primero se crea una BMI genérica utilizando datos de un grupo de participantes, y luego se adapta a cada uno de ellos durante cada sesión experimental.

Finalmente, debido a las diferencias encontradas entre los sujetos, sería interesante clasificarlos en grupos según su facilidad para controlar una BMI. Aquellos participantes que presenten mayores dificultades podrían requerir un mayor entrenamiento para lograr un mejor control y rendimiento.

La mayoría de las BMIs con EEG utilizan electrodos húmedos que utilizan un gel electrolítico como conductor entre el cuero cabelludo y el electrodo, lo que puede resultar incómodo para los usuarios y requerir un mantenimiento constante. Una posible línea de investigación para mejorar la usabilidad de las BMIs es la incorporación de equipos de electrodos secos. Los electrodos secos, en comparación con los electrodos húmedos, no requieren de la aplicación de geles conductores, lo que los hace más fáciles y rápidos de colocar. Además, eliminan la necesidad de limpieza y mantenimiento regular, lo que mejora la experiencia del usuario a largo plazo. Sin embargo, el uso de electrodos secos plantea desafíos en términos de calidad de la señal registrada. La impedancia más alta puede resultar en una mayor presencia de ruido y una menor sensibilidad para captar las señales cerebrales débiles. Por lo tanto, es fundamental investigar y desarrollar nuevas técnicas de procesamiento de señales y algoritmos de decodificación que permitan superar estas limitaciones.

Estas propuestas de investigación abren nuevas perspectivas para futuros estudios y contribuyen al avance del campo de la rehabilitación asistida por exoesqueletos e interfaces cerebro-máquina.

Bibliografía

- [1] M. Ortiz, L. Ferrero, E. Iáñez, J. M. Azorín, and J. L. Contreras-Vidal, “Sensory Integration in Human Movement: A New Brain-Machine Interface Based on Gamma Band and Attention Level for Controlling a Lower-Limb Exoskeleton,” *Frontiers in Bioengineering and Biotechnology*, vol. 8, p. 735, 2020. [Online]. Available: <https://www.frontiersin.org/article/10.3389/fbioe.2020.00735>
- [2] L. Ferrero, M. Ortiz, V. Quiles, E. Iáñez, and J. M. Azorín, “Improving Motor Imagery of Gait on a Brain–Computer Interface by Means of Virtual Reality: A Case of Study,” *IEEE Access*, vol. 9, pp. 49 121–49 130, 2021.
- [3] L. Ferrero, V. Quiles, M. Ortiz, E. Iáñez, and J. M. Azorín, “A BMI Based on Motor Imagery and Attention for Commanding a Lower-Limb Robotic Exoskeleton: A Case Study,” 2021.
- [4] L. Ferrero, M. Ortiz, V. Quiles, E. Iáñez, J. A. Flores, and J. M. Azorín, “Brain symmetry analysis during the use of a BCI based on motor imagery for the control of a lower-limb exoskeleton,” *Symmetry*, vol. 13, no. 9, 2021.
- [5] L. Ferrero, V. Quiles, M. Ortiz, E. Iáñez, Á. Gil-Agudo, and J. M. Azorín, “Brain-computer interface enhanced by virtual reality training for controlling a lower limb exoskeleton,” *iScience*, vol. 26, no. 5, p. 106675, 2023. [Online]. Available: <https://www.sciencedirect.com/science/article/pii/S2589004223007526>
- [6] G. L. Holmes and R. Khazipov, “Basic neurophysiology and the cortical basis of EEG,” *The Clinical Neurophysiology Primer*, pp. 19–33, 2007.
- [7] A. F. Jackson and D. J. Bolger, “The neurophysiological bases of EEG and EEG measurement: A review for the rest of us,” *Psychophysiology*, vol. 51, no. 11, pp. 1061–1071, 2014.
- [8] K. Venkatesh, “Spinal cord injury: pathophysiology, treatment strategies, associated challenges, and future implications,” pp. 125–151, 2019.

-
- [9] “Hospital Nacional de Paraplégicos.” [Online]. Available: <https://hnparaplegicos.sanidad.castillalamancha.es/es/pacientes/lesion-medular/preguntas-mas-frecuentes/lesion-medular>
- [10] M. Alcobendas-Maestro, E. López-Dolado, A. Esclarín de Ruz, and M. C. Valdizán-Vallador, “[Gait training in incomplete spinal cord injuries with body weight support].” *Revista de neurologia*, vol. 39, no. 5, pp. 406–410, sep 2004.
- [11] J. L. Pons, *Wearable Robots: Biomechatronic Exoskeletons*. Wiley, 2008.
- [12] D. Grasmücke, A. Zierjacks, O. Jansen, C. Fisahn, M. Sczesny-kaiser, M. Wessling, R. C. Meindl, T. A. Schildhauer, and M. Aach, “Against the odds: what to expect in rehabilitation of chronic spinal cord injury with a neurologically controlled Hybrid Assistive Limb exoskeleton. A subgroup analysis of 55 patients according to age and lesion level,” *Neurosurgical Focus*, vol. 42, no. May, 2017.
- [13] M. Ortiz, K. Nathan, J. M. Azorín, and J. L. Contreras-Vidal, “Brain-Machine Interfaces for Neurorobotics BT - Handbook of Neuroengineering,” N. V. Thakor, Ed. Singapore: Springer Nature Singapore, 2023, pp. 1817–1857. [Online]. Available: https://doi.org/10.1007/978-981-16-5540-1_{_}52
- [14] K. Lee, D. Liu, L. Perroud, R. Chavarriaga, and J. d. R. Millán, “A brain-controlled exoskeleton with cascaded event-related desynchronization classifiers,” *Robotics and Autonomous Systems*, vol. 90, pp. 15–23, 2017. [Online]. Available: <http://dx.doi.org/10.1016/j.robot.2016.10.005>
- [15] I. Lazarou, S. Nikolopoulos, P. C. Petrantonakis, I. Kompatsiaris, and M. Tsolaki, “EEG-Based Brain–Computer Interfaces for Communication and Rehabilitation of People with Motor Impairment: A Novel Approach of the 21st Century,” *Frontiers in Human Neuroscience*, vol. 12, 2018. [Online]. Available: <https://www.frontiersin.org/article/10.3389/fnhum.2018.00014>
- [16] T. Kirschstein and R. Köhling, “What is the Source of the EEG?” *Clinical EEG and Neuroscience*, vol. 40, no. 3, pp. 146–149, 2009. [Online]. Available: <https://doi.org/10.1177/155005940904000305>
- [17] R. P. Loreto and A. D. Carolina, “Aporte de los distintos métodos electroencefalográficos (eeg) al diagnóstico de las epilepsias,” *Revista Médica Clínica Las Condes*, vol. 24, no. 6, pp. 953–957, 2013. [Online]. Available: <https://www.sciencedirect.com/science/article/pii/S0716864013702499>
-

-
- [18] N. Padfield, J. Zabalza, H. Zhao, V. Masero, and J. Ren, “EEG-based brain-computer interfaces using motor-imagery: Techniques and challenges,” *Sensors (Switzerland)*, vol. 19, no. 6, pp. 1–34, 2019.
- [19] M. Rangaswamy and B. Porjesz, “From event-related potential to oscillations: genetic diathesis in brain (dys)function and alcohol dependence.” pp. 238–242, 2008.
- [20] M. J. Maguire and A. D. Abel, “What changes in neural oscillations can reveal about developmental cognitive neuroscience: Language development as a case in point,” *Developmental Cognitive Neuroscience*, vol. 6, pp. 125–136, 2013. [Online]. Available: <https://www.sciencedirect.com/science/article/pii/S1878929313000492>
- [21] S. Sur and V. K. Sinha, “Event-related potential: An overview.” *Industrial psychiatry journal*, vol. 18, no. 1, pp. 70–73, jan 2009.
- [22] C. C. Knight, *Encyclopedia of Sciences and Religions*, 2013.
- [23] S. Moratti, B. A. Clementz, Y. Gao, T. Ortiz, and A. Keil, “Neural mechanisms of evoked oscillations: stability and interaction with transient events.” *Human brain mapping*, vol. 28, no. 12, pp. 1318–1333, dec 2007.
- [24] E. Başar, “Brain oscillations in neuropsychiatric disease.” *Dialogues in clinical neuroscience*, vol. 15, no. 3, pp. 291–300, sep 2013.
- [25] P. D. Skosnik and J. A. Cortes-Briones, “Chapter 80 - Electroencephalography and Cannabis: From Event-Related Potentials to Oscillations,” V. R. B. T. N. o. D. A. Preedy and S. Misuse, Eds. San Diego: Academic Press, 2016, pp. 851–862. [Online]. Available: <https://www.sciencedirect.com/science/article/pii/B9780128002131000808>
- [26] P. A. Abhang, B. W. Gawali, and S. C. Mehrotra, “Chapter 2 - Technological Basics of EEG Recording and Operation of Apparatus,” in *Introduction to EEG- and Speech-Based Emotion Recognition*, P. A. Abhang, B. W. Gawali, and S. C. Mehrotra, Eds. Academic Press, 2016, pp. 19–50. [Online]. Available: <https://www.sciencedirect.com/science/article/pii/B9780128044902000026>
- [27] A. Salek-Haddadi, K. J. Friston, L. Lemieux, and D. R. Fish, “Studying spontaneous EEG activity with fMRI,” *Brain Research Reviews*, vol. 43, no. 1, pp. 110–133, 2003.
- [28] L. Iemi, M. Chaumon, S. M. Crouzet, and N. A. Busch, “Spontaneous Neural Oscillations Bias Perception by Modulating Baseline Excitability.” *The Journal of neuroscience : the official journal of the Society for Neuroscience*, vol. 37, no. 4, pp. 807–819, jan 2017.
-

-
- [29] C. Saavedra and L. Bougrain, “Processing Stages of Visual Stimuli and Event-Related Potentials,” in *The NeuroComp/KEOpS’12 workshop*, Bordeaux, 2012.
- [30] V. Quiles, L. Ferrero, E. Iáñez, M. Ortiz, Á. Gil-Agudo, and J. M. Azorín, “Brain-machine interface based on transfer-learning for detecting the appearance of obstacles during exoskeleton-assisted walking,” *Frontiers in Neuroscience*, vol. 17, 2023. [Online]. Available: <https://www.frontiersin.org/articles/10.3389/fnins.2023.1154480>
- [31] A. Seeland, L. Manca, F. Kirchner, and E. A. Kirchner, “Spatio-temporal comparison between ERD/ERS and MRCP-based movement prediction,” *BIOSIGNALS 2015 - 8th International Conference on Bio-Inspired Systems and Signal Processing, Proceedings; Part of 8th International Joint Conference on Biomedical Engineering Systems and Technologies, BIOSTEC 2015*, pp. 219–226, 2015.
- [32] A. Kilicarslan, S. Prasad, R. G. Grossman, and J. L. Contreras-Vidal, “High accuracy decoding of user intentions using EEG to control a lower-body exoskeleton,” *Conference proceedings : ... Annual International Conference of the IEEE Engineering in Medicine and Biology Society. IEEE Engineering in Medicine and Biology Society. Annual Conference*, vol. 2013, pp. 5606–5609, 2013. [Online]. Available: <https://pubmed.ncbi.nlm.nih.gov/24111008https://www.ncbi.nlm.nih.gov/pmc/articles/PMC3801445/>
- [33] B. Güntekin and E. Başar, “Review of evoked and event-related delta responses in the human brain,” *International Journal of Psychophysiology*, vol. 103, pp. 43–52, 2016.
- [34] A. Kaplan, D. Zhigulskaya, and D. A. Kiriyanov, “Studying the ability to control human phantom fingers in P300 brain-computer interface,” *Bulletin of Russian State Medical University*, 2016.
- [35] L. A. Farwell and E. Donchin, “Talking off the top of your head: toward a mental prosthesis utilizing event-related brain potentials,” *Electroencephalography and Clinical Neurophysiology*, vol. 70, no. 6, pp. 510–523, 1988.
- [36] N. S. Kwak, K. R. Müller, and S. W. Lee, “A convolutional neural network for steady state visual evoked potential classification under ambulatory environment,” *PLoS ONE*, vol. 12, no. 2, pp. 1–20, 2017.
- [37] N.-S. Kwak, K.-R. Müller, and S.-W. Lee, “A lower limb exoskeleton control system based on steady state visual evoked potentials,” *Journal of Neural Engineering*,
-

-
- vol. 12, no. 5, p. 056009, oct 2015. [Online]. Available: <http://stacks.iop.org/1741-2552/12/i=5/a=056009?key=crossref.d574e38494295e53b491abb83540a57c>
- [38] G. Pfurtscheller and F. H. Lopes Da Silva, “Event-related EEG/MEG synchronization and desynchronization: Basic principles,” *Clinical Neurophysiology*, vol. 110, no. 11, pp. 1842–1857, 1999.
- [39] N. Mizuguchi and K. Kanosue, “Changes in brain activity during action observation and motor imagery: Their relationship with motor learning,” *Progress in Brain Research*, vol. 234, pp. 189–204, 2017.
- [40] A. H. Do, P. T. Wang, C. E. King, S. N. Chun, and Z. Nenadic, “Brain-computer interface controlled robotic gait orthosis,” *Journal of NeuroEngineering and Rehabilitation*, vol. 111, 2013.
- [41] E. García-Cossio, M. Severens, B. Nienhuis, J. Duysens, P. Desain, N. Keijsers, and J. Farquhar, “Decoding sensorimotor rhythms during robotic-assisted treadmill walking for brain computer interface (BCI) applications,” *PLoS ONE*, vol. 10, no. 12, pp. 1–21, 2015.
- [42] E. López-Larraz, F. Trincado-Alonso, V. Rajasekaran, S. Pérez-Nombela, A. J. Del-Ama, J. Aranda, J. Minguez, A. Gil-Agudo, and L. Montesano, “Control of an Ambulatory Exoskeleton with a Brain–Machine Interface for Spinal Cord Injury Gait Rehabilitation ,” p. 359, 2016. [Online]. Available: <https://www.frontiersin.org/article/10.3389/fnins.2016.00359>
- [43] V. Rajasekaran, E. López-Larraz, F. Trincado-Alonso, J. Aranda, L. Montesano, A. J. Del-Ama, and J. L. Pons, “Volition-adaptive control for gait training using wearable exoskeleton: Preliminary tests with incomplete spinal cord injury individuals,” *Journal of NeuroEngineering and Rehabilitation*, vol. 15, no. 1, pp. 1–15, 2018.
- [44] M. Rodríguez-Ugarte, E. Iáñez, M. Ortiz, and J. M. Azorín, “Improving Real-Time Lower Limb Motor Imagery Detection Using tDCS and an Exoskeleton ,” p. 757, 2018. [Online]. Available: <https://www.frontiersin.org/article/10.3389/fnins.2018.00757>
- [45] A. M. Batula, J. A. Mark, Y. E. Kim, and H. Ayaz, “Comparison of Brain Activation during Motor Imagery and Motor Movement Using fNIRS,” *Computational Intelligence and Neuroscience*, vol. 2017, p. 5491296, 2017. [Online]. Available: <https://doi.org/10.1155/2017/5491296>
-

- [46] M. Lotze and U. Halsband, “Motor imagery,” *Journal of Physiology-Paris*, vol. 99, no. 4, pp. 386–395, 2006. [Online]. Available: <https://www.sciencedirect.com/science/article/pii/S0928425706000210>
- [47] S. P. Ahlfors, J. Han, F.-H. Lin, T. Witzel, J. W. Belliveau, M. S. Hämäläinen, and E. Halgren, “Cancellation of EEG and MEG signals generated by extended and distributed sources.” *Human brain mapping*, vol. 31, no. 1, pp. 140–149, jan 2010.
- [48] S. Y. Gordleeva, M. V. Lukoyanov, S. A. Mineev, M. A. Khoruzhko, V. I. Mironov, A. Y. Kaplan, and V. B. Kazantsev, “Exoskeleton control system based on motor-imaginary brain-computer interface,” *Sovremennyye Tehnologii v Medicine*, vol. 9, no. 3, pp. 31–36, 2017.
- [49] Y. He, D. Eguren, J. M. Azorín, R. G. Grossman, T. P. Luu, and J. L. Contreras-Vidal, “Brain-machine interfaces for controlling lower-limb powered robotic systems,” *Journal of Neural Engineering*, vol. 15, no. 2, 2018.
- [50] G. H. Klem, H. O. Lüders, H. H. Jasper, and C. Elger, “The ten-twenty electrode system of the International Federation. The International Federation of Clinical Neurophysiology.” *Electroencephalography and clinical neurophysiology. Supplement*, vol. 52, pp. 3–6, 1999.
- [51] K. GH, L. HO, J. HH, and E. C, “The ten-twenty electrode system of the International Federation. The International Federation of Clinical Neurophysiology,” *Electroencephalography and Clinical neurophysiology*, vol. 52, pp. 3–6, 1999.
- [52] R. Oostenveld and P. Praamstra, “The five percent electrode system for high-resolution EEG and ERP measurements,” *Clinical Neurophysiology*, vol. 112, no. 4, pp. 713–719, 2001.
- [53] A. Kilicarslan, R. G. Grossman, and J. L. Contreras-Vidal, “A robust adaptive denoising framework for real-time artifact removal in scalp EEG measurements,” *Journal of Neural Engineering*, vol. 13, no. 2, 2016.
- [54] E. J. McDermott, P. Raggam, C. Zrenner, S. Kirsch, P. Belardinelli, and U. Ziemann, “Artifacts in EEG-based BCI therapies: Friend or foe?” *Sensors*, vol. 22, no. 1, pp. 1–18, 2022.
- [55] P. Grosse, M. J. Cassidy, and P. Brown, “EEG-EMG, MEG-EMG and EMG-EMG frequency analysis: Physiological principles and clinical applications,” *Clinical Neurophysiology*, vol. 113, no. 10, pp. 1523–1531, 2002.

-
- [56] S. H. F. Syam, H. Lakany, R. B. Ahmad, and B. A. Conway, “Comparing Common Average Referencing to Laplacian Referencing in Detecting Imagination and Intention of Movement for Brain Computer Interface,” *MATEC Web of Conferences*, vol. 140, 2017.
- [57] C. D. Binnie, “EEG, paediatric neurophysiology, special techniques and applications,” 2003.
- [58] F. F. OFFNER, “The EEG as potential mapping: the value of the average monopolar reference.” *Electroencephalography and clinical neurophysiology*, vol. 2, no. 2, pp. 213–214, may 1950.
- [59] Y. He, K. Nathan, A. Venkatakrisnan, R. Rovekamp, C. Beck, R. Ozdemir, G. E. Francisco, and J. L. Contreras-Vidal, “An integrated neuro-robotic interface for stroke rehabilitation using the NASA X1 powered lower limb exoskeleton,” *2014 36th Annual International Conference of the IEEE Engineering in Medicine and Biology Society, EMBC 2014*, no. August, pp. 3985–3988, 2014.
- [60] A. R. Donati, S. Shokur, E. Morya, D. S. Campos, R. C. Moioli, C. M. Gitti, P. B. Augusto, S. Tripodi, C. G. Pires, G. A. Pereira, F. L. Brasil, S. Gallo, A. A. Lin, A. K. Takigami, M. A. Aratana, S. Joshi, H. Bleuler, G. Cheng, A. Rudolph, and M. A. Nicolelis, “Long-Term Training with a Brain-Machine Interface-Based Gait Protocol Induces Partial Neurological Recovery in Paraplegic Patients,” *Scientific Reports*, vol. 6, no. August, pp. 1–16, 2016.
- [61] P. L. Nunez and A. F. Westdorp, “The surface Laplacian, high resolution EEG and controversies.” *Brain topography*, vol. 6, no. 3, pp. 221–226, 1994.
- [62] S. K. Law, J. W. Rohrbaugh, C. M. Adams, and M. J. Eckardt, “Improving spatial and temporal resolution in evoked EEG responses using surface Laplacians.” *Electroencephalography and clinical neurophysiology*, vol. 88, no. 4, pp. 309–322, 1993.
- [63] T. R. Mullen, C. A. E. Kothe, Y. M. Chi, A. Ojeda, T. Kerth, S. Makeig, T.-P. Jung, and G. Cauwenberghs, “Real-Time Neuroimaging and Cognitive Monitoring Using Wearable Dry EEG.” *IEEE transactions on bio-medical engineering*, vol. 62, no. 11, pp. 2553–2567, nov 2015.
- [64] W. S. Brown, J. T. Marsh, and J. C. Smith, “Principal component analysis of ERP differences related to the meaning of an ambiguous word,” *Electroencephalography and Clinical Neurophysiology*, vol. 46, no. 6, pp. 709–714, 1979. [Online]. Available: <https://www.sciencedirect.com/science/article/pii/001346947990110X>
-

-
- [65] Y. Zhang, S. Prasad, A. Kilicarslan, and J. L. Contreras-Vidal, “Multiple kernel based region importance learning for neural classification of gait states from EEG signals,” *Frontiers in Neuroscience*, vol. 11, no. APR, pp. 1–11, 2017.
- [66] P. Comon, “Independent component analysis, A new concept?” *Signal Processing*, vol. 36, no. 3, pp. 287–314, 1994. [Online]. Available: <https://www.sciencedirect.com/science/article/pii/0165168494900299>
- [67] S. Amari and A. Cichocki, “Adaptive blind signal processing-neural network approaches,” *Proceedings of the IEEE*, vol. 86, no. 10, pp. 2026–2048, 1998.
- [68] J. F. Cardoso, “Blind signal separation: statistical principles,” *Proceedings of the IEEE*, vol. 86, no. 10, pp. 2009–2025, 1998.
- [69] A. Delorme and S. Makeig, “EEGLAB: an open source toolbox for analysis of single-trial EEG dynamics including independent component analysis.” *Journal of neuroscience methods*, vol. 134, no. 1, pp. 9–21, mar 2004.
- [70] Á. Costa, E. Iáñez, A. Úbeda, E. Hortal, A. J. Del-Ama, Á. Gil-Agudo, and J. M. Azorín, “Decoding the Attentional Demands of Gait through EEG Gamma Band Features,” *PloS one*, vol. 11, no. 4, pp. e0154136–e0154136, apr 2016. [Online]. Available: <https://pubmed.ncbi.nlm.nih.gov/27115740https://www.ncbi.nlm.nih.gov/pmc/articles/PMC4846000/>
- [71] M. Tariq, P. M. Trivailo, and M. Simic, “EEG-Based BCI Control Schemes for Lower-Limb Assistive-Robots,” *Frontiers in Human Neuroscience*, vol. 12, no. August, 2018.
- [72] S. N. Resalat and V. Saba, “A Study of Various Feature Extraction Methods on a Motor Imagery Based Brain Computer Interface System.” *Basic and clinical neuroscience*, vol. 7, no. 1, pp. 13–19, jan 2016.
- [73] P. Goldberg, D. Samson-Dollfus, and F. Greymy, “[Spectrum analysis: Fast Fourier Transform].” *Agressologie: revue internationale de physio-biologie et de pharmacologie appliquees aux effets de l’agression*, vol. 10, pp. Suppl:541–52, jun 1969.
- [74] G. Dumermuth and H. Fluehler, “Re-introduction of the direct Fourier transformation in EEG spectral analysis.” *Electroencephalography and clinical neurophysiology*, vol. 26, no. 4, p. 440, apr 1969.
- [75] M. Ortiz, M. Rodriguez-Ugarte, E. Iáez, and J. M. Azorín, “Comparison of different EEG signal analysis techniques for an offline lower limb motor imagery brain-computer interface,” in *2018 40th Annual International Conference of the IEEE Engineering in Medicine and Biology Society (EMBC)*, 2018, pp. 203–206.
-

-
- [76] A. R. Haig, E. Gordon, V. De Pascalis, R. A. Meares, H. Bahramali, and A. Harris, “Gamma activity in schizophrenia: evidence of impaired network binding?” *Clinical neurophysiology : official journal of the International Federation of Clinical Neurophysiology*, vol. 111, no. 8, pp. 1461–1468, aug 2000.
- [77] M. Hansson-Sandsten, “Evaluation of the optimal lengths and number of multiple windows for spectrogram estimation of SSVEP.” *Medical engineering & physics*, vol. 32, no. 4, pp. 372–383, may 2010.
- [78] D. Liu, W. Chen, Z. Pei, and J. Wang, “A brain-controlled lower-limb exoskeleton for human gait training,” *Review of Scientific Instruments*, vol. 88, no. 10, p. 104302, oct 2017. [Online]. Available: <http://aip.scitation.org/doi/10.1063/1.5006461>
- [79] K.-K. Poh and P. Marziliano, “Analysis of neonatal EEG signals using Stockwell transform.” *Annual International Conference of the IEEE Engineering in Medicine and Biology Society. IEEE Engineering in Medicine and Biology Society. Annual International Conference*, vol. 2007, pp. 594–597, 2007.
- [80] X. Li, M. Chu, T. Qiu, and H. Bao, “[An EMD based time-frequency distribution and its application in EEG analysis].” *Sheng wu yi xue gong cheng xue za zhi = Journal of biomedical engineering = Shengwu yixue gongchengxue zazhi*, vol. 24, no. 5, pp. 990–995, oct 2007.
- [81] K. I. Panoulas, L. J. Hadjileontiadis, and S. M. Panas, “Hilbert-Huang Spectrum as a new field for the identification of EEG event related de-/synchronization for BCI applications.” *Annual International Conference of the IEEE Engineering in Medicine and Biology Society. IEEE Engineering in Medicine and Biology Society. Annual International Conference*, vol. 2008, pp. 3832–3835, 2008.
- [82] L. Wang, G. Xu, J. Wang, S. Yang, and W. Yan, “Application of Hilbert-Huang transform for the study of motor imagery tasks.” *Annual International Conference of the IEEE Engineering in Medicine and Biology Society. IEEE Engineering in Medicine and Biology Society. Annual International Conference*, vol. 2008, pp. 3848–3851, 2008.
- [83] N. E. Huang, Z. Shen, S. R. Long, M. C. Wu, H. H. Shih, Q. Zheng, N. Yen, C. C. Tung, and H. H. Liu, “The empirical mode decomposition and the Hilbert spectrum for nonlinear and non-stationary time series analysis,” *Proceedings of the Royal Society of London. Series A: Mathematical, Physical and Engineering Sciences*, vol. 454, pp. 903–995, 1998.
-

- [84] C. M. Sweeney-Reed and S. J. Nasuto, “A novel approach to the detection of synchronisation in EEG based on empirical mode decomposition.” *Journal of computational neuroscience*, vol. 23, no. 1, pp. 79–111, aug 2007.
- [85] H. Ramoser, J. Müller-Gerking, and G. Pfurtscheller, “Optimal Spatial Filtering of Single Trial EEG During Imagined Hand Movement,” *IEEE transactions on rehabilitation engineering : a publication of the IEEE Engineering in Medicine and Biology Society*, vol. 8, pp. 441–446, jan 2001.
- [86] A. Barachant, S. Bonnet, M. Congedo, and C. Jutten, *Riemannian Geometry Applied to BCI Classification*, sep 2010.
- [87] A. Craik, Y. He, and J. Contreras-Vidal, “Deep learning for Electroencephalogram (EEG) classification tasks: A review,” *Journal of Neural Engineering*, vol. 16, feb 2019.
- [88] C. E. Solorzano-Espindola, E. Zamora, and H. Sossa, “Multi-subject classification of Motor Imagery EEG signals using transfer learning in neural networks,” *Proceedings of the Annual International Conference of the IEEE Engineering in Medicine and Biology Society, EMBS*, pp. 1006–1009, 2021.
- [89] M. Jobert, C. Tismer, E. Poiseau, and H. Schulz, “Wavelets-a new tool in sleep biosignal analysis.” *Journal of sleep research*, vol. 3, no. 4, pp. 223–232, dec 1994.
- [90] J. Muthuswamy and N. V. Thakor, “Spectral analysis methods for neurological signals.” *Journal of neuroscience methods*, vol. 83, no. 1, pp. 1–14, aug 1998.
- [91] J. S. Huang, W. S. Liu, B. Yao, Z. X. Wang, S. F. Chen, and W. F. Sun, “Electroencephalogram-Based Motor Imagery Classification Using Deep Residual Convolutional Networks,” *Frontiers in Neuroscience*, vol. 15, no. November, pp. 1–8, 2021.
- [92] O. Y. Kwon, M. H. Lee, C. Guan, and S. W. Lee, “Subject-Independent Brain-Computer Interfaces Based on Deep Convolutional Neural Networks,” *IEEE Transactions on Neural Networks and Learning Systems*, vol. 31, no. 10, pp. 3839–3852, 2020.
- [93] F. Škola, S. Tinková, and F. Liarokapis, “Progressive Training for Motor Imagery Brain-Computer Interfaces Using Gamification and Virtual Reality Embodiment,” *Frontiers in Human Neuroscience*, vol. 13, p. 329, 2019. [Online]. Available: <https://www.frontiersin.org/article/10.3389/fnhum.2019.00329>

-
- [94] T. P. Luu, Y. He, S. Brown, S. Nakagome, and J. L. Contreras-Vidal, “A closed-loop brain computer interface to a virtual reality avatar: Gait adaptation to visual kinematic perturbations,” in *2015 International Conference on Virtual Rehabilitation (ICVR)*, jun 2015, pp. 30–37.
- [95] S. Dalbayrak, O. Yaman, and T. Yılmaz, “Current and future surgery strategies for spinal cord injuries,” *World journal of orthopedics*, vol. 6, no. 1, pp. 34–41, jan 2015. [Online]. Available: <https://pubmed.ncbi.nlm.nih.gov/25621209><https://www.ncbi.nlm.nih.gov/pmc/articles/PMC4303788/>
- [96] T. T. Roberts, G. R. Leonard, and D. J. Cepela, “Classifications In Brief: American Spinal Injury Association (ASIA) Impairment Scale,” *Clinical orthopaedics and related research*, vol. 475, no. 5, pp. 1499–1504, may 2017. [Online]. Available: <https://pubmed.ncbi.nlm.nih.gov/27815685><https://www.ncbi.nlm.nih.gov/pmc/articles/PMC5384910/>
- [97] W. Chay and S. Kirshblum, “Predicting Outcomes After Spinal Cord Injury,” *Physical Medicine and Rehabilitation Clinics of North America*, vol. 31, no. 3, pp. 331–343, 2020. [Online]. Available: <https://www.sciencedirect.com/science/article/pii/S104796512030022X>
- [98] J. H. Martin, “Chapter 22 - Neuroplasticity of spinal cord injury and repair,” in *Neuroplasticity*, ser. Handbook of Clinical Neurology, A. Quartarone, M. F. Ghilardi, and F. Boller, Eds. Elsevier, 2022, vol. 184, pp. 317–330. [Online]. Available: <https://www.sciencedirect.com/science/article/pii/B9780128194102000175>
- [99] J. R. Walker and M. R. Detloff, “Plasticity in Cervical Motor Circuits following Spinal Cord Injury and Rehabilitation,” 2021.
- [100] G. M. Innocenti, “Chapter 1 - Defining neuroplasticity,” in *Neuroplasticity*, ser. Handbook of Clinical Neurology, A. Quartarone, M. F. Ghilardi, and F. Boller, Eds. Elsevier, 2022, vol. 184, pp. 3–18. [Online]. Available: <https://www.sciencedirect.com/science/article/pii/B9780128194102000011>
- [101] J. K. Lotter, C. E. Henderson, A. Plawecki, M. E. Holthus, E. H. Lucas, M. M. Ardestani, B. D. Schmit, and T. G. Hornby, “Task-Specific Versus Impairment-Based Training on Locomotor Performance in Individuals With Chronic Spinal Cord Injury: A Randomized Crossover Study.” *Neurorehabilitation and neural repair*, vol. 34, no. 7, pp. 627–639, jul 2020.
- [102] L. Avanzino, N. Gueugneau, A. Bisio, P. Ruggeri, C. Papaxanthis, and M. Bove, “Motor cortical plasticity induced by motor learning through mental practice.” *Frontiers in behavioral neuroscience*, vol. 9, p. 105, 2015.
-

- [103] C. Ruffino, C. Papaxanthis, and F. Lebon, “Neural plasticity during motor learning with motor imagery practice: Review and perspectives,” *Neuroscience*, vol. 341, pp. 61–78, 2017. [Online]. Available: <https://www.sciencedirect.com/science/article/pii/S0306452216306443>
- [104] L. Xu, M. Xu, T. P. Jung, and D. Ming, “Review of brain encoding and decoding mechanisms for EEG-based brain–computer interface,” *Cognitive Neurodynamics*, vol. 15, no. 4, pp. 569–584, 2021. [Online]. Available: <https://doi.org/10.1007/s11571-021-09676-z>
- [105] A. Gharabaghi, “What Turns Assistive into Restorative Brain-Machine Interfaces?” *Frontiers in Neuroscience*, vol. 10, p. 456, 2016. [Online]. Available: <https://www.frontiersin.org/article/10.3389/fnins.2016.00456>
- [106] R. Rupp, “Challenges in clinical applications of brain computer interfaces in individuals with spinal cord injury,” *Frontiers in neuroengineering*, vol. 7, p. 38, sep 2014. [Online]. Available: <https://pubmed.ncbi.nlm.nih.gov/25309420https://www.ncbi.nlm.nih.gov/pmc/articles/PMC4174119/>
- [107] S. Gordleeva, M. V. Lukoyanov, S. Mineev, M. A. Khoruzhko, V. Mironov, A. Kaplan, and V. Kazantsev, “Exoskeleton Control System Based on Motor-Imaginary Brain–Computer Interface,” *Sovremennye tehnologii v medicine*, vol. 9, p. 31, sep 2017.
- [108] M. Mousavi and V. R. de Sa, “Motor imagery performance from calibration to online control in EEG-based brain-computer interfaces,” in *2021 10th International IEEE/EMBS Conference on Neural Engineering (NER)*, 2021, pp. 491–494.
- [109] P. K. Parashiva and A. P. Vinod, “Online Hand Motor Imagery Direction Decoding using Brain Computer Interface,” pp. 17–20, 2021.
- [110] N. Padfield, K. Camilleri, T. Camilleri, S. Fabri, and M. Bugeja, “A Comprehensive Review of Endogenous EEG-Based BCIs for Dynamic Device Control,” *Sensors*, vol. 22, no. 15, 2022. [Online]. Available: <https://www.mdpi.com/1424-8220/22/15/5802>
- [111] A. Kline, C. Gaina Ghiroaga, D. Pittman, B. Goodyear, and J. Ronsky, “EEG differentiates left and right imagined Lower Limb movement,” *Gait & Posture*, vol. 84, pp. 148–154, 2021. [Online]. Available: <https://www.sciencedirect.com/science/article/pii/S0966636220306391>

-
- [112] C. Wang, X. Wu, Z. Wang, and Y. Ma, “Implementation of a Brain-Computer Interface on a Lower-Limb Exoskeleton,” *IEEE Access*, vol. 6, pp. 38 524–38 534, 2018.
- [113] P. Barria, A. Pino, N. Tovar, D. Gomez-Vargas, K. Baleta, C. A. R. Díaz, M. Múnica, and C. A. Cifuentes, “BCI-Based Control for Ankle Exoskeleton T-FLEX: Comparison of Visual and Haptic Stimuli with Stroke Survivors.” *Sensors (Basel, Switzerland)*, vol. 21, no. 19, sep 2021.
- [114] J. Choi, K. T. Kim, J. H. Jeong, L. Kim, S. J. Lee, and H. Kim, “Developing a Motor Imagery-Based Real-Time Asynchronous Hybrid BCI Controller for a Lower-Limb Exoskeleton.” *Sensors (Basel, Switzerland)*, vol. 20, no. 24, dec 2020.
- [115] S. Y. Gordleeva, S. A. Lobov, N. A. Grigorev, A. O. Savosenkov, M. O. Shamshin, M. V. Lukoyanov, M. A. Khoruzhko, and V. B. Kazantsev, “Real-Time EEG-EMG human-machine interface-based control system for a lower-limb exoskeleton,” *IEEE Access*, vol. 8, pp. 84 070–84 081, 2020.
- [116] F. Malouin, P. L. Jackson, and C. L. Richards, “Towards the integration of mental practice in rehabilitation programs. A critical review.” *Frontiers in human neuroscience*, vol. 7, p. 576, sep 2013.
- [117] M. Ortiz, E. Iáñez, J. Gaxiola, A. Kilicarslan, J. M. Azorín, and S. Member, “Assessment of motor imagery in gamma band using a lower limb exoskeleton,” in *IEEE International Conference on Systems, Man and Cybernetics (SMC)*. Bari: IEEE, 2019, pp. 2773–2778.
- [118] A. Singh, A. A. Hussain, S. Lal, and H. W. Guesgen, “A Comprehensive Review on Critical Issues and Possible Solutions of Motor Imagery Based Electroencephalography Brain-Computer Interface,” *Sensors*, vol. 21, no. 6, 2021. [Online]. Available: <https://www.mdpi.com/1424-8220/21/6/2173>
- [119] X. Zhang, Q. She, Y. Chen, W. Kong, and C. Mei, “Sub-band target alignment common spatial pattern in brain-computer interface.” *Computer methods and programs in biomedicine*, vol. 207, p. 106150, aug 2021.
- [120] L. Ferrero, V. Quiles, M. Ortiz, J. V. Juan, E. Iáñez, and J. M. Azorín, “Inter-session Transfer Learning in MI Based BCI for Controlling a Lower-Limb Exoskeleton,” in *Bio-inspired Systems and Applications: from Robotics to Ambient Intelligence*, J. M. Ferrández Vicente, J. R. Álvarez Sánchez, F. de la Paz López, and H. Adeli, Eds. Cham: Springer International Publishing, 2022, pp. 243–252.
-

-
- [121] H. He and D. Wu, “Transfer Learning for Brain-Computer Interfaces: A Euclidean Space Data Alignment Approach.” *IEEE transactions on bio-medical engineering*, vol. 67, no. 2, pp. 399–410, feb 2020.
- [122] Z. Khademi, F. Ebrahimi, and H. M. Kordy, “A review of critical challenges in MI-BCI: From conventional to deep learning methods,” *Journal of Neuroscience Methods*, vol. 383, no. October 2022, p. 109736, 2023. [Online]. Available: <https://doi.org/10.1016/j.jneumeth.2022.109736>
- [123] S. Becker, K. Dhindsa, L. Mousapour, and Y. Al Dabagh, “BCI Illiteracy: It’s Us, Not Them. Optimizing BCIs for Individual Brains,” in *2022 10th International Winter Conference on Brain-Computer Interface (BCI)*, 2022, pp. 1–3.
- [124] C. Vidaurre and B. Blankertz, “Towards a cure for BCI illiteracy.” *Brain topography*, vol. 23, no. 2, pp. 194–198, jun 2010.
- [125] V. J. Samar, A. Bopardikar, R. Rao, and K. Swartz, “Wavelet analysis of neuroelectric waveforms: a conceptual tutorial.” *Brain and language*, vol. 66, no. 1, pp. 7–60, jan 1999.
- [126] M. Ende, A. K. Louis, P. Maass, and G. Mayer-Kress, “EEG Signal Analysis by Continuous Wavelet Transform Techniques BT - Nonlinear Analysis of Physiological Data,” H. Kantz, J. Kurths, and G. Mayer-Kress, Eds. Berlin, Heidelberg: Springer Berlin Heidelberg, 1998, pp. 213–219.
- [127] A. Izenman, “Linear Discriminant Analysis,” in *Modern Multivariate Statistical Techniques*, Springer Texts in Statistics, Ed. New York: Springer.
- [128] B. D. Rainford and G. J. Daniell, “ μ SR frequency spectra using the maximum entropy method,” *Hyperfine Interactions*, vol. 87, no. 1, pp. 1129–1134, 1994. [Online]. Available: <https://doi.org/10.1007/BF02068515>
- [129] M. Torkamani-Azar, A. Jafarifarmand, and M. Cetin, “Prediction of Motor Imagery Performance based on Pre-Trial Spatio-Spectral Alertness Features.” *Annual International Conference of the IEEE Engineering in Medicine and Biology Society. IEEE Engineering in Medicine and Biology Society. Annual International Conference*, vol. 2020, pp. 3062–3065, jul 2020.
- [130] J. Solomon O M, “PSD computations using Welch’s method. [Power Spectral Density (PSD)],” United States, Tech. Rep., 1991. [Online]. Available: <https://www.osti.gov/biblio/5688766https://www.osti.gov/servlets/purl/5688766>
-

- [131] N. Leeuwis, A. Paas, and M. Alimardani, “Vividness of Visual Imagery and Personality Impact Motor-Imagery Brain Computer Interfaces.” *Frontiers in human neuroscience*, vol. 15, p. 634748, 2021.
- [132] M. Rodriguez Ugarte, E. Iáñez, M. García, and J. Azorin, “Personalized Offline and Pseudo-Online BCI Models to Detect Pedaling Intent,” *Frontiers in Neuroinformatics*, vol. 11, jul 2017.
- [133] C. Zich, M. De Vos, C. Kranczioch, and S. Debener, “Wireless EEG with individualized channel layout enables efficient motor imagery training,” *Clinical Neurophysiology*, vol. 126, no. 4, pp. 698–710, 2015. [Online]. Available: <http://dx.doi.org/10.1016/j.clinph.2014.07.007>
- [134] L. Ferrero, V. Quiles, M. Ortiz, E. Iáñez, and J. M. Azorín, “BCI Based on Lower-Limb Motor Imagery and a State Machine for Walking on a Treadmill,” *International IEEE EMBS Conference on Neural Engineering*, 2020.
- [135] T. Zhang, T. Liu, F. Li, M. Li, D. Liu, R. Zhang, H. He, P. Li, J. Gong, C. Luo, D. Yao, and P. Xu, “Structural and functional correlates of motor imagery BCI performance: Insights from the patterns of fronto-parietal attention network.” *NeuroImage*, vol. 134, pp. 475–485, jul 2016.
- [136] N. Robinson, K. P. Thomas, and A. P. Vinod, “Neurophysiological predictors and spectro-spatial discriminative features for enhancing SMR-BCI.” *Journal of neural engineering*, vol. 15, no. 6, p. 66032, dec 2018.

Anexo A. Compendio de publicaciones

En esta sección se adjuntan las publicaciones que forman parte del compendio de publicaciones de la presente tesis doctoral.



Sensory Integration in Human Movement: A New Brain-Machine Interface Based on Gamma Band and Attention Level for Controlling a Lower-Limb Exoskeleton

Mario Ortiz^{1,2*}, Laura Ferrero¹, Eduardo Iáñez¹, José M. Azorín¹ and José L. Contreras-Vidal²

¹ Brain-Machine Interface Systems Lab, Miguel Hernández University of Elche, Elche, Spain, ² Laboratory for Non-invasive Brain Machine Interfaces, Department of Electrical and Computer Engineering, University of Houston, Houston, TX, United States

OPEN ACCESS

Edited by:

Massimo Sartori,
University of Twente, Netherlands

Reviewed by:

Salvatore Andrea Pullano,
University Magna Graecia of
Catanzaro, Italy
Jakob Dideriksen,
Aalborg University, Denmark

*Correspondence:

Mario Ortiz
mortiz@umh.es

Specialty section:

This article was submitted to
Bionics and Biomimetics,
a section of the journal
Frontiers in Bioengineering and
Biotechnology

Received: 30 December 2019

Accepted: 10 June 2020

Published: 03 September 2020

Citation:

Ortiz M, Ferrero L, Iáñez E, Azorín JM
and Contreras-Vidal JL (2020)
Sensory Integration in Human
Movement: A New Brain-Machine
Interface Based on Gamma Band and
Attention Level for Controlling a
Lower-Limb Exoskeleton.
Front. Bioeng. Biotechnol. 8:735.
doi: 10.3389/fbioe.2020.00735

Brain-machine interfaces (BMIs) can improve the control of assistance mobility devices making its use more intuitive and natural. In the case of an exoskeleton, they can also help rehabilitation therapies due to the reinforcement of neuro-plasticity through repetitive motor actions and cognitive engagement of the subject. Therefore, the cognitive implication of the user is a key aspect in BMI applications, and it is important to assure that the mental task correlates with the actual motor action. However, the process of walking is usually an autonomous mental task that requires a minimal conscious effort. Consequently, a brain-machine interface focused on the attention to gait could facilitate sensory integration in individuals with neurological impairment through the analysis of voluntary gait will and its repetitive use. This way the combined use of BMI+exoskeleton turns from assistance to restoration. This paper presents a new brain-machine interface based on the decoding of gamma band activity and attention level during motor imagery mental tasks. This work also shows a case study tested in able-bodied subjects prior to a future clinical study, demonstrating that a BMI based on gamma band and attention-level paradigm allows real-time closed-loop control of a Rex exoskeleton.

Keywords: brain-machine interface, EEG, gamma band, lower-limb exoskeleton, motor imagery, human movement, sensory integration, Stockwell Transform

1. INTRODUCTION

Stroke, spinal cord injury (SCI), and limb loss are some of the most common causes of acquired motor disabilities in adults, being the restoration of motor function often incomplete. Normally, therapists try to recover some residual ability for movement when possible, acting over the distal physical level, trying to influence the neural system through mechanisms of neural plasticity (Ang and Guan, 2013). Traditional therapies focus on improving the functional ambulation for patients in the sub-acute phase, using overground training. This requires the design of preparatory exercises, the observation by a physical therapist and the direct manipulation of the limbs during gait over a regular surface, followed by supervised walking. Orthosis and prosthesis devices have

been developed in the last years in order to assist people with motor limitations (Contreras-Vidal et al., 2016). The introduction of these robotic devices into rehabilitation therapies can further improve them (Bortole et al., 2015). Regarding the control, EMG-based interfaces can be used to control prosthesis (Villarejo Mayor et al., 2017), but a Brain-Machine Interface (BMI) offers a more suitable option to control a mechanical device, such as a speller or a wheelchair (Li et al., 2014), and exoskeletons or robotic orthosis (Do et al., 2013; Kilicarslan et al., 2013; López-Larraz et al., 2016; Liu et al., 2017). In addition, a BMI can improve neuroplasticity during rehabilitation therapies through the cognitive engagement of the subject (Cramer, 2008; Gharabaghi, 2016; Barrios et al., 2017), a fact that has been proved in clinical studies (Donati et al., 2016).

One of the most common paradigms used for BMIs to decode the brain activity is motor imagery (MI). It has been demonstrated that the mental task of imaging a movement produces similar brain patterns to the actual motion (Stippich et al., 2002; Bakker et al., 2007; Batula et al., 2017). Feature extraction of MI is usually based on the frequency analysis of the subject's electroencephalographic signals (EEG) in alpha (8 – 12 Hz) and beta bands (12 – 32 Hz) (Pfurtscheller et al., 2006), or delta bands (0.1 – 4 Hz) (Bradberry et al., 2010; Presacco et al., 2011). However, there are not many studies that focus on gamma bands (32 – 100 Hz). Recently, the gamma band has been related to gait attention (Costa et al., 2016; Costa-García et al., 2019). However, the actual action of walking does not demand high attention from the individual, as it is usually involving a subconscious mental task. Besides, the subject can be affected by external sensory distractions that can reduce the level of cognitive engagement associated with the MI task. For this reason, it is important to assess the attention level that the subject keeps during the mental task of controlling the robotic device. This way, it can be assured that the cognitive engagement of the subject is high during the therapy, and that the control outputs are accurate and associated with the mental process of rehabilitation. This allows to turn assistive BMIs into restorative BMIs (Gharabaghi, 2016).

The present research combines two different paradigms in order to propose a new BMI for controlling a lower-limb exoskeleton. First, a new BMI based on MI for gamma band is presented. The current work expands the initial research developed in Ortiz et al. (2019), studying the real-time feasibility of the new MI paradigm in an opened-loop and closed-loop control scenario. Second, the BMI proposed in Costa-García et al. (2019) is adapted to the current research in order to evaluate the attention to gait based on a dual task paradigm. The attention level provides this way, a measurement of the cognitive engagement of the subject during the use of an exoskeleton, fact that has not been studied previously in literature. This information could be provided during rehabilitation therapies to the subject and clinical staff to assess the degree of engagement during the MI mental task. Finally, the viability of the combination of the attention level to gait as a modifier for the initial MI paradigm is studied. The objective is to see if the combination of both paradigms allows to operate the exoskeleton with a higher accuracy. This new approach has been tested with

several able-bodied volunteers, as a preliminary study before its employment with patients in a second stage of the research. The results show that the proposed BMI can be used for real-time closed-loop operation of a Rex exoskeleton.

2. MATERIALS AND METHODS

This section describes the experimental setup, the equipment used, the data processing methods and the indices used for assessment.

2.1. Equipment

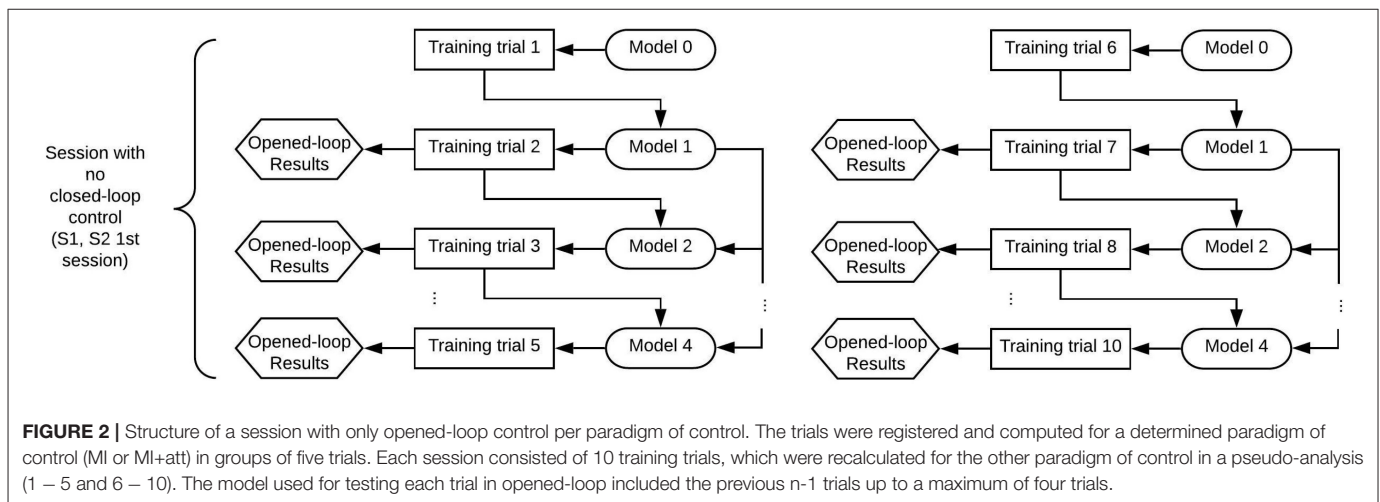
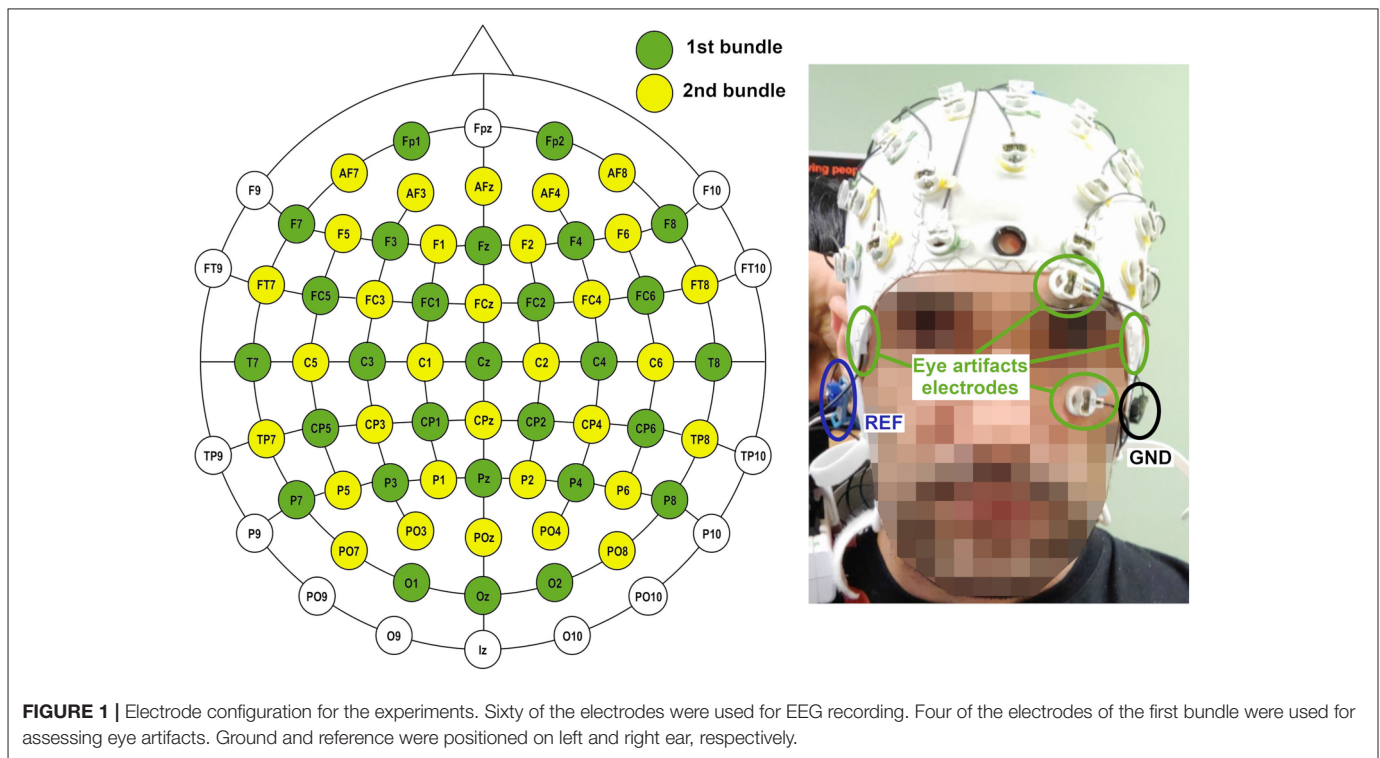
Data acquisition was accomplished by two non-invasive bundles of 32 wet scalp electrodes over an easyCap unit (Brain Products GmbH, Germany). The cap followed the 10–10 distribution of the international system. Four of the electrodes of the first bundle (see **Figure 1**) were placed around the eyes in a bipolar setup to assess the contribution of blinking to artifacts. Reference and ground electrodes were positioned on both ears. Data were transferred by wireless communication using a Move transmitter (Brain Products GmbH, Germany) for their posterior amplification by two brainAmp units (Brain Products GmbH, Germany) and their processing and recording in a laptop.

The exoskeleton used was the Rex (Rex Bionics, New Zealand). The exoskeleton was controlled by wireless communication. The feedback information of the current status of the Rex was acquired by the computer through a wire serial port communication with a custom developed software. Rex exoskeleton has several characteristics which make it different from other lower-limb exoskeletons. First, it is a self-standing exoskeleton that does not require any crutches and that allows a full standing walking without any vertical inclination. In addition, its walking pattern is very peculiar and far from the anthropomorphic usual gait. The choice of this exoskeleton was made based on the movement limitations it provides. In a Rex exoskeleton, the limbs of the subject are tightly attached to the robotic prosthesis by several straps, avoiding any lower limb movement. This way, the subject can only move their legs when the exoskeleton does, avoiding any lower-limb movement not commanded by the BMI.

2.2. Experimental Setup

2.2.1. Subjects

Four able-bodied subjects (S1–S4) took part in the experiments. The subjects did not report any known disease and participated voluntarily in the research, giving written and informed consent. All the procedures were approved by the Institutional Review Board of the University of Houston, TX (USA). The research included two different experiments. S1 and S2 participated in the initial opened-loop experiments, which were used to set up the initial algorithms of both BMIs (only MI and MI+attention). Additionally, subjects S2–S4 participated in the sessions which were designed with the objective to test the initial results in a closed-loop control scenario. S1 could not participate in the closed-loop experiments due to malfunctioning of the electrodes.



2.2.2. Subject Preparation

Preparation of the subject included two different steps. First the limb length of the exoskeleton was adjusted to the subject. After that, the electrodes were gelled to a value lower than $30k\Omega$. Electrode's impedance was checked before starting the trials and after finishing to be sure no electrodes were marginally over the $30k\Omega$ value. Full process for both tasks could take around an hour. Before starting data collection, a medical mesh was positioned over the cap to avoid any wire movement and mitigate motion artifacts. Before starting, several runs of walking by manual control were accomplished in order to get the subject used to the Rex movement.

2.2.3. Protocols

Figures 2, 3 show the structure of both kind of sessions (only opened-loop control and with closed-loop control). First sessions of the research included only training trials that were controlled in opened-loop. Once the paradigms were set-up based on the first sessions data, experimental sessions included test trials which were controlled in closed-loop. Following paragraphs detail the characteristic of both kind of trials.

2.2.3.1. Training trials

Training trials were the ones used for creating the classifier model of each paradigm control (MI or MI+attention). As

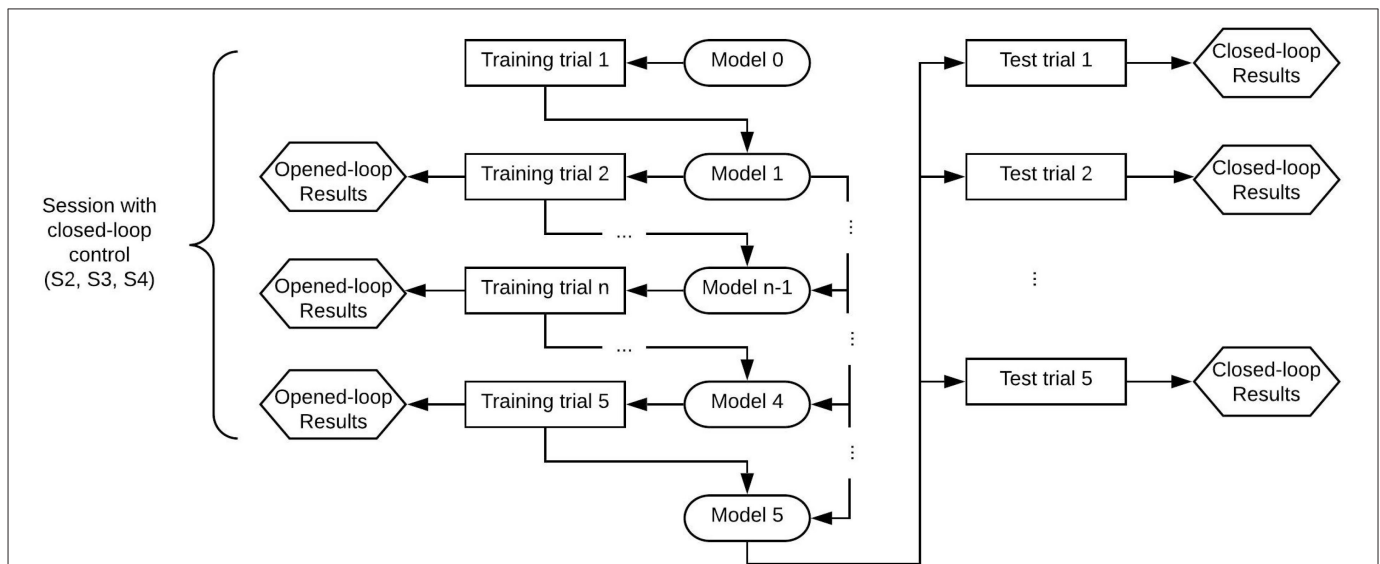


FIGURE 3 | Structure of a session with closed-loop control per paradigm of control. The subject performed the whole diagram once per each paradigm of control (MI and MI+att). Each paradigm consisted of five training and five tests trials, so each session consisted of 20 trials. The test trials were tested with the specific trained model.

the developed tool always works in real time, first training trial needs a generic model 0 (randomized data) in order to be processed. The output results of the first training trial were not considered for this reason, as the trial was classified with a model which contains data that was not related to the subject. Subsequent training trials were tested in opened-loop control with the model of the previous $n-1$ trials of the subject. As real-time analysis can be done for only a specific algorithm of control (MI or MI+attention), trials were run with an specific kind of model paradigm. However, a pseudo-online analysis for the other control paradigm was run to compare the performance of both paradigms, as it will be seen in results section.

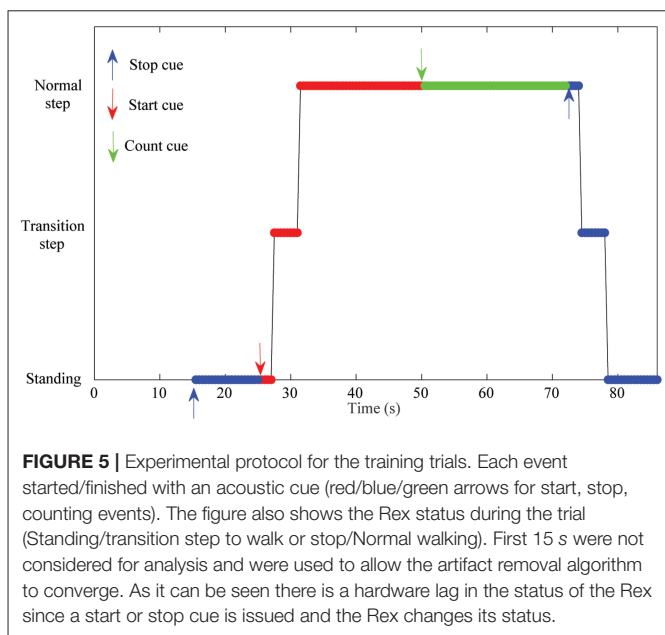
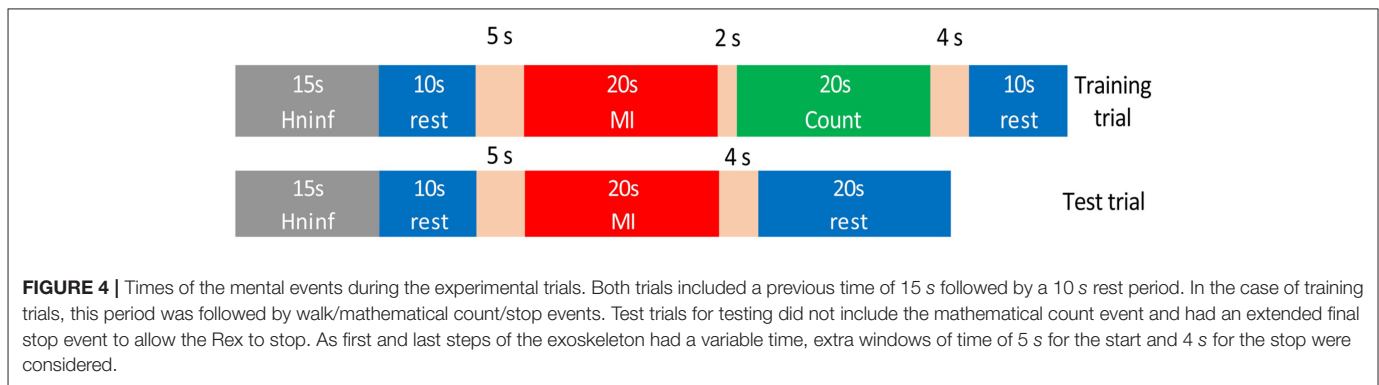
The protocol of a training trial included three different mental tasks (see **Figure 4**). First, 15 s were not used for classification as they were needed for the convergence of the H^∞ eye blinking artifact removal algorithm (Kilicarslan et al., 2016). In addition, these seconds helped the subject to feel relaxed before the start of the trial. After that, an acoustic cue marked the start of a rest/standing event, which ended by another acoustic cue for starting the MI event and the Rex activation. After at least 20 s of normal exoskeleton walking, a new acoustic cue indicated the start of a reverse mental count. This mathematical task substituted the original mathematical operations used in Costa-García et al. (2019) for the assessment of the low attention to gait, as it was difficult to attach a tablet to the Rex exoskeleton without disturbing the subject. The mental operation consisted of an accumulative counting of $1,000 \pm 7$. The \pm was changed randomly between trials to avoid the repetition of the numbers and any memorization of the operations by the subject. The counting event was used as a distracting mental task to assure that the focus of the subject was not on the gait during the Rex walking. This counting also worked as a control class to

detect if the output differences in the MI class were related to motion artifacts. As the Rex is moving in the same way during MI and counting periods, the output differences were just related to the mental processes. In addition, to take into account the time that the exoskeleton needs to perform the transition step to start or to stop, additional windows of time of 5 s for the start (2 s for the cue influence +3 s for the transition step) and 4 s for the stop were considered. Status of the Rex can be seen in **Figure 5** operating in an opened-loop control. As it can be seen in the image, there is some inherent lag since the real command is issued, which in training trials is coincidental with difference between the acoustic cue (start or stop) and the moment the Rex initiates the transition step or achieves the reference status (normal walking or standing position).

2.2.3.2. Test trials

Test trials were run in real-time closed-loop control in order to assess the BMI behavior. The model that used the test trials consisted of the previous five training trials acquired.

The trials used for testing the BMIs were similar to the training ones, but without the count event, see lower part of **Figure 4**. In order to give enough time for the Rex to stop, the final rest event was expanded to 20 s, as the lag introduced by the Rex between the issue of a stop command and an actual stop can last over 7 s depending on the position of the mechanical limbs. This is because final standing position must leave both limbs in parallel, requiring sometimes to fulfill a full last step plus the transition step before stopping. The command to start or to stop the Rex was issued only when a decision command output was created by the BMI based on the output of the classifier.



2.3. Signal Processing

The whole signal processing scheme can be seen in **Figure 6**. The following paragraphs will describe it for the different processing paradigms.

2.3.1. Initial Pre-processing

One of the most difficult problems a BMI based on non-invasive EEG must confront is the presence of artifacts which could spoil the information contained in the EEG signal. This is especially difficult in the case of real-time algorithms, as no offline analysis mitigation is possible. The movement of the Rex is slow enough to not have important motion artifacts. Nevertheless, the electrode’s wires were carefully attached using plastic clamps and a medical mesh was placed over the cap in order to avoid any fluctuation of the wires. In addition, subjects were advised to avoid any swallowing or chewing during the experiment. In order to mitigate the artifacts associated with eye blinking, H^∞ (Kilicarslan et al., 2016) algorithm was applied (see **Figure 1** for detail of the electrodes used for H^∞). As the algorithm needed to work in a real-time scenario, the sampling frequency of the

original data was resampled from 1 kHz to 200Hz, applying each sample for a variable state function for an anti-aliasing low-pass filter. The filter was designed to maintain the Shannon sampling theorem requirements, with cut-off frequency equal to the new Nyquist frequency (Vaidyanathan, 1993). The 200 Hz frequency was chosen as a compromise between frequency resolution (allowing the extraction of γ band) and the processing speed of an epoch of 1 s length. This value was based on the preliminary analysis of former Rex data by the lab and the first of the opened-loop sessions. Time processing was an important issue as each epoch shifted every 0.5 s. Therefore, the whole processing time since an epoch was collected and a command decision was taken (see **Figure 6**) should be below 0.5 s for all the epochs in a trial. This was accomplished for the pseudo-online and online analyses requiring and optimization of the code not usually needed in an offline analysis.

After the signal was resampled and free of ocular artifacts, a standardization process was accomplished. This step is important to give the same weight to different electrodes for the MI and attention paradigms and to avoid that the changes in the EEG voltages of the subject between training and test trials can affect the classification. The standardization process was similar to the one presented in Costa et al. (2016) using the maximum visual threshold (MV). For each electrode i , it is computed based on its voltage V , and updated for each epoch $m = 1 : N$ of the trial, with a length of L samples as:

$$MV^i = \frac{1}{N} \sum_{m=1}^N \max \left[abs \left(V_{(m-1) \cdot L + 1 : m \cdot L}^i \right) \right] \quad (1)$$

Being the standardized voltage of the electrode i per each sample at time t :

$$SV^i(t) = \frac{V^i(t)}{\frac{1}{60} \sum_{j=1}^{60} MV^j} \quad (2)$$

For the first epoch of the first training trial, the BMI takes the MV thresholds of the generic model 0 file, based on the data of a former subject. This information is updated for each epoch, converging to a stable value after several seconds, so it does not affect the epochs in the events under analysis. Following trials use the updated thresholds of previous trials, so model 0 is just

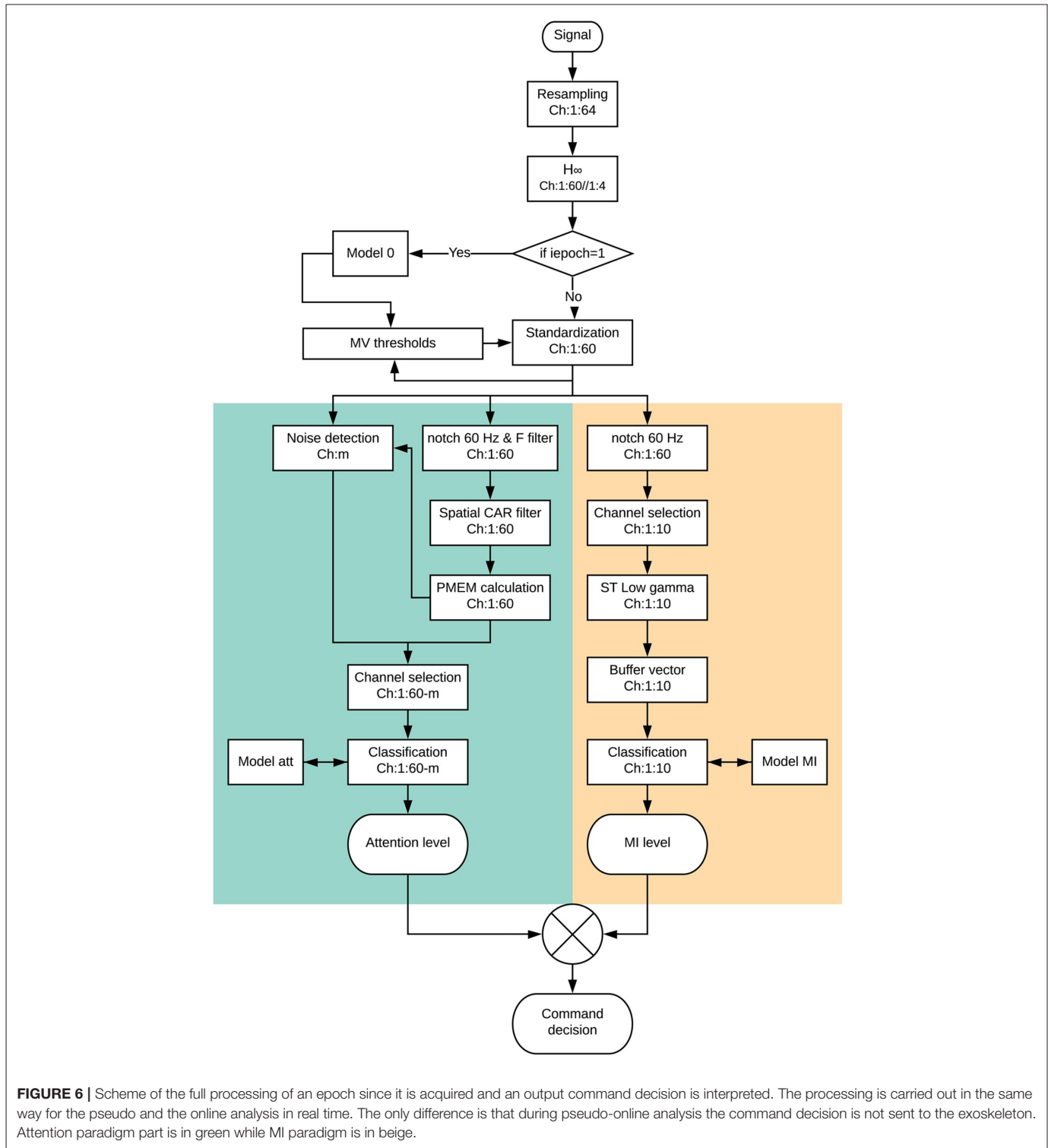


FIGURE 6 | Scheme of the full processing of an epoch since it is acquired and an output command decision is interpreted. The processing is carried out in the same way for the pseudo and the online analysis in real time. The only difference is that during pseudo-online analysis the command decision is not sent to the exoskeleton. Attention paradigm part is in green while MI paradigm is in beige.

used for the initial seconds of the first training trial as a way to accelerate the MV convergence.

2.3.2. Attention Level Paradigm

The attention level BMI is based on the previous research published in Costa-García et al. (2019). However, it is

particularized for the 60 EEG channels of the proposed setup instead of the original 31 channels, and the mental tasks of this research, as it is not possible for the Rex to follow ground stamps.

The first step is to detect the presence of any residual noise in the signal. An epoch of electrode *i* is considered as noisy if the instant MV threshold is over 150 μV , its instant kurtosis is over

15 μV , and its spectral power obtained by the maximum entropy method is not over 14 μV^2 .

Regarding the data processing, first a notch filter at 60 Hz and a fourth order Butterworth band-pass filter (5–90 Hz) is applied to the epoch, followed by a spatial Common Average Reference filter (McFarland et al., 1997). After that, the power spectral density of the channel is computed by the maximum entropy method (Rainford and Daniell, 1994) for the bands between 30–55 and 65–90 Hz. Bands were changed from the original research due to the different line frequency in the USA.

In order to consider an epoch as valid for attention level assessment, at least 21 channels must be not noisy. If this is not the case, the attention level is considered as the one of the previous epoch (please check Costa-García et al., 2019 for further information of the method). This means that the feature data vector can range between 21 and 60 data. Nevertheless, due to the extended number of channels in this research, and the preliminary artifact filters, this was not needed in practice, as the noise content was below the original research.

For the classification, three different classes were considered: rest, count and walk. Rest class contains the epochs of the standing rest periods of the Rex (standing blue parts in **Figure 5**, about 20 s); count data consists of the 20 s of walking mathematical operations (green part in **Figure 5** neglecting the 2 s after the count cue); and walk class is based on the normal step walking periods (upper red part in **Figure 5**, about 20 s). Due to the uncertain time needed to do the transition steps, rest and walk periods can have slightly different number of epochs. However, the difference is not high enough to unbalance the classes.

The classifier uses a Linear Discriminant Analysis (LDA) algorithm, which is a generalization of Fishers Discriminant classifier (Izenman, 2013). For the opened-loop analysis, the model is created using the data-set of the previous training trials. This means that trial i is classified with the information of training trials $1:i-1$. In the case of the closed-loop testing, the model is created with the five associated training trials (see **Figures 2, 3**). The first training trial needs a generalized model 0 to be processed as there is not previous model data and the tool works always in real-time for all the registers. This output can not be used for assessment as it is not relevant. This is the reason why opened-loop analysis shows only the information of training trials $2-5$.

After each epoch is classified, a weight is assigned depending on the output label. If the output corresponds to a rest or count label, an attention value of 0 is assigned and if it is a walk a 1. This value is then averaged for the last 10 epochs. This means that for obtaining a maximum attention value of 1, 10 consecutive epochs must be classified (5 s due to the shifting). Considering the data acquisition lag (+0.5 s) means that at least 5.5 s are needed to achieve a perfect attention level. This is important to understand that certain lag is inherent to the assessment method. This way, a medium level attention is considered when it is over 0.25 and a high level over 0.5 (around 3 s of consecutive walk detection). An example of the attention level can be seen in **Figure 7** as the bars of the attention paradigm image (down). Each of the classifications can be seen in the image as a ●.

2.3.3. Motor Imagery Paradigm

The MI BMI is based on the preliminary study developed in Ortiz et al. (2019). In that research, a BMI based on γ band was presented and the conclusion extracted was that γ band could be used for commanding an exoskeleton with a low false positive ratio. However, the study was limited to one subject and tested in an offline scenario. In the present research some changes have been done to the former BMI to allow its use in real time and in coordination with the attention level BMI for commanding the Rex exoskeleton in closed-loop control.

As it can be seen in **Figure 5**, data is first notch filtered at 60 Hz. The rest of the processing is applied to the central electrodes associated with MI tasks: Fz, FC1, FCz, FC2, C1, Cz, C2, CP1, CPz, and CP2.

Regarding the feature extraction, this is done using Stockwell Transform (ST) for each epoch (Stockwell et al., 1996). Although ST is applied to the whole epoch (1 s), in order to avoid border effects the information considered is extracted from 0.25 to 0.75 s of each epoch. This means, that each epoch overlaps information for a quarter of second, as epochs are shifted at a 0.5 s pace. Once ST is computed, the instantaneous power of the voices from 30 to 55 Hz lower γ band is added. This changes from the original research that used the maximum peaks of the low and high γ bands. Preliminary studies using the S1, and S2 training data revealed that high γ band did not produce a significant improvement of accuracy, while its no consideration kept the processing times below the shifting time. Besides, the addition of power, instead of the computation of the maximum peak, produced slightly better results without affecting the computation times.

The buffer for smoothing the output was extended to 4 s in this research (this contains data since 4.5 s due to +0.5 s needed for acquisition). This is a compromise between 3 s needed for a medium attention level and the 5.5 s for a high attention level. An example for the smoothed value of electrode Cz can be seen as standardized power in the upper image of **Figure 7**.

This smoothed value is averaged afterwards for each epoch to obtain the associated feature of each electrode. This is another difference in comparison with the former research, as the calculation of the features is done by each individual electrode and epoch and its value is not averaged for the 10 electrodes (Ortiz et al., 2019). This allows to use the 10 features per epoch as a vector data for the LDA classifier.

Regarding the classifier, only two classes are considered, walk and rest, instead of the three classes of the attention model. Similarly to the attention BMI, depending on the output label of the classifier, a 0 is assigned to each epoch for a rest detection and a 1 for walk. This way, the MI level is computed in an analog way to the attention paradigm, see MI paradigm (center) image of **Figure 7**. In the same way than the attention paradigm, the MI level is shown as bars and the classifier output as a ●.

2.3.4. Command Decision

Once the MI and attention levels are assessed, they are used to create a decision for the output command of the BMI. In the case of the opened-loop trials, the information is recorded for its evaluation, while in the case of closed-loop trials it is sent to

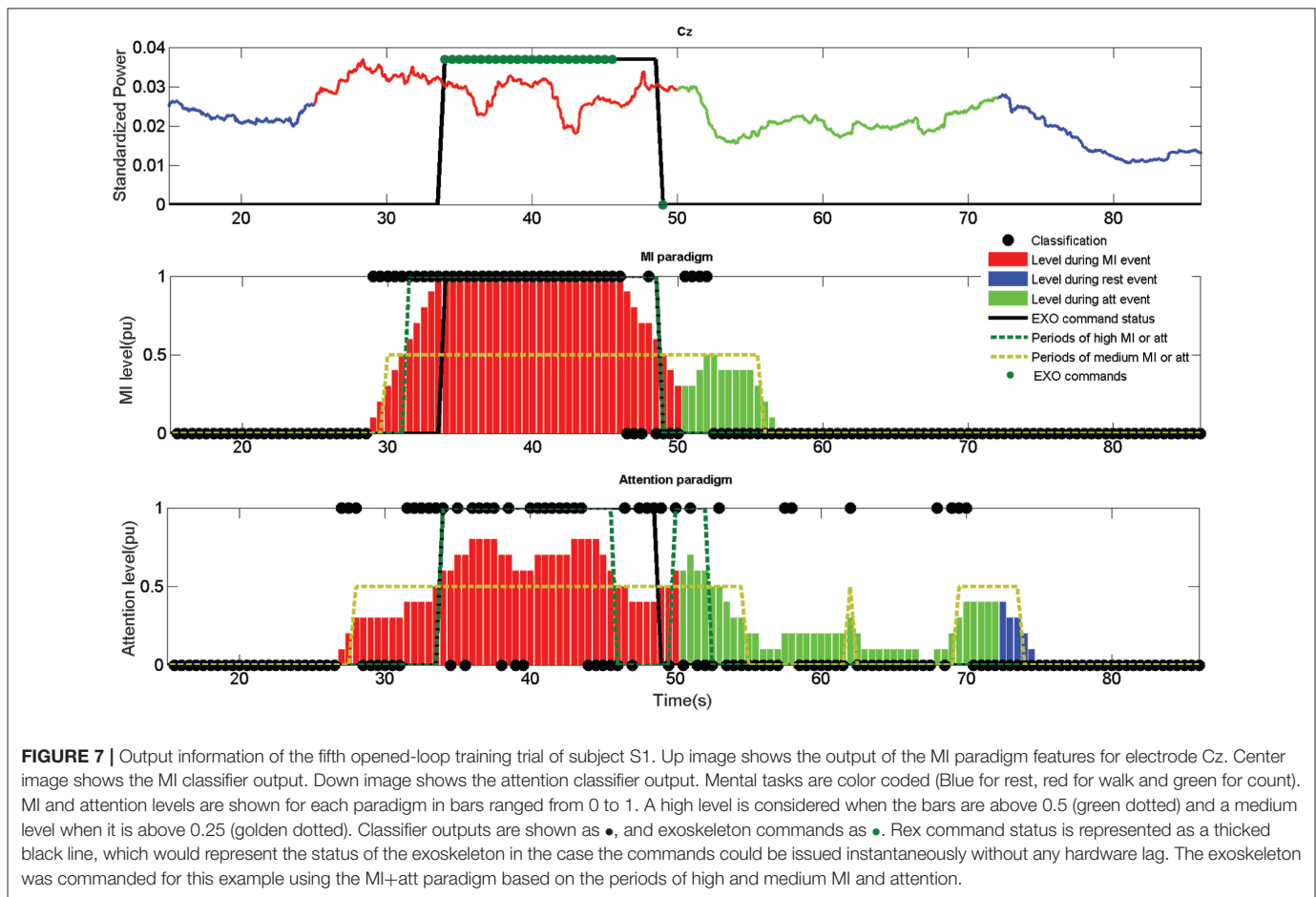


FIGURE 7 | Output information of the fifth opened-loop training trial of subject S1. Up image shows the output of the MI paradigm features for electrode Cz. Center image shows the MI classifier output. Down image shows the attention classifier output. Mental tasks are color coded (Blue for rest, red for walk and green for count). MI and attention levels are shown for each paradigm in bars ranged from 0 to 1. A high level is considered when the bars are above 0.5 (green dotted) and a medium level when it is above 0.25 (golden dotted). Classifier outputs are shown as ●, and exoskeleton commands as ●. Rex command status is represented as a thick black line, which would represent the status of the exoskeleton in the case the commands could be issued instantaneously without any hardware lag. The exoskeleton was commanded for this example using the MI+att paradigm based on the periods of high and medium MI and attention.

the exoskeleton providing feedback to the subject. Two different command rules were tested depending on the paradigms used: MI and MI+att.

First control method (MI) only uses the information of the MI levels, creating an output command when its value is over 0.5. To simulate the time needed for the exoskeleton to finish a step, it is not possible to send two different commands in a timelapse of 3 s. This does not affect the behavior of the control in a closed-loop scenario, as the hardware cannot process opposite commands during a step. However, it provides a more realistic output of the commands and indices for opened-loop trials. An example of a closed-loop control using just the MI control can be seen in **Figure 8**.

Second control method (MI+att) combines both paradigms to make a command decision. The requisite of no-different commands within a 3 s period is also present. The rules are more complex and can be summed as:

- If no command was issued since 3 s.
 - If $MI > 0.5$ and $att > 0.5$, walk (high MI and att).
 - If $MI < 0.5$ and $att < 0.5$, stop (medium or less MI and att, can be accounted while in standing position).
 - if $EXO\ command = 1$ and $MI < 0.5$ and $att < 0.25$, stop (during walking, medium or low MI with low att).

- else
 - If $EXO\ command = 1$ and $MI_{epoch_i} > 0.25$ and $MI_{epoch_{i-1}} > 0.25$ or $att > 0.25$, reinforcing walk (during walking, at least medium MI for current and previous epoch or medium att for current one).

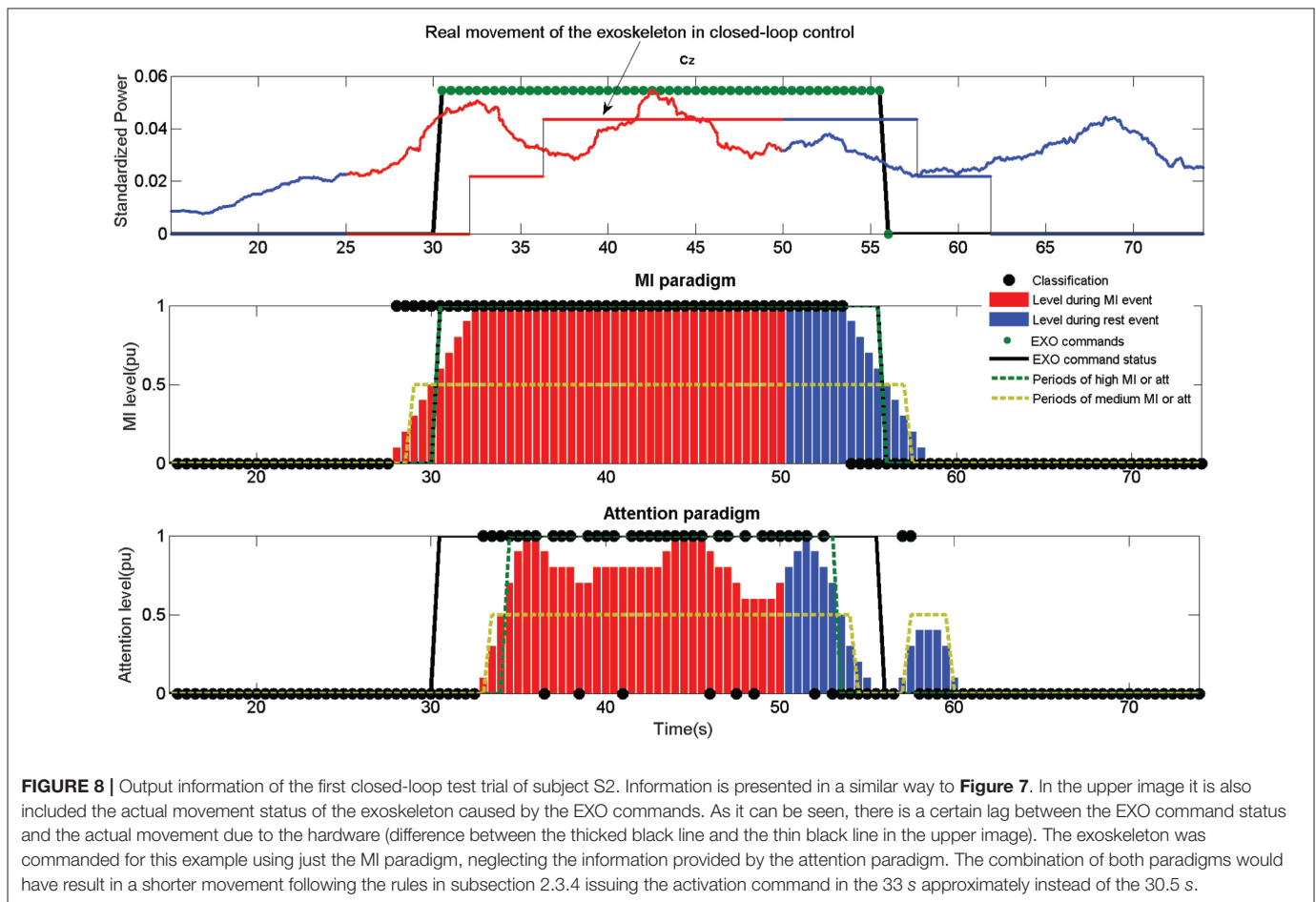
Reinforcing commands are needed to assure that the exoskeleton goes on walking, as the absence of a walking command makes the Rex to stop.

2.4. Indices for Assessment the BMI Performance

One of the most important aspects to evaluate the performance of a BMI is to correctly define the indices considered for its evaluation. Literature is not always precise in the definition of them, which can cause difficulties to compare the results. This subsection tries to overcome this difficulty clearly defining all the indices that are going to be used for the BMI assessment in a quantitative and qualitative way.

2.4.1. True Positive Ratio (TPR)

It indicates the percentage of walking events that are executed during a walking event. As the trials have only a walking event, this value can be only 0% or 100% per trial, indicating the average



value the percentage of trials with true activations. The qualitative scale would be: poor < 50%, average \geq 50%, good \geq 65%, very good \geq 75%, and excellent \geq 85%.

2.4.2. Accuracy (Acc)

It indicates the number of correct commands issued with respect to the total number of commands. A correct command is when a walk or stop command is computed in a walk or stop event, respectively. The qualitative scale is the same of TPR.

2.4.3. False Positives (FP) and False Positives per Minute (FP/min)

This is one of the most important indices, as it quantifies the number of walking commands issued during rest or count periods. One of the objectives of the research is to kept this number as low as possible, even if it limits the accuracy of the BMI. For the real-time control of an exoskeleton, it is an important problem if the exoskeleton is activated when it is not desired, as it could be frustrating for the patient during therapies or make the control unusable for assistance. This index is usually computed per minute, which is also included for comparison of the different performances. The qualitative scale for the FP is: poor > 2, average \leq 2, good \leq 1.5, very good \leq 1, and excellent \leq 0.5.

2.4.4. Percentage per Epoch and Paradigm

There are three different indices: %MI, %att, and %Command. The first two indicate the accuracy of each classifier paradigm, as the number of correct detections divided by the number of total detections. Detections can be seen in **Figures 7–9** as •. A correct detection value would be 1 for walk events and 0 for the other events. The third one is based on the percentage of epochs with correct EXO command status. It is important to notice that due to the way the algorithms work (averaging previous epochs and outputs in the case of the MI and attention levels), it is not possible to have a 100% accuracy as it would need at least several seconds of perfect features to compute a change of event. The qualitative scale would be: poor < 50%, average \geq 50%, good \geq 60%, very good \geq 70%, and excellent \geq 80%.

2.4.5. Lags in Command

It can be computed for the commands (opened-loop) and for the exoskeleton (closed-loop). As the second one is hardware dependent, it does not provide any information of the BMI performance. They are a quantitative value of the time needed to change the status since a cue is established. For instance, the time needed to walk or to send the walk command since the walking acoustic cue is issued. There is not a qualitative scale,

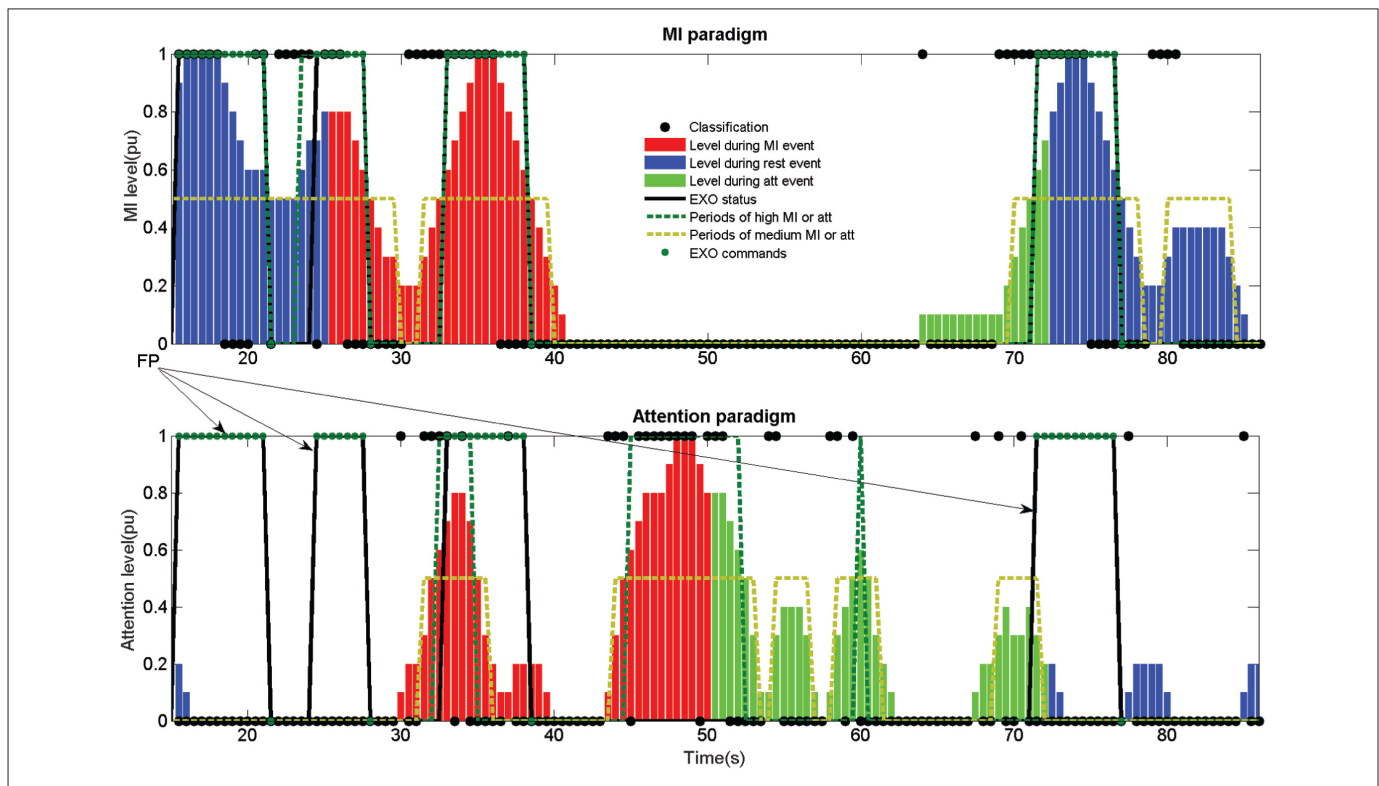


FIGURE 9 | Example of an erroneous classification in an opened-loop trial. The image corresponds to the training trial 5 of subject S4. The poor %MI classification (52.8%) produced three FP and an Acc of 37.5%. If the attention paradigm had been considered, the three FP marked by the arrows would not have been computed. However, the exoskeleton would have been activated for a shorter period of time (between 33 and 38 s), stopping before the count event starts. This would have had a 50% Acc as the stop would have been commanded before the MI period ended. Compare **Table 1** results for both paradigms of training trial 5 of S4.

but a good value would be <10 s for the EXO command having in consideration the lag of the algorithms and the exoskeleton.

3. RESULTS

As previously stated, all the trials (training and test) were processed in a real-time (online) scenario. Training trials were executed in opened-loop control while test trials were executed in closed-loop control. Each trial was performed following a determined method of control (MI or MI+att). In the case of closed-loop control tests, the method of control corresponds to the one used when registered. However, in the case of training trials, they were simulated again using a pseudo-online analysis. For this reason, training trials show the results of both methods of control and test trials only the method that was actually executed in real time.

3.1. Opened-Loop Results

Table 1 shows the results obtained for the training trials. When there was not an activation of the exoskeleton, there is a “-” under Acc index. The results by subject and algorithm of control can be seen in **Tables 2, 3** based on the section 2.4 indices.

Regarding the method of control (**Table 2**), the main differences appear for the TPR and FP. The fact that MI+Att requires to keep a level of attention makes harder to activate the exoskeleton, but provides less FP. For the same reason, when

both paradigms are used, the lags for starting are longer and for stopping shorter, as the time the exoskeleton is going to be moving is shorter. Nevertheless, there is not a significant difference between the %Command of both control methods, because a shorter walking time provides less time walking during walking periods, but less time walking during the last rest period, compensating the %Command value between both events. Therefore, it could be said that MI+Att makes the control safer, but less responsive.

Regarding the subject performance (**Table 3**), the Acc results vary depending on the subject ($p < 0.05$), with S1 and S2 having values for the classifiers over 75% in average. The subject with lower results is S4, which shows a high TPR 75% with a an Acc around 53.1%, which indicates that the BMI is activating the exoskeleton during the walking events (TPR), but for a short time (low Acc). This irregularity, specifically in the %MI, causes a higher value of FP when the attention paradigm is not considered (see **Figure 9**). Another fact to take into account is that the last trial uses more information for its model than the second trial, which uses just the first trial. This does not have to be negative in all the cases, since the consideration of a spoiled training trial in the model could be more negative for its use in the classification.

3.2. Closed-Loop Results

Once the five training trials were done for each control option, the test trials were registered. They were carried out after the

TABLE 1 | Results of the analysis of the training trials.

Subject	Control	Trial	TPR	Acc	FP	FP/min	%MI	%Att	%Command	Lag start	Lag stop	Subject	Control	Trial	TPR	Acc	FP	FP/min	%MI	%Att	%Command	Lag start	Lag stop	
S1	MI+att pseudo	2	100	50	1	0	83.1	74.7	73.2	13	-	S2	MI+att pseudo	2	100	100	0	0	79.6	63.4	75.4	15.0	3.5	
		3	100	75	0	0	81	82.4	70.4	14	5			3	0	-	0	0	71.1	66.9	64.8	-	-	
		4	100	50	0	0	76.8	76.1	70.4	6.5	-			4	0	-	0	0	76.1	67.6	64.8	-	-	
		5	100	50	0	0	87.3	78.9	85.9	9	-			5	100	50	0	0	71.1	74.7	70.4	15	19	
		Avg	100	56.3	0.25	0.0	82.0	78.0	75.0	10.6	5.0			Avg	50.0	75.0	0.00	0.0	74.5	68.1	68.8	15.0	11.3	
	MI opened-loop	2	100	50	1	1.8	83.1		83.1	5.5	-		MI opened-loop	2	100	100	0	0	79.6		79.6	15.0	0.5	
		3	100	100	0	0	81.0		74.7	14.0	5.0			3	100	50	0	0	71.1		70.4	16.5	-	
		4	100	50	1	1.8	76.8		70.4	6.5	-			4	100	50	0	0	76.1		78.9	10.5	-	
		5	100	50	0	0	87.3		89.4	6.5	-			5	100	50	0	0	71.1		70.4	15.0	19.0	
		Avg	100	62.5	0.50	0.9	82.0		79.4	8.1	5.0			Avg	100	62.5	0.00	0.0	74.5		74.8	14.3	9.8	
	MI+att pseudo	7	100	100	0	0	88.7	77.5	91.6	6.0	1.0		1st session	MI+att pseudo	7	0	-	0	0	64.8	64.8	64.8	-	-
		8	100	75	0	0	85.2	72.5	71.8	9.0	4.0				8	100	100	0	0.0	69.0	66.9	66.2	23.5	1.5
		9	100	100	0	0	81.0	78.2	66.2	19.0	6.0				9	100	62.5	1	1.8	61.3	69.0	67.6	13.0	2.5
		10	100	100	0	0	91.6	63.4	77.5	8.0	9.0				10	0	-	0	0	64.8	72.5	64.8	-	-
		Avg	100	93.8	0.00	0.0	86.6	72.9	76.8	10.5	5.0				Avg	50.0	81.3	0.25	0.4	65.0	68.3	65.8	18.3	2.0
MI opened-loop	7	100	100	0	0	88.7		84.5	6.0	6.0	MI opened-loop	7		100	50	3	5.3	64.8		59.2	6.5	4.0		
	8	100	75	0	0	85.2		78.9	5.5	4.0		8		100	66.7	1	1.8	69.0		66.9	13.5	3.0		
	9	100	100	0	0	81.0		73.9	9.5	10.0		9		100	100	0	0	61.3		59.9	7.5	22.0		
	10	100	100	0	0	91.6		85.2	5.5	6.0		10		0	-	0	0	64.8		64.8	-	-		
	Avg	100	93.8	0.00	0.0	86.6		80.6	6.6	6.5		Avg		75	72.2	1.00	1.8	65.0		62.7	9.2	9.7		
S2	MI+att pseudo	2	100	100	0	0	83.1	81.0	81.0	8.5	6.0	S3		MI+att pseudo	2	0	-	0	0.0	61.3	71.8	64.8	-	-
		3	100	100	0	0.0	87.3	86.6	83.1	7.0	6.0				3	100	50	0	0.0	62.0	69.0	73.9	9.0	-
		4	100	100	0	0.0	85.2	81.7	76.1	11.0	7.0				4	100	100	0	0.0	90.9	77.5	92.3	6.5	0.5
		5	100	75	0	0.0	85.9	77.5	80.3	9.0	8.0				5	100	75	0	0.0	71.1	70.4	71.8	13.0	2.5
		Avg	100.0	93.8	0.00	0.0	85.4	81.7	80.1	8.9	6.8				Avg	75.0	75.0	0.00	0.0	71.3	72.2	75.7	9.5	1.5
	MI opened-loop	2	100	75	1	1.8	83.1		78.9	8.5	4.5		MI opened-loop	2	0	50	1	1.8	61.3		58.5	-	-	
		3	100	100	0	0.0	87.3		83.1	7.0	6.0			3	100	50	1	1.8	62.0		64.8	8.5	-	
		4	100	100	0	0.0	85.2		79.6	11.0	4.5			4	100	100	0	0.0	90.9		92.3	4.0	2.5	
		5	100	100	0	0.0	85.9		84.5	9.0	3.0			5	100	50	3	5.3	71.1		74.7	-	2.5	
		Avg	100.0	93.8	0.25	0.4	85.4		81.5	8.9	4.5			Avg	75.0	62.5	1.25	2.2	71.3		72.5	6.3	2.5	
	MI+att opened-loop	7	0	-	0	0.0	64.8	64.8	64.8	-	-		MI+att opened-loop	7	100	75	1	1.8	63.4	55.6	62.0	21.0	4.0	
		8	100	100	0	0.0	69.0	66.9	64.1	23.5	3.0			8	100	50	0	0.0	63.4	79.6	69.0	11.0	-	
		9	100	75	0	0.0	61.3	69.0	63.4	13.0	11.0			9	100	50	2	3.5	71.8	71.1	66.2	6.5	-	
		10	0	-	0	0.0	64.8	72.5	64.8	-	-			10	100	50	0	0.0	77.5	76.8	88.0	7.0	-	
		Avg	50.0	87.5	0.00	0.0	65.0	68.3	64.3	18.3	7.0			Avg	100.0	56.3	0.75	1.3	69.0	70.8	71.3	11.4	4.0	

(Continued)

TABLE 1 | Continued

Subject	Control	Trial	TPR	Acc	FP	FP/min	%MI	%Att	%Command	Lag start	Lag stop	Subject	Control	Trial	TPR	Acc	FP	FP/min	%MI	%Att	%Command	Lag start	Lag stop	
	MI pseudo	7	100	50	3	5.3	64.8		59.2	6.5	–		MI pseudo	7	100	66.7	2	3.5	63.4		57.8	21.0	4.0	
		8	100	66.7	1	1.8	69.0		66.9	13.5	3.0			8	100	50	1	1.8	63.4		63.4	11.0	–	
		9	100	100	0	0.0	61.3		59.9	7.5	22.0			9	100	50	2	3.5	71.8		69.7	8.0	–	
		10	0	–	0	0.0	64.8		64.8	–	–			10	100	100	0	0.0	77.5		80.3	7.0	8.0	
		Avg	75.0	72.2	1.00	1.8	65.0		62.7	9.2	12.5			Avg	100.0	66.7	1.25	2.2	69.0		67.8	11.8	6.0	
S4	MI+att pseudo	2	0	50	1	1.8	45.1	59.9	56.3	–	–			MI opened-loop	2	100	75	1	1.8	45.1		38.7	20.5	5.5
		3	100	50	1	1.8	54.2	61.3	62.0	5.0	–				3	100	50	2	3.5	54.2		58.5	5.0	–
		4	100	57.1	3	5.3	28.2	59.9	36.6	18.5	7.0				4	100	60	2	3.5	28.2		24.7	18.5	4.5
		5	100	50	0	0.0	52.8	69.7	72.5	8.0	–				5	100	37.5	3	5.3	52.8		58.5	8.0	–
		Avg	75.0	51.8	1.25	2.2	45.1	62.7	56.9	10.5	7.0				Avg	100	55.6	2.00	3.5	45.1		45.1	13.0	5.0
	MI+att opened-loop	7	0	–	0	0.0	71.8	66.2	64.8	–	–			MI pseudo	7	100	50	2	3.5	71.8		61.3	13.0	–
		8	100	50	1	1.8	71.8	66.2	59.9	14.0	–				8	100	66.7	1	1.8	71.8		66.2	1.5	6.0
		9	0	50	1	1.8	56.3	66.2	59.2	–	–				9	0	50	1	1.8	56.3		59.2	–	–
		10	100	50	0	0.0	73.9	74.7	76.1	11.0	–				10	100	50	1	1.8	73.9		70.4	4.5	–
		Avg	50.0	50.0	0.50	0.9	68.5	68.3	65.0	12.5	–				Avg	75.0	54.2	1.25	2.2	68.5		64.3	6.3	6.0

The trials were also tested in a pseudo-online analysis for the type of control not used during the opened-loop session. Averaged very good results using the qualitative scale are in bold, while poor in red.

TABLE 2 | Results of the training trials averaged per method of control.

Control	TPR	Acc	FP	FP/min	%MI	%Att	%Command	Lag start	Lag Stop
MI+Att	75.0 ± 43.9	70.9 ± 34.8	0.30 ± 0.65	0.49 ± 1.13	71.2 ± 13.3	71.1 ± 7.0	70.0 ± 10.3	11.8 ± 6.8	5.6 ± 4.1
MI	90.0 ± 30.4	69.5 ± 26.8	0.85 ± 1.00	1.50 ± 1.77	71.2 ± 13.3		69.1 ± 13.2	9.6 ± 5.5	6.8 ± 5.6

Averaged very good results using the qualitative scale are in bold. No poor results were achieved for the averaged indices per method of control.

TABLE 3 | Results of the training trials averaged per subject.

Subject	TPR	Acc	Fp	Fp/min	%Mi	%Att	%Command	Lag start	Lag stop
S1	100.0 ± 0.0	76.6 ± 23.2	0.19 ± 0.40	0.22 ± 0.60	84.3 ± 4.7	75.4 ± 5.7	77.9 ± 7.7	9.0 ± 4.0	5.6 ± 3.4
S2	75.0 ± 44.0	80.0 ± 21.8	0.31 ± 0.78	0.55 ± 1.38	72.4 ± 9.0	71.6 ± 6.9	70.1 ± 8.0	11.9 ± 4.8	7.6 ± 6.9
S3	87.5 ± 34.2	64.4 ± 20.5	0.81 ± 0.98	1.43 ± 1.73	70.2 ± 9.8	71.5 ± 7.4	71.8 ± 11.2	10.3 ± 5.3	3.4 ± 2.3
S4	75.0 ± 44.7	53.1 ± 8.7	1.25 ± 0.93	2.21 ± 1.64	56.8 ± 15.2	65.5 ± 5.1	57.8 ± 13.6	10.6 ± 6.3	5.8 ± 1.0

No poor results were achieved for the averaged indices per subject. Averaged very good results using the qualitative scale are in bold.

training in sequence. This means five training sessions for MI followed by five tests for MI and then five training sessions for MI+att followed by five tests for MI+att. **Table 4** shows the closed-loop results obtained.

Looking at **Table 4**, some facts can be extracted. The most obvious one is that S3 was not able to make the BMI work in closed-loop control. Rex was hardly activated during the tests. This contrasts with the results obtained by the subject in the opened-loop trials. However, S2 and S4 obtained a good performance for the MI control with a high number of activations of the exoskeleton during walking periods (TPR) and a proper activation of the commands (Acc). Nevertheless, classifier accuracies were a bit lower than in the opened-loop scenario.

In the case of the %EXO index, i.e., the time that the Rex is standing or walking during the correct events, achieved a value of 56.3 and 51.2 for subjects S2 and S4. This, a priori low value, is caused by two causes. First the algorithms need several seconds of correct features in order to achieve a command decision (sections 2.3.2 and 2.3.3). Second, Rex has an inherent lag for responding to the commands which is very variable, especially in the case of a stop, as it depends on the limbs position when the command is issued. This information can be calculated by the difference between Start exo and Lag start, and between Stop exo and Lag stop from the data in **Table 4**. Rex lags were in average 2.8 s for the start and 5.4 s for the stop, times which are added to the command lag decision. For instance, looking at **Figure 8**, which corresponds to the 1st MI test trial of S2, it lags 8 s for the start and 12.5 s for the stop. This makes a %EXO of only 67.0%, for a excellent classifier trial (89.8%MI and 77.1%Att). Another consequence that can be extracted from the results is that the MI control performs better than the MI+att for S2 and S4. In the same way than in the opened-loop trials, the combination of the paradigms makes the BMI more conservative, avoiding the activation of the Rex in two of the five test trials for both subjects.

4. DISCUSSION

The MI paradigm is based on gamma band. This is not a band that it is usually considered in literature and only a few studies prior to our previous research (Ortiz et al., 2019) have considered

it (Seeber et al., 2015). Two were the main reasons to focus on this band instead of θ , α , or β bands. First, γ band is less affected by low frequency noise. In the research, an active filter was applied to mitigate eye blinking (H^∞) and passive mitigation (mesh, clamps) to avoid wire oscillations or muscle noise (no swallowing or chewing). However, as the whole tool works in real time, no other offline mitigation techniques can be applied, such as independent component analysis (ICA) (Delorme and Makeig, 2004), so this band can be less affected by motion noise. Second, γ band is associated with attentive focus (Rao, 2013) and gait attention (Costa et al., 2016; Costa-García et al., 2019). For this reason, the attention level paradigm reinforces the MI paradigm by requiring a high focus of the subject during the walk events. This produces that the proposed BMI obtains sometimes a lower accuracy than other MI paradigms in the literature, but with a lower value in FP/min, which was one of the priority objectives of the research. This can be seen comparing the results of this research with the ones presented in the review of lower-limb exoskeletons by He et al. (2018). FP/min is only provided in the study by Do et al. (2013) achieving a 7.42 ± 2.85 FP/min. This is substantially higher than the FP/min presented in this article, which rarely go beyond 2 FP/min and are in most cases below 1 FP/min. The comparison with accuracy can be hard, as the way it is accounted can vary from different researches. Table 2 of He et al. (2018) varies from 68 to 99% depending on the study. This value can be confronted with the Acc index for the whole BMI or with %MI or %Att for the individual paradigms. Accuracy is in the range of the literature studies except for S4 and the closed-loop trials of S3.

Results by subject also indicate one of the most common problems of BMI studies, which it is the high dependency of the results on the individual. The fact that the tool provides performance indices since the second trial could help to detect subjects that are having troubles with the BMI. This is especially important in the case of ACV or stroke patients, which could also have cognitive difficulties which could make them unable to use the BMI, even if they have been selected as suitable in the previous clinical selection stage. A quick detection of these problems could help clinicians to adapt the therapy in these cases, for instance only applying an opened-loop control to the

TABLE 4 | Results of the analysis of the test trials.

Subject	Control	Trial	TPR	Acc	FP	FP/min	%MI	%Att	%Command	%EXO	Lag start	Start exo	Lag stop	Stop exo
S2	MI	1	100	100	0	0.00	89.8	77.1	82.2	67.0	5.5	8.0	6.0	12.5
		2	100	100	0	0.00	79.7	60.2	78.8	68.6	13.0	14.6	0.5	3.4
		3	100	75	0	0.00	67.8	55.1	59.3	57.6	12.0	13.6	7.0	10.0
		4	100	100	0	0.00	64.4	65.3	55.1	39.8	13.5	16.0	14.0	19.9
		5	100	100	0	0.00	70.3	64.4	62.7	48.3	13.5	16.0	9.5	15.5
	Avg	100.0	95.0	0.00	0.00	74.4	64.4	67.6	56.3	11.5	13.6	7.4	12.2	
	MI+att	1	0	50	1	1.76	38.1	43.2	38.1	24.6	–	–	12.5	19.1
		2	0	–	0	0.00	44.1	59.3	57.6	57.6	0.0	–	–	–
		3	0	–	0	0.00	66.1	72.0	57.6	57.6	–	–	–	–
		4	100	100	0	0.00	71.2	57.6	62.7	50.0	21.0	23.5	0.0	7.0
5		100	50	1	1.76	68.6	67.8	59.3	49.2	13.0	14.5	5.5	13.3	
Avg	40.0	66.7	0.40	0.71	57.6	60.0	55.1	47.8	17.0	19.0	6.0	13.1		
S3	MI	1	0	–	0	0.00	52.5	52.5	57.6	57.6	–	–	–	–
		2	0	0	1	1.30	48.3	58.5	46.6	50.0	–	–	–	–
		3	0	0	2	2.61	38.1	42.4	38.1	36.4	–	–	–	–
		4	100	100	0	0.00	62.7	48.3	54.2	43.2	24.5	27.5	3.0	11.0
		5	0	50	1	1.30	39.8	39.0	44.1	34.8	–	–	–	–
	Avg	20.0	37.5	0.80	1.04	48.3	48.1	48.1	44.4	24.5	27.5	3.0	11.0	
	MI+att	1	0	–	0	0.00	56.8	54.2	57.6	57.6	–	–	–	–
		2	0	–	0	0.00	57.6	61.0	57.6	57.6	–	–	–	–
		3	0	–	0	0.00	46.6	54.2	57.6	57.6	–	–	–	–
		4	0	0	1	1.30	48.3	48.3	52.5	56.8	–	–	–	–
5		0	–	0	0.00	49.2	51.7	57.6	57.6	–	–	–	–	
Avg	0.0	0.0	0.20	0.26	51.7	53.9	56.6	57.5	–	–	–	–		
S4	MI	1	100	62.5	2	2.61	56.8	60.2	52.5	40.7	7.5	9.5	1.5	7.0
		2	0	50	2	2.61	39.8	60.2	37.3	33.9	–	–	–	–
		3	100	50	1	1.30	50.9	56.8	60.2	57.6	0.0	1.6	–	–
		4	100	50	1	1.30	60.2	61.9	54.2	59.3	9.5	11.5	7.0	13.3
		5	100	66.7	1	1.30	67.0	61.0	70.3	64.4	3.5	6.0	0.0	3.0
	Avg	80.0	55.8	1.40	1.83	54.9	60.0	54.9	51.2	5.1	7.2	2.8	7.8	
	MI+att	1	100	75	1	1.30	60.2	59.3	52.5	28.0	21.0	22.6	0.0	6.0
		2	100	75	0	0.00	58.5	63.6	67.8	60.2	13.0	15.5	3.5	7.5
		3	0	–	0	0.00	48.3	56.8	57.6	57.6	–	–	–	–
		4	0	–	0	0.00	51.5	55.9	57.6	57.6	–	–	–	–
5		100	50	1	1.30	62.7	54.2	57.6	61.0	5.0	6.5	4.4	6.4	
Avg	60	66.7	0.40	0.52	56.2	58.0	58.6	52.9	13.0	14.9	2.6	6.6		

All the tests were done in closed-loop control. Averaged results considered very good using the qualitative scale are in bold, while poor in red.

exoskeleton. In addition, the degree of expertise of the subject with a BMI is a factor that improves the performance. In this study, only one session per subject (except for S2) was carried out, which does not allow to study the evolution of each individual with the different sessions.

Another important factor to consider is the use of erroneous trials to create the model, as it affects the classifier output. One BMI based on attention is more subject to distractions which could cause erroneous training trials, but MI or rest events are also affected by mental distractions. Even as environment conditions can up to a certain point be controlled, mental distractions are hard to detect beyond the subject's feedback. In this research, each training trial is checked in real time with the model created with previous training data which allows to discharge bad training trials to avoid spoiling the posterior

performance of the BMI. For instance, the fourth training trial of S4 should have been neglected for model creation due to achieving just a %MI of 28.2% (Table 1). This trial filtering for the model creation was not considered in this research to limit the length of the sessions and to compare all the subjects in the same conditions. However, it will be something to apply in future researches avoiding any trial with %MI or %Att below 70% to improve model output when used in the closed-loop trials.

The proposed BMI has been designed to serve as a tool for rehabilitation therapies helping the subject to keep a high cognitive engagement during a trial. The attention level paradigm helps to improve the FP/min index, but makes the BMI less responsive with lower Acc and TPR, and less activation time of the exoskeleton (%Command). A revision of the command decision rules explained in subsection 2.3.4 could help to improve

the results. Another option would be to offer the attention level as a feedback that could enhance the mental engagement of the subject during the walk events, or reduce it during the rest events. Additionally, the order of the application of the control methods could have affected the subjects due to fatigue. A high fatigue produces a low attention to the mental task of MI. Looking at **Table 1**, this is sustained by the classifier percentages. The training trials value for 7 – 10 trials (MI+att opened-loop trials) were in almost all the cases lower than for 2 – 5 trials which were the ones used for the model of the MI+att closed-loop trials. The length of the experiments is another key factor to consider. As two different methods of control were tested, closed-loop sessions extended to 3 h, indicating the subjects that fatigue was clearly present in the last test trials. This could be the reason of the lower test results of S3 and the MI+att of S2 (**Table 4**). Protocols must be improved in order to avoid sessions over an hour and a half since the beginning of the preparation of the subject, even if the actual active time of the session is below an hour, all the preparation times must be reduced.

5. CONCLUSIONS

During this research, a new BMI based on MI in γ band has been tested with a Rex exoskeleton in real time, not only in opened-loop control, but also in closed-loop control. In addition, an innovative BMI to assess the level of attention to gait has been implemented and combined with the former BMI. Two of the experimental subjects were able to control the exoskeleton in closed-loop control with very low FP, which was one of the main objectives to achieve.

Regarding the combination of the attention level with the MI paradigm, it provided similar results in opened-loop trials, but activating the exoskeleton in a more conservative way with slightly fewer FP and times of activation. However, the length of the proposed protocols was so long that the induced fatigue affected the results of the closed-loop test trials. Independently of its use in the closed-loop control, the attention level can be used as a way to give feedback to the subject and to inform the clinical supervisor of the cognitive engagement of the subject.

The experimental sessions fulfilled, show a case of study for the validation of the proposal, which has been validated as a promising technique to operate an exoskeleton in rehabilitation therapies which imply the cognitive engagement of the subject. Future research, will explore how the expertise of the subject can affect both paradigms during several sessions. In addition, the flaws detected in the current proposal will be corrected in future implementations of the BMI, such as limiting the fatigue of the subject with shorter sessions and assuring that the model training

trials are not inducing errors in the classifier. All of this, in order to allow its future implementation with non able-bodied subjects in a clinical study.

DATA AVAILABILITY STATEMENT

The datasets presented in this article are not readily available because of University of Houston IRB restrictions. Requests to access the datasets should be directed to Dr. Contreras-Vidal.

ETHICS STATEMENT

The studies involving human participants were reviewed and approved by Institutional Review Board of the University of Houston, TX (USA). The patients/participants provided their written informed consent to participate in this study.

AUTHOR CONTRIBUTIONS

MO and JA: conceptualization of the project. MO: methodology, formal analysis, investigation, and data curation. MO, LF, and EI: software development. MO and EI: validation. JC-V: resources and supervision. MO and LF: writing original draft preparation. MO, LF, EI, JC-V, and JA: writing, review, and editing. MO, JC-V, and JA: project administration and funding acquisition. All authors contributed to the article and approved the submitted version.

FUNDING

This research was funded by the Spanish Ministry of Science and Innovation through grant CAS18/00048 José Castillejo; by the Spanish Ministry of Science and Innovation, the Spanish State Agency of Research, and the European Union through the European Regional Development Fund in the framework of the project Walk–Controlling lower-limb exoskeletons by means of brain-machine interfaces to assist people with walking disabilities (RTI2018-096677-B-I00); and by the Consellería de Innovación, Universidades, Ciencia y Sociedad Digital (Generalitat Valenciana), and the European Social Fund in the framework of the project Desarrollo de nuevas interfaces cerebro-máquina para la rehabilitación de miembro inferior (GV/2019/009).

ACKNOWLEDGMENTS

Authors would like to thank especially Kevin Nathan and the rest of the laboratory of JC-V for their help during the experimental trials, and Atilla Kilicarslan for his help with the implementation of H^∞ algorithm.

REFERENCES

Ang, K. K., and Guan, C. (2013). Brain-computer interface in stroke rehabilitation. *J. Comput. Sci. Eng.* 7, 139–146. doi: 10.5626/JCSE.2013.7.2.139

Bakker, M., De Lange, F. P., Stevens, J. A., Toni, I., and Bloem, B. R. (2007). Motor imagery of gait: a quantitative approach. *Exp. Brain Res.* 179, 497–504. doi: 10.1007/s00221-006-0807-x

Barrios, L. J., Hornero, R., Pérez-turiel, J., Pons, J. L., Vidal, J., and Azorín, J. M. (2017). Revista Iberoamericana de Automática e Informática Industrial.

- Rev. Iberoam. Autom. Inform. Ind. 14, 346–354. doi: 10.1016/j.riai.2017.06.003
- Batula, A. M., Mark, J. A., Kim, Y. E., and Ayaz, H. (2017). Comparison of brain activation during motor imagery and motor movement using fNIRS. *Comput. Intell. Neurosci.* 2017:5491296. doi: 10.1155/2017/5491296
- Bortole, M., Venkatakrishnan, A., Zhu, F., Moreno, J. C., Francisco, G. E., Pons, J. L., et al. (2015). The H2 robotic exoskeleton for gait rehabilitation after stroke: early findings from a clinical study wearable robotics in clinical testing. *J. Neuroeng. Rehabil.* 12:54. doi: 10.1186/s12984-015-0048-y
- Bradberry, T. J., Gentili, R. J., and Contreras-Vidal, J. L. (2010). Reconstructing three-dimensional hand movements from noninvasive electroencephalographic signals. *J. Neurosci.* 30, 3432–3437. doi: 10.1523/JNEUROSCI.6107-09.2010
- Contreras-Vidal, J. L., Bhagat, N. A., Brantley, J., Cruz-Garza, J. G., He, Y., Manley, Q., et al. (2016). Powered exoskeletons for bipedal locomotion after spinal cord injury. *J. Neural Eng.* 13:031001. doi: 10.1088/1741-2560/13/3/031001
- Costa, A., Iáñez, E., Úbeda, A., Hortal, E., Del-Ama, A. J., Gil-Agudo, A., et al. (2016). Decoding the attentional demands of gait through EEG gamma band features. *PLoS ONE* 11:e0154136. doi: 10.1371/journal.pone.0154136
- Costa-García, A., Iáñez, E., Del-Ama, A., Gil-Águdo, A., and Azorín, J. (2019). EEG model stability and online decoding of attentional demand during gait using gamma band features. *Neurocomputing* 360, 151–162. doi: 10.1016/j.neucom.2019.06.021
- Cramer, S. C. (2008). Repairing the human brain after stroke. II. Restorative therapies. *Ann. Neurol.* 63, 549–560. doi: 10.1002/ana.21412
- Delorme, A., and Makeig, S. (2004). EEGLAB: an open source toolbox for analysis of single-trial EEG dynamics including independent component analysis. *J. Neurosci Methods* 134, 9–21. doi: 10.1016/j.jneumeth.2003.10.009
- Do, A. H., Wang, P. T., King, C. E., Chun, S. N., and Nenadic, Z. (2013). Brain-computer interface controlled robotic gait orthosis. *J. Neuroeng. Rehabil.* 10:111. doi: 10.1186/1743-0003-10-111
- Donati, A. R. C., Shokur, S., Morya, E., Campos, D. S. F., Moioli, R. C., Gitti, C. M., et al. (2016). Long-term training with a brain-machine interface-based gait protocol induces partial neurological recovery in paraplegic patients. *Sci. Rep.* 6:30383. doi: 10.1038/srep30383
- Gharabaghi, A. (2016). What turns assistive into restorative brain-machine interfaces? *Front. Neurosci.* 10:456. doi: 10.3389/fnins.2016.00456
- He, Y., Eguren, D., Azorín, J. M., Grossman, R. G., Luu, T. P., and Contreras-Vidal, J. L. (2018). Brain-machine interfaces for controlling lower-limb powered robotic systems. *J. Neural Eng.* 15:021004. doi: 10.1088/1741-2552/aaa8c0
- Izenman, A. J. (2013). *Modern Multivariate Statistical Techniques*. New York, NY: Springer, 237–280. doi: 10.1007/978-0-387-78189-1_8
- Kilicarslan, A., Grossman, R. G., and Contreras-Vidal, J. L. (2016). A robust adaptive denoising framework for real-time artifact removal in scalp EEG measurements. *J. Neural Eng.* 13:026013. doi: 10.1088/1741-2560/13/2/026013
- Kilicarslan, A., Prasad, S., Grossman, R. G., and Contreras-Vidal, J. L. (2013). “High accuracy decoding of user intentions using EEG to control a lower-body exoskeleton,” in *Proceedings of the Annual International Conference of the IEEE Engineering in Medicine and Biology Society, EMBS* (Osaka), 5606–5609. doi: 10.1109/EMBC.2013.6610821
- Li, J., Ji, H., Cao, L., Zang, D., Gu, R., Xia, B., et al. (2014). Evaluation and application of a hybrid brain computer interface for real wheelchair parallel control with multi-degree of freedom. *Int. J. Neural Syst.* 24:1450014. doi: 10.1142/S0129065714500142
- Liu, D., Chen, W., Chavarriaga, R., Pei, Z., and Millán, J., d. R. (2017). Decoding of self-paced lower-limb movement intention: a case study on the influence factors. *Front. Hum. Neurosci.* 11:560. doi: 10.3389/fnhum.2017.00560
- López-Larraz, E., Trincado-Alonso, F., Rajasekaran, V., Pérez-Nombela, S., Del-Ama, A. J., Aranda, J., et al. (2016). Control of an ambulatory exoskeleton with a brain-machine interface for spinal cord injury gait rehabilitation. *Front. Neurosci.* 10:359. doi: 10.3389/fnins.2016.00359
- McFarland, D. J., McCane, L. M., David, S. V., and Wolpaw, J. R. (1997). Spatial filter selection for EEG-based communication. *Electroencephalogr. Clin. Neurophysiol.* 103, 386–394. doi: 10.1016/S0013-4694(97)00022-2
- Ortiz, M., Ianez, E., Gaxiola, J., Kilicarslan, A., Contreras-Vidal, J., and Azorin, J. M. (2019). “Assessment of motor imagery in gamma band using a lower limb exoskeleton,” in *2019 IEEE International Conference on Systems, Man and Cybernetics (SMC)* (Bari: IEEE), 2773–2778. doi: 10.1109/SMC.2019.8914483
- Pfurtscheller, G., Brunner, C., Schlögl, A., and Lopes da Silva, F. H. (2006). Mu rhythm (de)synchronization and EEG single-trial classification of different motor imagery tasks. *Neuroimage* 31, 153–159. doi: 10.1016/j.neuroimage.2005.12.003
- Presacco, A., Goodman, R., Forrester, L., and Contreras-Vidal, J. L. (2011). Neural decoding of treadmill walking from noninvasive electroencephalographic signals. *J. Neurophysiol.* 106, 1875–1887. doi: 10.1152/jn.00104.2011
- Rainford, B. D., and Daniell, G. J. (1994). μ SR frequency spectra using the maximum entropy method. *Hyperfine Interact.* 87, 1129–1134. doi: 10.1007/BF02068515
- Rao, R. P. N. (2013). *Brain-Computer Interfacing: An Introduction*. Cambridge: Cambridge University Press.
- Seeber, M., Scherer, R., Wagner, J., Solis-Escalante, T., and Müller-Putz, G. R. (2015). High and low gamma EEG oscillations in central sensorimotor areas are conversely modulated during the human gait cycle. *Neuroimage* 112, 318–326. doi: 10.1016/j.neuroimage.2015.03.045
- Stippich, C., Oehmman, H., and Sartor, K. (2002). Somatotopic mapping of the human primary sensorimotor cortex during motor imagery and motor execution by functional magnetic resonance imaging. *Neurosci. Lett.* 331, 50–54. doi: 10.1016/S0304-3940(02)00826-1
- Stockwell, R., Mansinha, L., and Lowe, R. (1996). Localization of the complex spectrum: the S transform. *IEEE Trans. Signal Process.* 44, 998–1001. doi: 10.1109/78.492555
- Vaidyanathan, P. (1993). *Multirate Systems and Filter Banks*. Prentice-Hall. Englewood Cliffs, NJ: Prentice Hall.
- Villarejo Mayor, J. J., Costa, R. M., Frizera-Neto, A., and Bastos, T. F. (2017). Decodificación de Movimientos Individuales de los Dedos y Agarre a Partir de Señales Mioeléctricas de Baja Densidad. *Rev. Iberoam. Autom. Inform. Ind.* 14, 184–192. doi: 10.1016/j.riai.2017.02.001

Conflict of Interest: The authors declare that the research was conducted in the absence of any commercial or financial relationships that could be construed as a potential conflict of interest.

Copyright © 2020 Ortiz, Ferrero, Iáñez, Azorín and Contreras-Vidal. This is an open-access article distributed under the terms of the Creative Commons Attribution License (CC BY). The use, distribution or reproduction in other forums is permitted, provided the original author(s) and the copyright owner(s) are credited and that the original publication in this journal is cited, in accordance with accepted academic practice. No use, distribution or reproduction is permitted which does not comply with these terms.

Received March 9, 2021, accepted March 19, 2021, date of publication March 26, 2021, date of current version April 5, 2021.

Digital Object Identifier 10.1109/ACCESS.2021.3068929

Improving Motor Imagery of Gait on a Brain–Computer Interface by Means of Virtual Reality: A Case of Study

L. FERRERO^{ID}, (Member, IEEE), M. ORTIZ^{ID}, (Member, IEEE), V. QUILES^{ID}, (Member, IEEE), E. IÁÑEZ^{ID}, (Member, IEEE), AND J. M. AZORÍN^{ID}, (Senior Member, IEEE)

Brain–Machine Interface Systems Laboratory, Miguel Hernández University of Elche, 03202 Elche, Spain

Corresponding author: L. Ferrero (lferrero@umh.es)

This work was supported in part by the Spanish Ministry of Science and Innovation, the Spanish State Agency of Research, and the European Union through the European Regional Development Fund in the framework of the project Walk–Controlling lower-limb exoskeletons by means of brain–machine interfaces to assist people with walking disabilities under Grant RTI2018-096677-B-I00, in part by the Consellería de Innovación, Universidades, Ciencia y Sociedad Digital (Generalitat Valenciana), and in part by the European Social Fund in the framework of the project Desarrollo de nuevas interfaces cerebro–máquina para la rehabilitación de miembro inferior under Grant GV/2019/009.

ABSTRACT Motor imagery (MI) is one of the most common paradigms used in brain–computer interfaces (BCIs). This mental process is defined as the imagination of movement without any motion. In some lower-limb exoskeletons controlled by BCIs, users have to perform MI continuously in order to move the exoskeleton. This makes it difficult to design a closed-loop control BCI, as it cannot be assured that the analyzed activity is not related to motion instead of imagery. A possible solution would be the employment of virtual reality (VR). During VR training phase, subjects could focus on MI avoiding any distraction. This could help the subject to create a robust model of the BCI classifier that would be used later to control the exoskeleton. This paper analyzes if gait MI can be improved when VR feedback is provided to subjects instead of visual feedback by a screen. Additionally, both types of visual feedback are analyzed while subjects are seated or standing up. From the analysis, visual feedback by VR was related to higher performances in the majority of cases, not being relevant the differences between standing and being seated. The paper also presents a case of study for the closed-loop control of the BCI in a virtual reality environment. Subjects had to perform gait MI or to be in a relaxation state and based on the output of the BCI, the immersive first person view remained static or started to move. Experiments showed an accuracy of issued commands of 91.0 ± 6.7 , being a very satisfactory result.

INDEX TERMS Brain–computer interface, EEG, motor imagery, common spatial patterns, virtual reality.

I. INTRODUCTION

Motor Imagery (MI) is defined as the mental process of imaging a motion act without actually executing any movement [1]. It is one of the most commonly used control paradigms in brain–computer interfaces (BCIs), as motion imagery produces similar brain patterns to the ones associated with the execution of the movement [2]–[4].

The cognitive involvement of a patient can improve rehabilitation processes thanks to neuroplasticity [5]. This has been demonstrated in clinical studies [6]. Therefore, the use of this paradigm can be used not only for the control of

mechatronic devices, but as an actively part in rehabilitation therapies.

However the MI performance is affected by several conditions. First, it requires a high focus of the subject during the training of the BCI to adjust the classifier. Any distraction by the subject can easily spoil the data affecting the quality of the classifier model. Therefore, a high control of the experimental conditions are needed, avoiding any external noise or motions. On the other hand, when MI is applied to event related de-synchronization (ERD/ERS) [7], it is important to assure that the MI epochs considered do not contain any data after the actual start of motion. If this is not accomplished, it is difficult to state that the ERD/ERS detection is caused by imagery instead of actual motion activity or

The associate editor coordinating the review of this manuscript and approving it for publication was Gang Wang^{ID}.

artifacts. Indeed, accuracy drops when only epochs before the motion are considered for the classifier creation as it is shown in literature [8], [9]. However, in a restorative therapy it is important to use MI as a continuous mental act instead of an event related act (motion intention) to favor the neuroplasticity mechanisms [5]. If MI is used in a brain-machine interface in combination with a mechanic device, such as an exoskeleton or orthosis, the patient receives the feedback of the BCI classification as the motion of the device in a closed-loop control. This means that the MI act is actually performed during motion, which could not be considered as a proper MI act by its definition. This makes really hard to develop a closed-loop control BCI based on maintained MI. A way to avoid motion artifacts could be to focus on gamma band (>30Hz) [10] instead of sensory motor bands (alpha and low beta band 8-19Hz) or applying state of the art real-time motion artifact techniques [11]. However, this cannot assure that the analyzed activity is not related to motion instead of imagery. Specifically, in the case of BCIs for lower-limb closed-loop control of exoskeletons there are not many investigations in literature, and they usually do not apply a maintained MI paradigm, but ERD/ERS as in [12], [13], Motion Related Cortical Potentials [14] as in [15], Steady State Visual Potentials such as in [16]–[18] and combinations of them [19], [20].

An effective way to adjust the model of a BCI based on MI for its application in closed-loop control could be virtual reality (VR). In this case, the environment can easily isolate the subject from any external perturbation. In addition, motion feedback can be provided through the VR environment in an immersive way without executing any movement. Some works have explored the combination of BCI with VR or virtual screen feedback. For instance, in [21] a virtual avatar was applied in combination with a treadmill for closed-loop control of a BCI. However, the feedback included motion and the avatar was shown to the subject by a screen interface, which could not be considered as a proper immersive VR environment. In addition, the majority of studies that have employed VR are focused on hand MI [22]–[24] or a combination of hand with foot MI [25]. Reference [26] shows an study with VR to promote foot motor imagery but in an open-loop approach.

Filter Bank Common Spatial Patterns (FBCSP) is a decoding algorithm which is based on spectral and spatial features [27]. Whereas there are many studies that has tested this algorithm with offline competition datasets to distinguish among different motor imagery tasks [28], [29], there are only a few that have applied this methodology for the closed-loop control of an external device [30]. Additionally, in the literature there are different variants of FBCSP that have reported higher accuracies in offline competition datasets [31], [32]. However, they have not been tested in an online approach applied to the whole EEG signal trial, but only to selected fragments to be processed. In addition, these FBCSP variants need to estimate hyperparameters for the selection of optimal features, which is time consuming and would

affect the experimental length of online trials. Consequently, it difficult its application for a real experiment with patients in which the duration of the session is crucial, as otherwise subjects could suffer from fatigue.

The current research explores the use of VR as a mean to improve the MI task execution. This could help the subjects during the training phase of the classifier. This is performed in open-loop control in order to create a classifier model able to separate the classes. Usually, the classes to consider are rest vs. MI walk, and it is critical for the subject to be focused on the mental tasks avoiding any external distraction in order to create a robust model to be used during the closed-loop test trials.

The paper is organized in two experiments. In both, FBCSP was employed for pattern decoding. First experiment explored the use of an immersive VR environment in comparison to a screen interface. In order to take into account balance issues during MI, both experiments were repeated while the subject was seated and standing up. This first step of the research assessed the accuracy of the proposed BCI as the index to compare the performance of the different interfaces. The second part of the research presented a case of study for the closed-loop control of the VR environment by means of the BCI.

II. MATERIAL AND METHODS

A. PARTICIPANTS

Five subjects participated in the study (mean age 29.8 ± 6.46). They were informed about the experiments and signed an informed consent in accordance with the Declaration of Helsinki They did not report any known disease and had no movement impairment. All subjects had some experience with BCI, but not with the same experimental setup or VR. All procedures were approved by the Responsible Research Office of Miguel Hernández University of Elche.

B. EQUIPMENT

EEG signals were recorded with a 32 electrode system acti-Cap (Brain Products GmbH, Germany). The electrodes (FZ, FC5, FC1, FCZ, FC2, FC6, C3, Cz, C4, CP5, CP1, CP2, CP6, P3, Pz, P4, PO7, PO3, PO4, PO8, FC3, FC4, C5, C1, C2, C6, CP3, CPz, CP4, P1, P2) were placed following the 10-10 international system, on an actiCAP (Brain Products GmbH, Germany). The signals of each channel were amplified using a BrainVision BrainAmp amplifier (Brain Products GmbH, Germany), and then transmitted to the BrainVision recorder software (Brain Products GmbH, Germany). Ground and reference electrodes were located in the right and left ear lobe respectively.

The VR hardware and software used consisted of a VIVE HTC headset (HTC, Taiwan) (2160×1200 resolution, 1080×1200 per eye, 90 Hz refresh rate) that participants wore, two base stations that tracked the exact location of the headset and Steam software (Valve, United States).

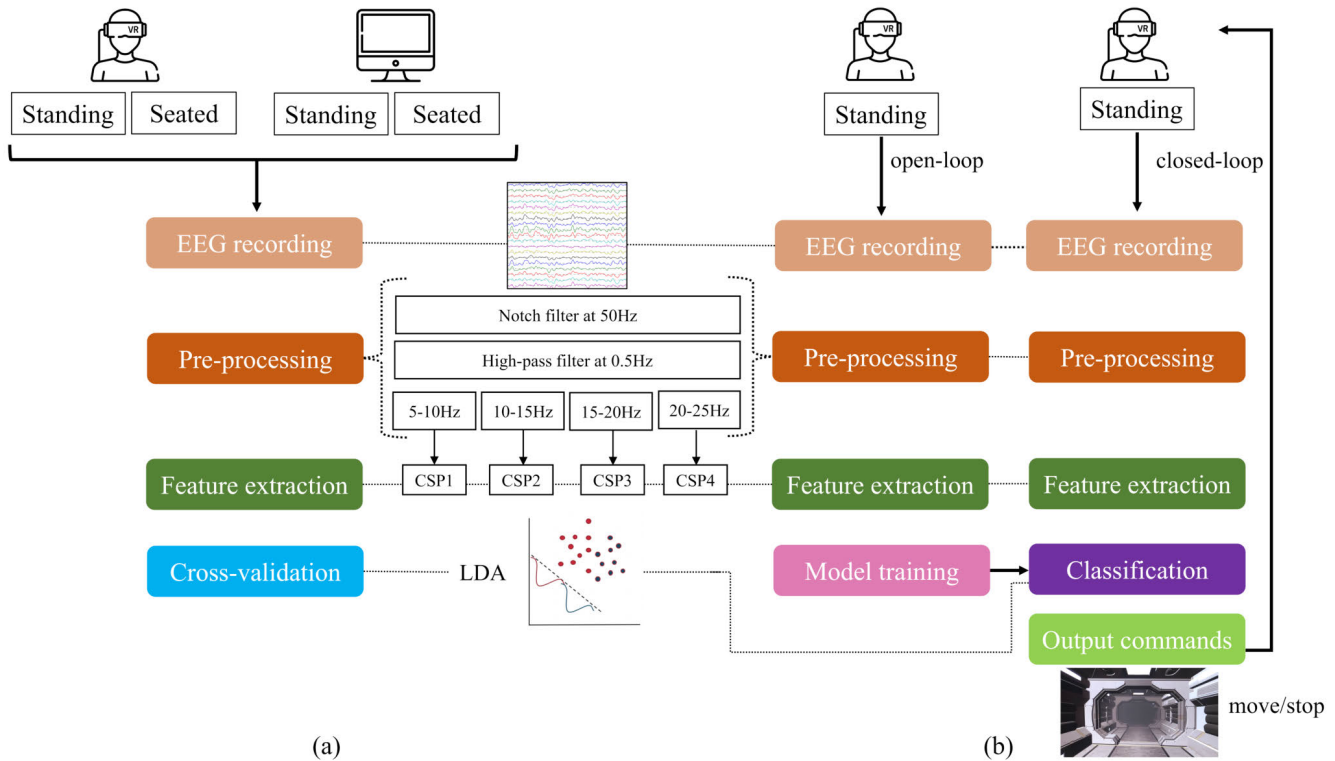


FIGURE 1. Experimental design. In experiment 1 (a), 4 approaches of BCI with visual feedback were tested offline and results were compared. In experiment (b), subjects first performed trials in which the visual feedback was predefined and these trials were employed to train the BCI classifier. Afterwards, subjects performed closed-loop trials in which the visual feedback changed based on the output of the BCI classifier previously trained. First, data was recorded. Then, it was pre-processed with different frequency filters and common spatial patterns were extracted from each frequency band. Finally, the algorithm performed a classification in two events: MI or relax.

C. EXPERIMENTAL DESIGN

Two different experiments were conducted in which users had to perform MI of gait. The objective was to investigate if it is possible to differentiate between periods of MI and resting state while subjects get only visual feedback. In the first experiment, different approaches for the visual feedback were compared and the performances were calculated offline. In the second experiment, the approach that showed the highest performance in experiment 1 was employed for closed-loop online sessions. The schema of the experimental setup can be seen in Fig. 1.

1) EXPERIMENT 1

In this experiment the BCI performance was compared when users got visual feedback using a screen or a VR environment. Visual environment consisted of an star-ship corridor. The corridor followed a repetitive pattern to avoid any visual distraction, but allowing an easy perception of speed and motion. During the MI periods, the first person view moved recreating the gait action through the VR corridor, creating a realistic motion sensation thanks to some minor balancing motion animations of the camera. Otherwise, first person view was static during periods of resting. An example of the screen view of the corridor can be seen in Fig. 2. Two other conditions were compared: when subjects were physically standing still and when they were seated in a chair.

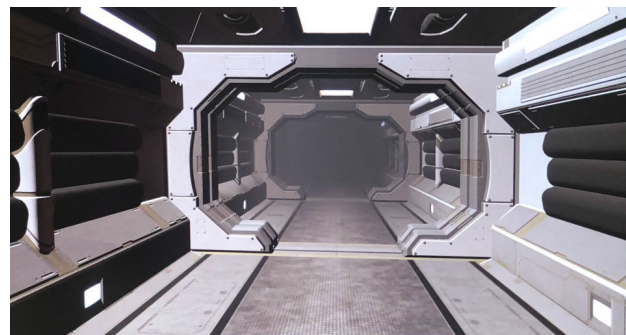


FIGURE 2. Visual feedback. During the experiment, users get visual feedback that is a corridor that can move as if the user is walking through it or it can be static.

The objective of this comparison was to study if the feeling of stability, especially when using VR, has an effect on the performance. The sequence of experiments with these four conditions was randomized for each subject. Fig. 3 shows an example of a participant with VR and standing.

Subjects had to perform trials with a series of mental tasks as can be seen in Fig. 4(a). They had to alternate periods of motor imagery of walking with resting. There was a visual cue that indicated the beginning of each task. In order to avoid visual evoked potentials, the period of 2 seconds after the cue was labelled as preparation task and was not considered for further analysis. The protocol had an extra class called ‘Free’

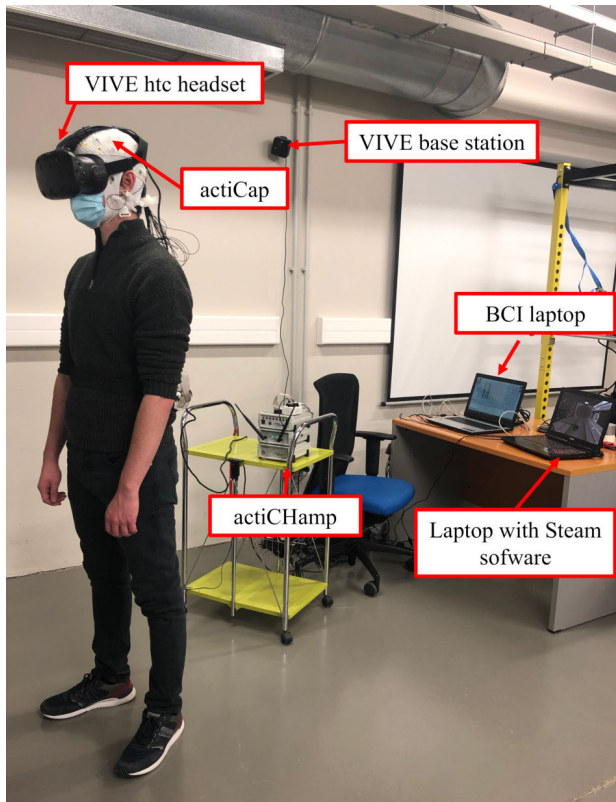


FIGURE 3. Participant doing a trial with visual feedback provided by virtual reality equipment. One laptop runs the BCI algorithm and the other one controls the virtual reality environment.

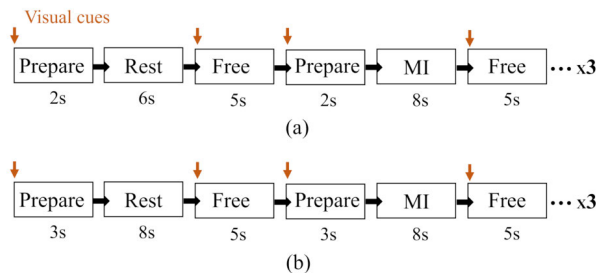


FIGURE 4. Protocol of trials for experiment 1 (a) and experiment 2 (b).

in which subjects could rest and do free tasks as swallowing or blinking. The protocol of Fig. 4(a). was repeated 6-8 times for each one of the 4 approaches: VR+ standing, VR+ sitting, screen + standing, screen + sitting. Two subjects performed a session with 8 trials of each procedure and the other one participated in two sessions, but with 6 trials. The reduction to 6 trials in the third subject was done in order to limit the protocol times based on the feedback of the first two subjects to avoid fatigue.

2) EXPERIMENT 2

The approach in which subjects were standing still and using VR was employed for closed-loop online sessions. The first part of the session consisted of the open-loop trials used for the classifier training and the second part of the closed-loop trials used to test the performance of the BCI in real time.

The protocol of each kind of trial can be seen in Fig. 4(b). In the first part of the session, each subject performed the 10 open-loop training trials. In addition, the performance of these training trials was calculated offline following a leave-one-out cross-validation. Afterwards, each subject performed 5 closed-loop trials. While in open-loop trials, first person view feedback was previously defined based on the protocol as in experiment 1, in closed-loop trials, first person view motion was based on the output of the BCI.

D. BRAIN COMPUTER INTERFACE

The BCI consisted of four phases of pre-processing, feature extraction, classification and issuing commands.

For both experiments, EEG signals were recorded at a sampling frequency of 500Hz. In experiment 1, data were analysed offline following a pseudo-online approach, whereas all the analysis was done online in experiment 2. From each trial, epochs of 1s with 0.5s of shifting were extracted and processed.

1) PRE-PROCESSING

The first pre-processing step was a notch filter at 50Hz to remove the contribution of the power line. It was followed by a high-pass filter at 0.5Hz. For feature extraction, FBCSP algorithm [27] was employed to get spatial features associated with different frequency bands. As the first stage of FBCSP algorithm, a filter bank of band-pass filters was applied to study different frequency bands. Focusing on the MI, 4 band-pass filters were applied to get alpha and beta waves: 5-10Hz, 10-15Hz, 15-20Hz, 20-25Hz. In order to mitigate artifacts caused by the movement of electrodes or wires, they were fixed with clamps and a medical mesh. Additionally, subjects were asked to not blink, swallow or chew during periods of MI and resting state.

2) FEATURE EXTRACTION

Discriminant characteristics associated with each brain task were extracted from each pre-processed windows of data for classifier training and testing. The second stage of FBCSP algorithm was applied to signals from each filtered frequency band. It designs spatial filters that enhance the differences between two types of EEG patterns in terms of their variances [33]. Thus, given an EEG signal, X , that has $N * T$ dimensions, in which N is the number of channels and T is the number of samples, the algorithm estimates a matrix of spatial filters W . In this case, the two classes to discriminate are MI (X_1) and rest (X_2). The normalized covariance matrix for each class is

$$C_1 = \frac{X_1 X_1^T}{\text{trace}(X_1 X_1^T)}, \quad C_2 = \frac{X_2 X_2^T}{\text{trace}(X_2 X_2^T)}. \quad (1)$$

\bar{X}_1 y \bar{X}_2 are calculated by averaging over all the signals from each class. The composite spatial covariance matrix is obtained with the sum of these averaged normalized covariance matrices and can be factorized as

$$C = \bar{C}_1 + \bar{C}_2 = U_0 \Sigma U_0^T. \quad (2)$$

U_0 and Σ are the eigenvectors and the diagonal matrix of eigenvalues respectively. The transformation (3). converts the averaged normalized covariance matrices as (4).

$$P = \Sigma^{1/2} U_0^T \quad (3)$$

$$S_1 = P \overline{C_1} P^T, \quad S_2 = P \overline{C_2} P^T \quad (4)$$

The factorization of S_1 and S_2 are computed as (5). They have common eigenvectors, and the sum of both matrices of eigenvalues is the identify matrix. Therefore, for an eigenvector, if S_1 has the eigenvalue s_1 , S_2 will have $s_2 = 1 - s_1$.

$$S_1 = U \Sigma_1 U^T, \quad S_2 = U \Sigma_2 U^T \text{ and } \Sigma_1 + \Sigma_2 = I \quad (5)$$

The projection matrix is obtained as

$$W = U^T P. \quad (6)$$

The original signal S can be projected into another space of uncorrelated components. Columns of W^{-1} are the spatial patterns.

$$Z = WX \quad (7)$$

The resulting signal Z has the same dimensions as S ($N * T$), but first and last rows are the components whose variances are more suitable for discrimination between the two classes. These components are associated with the largest eigenvalues of Σ_1 and Σ_2 . Consequently, only the variances of the m first and last components of Z are considered for feature extraction, which is defined as Z_p .

The variances of Z_p are computed and normalized with the logarithm as

$$f_p = \log \frac{\text{var}(Z_p)}{\sum_{i=1}^{2m} Z_p}. \quad (8)$$

Finally, f_p is the vector of features and has $(fbands * 2 * m) * T$ dimension. In this case, since there are 4 frequency bands filtered out and m was set to 4, the dimension is $32 * T$.

3) CLASSIFICATION

The classifier employed for both experiments was the Linear Discriminant Analysis (LDA). In experiment 1, trials were evaluated performing cross-validation leave-one-out for each approach separately: VR + standing, VR + sitting, screen + standing, screen + sitting. Once the vector of features, f_p , was obtained for each epoch of data for all the trials of each approach, the classifier was trained with all the trials but one, and tested with the unused one. This process was repeated using every trial once as test.

In experiment 2, the classifier was trained with open-loop trials. Afterwards, during closed-loop trials, each epoch of data was classified as MI or resting state in real time.

4) OUTPUT COMMANDS

In closed-loop trials of experiment 2, VR environment was controlled by commands issued by the BCI. The commands

were chosen based on the prediction of the classifier and the following rules:

- During the periods of free and preparation tasks, commands cannot be issued. The first two seconds of preparation are not considered to avoid any evoked potential due to the user interface message shown to the subject at the beginning of the prepare rest or MI tasks.
- The prediction of the classifier was 1 for MI and 0 for resting state. This prediction was averaged every 3s. If the resulting index was higher or equal than 0.7, the command issued was to move the environment and if it was lower than 0.7, the command issued was to stop.
- During 3s new commands cannot be sent.

E. EVALUATION

As mentioned previously in II-D3, trials of experiment 1 were evaluated using cross-validation leave-one-out. The same method was employed for the open-loop trials of experiment 2. The performance was assessed with the percentage of correctly classified epochs of data during MI and resting state tasks. On the other hand, the performance of closed-loop trials of experiment 2 was evaluated with the following indices:

- Accuracy: percentage of epochs of data correctly classified.
- %Commands: percentage of epochs of data with correct commands.
- Accuracy commands: percentage of correct commands issued.
- True Positive Ratio (TPR): percentage of MI periods (each trial has 3) in which the VR environment is moving.
- False Positives (FP) and False Positives per minute (FP/min): moving commands issued during rest periods.

III. RESULTS

In this section, the results of the experiments described are presented.

A. EXPERIMENT 1

In experiment 1, subjects performed trials with periods of MI and resting while they were receiving visual feedback with VR or a screen. Additionally, they were standing up or seated. Results are shown in Table 1.

An statistical analysis was performed in Rstudio to test if the differences among the procedures were significant. The chosen test was the repeated-measures ANOVA to study the differences between VR/screen and standing/seated. Firstly, the assumptions made by the ANOVA were verified:

- No significant outliers were identified.
- Shapiro-Wilk test was employed to assess if the performance indices obtained with each protocol followed a normal distribution. Results showed that all groups followed a normal distribution with a $p_{value} < 0.05$.

TABLE 1. Results obtained in experiment 1.

Subject	Session	Visual	Position	%total	%MI	%rest
S11	1	VR	Standing	68.1 ± 12.7	64.9 ± 7.6	71.4 ± 5.4
	1	VR	Seated	75.5 ± 11.7	69.2 ± 18.2	81.8 ± 8.9
	1	Screen	Standing	62.9 ± 8.8	68.1 ± 17.7	57.8 ± 7.11
	1	Screen	Seated	65.2 ± 6.2	62.2 ± 11.5	68.2 ± 12.7
S12	1	VR	Standing	81.2 ± 7.0	81.4 ± 9.57	81.0 ± 9.0
	1	VR	Seated	76.9 ± 13.5	80.6 ± 11.8	73.2 ± 30.8
	1	Screen	Standing	71.2 ± 10.3	73.7 ± 15.0	68.8 ± 22.7
	1	Screen	Seated	78.3 ± 8.7	79.0 ± 13.6	77.6 ± 14.8
S13	1	VR	Standing	58.1 ± 6.3	62.8 ± 12.4	53.5 ± 14.6
	1	VR	Seated	59.1 ± 7.0	58.5 ± 15.6	59.7 ± 19.8
	1	Screen	Standing	66.5 ± 4.4	64.2 ± 12.3	68.8 ± 9.6
	1	Screen	Seated	57.5 ± 8.5	55.7 ± 10.8	59.4 ± 8.9
	2	VR	Standing	71.2 ± 8.0	73.1 ± 11.2	69.4 ± 12.2
	2	VR	Seated	65.1 ± 9.9	67.0 ± 16.7	63.2 ± 16.3
	2	Screen	Standing	75.6 ± 7.0	70.9 ± 12.6	80.2 ± 9.4
	2	Screen	Seated	60.0 ± 4.0	60.6 ± 9.4	59.4 ± 9.3

Performances of each subject in 4 different protocols. Variables %total,%MI and %rest show the average accuracy per epoch in total and only for MI and resting tasks respectively. Additionally, the parameter Session is 1 for subjects S11 and S12 because they only participated in one experiment and it has two values for subject S13.

- The variances of the differences between protocols must be equal, which is defined as sphericity. This assumption was tested with the Mauchly's Test and the results confirmed it ($p_{value} < 0.05$).

The repeated-measures ANOVA was used to study the differences of subject performances based on the visual feedback and the position of the user. The accuracy was defined as the percentage of correctly classified epochs per trial. From the results of these tests, no significant differences were identified between VR and screen, standing and seated and the combination of both ($p_{value} > 0.05$).

Since subjects showed different behaviour to the protocols, it was tested if there were statistical significant differences among them with one-way ANOVA. Firstly, it was tested the normality assumption for the data of each group with the Shapiro-Wilk test. Results revealed that data of S11 and S13 followed a normal distribution but data of S12 did not. Therefore, the non-parametrical test Kruskal-Wallis was employed with a pairwise Mann-Whitney test. Performance of S12 differs significantly from S11 and S13. The average accuracy for subject S12 was 76.89 ± 10.14 , 67.94 ± 10.20 for subject S11 and 64.14 ± 7.13 for subject S13.

Finally, the data from each subject was analyzed independently. Two-way ANOVA was applied for S11 and S13 because normality and homoscedasticity assumptions were verified. However, in case of S12 the normality assumption was not fulfilled so the Kruskal-Wallis test was employed. Results from S11 and S13 showed significant differences in terms of the visual feedback.

Although some subjects indicated they experienced fatigue, the average performance of the last procedure was similar. It is difficult to say which procedure was the best in terms of performance due to significant differences among users. However, VR and standing had the highest accuracy in the majority of subjects.

B. EXPERIMENT 2

Experiment 2 was divided in two parts. First, subjects performed open-loop trials in order to train the BCI classifier.

TABLE 2. Results obtained in open-loop trials in experiment 2.

Subject	N	% total	%MI	%rest
S21	1	77.08	100.00	54.17
	2	76.04	89.58	62.50
	3	78.13	83.33	72.92
	4	79.17	93.75	64.58
	5	82.29	91.67	72.92
	6	95.83	97.92	93.75
	7	83.33	75.00	91.67
	8	83.33	87.50	79.17
	9	79.17	75.00	83.33
	10	88.54	87.50	89.58
	avg.	82.3±6.0	88.1±13.4	76.5±13.4
S22	1	82.29	97.92	66.67
	2	91.67	97.92	85.42
	3	82.29	70.83	93.75
	4	94.79	91.67	97.92
	5	79.17	68.75	89.58
	6	87.50	83.33	91.67
	7	88.54	85.42	91.67
	8	86.46	85.42	87.50
	9	73.96	62.50	85.42
	10	79.17	79.17	79.17
	avg.	84.6±6.4	82.3±8.8	86.9±8.8

Performances of open-loop trials. Each subject performed 10 trials and %total,%MI and %rest show the average accuracy per epoch in total, MI and resting tasks respectively. N is the number of the trial that goes from to 10.

Afterwards, they performed closed-loop trials in which the visual feedback of the VR environment could change based on the output of the BCI.

Results of open-loop trials are reported in terms of accuracy of correctly classified epochs as experiment 1. They can be seen in Table 2. The total average classification accuracy of subject S21 is 82.3 ± 6.0 and the accuracies in MI and relax events are 88.1 ± 13.4 and 76.5 ± 13.4 respectively. Regarding S22, the average classification accuracies are 84.6 ± 6.4 in total, 82.3 ± 8.8 in MI events and 86.9 ± 8.8 in relax events.

Table 3 summarizes the performance of closed-loop trials. The average value of Accuracy is 71.7 ± 8.9 for S21 and 77.3 ± 8.6 for S22. This metric is equivalent to %total of open-loop trials. %Commands also provides a measure that is evaluated per epoch, but it is focused on the commands

TABLE 3. Results obtained in closed-loop trials in experiment 2.

Subject	N	Accuracy	%Commands	TPR	FP	FP/min
S21	1	71.9	88.5	100.0	2.0	5.0
	2	70.8	97.9	100.0	3.0	7.5
	3	69.8	95.8	100.0	2.0	5.0
	4	60.4	82.3	100.0	2.0	5.0
	5	85.4	92.7	100.0	1.0	2.5
avg.		71.7±8.9	91.5±6.2	100.0±0.0	2.0±0.7	5.0±1.8
S22	1	78.1	93.8	100.0	0.0	0.0
	2	63.5	100.0	100.0	3.0	7.5
	3	79.2	86.5	100.0	0.0	0.0
	4	87.5	90.6	100.0	0.0	0.0
	5	78.1	81.3	100.0	1.0	2.5
avg.		77.3±8.6	90.4±7.1	100.0±0.0	0.8±1.3	2.0±3.3

Performances of closed-loop trials. N is the number of the trial that goes from 1 to 5.

issued. From the results, it can be pointed out that %Commands is always higher than Accuracy. On the other hand, TPR is 100% for all trials, which means that there is an activation in all MI events. Regarding FP/min, S22 had a lower rate of False Positives than S12. A similar pattern of results was obtained in open-loop trials in which S22 had higher Accuracy in relax events.

The spatial patterns of motor imagery and relax of S21 and S22 can be seen in Fig. 5 and Fig. 6 respectively. Results from S21 show that electrodes CP1 and CP2 seem to have a relevant role in MI of gait in frequencies from 5 to 20Hz. In relax events, electrode Pz is the one highlighted at 15-25Hz. Regarding S22, the patterns are different. In relax events, the most significant electrode is FCz followed by FC1 and FC2 at 15-25Hz. In MI of gait, the distribution of relevant areas is scattered for all frequency bands considered.

IV. DISCUSSION

Results from experiment 1 showed that visual feedback provided by VR was related to higher performances in the majority of cases. However, no statistically significant differences were found. With regard to the position of the user, there were not notable differences between standing and being seated. Intrinsic within-subject differences may affect performances more than other factors, such as procedure. A similar conclusion was reached by [24], although their work was focused on hand MI. They compared the performance of users and their embodiment when they were using VR or watching a screen. Whereas they found a trend for better performance and embodiment in VR, they could not find significant differences.

In experiment 2, the percentage of correctly issued commands (%Commands) is slightly superior than the percentage of correct outputs (Accuracy) and in some cases, the difference is considerable. This might be due to the fact that maintaining MI or a state of relaxation during long periods can be challenging. It is easy that subjects can get distracted and eventually center their attention in another task. Therefore, by averaging the output of the classifier, short deviations can be mitigated. These findings are in line with the research shown in [10].

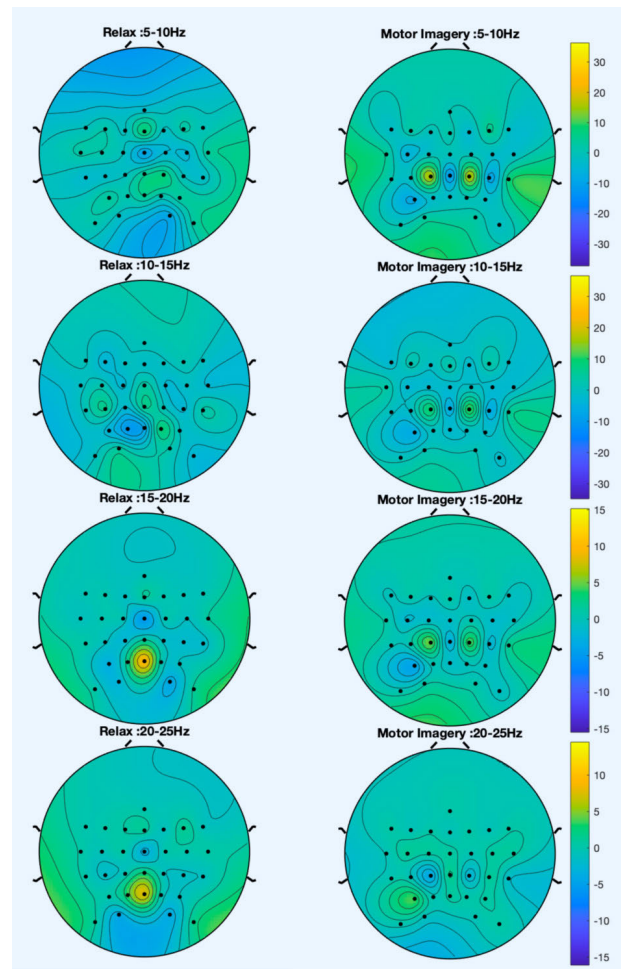


FIGURE 5. Spatial patterns for subject S21 that best discriminate between rest and MI classes.

The spatial patterns from subjects S21 and S22 show inter-subject variability with respect to the MI pattern. A similar conclusion was reached by [34]. They found different optimal spectro-spatial characteristics across subjects and sessions which could be explained by the non-stationary nature of EEG but also unknown factors. In addition, the FBCSP methodology was employed with a motor imagery competition dataset and the spatial patterns showed dissimilarities across subjects [27].

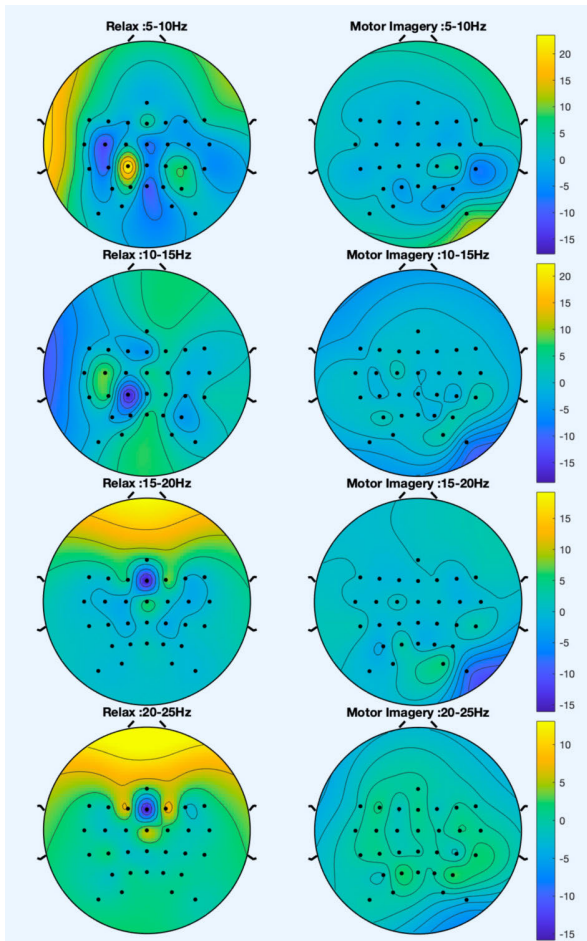


FIGURE 6. Spatial patterns for subject S22 that best discriminate between rest and MI classes.

Inter-subject differences with regards to MI BCI performance as well as underlying neural mechanisms remain unclear. Reference [35] studied which characteristics of the fronto-parietal attention network (FPAN) could play a relevant role in the prediction of the performance of the BCI. They observed that certain FPAN structural and functional features could be associated with higher or lower performance. Furthermore, the presence of certain cognitive states during resting state also appears to be associated with the performance [34].

In line with previous studies, the current work addressed inter-subject variability with subject specific modeling BCI [35]. CSP are adapted to every subject and session.

Since it was demonstrated that some users find it more difficult to modulate brain rhythms in a volitional way, future research could focus on adaptive training approaches. So for example, some subjects could need more training sessions or more trials in opened-loop control before starting with closed-loop control. There are some methodologies in the literature that have demonstrated to predict the BCI performance of a user [36]–[38]. Therefore, these neurological predictors could be employed to identify which individuals would need more training and more assistance by the researchers before starting the experiment.

On the other hand, it is important to highlight that the percentage of correctly classified epochs is lower in closed-loop trials (Accuracy) than in open-loop trials (%total). This does seem to depend on the fact that during closed-loop trials, subjects know how good they are performing, so they have an additional element that could affect their focus on the mental task. Similar results were reported by [25] in which it was performed hand and foot MI; and [39], where hand MI is studied using an exoskeleton located next to the subjects as feedback.

When comparing the results to [25], the average Accuracy of online closed-loop sessions is slightly superior in our proposed algorithm. However, their experiment is based on the classification between hand and foot MI and our approach is based on the distinction between MI of gait and rest.

Reference [26] shows a study with VR and functional electrical stimulation to enhance foot MI in an open-loop approach. The average accuracy was 78.1 ± 7.6 for VR and $84.8.1 \pm 7.0$ for the combination of VR with stimulation. These metrics can be confronted with %total in open-loop trials from experiment 2. While the performance is slightly superior for the appliance of functional electrical stimulation, the results achieved with our algorithm are higher in terms of non-stimulated VR.

Even though the study of [21] had a different experimental setup including a treadmill, it was based on foot MI, providing visual feedback through a screen. They reported an accuracy of 71% correctly classified epochs in open-loop trials and 70% in closed-loop trials. By comparing these metrics to %total in open-loop trials and %Commands in closed-loop trials, our approach showed a greater performance.

In [40], it is presented a BCI based on three brain tasks (left hand MI, right hand MI and foot MI) in which users did not get any feedback during training. Although it is not a direct comparison between foot MI and rest, the accuracy obtained during foot MI in training phase can be confronted to %MI from our open-loop trials. It is shown an average accuracy of 80.5 ± 5.9 which is lower than the results from our approach. Consequently, results suggest that the employment of visual feedback can enhance the realization of MI.

The performance of maintained MI or rest state can be challenging for subjects as they can be suddenly distracted from their task. As a consequence, the feedback from the VR environment can be negative, i.e. different from what was expected, and false movements or false stops can happen. Previous studies have assessed the level of attention of the subject during the experiment and based on it, the output commands were adapted so the number of false positives can be reduced [10]. Future research could combine our MI BCI with another one that measures the concentration/attention of subjects.

V. CONCLUSION

In this paper, it is proposed the employment of VR to provide real-time feedback when subjects are performing MI of gait. Since subjects are static, it can be assured that the BCI

algorithm is detecting MI and not the actual brain activity associated with motion. Firstly, it was compared if the immersion of the subject in the visual feedback paid a relevant role. It was checked that the visual feedback provided by VR was related to higher performances in most of the cases. On the other hand, the stability of the subject was also studied, but not differences were found between being seated or standing during the trials. Secondly, two subjects took part in online closed-loop sessions. They first performed some trials to train the classifier and then, they performed trials in which they received feedback in the VR environment based on the output of the BCI. The average accuracy in open-loop trials was 83.5 ± 6.2 . Regarding closed-loop trials, the average accuracy of predictions was 74.5 ± 8.8 . and the average accuracy of commands, 91.0 ± 6.7 . These real-time closed-loop results improve the outputs of other methodologies presented in literature.

Future work could design experiments that start with initial VR sessions. Therefore, subjects could learn to modulate their brain rhythms in an immersive environment that mitigates external distractions. Additionally, as the feedback provided by the VR environment is only visual, it is safer than any motion-related feedback, especially for users with motor disabilities with limited experience in the use of orthosis. Therefore, subjects could start with a BCI that controls a VR environment and when a certain level of performance is achieved, they could try other controlled devices, such as robotic exoskeletons.

Future research will study the introduction of a BCI with preliminary VR sessions before the subject employs a lower-limb exoskeleton in closed-loop control. It will assess the possibility to improve the BCI control success rate, but also the reduction of the training time needed to control successfully the exoskeleton.

REFERENCES

- [1] M. Jeannerod, "Mental imagery in the motor context," *Neuropsychologia*, vol. 33, no. 11, pp. 1419–1432, Nov. 1995.
- [2] C. Stippich, H. Oehmann, and K. Sartor, "Somatotopic mapping of the human primary sensorimotor cortex during motor imagery and motor execution by functional magnetic resonance imaging," *Neurosci. Lett.*, vol. 331, no. 1, pp. 50–54, Oct. 2002.
- [3] M. Bakker, F. P. de Lange, J. A. Stevens, I. Toni, and B. R. Bloem, "Motor imagery of gait: A quantitative approach," *Exp. Brain Res.*, vol. 179, no. 3, pp. 497–504, May 2007.
- [4] A. M. Batula, J. A. Mark, Y. E. Kim, and H. Ayaz, "Comparison of brain activation during motor imagery and motor movement using fNIRS," *Comput. Intell. Neurosci.*, vol. 2017, May 2017, Art. no. 5491296.
- [5] A. Gharabaghi, "What turns assistive into restorative brain-machine interfaces?" *Frontiers Neurosci.*, vol. 10, p. 456, Oct. 2016.
- [6] J. Liu, M. Abd-El-Barr, and J. H. Chi, "Long-term training with a brain-machine interface-based gait protocol induces partial neurological recovery in paraplegic patients," *Neurosurgery*, vol. 79, no. 6, pp. N13–N14, Dec. 2016.
- [7] G. Pfurtscheller, C. Neuper, D. Flotzinger, and M. Pregenzer, "EEG-based discrimination between imagination of right and left hand movement," *Electroencephalogr. Clin. Neurophysiol.*, vol. 103, no. 6, pp. 642–651, Dec. 1997.
- [8] E. Hortal, A. Úbeda, E. Iáñez, J. M. Azorín, and E. Fernández, "EEG-based detection of starting and stopping during gait cycle," *Int. J. Neural Syst.*, vol. 26, no. 7, Nov. 2016, Art. no. 1650029.
- [9] M. Ortiz, M. Rodríguez-Ugarte, E. Iáñez, and J. M. Azorín, "Application of the stockwell transform to electroencephalographic signal analysis during gait cycle," *Frontiers Neurosci.*, vol. 11, p. 660, Nov. 2017.
- [10] M. Ortiz, L. Ferrero, E. Iáñez, J. M. Azorín, and J. L. Contreras-Vidal, "Sensory integration in human movement: A new brain-machine interface based on gamma band and attention level for controlling a lower-limb exoskeleton," *Frontiers Bioeng. Biotechnol.*, vol. 8, p. 735, Sep. 2020.
- [11] A. Kilicarslan and J. L. C. Vidal, "Characterization and real-time removal of motion artifacts from EEG signals," *J. Neural Eng.*, vol. 16, no. 5, Sep. 2019, Art. no. 056027.
- [12] A. H. Do, P. T. Wang, C. E. King, S. N. Chun, and Z. Nenadic, "Brain-computer interface controlled robotic gait orthosis," *J. NeuroEng. Rehabil.*, vol. 10, no. 1, p. 111, 2013.
- [13] K. Lee, D. Liu, L. Perroud, R. Chavarriaga, and J. D. R. Millán, "A brain-controlled exoskeleton with cascaded event-related desynchronization classifiers," *Robot. Auto. Syst.*, vol. 90, pp. 15–23, Apr. 2017.
- [14] H. Shibasaki and M. Hallett, "What is the Bereitschaftspotential?" *Clin. Neurophysiol.*, vol. 117, no. 11, pp. 2341–2356, Nov. 2006.
- [15] A. Kilicarslan, S. Prasad, R. G. Grossman, and J. L. Contreras-Vidal, "High accuracy decoding of user intentions using EEG to control a lower-body exoskeleton," in *Proc. 35th Annu. Int. Conf. IEEE Eng. Med. Biol. Soc. (EMBC)*, Osaka, Japan, Jul. 2013, pp. 5606–5609.
- [16] N.-S. Kwak, K.-R. Müller, and S.-W. Lee, "A lower limb exoskeleton control system based on steady state visual evoked potentials," *J. Neural Eng.*, vol. 12, no. 5, Oct. 2015, Art. no. 056009.
- [17] X. Zhang, G. Xu, J. Xie, M. Li, W. Pei, and J. Zhang, "An EEG-driven lower limb rehabilitation training system for active and passive co-stimulation," in *Proc. 37th Annu. Int. Conf. IEEE Eng. Med. Biol. Soc. (EMBC)*, Milano, Italy, Aug. 2015, pp. 4582–4585.
- [18] K. Gui, H. Liu, and D. Zhang, "Toward multimodal human-robot interaction to enhance active participation of users in gait rehabilitation," *IEEE Trans. Neural Syst. Rehabil. Eng.*, vol. 25, no. 11, pp. 2054–2066, Nov. 2017.
- [19] D. Liu, W. Chen, Z. Pei, and J. Wang, "A brain-controlled lower-limb exoskeleton for human gait training," *Rev. Sci. Instrum.*, vol. 88, no. 10, Oct. 2017, Art. no. 104302.
- [20] V. Rajasekaran, E. López-Larraz, F. Trincado-Alonso, J. Aranda, L. Montesano, A. J. Del-Ama, and J. L. Pons, "Volition-adaptive control for gait training using wearable exoskeleton: Preliminary tests with incomplete spinal cord injury individuals," *J. NeuroEng. Rehabil.*, vol. 15, no. 1, pp. 1–15, Dec. 2018.
- [21] T. P. Luu, Y. He, S. Brown, S. Nakagome, and J. L. Contreras-Vidal, "A closed-loop brain computer interface to a virtual reality avatar: Gait adaptation to visual kinematic perturbations," in *Proc. Int. Conf. Virtual Rehabil. (ICVR)*, Valencia, Spain, Jun. 2015, pp. 30–37.
- [22] F. Škola, S. Tinková, and F. Liarokapis, "Progressive training for motor imagery brain-computer interfaces using gamification and virtual reality embodiment," *Frontiers Hum. Neurosci.*, vol. 13, p. 329, Sep. 2019.
- [23] J. W. Choi, S. Huh, and S. Jo, "Improving performance in motor imagery BCI-based control applications via virtually embodied feedback," *Comput. Biol. Med.*, vol. 127, Dec. 2020, Art. no. 104079.
- [24] J. M. Juliano, R. P. Spicer, A. Vourvopoulos, S. Lefebvre, K. Jann, T. Ard, E. Santarnecchi, D. M. Krum, and S.-L. Liew, "Embodiment is related to better performance on a brain-computer interface in immersive virtual reality: A pilot study," *Sensors*, vol. 20, no. 4, p. 1204, Feb. 2020.
- [25] S. N. Resalat and V. Saba, "A study of various feature extraction methods on a motor imagery based brain computer interface system," *Basic Clin. Neurosci.*, vol. 7, no. 1, pp. 13–19, Jan. 2016.
- [26] S. Ren, W. Wang, Z.-G. Hou, X. Liang, J. Wang, and W. Shi, "Enhanced motor imagery based brain-computer interface via FES and VR for lower limbs," *IEEE Trans. Neural Syst. Rehabil. Eng.*, vol. 28, no. 8, pp. 1846–1855, Aug. 2020.
- [27] K. K. Ang, Z. Y. Chin, H. Zhang, and C. Guan, "Filter bank common spatial pattern (FBCSP) in brain-computer interface," in *Proc. IEEE Int. Joint Conf. Neural Netw., IEEE World Congr. Comput. Intell.*, Jun. 2008, pp. 2390–2397.
- [28] W. Abbas and N. A. Khan, "FBCSP-based multi-class motor imagery classification using BP and TDP features," in *Proc. 40th Annu. Int. Conf. IEEE Eng. Med. Biol. Soc. (EMBC)*, Jul. 2018, pp. 215–218.
- [29] K. K. Ang, Z. Y. Chin, C. Wang, C. Guan, and H. Zhang, "Filter bank common spatial pattern algorithm on BCI competition IV datasets 2a and 2b," *Frontiers Neurosci.*, vol. 6, pp. 1–9, Mar. 2012.

- [30] J. Choi, K. T. Kim, J. H. Jeong, L. Kim, S. J. Lee, and H. Kim, "Developing a motor imagery-based real-time asynchronous hybrid BCI controller for a lower-limb exoskeleton," *Sensors*, vol. 20, no. 24, p. 7309, Dec. 2020.
- [31] Y. Zhang, G. Zhou, J. Jin, X. Wang, and A. Cichocki, "Optimizing spatial patterns with sparse filter bands for motor-imagery based brain-computer interface," *J. Neurosci. Methods*, vol. 255, pp. 85–91, Nov. 2015.
- [32] Y. Jiao, T. Zhou, L. Yao, G. Zhou, X. Wang, and Y. Zhang, "Multi-view multi-scale optimization of feature representation for EEG classification improvement," *IEEE Trans. Neural Syst. Rehabil. Eng.*, vol. 28, no. 12, pp. 2589–2597, Dec. 2020.
- [33] H. Ramoser, J. Muller-Gerking, and G. Pfurtscheller, "Optimal spatial filtering of single trial EEG during imagined hand movement," *IEEE Trans. Rehabil. Eng.*, vol. 8, no. 4, pp. 441–446, Dec. 2000.
- [34] N. Robinson, K. P. Thomas, and A. P. Vinod, "Neurophysiological predictors and spectro-spatial discriminative features for enhancing SMR-BCI," *J. Neural Eng.*, vol. 15, no. 6, Dec. 2018, Art. no. 066032.
- [35] T. Zhang, T. Liu, F. Li, M. Li, D. Liu, R. Zhang, H. He, P. Li, J. Gong, C. Luo, D. Yao, and P. Xu, "Structural and functional correlates of motor imagery BCI performance: Insights from the patterns of fronto-parietal attention network," *NeuroImage*, vol. 134, pp. 475–485, Jul. 2016.
- [36] M. Torkamani-Azar, A. Jafarifarmand, and M. Cetin, "Prediction of motor imagery performance based on pre-trial spatio-spectral alertness features," in *Proc. 42nd Annu. Int. Conf. IEEE Eng. Med. Biol. Soc. (EMBC)*, Montreal, QC, Canada, Jul. 2020, pp. 3062–3065.
- [37] C. Jeunet, B. N'Kaoua, S. Subramanian, M. Hachet, and F. Lotte, "Predicting mental imagery-based BCI performance from personality, cognitive profile and neurophysiological patterns," *PLoS ONE*, vol. 10, no. 12, Dec. 2015, Art. no. e0143962.
- [38] H.-I. Suk, S. Fazli, J. Mehnert, K.-R. Müller, and S.-W. Lee, "Predicting BCI subject performance using probabilistic spatio-temporal filters," *PLoS ONE*, vol. 9, no. 2, Feb. 2014, Art. no. e87056.
- [39] S. Y. Gordleeva, M. V. Lukoyanov, S. A. Mineev, M. A. Khoruzhko, V. I. Mironov, A. Y. Kaplan, and V. B. Kazantsev, "Exoskeleton control system based on motor-imaginary brain-computer interface," *Sovremennye Tehnologii V Med.*, vol. 9, no. 3, pp. 31–36, Sep. 2017.
- [40] C. Wang, X. Wu, Z. Wang, and Y. Ma, "Implementation of a brain-computer interface on a lower-limb exoskeleton," *IEEE Access*, vol. 6, pp. 38524–38534, 2018.



L. FERRERO (Member, IEEE) was born in Alicante, Spain, in 1995. She received the degree in biomedical engineering from the Technical University of Valencia, in 2017, and the M.Sc. degree in data science from the Technical University of Madrid and the Eindhoven University of Technology, in 2019. She is currently pursuing the Ph.D. degree in industrial and telecommunication technology.

She is currently working as a Researcher with the Brain–Machine Interface Systems Laboratory, Miguel Hernández University of Elche, Spain. Her current research interest includes control of lower-limb exoskeletons by means of brain–machine interfaces.



M. ORTIZ (Member, IEEE) was born in Murcia, Spain, in 1978. He received the degree in industrial engineering and the Ph.D. degree from the Universidad Politécnica de Cartagena, in 2002 and 2016, respectively.

In 2019, he was a Visiting Researcher with the Non-invasive Brain–Machine Interface Systems Laboratory, University of Houston. He is currently an Associate Professor with the Department of Mechanical Engineering and Energy and a member

of the Brain–Machine Interface Systems Laboratory, Miguel Hernández University of Elche, Spain. His research interests include mathematical transforms applied to electrical signal processing, neural network applications for signal classification, and brain–machine interfaces.



V. QUILES (Member, IEEE) received the degree in industrial technical engineering specialized in electronics from the Miguel Hernández University of Elche, Spain, in 2017, and the master's degree in artificial intelligent from the Polytechnic University of Madrid, in 2017. He is currently pursuing the Ph.D. degree in industrial and telecommunication technology with the Brain–Machine Interface Systems Laboratory, Miguel Hernández University of Elche.

In 2019, he worked as a Research Assistant in collaboration with San Vicente del Raspeig Hospital, Alicante, Spain. His main research interest includes appliance of new IA techniques in order to decode brain signals.



E. IÁÑEZ (Member, IEEE) received the M.Sc. degree in telecommunication engineering and the Ph.D. degree in communication and industrial technologies from the Miguel Hernández University of Elche, Spain, in 2007 and 2012, respectively. He is currently a Scientific Researcher with the Brain–Machine Interface Systems Laboratory, Miguel Hernández University of Elche. He is focused on brain–computer interfaces (BCI) (non-invasive brain interfaces) and multimodal

human–robot interfaces (integrating brain, ocular, and haptic information). His current research interests include human–robot and human–computer interfaces.



J. M. AZORÍN (Senior Member, IEEE) received the M.Sc. degree in computer science from the University of Alicante, Spain, in 1997, and the Ph.D. degree in telerobotics from the Miguel Hernández University of Elche, Spain, in 2003.


He is currently the Director of the Brain–Machine Interface Systems Laboratory and a Full Professor with the Department of Systems Engineering and Automation, Miguel Hernández University of Elche. He has been a Visiting Pro-

fessor with the University of Houston, USA, and Imperial College London, U.K. Since 1999, he has been active in research within several projects on advanced robotics. Over the last years, his research has been funded by prestigious grants from the European Union, other international government agencies, and Spain. He has been the PI of more than 20 research projects, and his research has resulted in more than 200 technical articles and three patents. His current research interests include brain–computer interfaces, neuro-robotics, assistive robotics, and rehabilitation robotics. Since February 2012, he has been a member of the Publication Board of the IEEE Robotics and Automation Society, the Advisory Committee of the IEEE Systems Council, the IEEE Engineering in Medicine and Biology Society, and the Spanish Association inside the International Federation of Automatic Control (CEA-IFAC). He was a recipient of the "Best Thesis in the Department of Industrial Systems Engineering" from the Miguel Hernández University of Elche, in 1996. He is currently a Distinguished Lecturer of the IEEE Systems Council.

...

Article

A BMI Based on Motor Imagery and Attention for Commanding a Lower-Limb Robotic Exoskeleton: A Case Study

Laura Ferrero * , Vicente Quiles, Mario Ortiz , Eduardo Iáñez  and José M. Azorín 

Brain-Machine Interface System Lab, Miguel Hernández University of Elche, 03202 Elche, Spain; vquiles@umh.es (V.Q.); mortiz@umh.es (M.O.); eianez@umh.es (E.I.); jm.azorin@umh.es (J.M.A.)

* Correspondence: lferrero@umh.es

Abstract: Lower-limb robotic exoskeletons are wearable devices that can be beneficial for people with lower-extremity motor impairment because they can be valuable in rehabilitation or assistance. These devices can be controlled mentally by means of brain–machine interfaces (BMI). The aim of the present study was the design of a BMI based on motor imagery (MI) to control the gait of a lower-limb exoskeleton. The evaluation is carried out with able-bodied subjects as a preliminary study since potential users are people with motor limitations. The proposed control works as a state machine, i.e., the decoding algorithm is different to start (standing still) and to stop (walking). The BMI combines two different paradigms for reducing the false triggering rate (when the BMI identifies irrelevant brain tasks as MI), one based on motor imagery and another one based on the attention to the gait of the user. Research was divided into two parts. First, during the training phase, results showed an average accuracy of $68.44 \pm 8.46\%$ for the MI paradigm and $65.45 \pm 5.53\%$ for the attention paradigm. Then, during the test phase, the exoskeleton was controlled by the BMI and the average performance was $64.50 \pm 10.66\%$, with very few false positives. Participants completed various sessions and there was a significant improvement over time. These results indicate that, after several sessions, the developed system may be employed for controlling a lower-limb exoskeleton, which could benefit people with motor impairment as an assistance device and/or as a therapeutic approach with very limited false activations.

Keywords: brain–machine interfaces; EEG; exoskeleton; motor imagery



Citation: Ferrero, L.; Quiles, V.; Ortiz, M.; Iáñez, E.; Azorín, J.M. A BMI Based on Motor Imagery and Attention for Commanding a Lower-Limb Robotic Exoskeleton: A Case Study. *Appl. Sci.* **2021**, *11*, 4106. <https://doi.org/10.3390/app11094106>

Academic Editor: Carlos A. Jara

Received: 28 February 2021

Accepted: 29 April 2021

Published: 30 April 2021

Publisher's Note: MDPI stays neutral with regard to jurisdictional claims in published maps and institutional affiliations.



Copyright: © 2021 by the authors. Licensee MDPI, Basel, Switzerland. This article is an open access article distributed under the terms and conditions of the Creative Commons Attribution (CC BY) license (<https://creativecommons.org/licenses/by/4.0/>).

1. Introduction

Robotic exoskeletons are wearable devices that can enhance physical performance and provide movement assistance. In the case of lower-limb robotic exoskeletons, they can be beneficial for people with motor impairment in the lower extremities as they can assist the gait and facilitate rehabilitation [1]. The combination of lower-limb robotic exoskeletons with brain–machine interfaces (BMI), which are systems that decode neural activity to drive output devices, offers a new method to provide motor support. Thus, patients could walk while being assisted by an exoskeleton that is controlled by their brain activity.

In the literature, there are different BMI control paradigms for lower-limb exoskeletons based on brain changes. The most common ones are steady-state visually evoked potentials [2], which are based on visual stimuli; motion-related cortical potentials [3–6], which are produced between 1500 and 500 ms before the execution of the movement, and event-related desynchronization/synchronization (ERD/ERS), which is considered to indicate the activation and posterior recovery of the motor cortex during preparation and completion of a movement [7–9]. BMI based on ERD/ERS are usually employed to detect motion intention [3,6,10]. Similar ERD/ERS patterns are produced during motor imagery (MI), which consists of the imagination of a movement [11–13]. When performing MI, in contrast to external stimuli, brain changes are induced voluntarily and internally by the subject. BMI based on MI have the objective of identifying different MI tasks or differentiat-

ing between MI and an idle state [5,14–16]. The work of [16] combined MI with eye blinks as a control criterion.

The main limitation of MI is that patients have to maintain it for long periods in order to force the external device to perform any action. However, contrary to instantaneous brain changes, such as MRCP or motion intention, continuous cognitive involvement of a patient during the assisted motion can induce mechanisms of neuroplasticity. Neuroplasticity is the ability of the brain to reorganize its structure and promote rehabilitation [17]. The performance of maintained brain tasks can be challenging as it requires high focus from the user during the whole experiment and any external influence could easily disturb it. Previous studies have tried to evaluate the level of attention of a subject during the control of the external device [18] and some of them have considered it as a control paradigm for a lower-limb BMI [15]. BMI systems need a training phase in which the model is calibrated for each subject and then it is tested with with new data. In [5,14–16], during the training phase, participants alternated periods of MI with idle state and the output device was only moving during MI. Nevertheless, since BMI focus on sensorimotor rhythms, it is difficult to ensure that it is not considering the actual motion instead of motor imagery.

In our previous work [19], we designed a lower-limb MI BMI to control a treadmill and it was tested with able-bodied subjects. The BMI combined the paradigm of MI with another one that measured the level of attention that users had during MI tasks. In the test phase, i.e., when the output device was commanded by the BMI, the treadmill was only activated when the attention measured was higher than a certain threshold, reducing the number of false triggers. In order to ensure that motion artifacts did not affect the BMI classifier model, the training phase consisted of two types of trials: full standing and full motion trials. The mental tasks to perform were the same for both types, alternating periods of MI with idle state. Both types of trials allowed the creation of two different classifier models to be applied depending on the status of the subject: gait and stand.

In this study, the BMI designed in [19] was adapted for the control of the gait of a lower-limb exoskeleton and it was evaluated with able-bodied subjects. The combination of this BMI with a lower-limb exoskeleton is a promising and intuitive assistive approach for people with motor impairment. In addition, it could potentially benefit people with cortical damage (e.g., after a stroke) as a therapeutic approach for the recovery of lost motor function. Participants were trained over 2–5 days to assess the effect of practice on the performance. Each day's session was divided into two parts: the training and test phases. During training, subjects performed trials in which the exoskeleton was walking the entire time and trials in which it was standing. In the test phase, the exoskeleton provided real-time feedback in a closed-loop control scenario. This is a previous step in the development of a BMI that will reinforce rehabilitation and/or assist the gait for patients with neurological damage.

2. Materials and Methods

2.1. Participants

Two subjects participated in the study (mean age 23.5 ± 3.5). They did not report any known disease and had no movement impairment. They did not have any previous experience with BMI. They were informed about the experiments and signed an informed consent form in accordance with the Declaration of Helsinki. All procedures were approved by the Responsible Research Office of Miguel Hernández University of Elche.

2.2. Equipment

Brain activity was recorded with electroencephalography (EEG). A 32-electrode system actiCap (Brain Products GmbH, Germany) was employed to record EEG signals. The 27 channels selected for acquisition were: F3, FZ, FC1, FCZ, C1, CZ, CP1, CPZ, FC5, FC3, C5, C3, CP5, CP3, P3, PZ, F4, FC2, FC4, FC6, C2, C4, CP2, CP4, C6, CP6, P4. They were placed following the 10-10 international system on an actiCAP (Brain Products GmbH, Germany). Four electrodes were located next to the eyes to record electrooculography

(EOG) and ground and reference electrodes were located on the right and left ear lobes, respectively. Each channel signal was amplified with BrainVision BrainAmp amplifier (Brain Products GmbH, Germany). Finally, signals were transmitted wirelessly to the BrainVision recorder software (Brain Products GmbH, Germany).

H3 exoskeleton (Technaid, Madrid, Spain) was employed to assist the movement and participants used crutches as support. Control start/stop gait commands were sent via Bluetooth. The experimental setup can be seen in Figure 1.

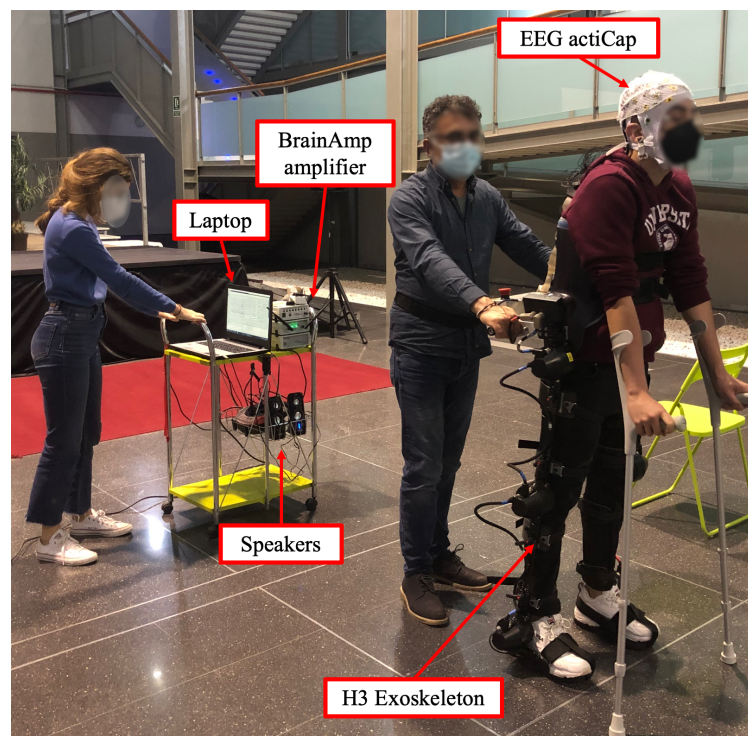


Figure 1. Experimental setup.

2.3. Experimental Design

Each participant completed several sessions and each session was divided into two parts. The first part consisted of the training phase, in which the exoskeleton was in opened-loop control. Thus, it was remotely controlled by the laptop with predefined commands based on the mental tasks to be registered and not by the output of the BMI classifier. Afterwards, the second part of the session allowed assessment of the BMI performance during closed-loop control of the exoskeleton. Commands issued by the BMI were sent to the exoskeleton in real time based on the decoding of the brain activity obtained as output of the BMI classifier, receiving the subjects' real-time feedback on their performance.

2.3.1. Training Phase

In the first part of each session, subjects performed 20 trials. Each trial consisted of a sequence of three mental tasks: MI of the gait, idle state and regressive count. For idle state, participants were asked to be as relaxed as possible. The regressive count was randomly changed every trial and consisted of a number between 300 and 1000 and a subtrahend between 1 and 9. For example, if they were given the count 500-4, they had to compute the series of subtractions of 496, 492, 488... until they had to perform the following task. This task aims to focus the subject on a demanding mental task very different to MI in order to assess a low level of attention to gait. The protocol can be seen in Figure 2a. There was a voice message that indicated the beginning of each task: 'Relax', 'Imagine', '500-5'. The message for the regressive count indicated a different mathematical operation

each time. In order to avoid evoked potentials, the 4 s period after auditory cues was not considered for further analysis.

During the session, subjects used crutches to maintain stability. In addition, a member of the research staff softly held the exoskeleton to prevent any possible loss of balance or fall. Ten of the training trials were performed in a full no-motion status and the other ten in a full motion status assisted by the exoskeleton. These trials were employed to train two different BMI classifiers: StandClassifiers (with non-motion trials) and GaitClassifiers (with full motion trials).

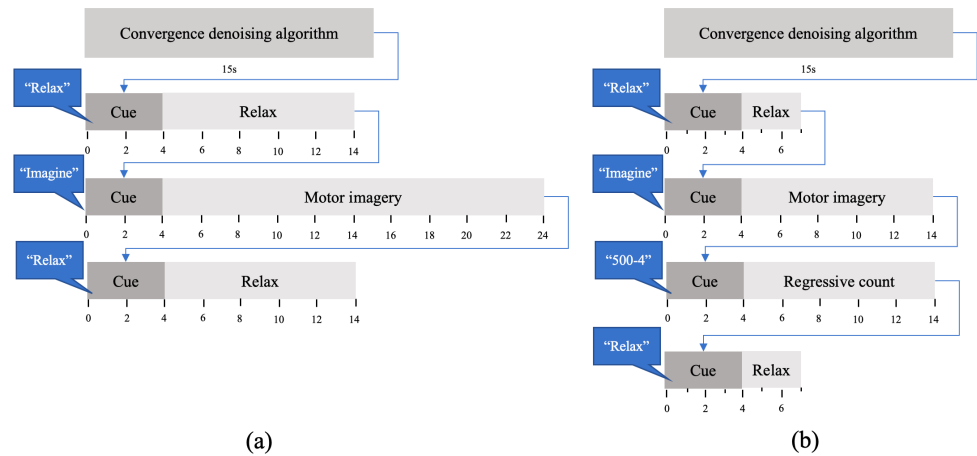


Figure 2. (a) The protocol of opened-loop trials and (b) the protocol of close-loop trials.

2.3.2. Test Phase

In the second part of each session, the BMI was tested in closed-loop control with the two groups of classifiers obtained with the data of the training phase (StandClassifiers, GaitClassifiers). Subjects performed five trials, whose protocol can be seen in Figure 2b. The transition between tasks was indicated with voice messages for ‘Relax’ and ‘Imagine’ tasks. Notice that no ‘Regression count’ task was considered, as attention level to gait was computed based on the information from training, but there was no need to implement a low-level gait attention task in the testing trials.

2.4. Brain Machine Interface

The presented BMI had the following steps: data acquisition, pre-processing, feature extraction, classification, exoskeleton control and evaluation.

As indicated before, this BMI was based on two paradigms: MI and attention. The first one was based on the distinction between MI of the gait and an idle state, so only data associated with these brain tasks were considered to train the classifiers (relax and motor imagery). With regard to the attention paradigm, it measured the level of attention to gait. Therefore, it had the objective of differentiating between the attention of the subject during MI and the attention during irrelevant tasks. For this paradigm, all brain tasks from training trials were contemplated (relax, motor imagery and regressive count). While the attention to the gait was assumed to be high during MI tasks, it was assumed to be low during regressive count and idle state. The schema of the BMI can be seen in Figure 3.

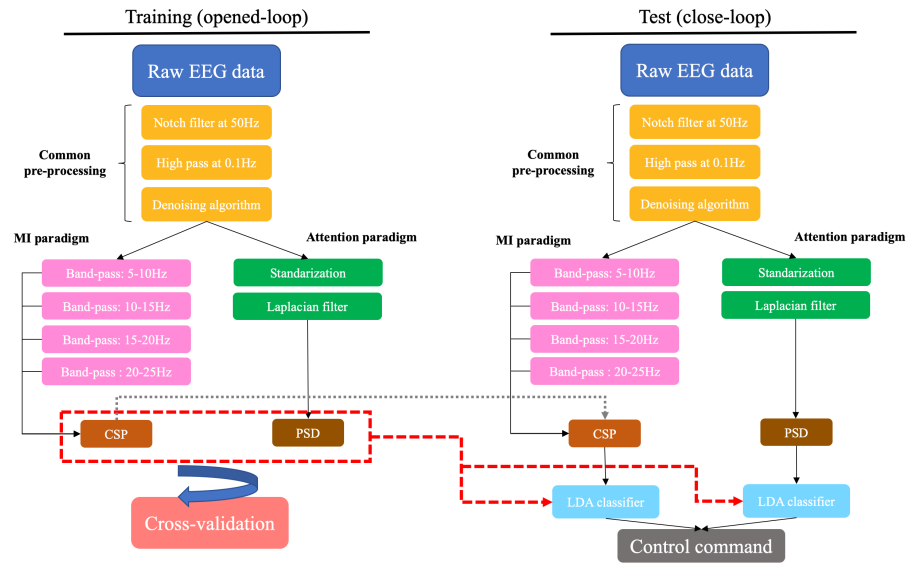


Figure 3. Brain–machine interface (BMI) scheme. During training, the exoskeleton was in opened-loop control, and for testing, it was in closed-loop control. The BMI used two different paradigms: one based on motor imagery of gait and another one based on the user’s level of attention to gait. Both paradigms shared some steps of pre-processing but there were additional different steps for each one. Then, two different feature extraction methods were employed. Trials from the training phase were used to train the BMI classifiers for testing.

2.4.1. Data Acquisition

EEG signals were recorded at a sampling frequency of 200 Hz. Then, epochs of 1 s with 0.5 s of shifting were extracted and processed.

2.4.2. Pre-Processing

The pre-processing stage started with two frequency filters: a notch filter at 50 Hz to remove the contribution of the power line and a high-pass filter at 0.1 Hz. In order to reduce motion artifacts, electrode wires were fixed with clamps and a medical mesh. The movement of jaw muscles can generate signal artifacts, so subjects were asked to not swallow or chew while they were performing MI, regressive count or were in a idle state.

The H_{∞} denoising algorithm was applied to mitigate the presence of eye artifacts and signal drifts [5]. This algorithm estimates the contribution of the EOG and a constant parameter to the EEG signal and removes it. Afterwards, there were two different pre-processing lines, one for each paradigm.

For the MI paradigm, a filter bank comprising multiple band-pass filters was applied to the data after the H_{∞} denoising algorithm. Four band-pass filters were employed to obtain data associated with alpha and beta rhythms.

Regarding the attention paradigm, EEG signals from each channel were first standardized following the process presented in [20]. For each channel, the maximum visual threshold was computed as the mean of the 6 highest values of the signal. This value was iteratively updated for each epoch and it was used to standardize the data as

$$SV(t)_{ch} = \frac{V(t)_{ch}}{\frac{1}{C_h} \sum_{j=1}^{C_h} MVThreshold_j} \tag{1}$$

The signal of each chanel, $V(t)_{ch}$, was normalized taking into consideration the maximum visual threshold ($MVThreshold$) of all the EEG channels. Subsequently, the surface Laplacian filter was used to reduce spatial noise and enhance the local activity of each electrode [21].

2.4.3. Feature Extraction

The following step of the BMI has the objective of computing the characteristics of the EEG during each brain task that could be discriminating.

For the MI paradigm, common spatial patterns (CSP) [22] are computed for each frequency band. CSP estimate a spatial transformation that maximizes the discriminability between two brain patterns. If X is the EEG that has $N * T$ dimensions, which are the number of channels and number of samples, respectively, the CSP algorithm estimates a matrix of spatial filters W that discriminates between two classes: (X_1) and (X_2). Firstly, the normalized covariance matrices are computed for each class as in

$$C_1 = \frac{X_1 X_1^T}{\text{trace}(X_1 X_1^T)}, C_2 = \frac{X_2 X_2^T}{\text{trace}(X_2 X_2^T)}. \quad (2)$$

These matrices are computed for each trial and \bar{C}_1 and \bar{C}_2 are calculated by averaging over all trials of the same class. The averaged covariance matrices are combined to result in the composite spatial covariance matrix that can be factorized as

$$C = \bar{C}_1 + \bar{C}_2 = U_0 \Sigma U_0^T. \quad (3)$$

U_0 is a matrix of eigenvectors and Σ is the diagonal matrix of eigenvalues. The averaged covariance matrices are transformed as

$$P = \Sigma^{1/2} U_0^T, \quad (4)$$

$$S_1 = P \bar{C}_1 P^T, S_2 = P \bar{C}_2 P^T. \quad (5)$$

S_1 and S_2 have common eigenvectors, and the sum of both matrices of eigenvalues is the identity matrix.

$$S_1 = U \Sigma_1 U^T, S_2 = U \Sigma_2 U^T \text{ and } \Sigma_1 + \Sigma_2 = I \quad (6)$$

The projection matrix is obtained as

$$W = U^T P. \quad (7)$$

Z is the projection of the original EEG signal S into another space. Columns of W^{-1} are the spatial patterns.

$$Z = W X \quad (8)$$

Although Z has $N * T$ dimensions, the first and last rows are the components that can be better discriminated in terms of their variance. Therefore, for feature extraction, only the m first and last components of Z are considered. Z_p is the subset of Z and the variances of each component are computed and normalized with the logarithm as

$$f_p = \log \frac{\text{var}(Z_p)}{\sum_{i=1}^{2m} Z_p}. \quad (9)$$

f_p is the vector of features and has $(fbands * 2 * m) * T$ dimension. m was set to 4, and in the pre-processing phase, 4 band-pass filters were employed so the dimension is $32 * T$.

For the attention paradigm, power spectral estimation by Maximum Entropy Method (MEM) was used to obtain features associated with each task. The signal of each electrode was estimated as an autoregressive model in which the known autocorrelation coefficients were calculated and the unknown coefficients were estimated by maximizing the spectral entropy [23]. Afterwards, the autocorrelation coefficients were used to compute the power spectrum that was compatible with the fragment of the signal analyzed, but it was also evasive regarding unseen data. Afterwards, only the power of the frequencies in the gamma band was considered [15].

2.4.4. Classification

Training trials of each session were evaluated using leave-one-out cross-validation. Each trial was once used as a test and the remaining trials conformed to the training group. This process was performed independently for trials in which subjects were standing (10 trials) and trials in which they were in motion (10 trials). Linear Discriminant Analysis (LDA) [24] classifiers were created depending on the subject status—full standing trials (StandClassifiers) and full motion trials (GaitClassifiers)—each one with two different models based on the decoding paradigm: MI and attention paradigms. As stated above, whereas LDA classifiers of the MI paradigm were only trained with data from MI and idle state, LDA classifiers of the attention paradigm were trained with data from all brain tasks (idle, regressive count, MI).

Concerning the test phase, the developed BMI was designed as a state machine system in which a group of classifiers was chosen based on the status of the exoskeleton. This way, if the subject is in a standing position, the MI and attention classifiers of the full standing trials (StandClassifiers) are used to decide if the exoskeleton keeps standing or starts moving, but if the subject is moving, the MI and attention classifiers obtained by the full motion trials (GaitClassifiers) are used to continue walking or to stop. Predictions from both paradigms were combined to decode control commands. Its design can be seen in Figure 4. In summary, in each test trial, subjects started standing with the exoskeleton and StandClassifiers were employed. The system could decode stop or walk commands based on the prediction of their MI and attention classifiers. When a walk command was sent to the exoskeleton, it started the gait and the system was changed to Gait state. Consequently, GaitClassifiers were employed afterwards. Again, the system could decode stop or walk commands, but when a stop command was issued, the exoskeleton stopped the gait and the system changed to Stand state again.

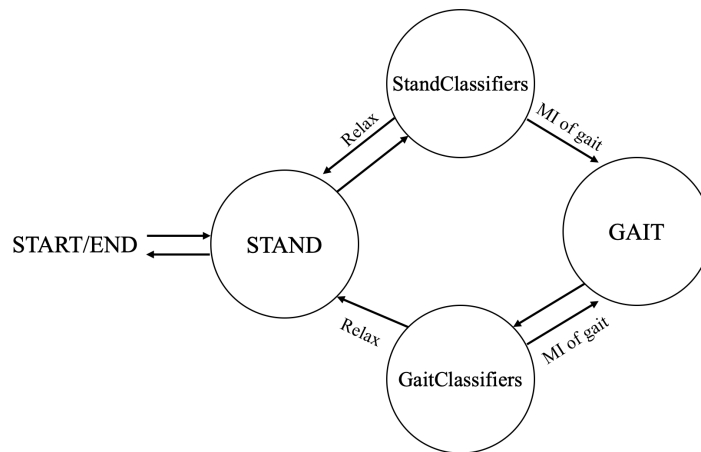


Figure 4. State machine design of the brain–machine interface (BMI). There are two states, gait and stand, that depend on the exoskeleton status. Each state is associated with two different classifiers, one for each paradigm, that will be used to give decode control commands.

2.4.5. Exoskeleton Control

In the test phase, the exoskeleton was controlled by BMI decoded commands. MI classifiers could predict two classes, 0 for idle state and 1 for MI, and attention classifiers could predict a 0 for low attention to gait and a 1 for high attention. These predictions were averaged every 10 s, which resulted in MI and attention indices that ranged from 0 to 1. Control commands were selected based on the following rules:

- During 5 s, new commands cannot be issued.
- If subject was standing:

- If the MI index was higher than or equal than 0.7 or the MI index was higher than or equal than 0.6 and the attention index was higher than or equal to 0.4, a move command was issued and the exoskeleton started the gait.
- Otherwise, the exoskeleton kept standing.
- If the subject was walking:
 - If the MI index was lower than or equal to 0.4, a stop command was issued and the exoskeleton stopped the gait.
 - Otherwise, it kept walking.

2.5. Evaluation

The accuracy of training trials was defined as the percentage of correctly classified epochs during each brain task. This metric was computed separately for trials in which participants were moving and trials in which they were static. Furthermore, the performance of closed-loop trials was assessed with the following indices:

- %MI and %Att: percentage of epochs of data correctly classified for each paradigm.
- %Commands: percentage of epochs of data with correct control commands.
- Accuracy commands: percentage of correct commands issued.
- True positive ratio (TPR): percentage of MI periods in which a walking event is executed. There is only an event of MI per trial, so this value can only be 0 or 100% per trial.
- False positives (FP) and false positives per minute (FP/min): moving commands issued during rest periods.

Transition events were not considered for the computation of evaluation metrics.

3. Results

During training, participants wore the exoskeleton in an opened-loop control. Each subject completed several sessions, and on each of them, they completed 20 trials: 10 trials standing still and 10 trials walking. Results from subjects S1 and S2 are shown in Tables 1 and 2, respectively. It must be noted that they did not have the same amount of practice since they participated in a different number of sessions. Two different BMI paradigms were carried out. For the MI paradigm, S1 reached an average accuracy of $72.77 \pm 6.61\%$ with a difference of around 6% between the two conditions, standing and walking. In the last session, S2 achieved an average accuracy of 64.11 ± 9.98 with a difference of 20% between the two approaches. With respect to the attention paradigm, S1 obtained an accuracy of 65.06 ± 6.44 with a difference of 8%, and S2 achieved 65.83 ± 4.43 and a 10% difference. The average accuracy of the MI and attention paradigm was $68.44 \pm 8.46\%$ and $65.45 \pm 5.53\%$, respectively.

Figures 5 and 6 show the spatial patterns of S1 and S2 in their last session. Moreover, in order to provide a comparison under the same conditions, Figure 7 shows the spatial patterns of S3 in the second session. The spatial patterns estimated during trials without movement show that for S1 and S2, electrode FCz seems to have a relevant role in the discrimination of idle state. During MI events, the most significant electrodes for both subjects are peripheral as FC5. However, results from S2 show that in the 5–10 Hz band, C2 and CPz are relevant to the MI of gait. Regarding trials in which participants are walking, the distribution of relevant areas seems scattered for idle state and for MI; peripheral electrodes are also highlighted.

When comparing the spatial patterns of S2 in two different sessions, the main similarities can be found in the stand trials. CPz and Cz are highlighted for the relax class and electrode FC5 seems to be significant for the MI class.

3.1. Training Phase

Table 1. Results from training, subject S1. Trials with opened-loop control of the exoskeleton.

		Session 1	Session 2
Stand	%MI	59.29 ± 10.51	69.64 ± 7.62
	%Att	57.38 ± 9.27	60.83 ± 7.58
Gait	%MI	58.93 ± 11.60	75.89 ± 5.41
	%Att	65.83 ± 8.57	69.29 ± 5.04

Table 2. Results from training, subject S2. Trials with opened-loop control of the exoskeleton.

		Session 1	Session 2	Session 3	Session 4	Session 5
Stand	%MI	53.32 ± 8.59	69.64 ± 8.70	65.54 ± 5.12	64.2 ± 11.45	74.11 ± 6.14
	%Att	63.95 ± 4.44	62.57 ± 8.77	58.21 ± 8.76	59.52 ± 8.44	60.83 ± 5.48
Gait	%MI	50.26 ± 7.54	54.17 ± 8.75	62.50 ± 8.91	59.82 ± 10.11	54.11 ± 12.71
	%Att	61.05 ± 5.13	63.36 ± 2.84	61.55 ± 7.21	65.71 ± 6.82	70.83 ± 3.04

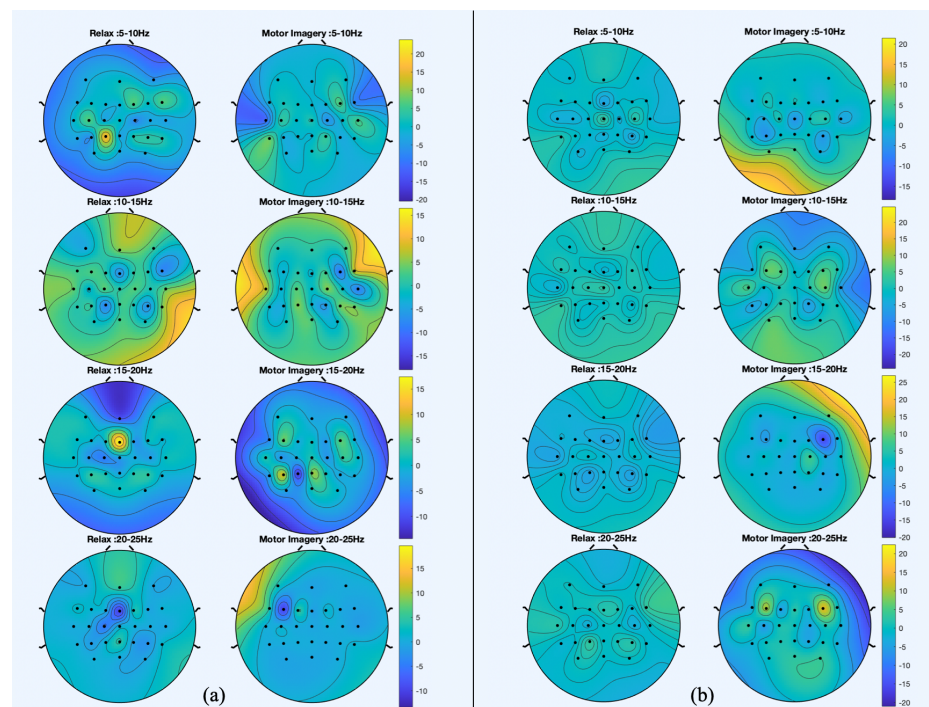


Figure 5. Spatial patterns for the session of S1 that best discriminate between motor imagery (MI) and idle state. (a) The spatial patterns from trials in which participant was standing still and (b) the spatial patterns from trials in which they were walking with the exoskeleton.

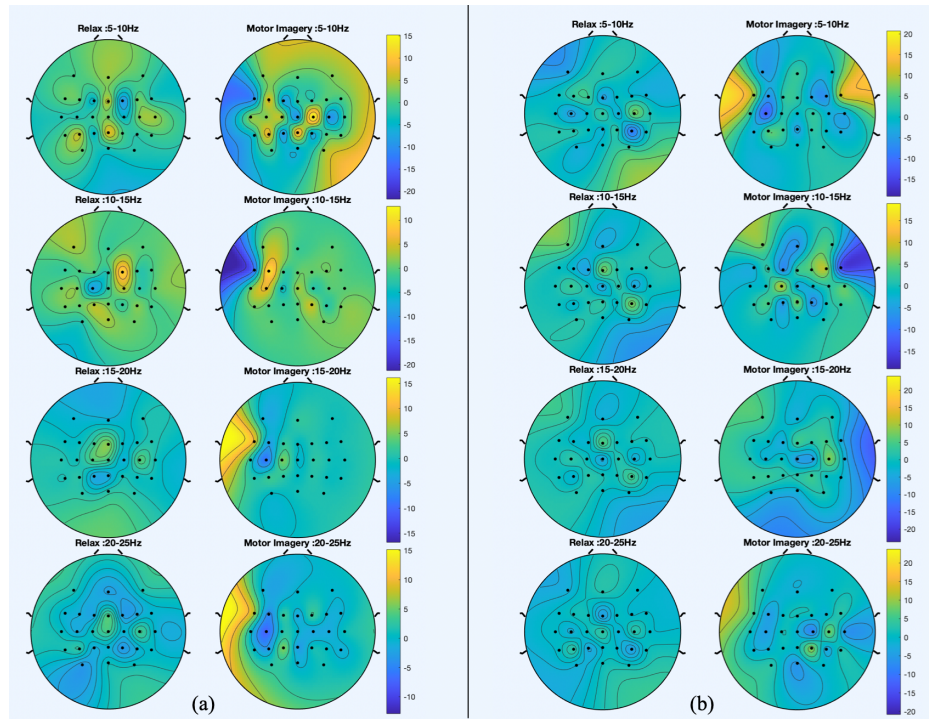


Figure 6. Spatial patterns for the session of S2 that best discriminate between motor imagery (MI) and idle state. (a) The spatial patterns from trials in which participant was standing still and (b) the spatial patterns from trials in which they were walking with the exoskeleton.

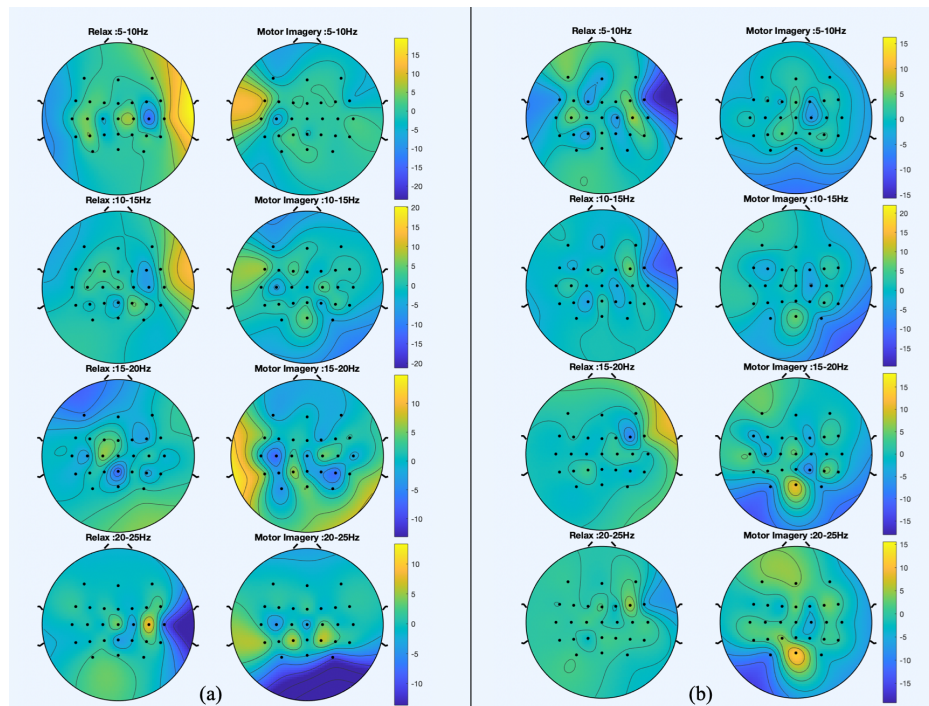


Figure 7. Spatial patterns for the fifth session of S2 that best discriminate between motor imagery (MI) and idle state. (a) The spatial patterns from trials in which participant was standing still and (b) the spatial patterns from trials in which they were walking with the exoskeleton.

3.2. Test Phase

The exoskeleton was controlled by the BMI decoded commands and the BMI classifiers were trained with training trials. Tables 3–5 summarize the results from closed-loop trials. TPR is 100% in the majority of trials, which means that the exoskeleton was activated at least once during the MI event. The number of false positive activations during idle state ranged from 0 to 2. Regarding %Commands, it improved by 13% from the first to the last session of S2, although their performance in each session was not always superior to the previous one. In the last session, the average %Commands for both subjects was $64.50 \pm 10.66\%$.

Table 3. Test results, subject S1. Trials in close-loop control.

		Trial 1	Trial 2	Trial 3	Trial 4	Trial 5	Avg.
Session 1	%MI	64.13	50.00	48.91	61.96	56.52	56.30
	%Att	51.09	58.70	53.26	47.83	55.43	53.26
	%Commands	63.00	78.00	62.00	60.00	83.00	69.20
	Acc. commands	50.00	50.00	50.00	0.00	50.00	40.00
	TPR	100.00	100.00	100.00	0.00	100.00	80.00
	FP	1.00	0.00	1.00	0.00	0.00	0.40
	FP/min	2.31	0.00	2.31	0.00	0.00	0.92
Session 2	%MI	61.96	52.17	50.00	60.87	57.61	56.52
	%Att	64.13	46.74	61.96	60.87	57.61	58.26
	%Commands	60.00	57.00	63.00	57.00	69.00	61.20
	Acc. commands	75.00	75.00	75.00	50.00	66.67	68.33
	TPR	100.00	100.00	100.00	100.00	100.00	100.00
	FP	1.00	1.00	1.00	1.00	1.00	1.00
	FP/min	2.31	2.31	2.31	2.31	2.31	2.31

Table 4. Test results, first two sessions of subject S2. Trials in close-loop control.

		Trial 1	Trial 2	Trial 3	Trial 4	Trial 5	Avg.
Session 1	%MI	50	44.57	43.48	42.39	43.48	44.78
	%Att	47.83	56.52	53.26	53.26	50	52.17
	%Commands	59.00	54.00	53.00	53.00	53.00	54.40
	Acc. commands	0.00	0.00	0.00	0.00	0.00	0.00
	TPR	100.00	100.00	100.00	100.00	100.00	100.00
	FP	1.00	1.00	1.00	1.00	1.00	1.00
	FP/min	2.31	2.31	2.31	2.31	2.31	2.31
Session 2	%MI	46.74	60.87	48.91	54.35	52.17	52.61
	%Att	56.52	59.78	43.48	66.3	64.13	58.04
	%Commands	59.00	53.00	37.00	76.00	68.00	58.60
	Acc. commands	0.00	100.00	0.00	66.67	100	53.33
	TPR	100.00	100.00	0.00	100.00	100.00	80.00
	FP	1.00	0.00	1.00	1.00	0.00	0.60
	FP/min	2.31	0.00	2.31	2.31	0.00	1.38

Table 5. Test results, last three sessions of subject S2. Trials in close-loop control.

		Trial 1	Trial 2	Trial 3	Trial 4	Trial 5	Avg.
Session 3	%MI	63.04	46.74	52.17	48.91	46.74	51.52
	%Att	45.65	44.57	55.43	52.17	50	49.56
	%Commands	67.00	81.00	75.00	63.00	63.00	69.80
	Acc. commands	60.00	60.00	75.00	40.00	50.00	57.00
	TPR	100.00	100.00	100.00	100.00	100.00	100.00
	FP	2.00	1.00	1.00	2.00	2.00	1.60
	FP/min	4.62	2.31	2.31	4.62	4.62	3.69
Session 4	%MI	53.26	64.13	45.65	58.7	58.7	56.09
	%Att	58.7	56.52	75	55.43	71.74	63.48
	%Commands	57.00	64.00	57.00	78.00	65.00	64.20
	Acc. commands	0.00	100.00	0.00	75.00	50.00	45.00
	TPR	100.00	100.00	100.00	100.00	100.00	100.00
	FP	1.00	0.00	1.00	1.00	1.00	0.80
	FP/min	2.31	0.00	2.31	2.31	2.31	1.85
Session 5	%MI	59.78	56.52	59.78	59.78	61.96	59.56
	%Att	70.65	70.65	59.78	67.39	56.52	65.00
	%Commands	56.00	73.00	52.00	88.00	70.00	67.80
	Acc. commands	40.00	66.67	100.00	100.00	33.33	68.00
	TPR	100.00	100.00	100.00	100.00	100.00	100.00
	FP	2.00	1.00	0.00	0.00	2.00	1.00
	FP/min	4.62	2.31	0.00	0.00	4.62	2.31

4. Discussion

Contrary to the findings of our previous work on a BMI-controlled treadmill [19], we found significant differences between opened-loop trials in which subjects were standing and when they were walking. It is important to note that walking assisted by an exoskeleton is a more complex task than walking on a treadmill, so subjects must be concentrated. Consequently, it is more difficult for them to perform other brain tasks such as MI or regressive count. In addition, when comparing the results from closed-loop trials, the average percentage of epochs with correct commands was 64.5% with the exoskeleton and 75.6% with the treadmill. A possible explanation for this contrast could be also related to the complexity of the movement with the exoskeleton.

On the other hand, the attention paradigm showed worse performance than the MI paradigm in opened-loop trials, which is consistent with the findings of our previous work [19]. However, in line with our previous work with an exoskeleton [15], this difference is not as evident in closed-loop trials. Therefore, future BMI designs could rely more on the attention paradigm for the activation of the exoskeleton.

While results from the MI paradigm showed an increasing trend throughout sessions, this pattern is not as evident for the attention paradigm. Our results for the MI paradigm are in consonance with the conclusions from [25]. Performing MI is not an intuitive activity for novel participants and practice could promote the modulation and enhance brain activity patterns. Nevertheless, with regard to the attention of the user, the performance does not seem to improve with practice. The attention is something that people train on daily basis, so this could explain why a few sessions cannot further improve it.

There are not many investigations in the literature that developed BMI based on lower-limb MI without other external stimuli [2] and they are usually based on motion intention [3,6,10]. In addition, the works of [4,26] employed upper-limb MI to control a lower-limb exoskeleton. Reference [26] showed a percentage of correct commands issued every 4.5 s of 66% and [4] of 80.16% but the BMI was only employed to start the gait and not to stop it. These values can be compared with the %Commands of the present paper. Although superior results are achieved with upper-limb MI, this paradigm cannot be applied to promote neuroplasticity.

In [16], a BMI was presented that employed a combination of MI with eye blinking as a control paradigm, and an accuracy of 86.7% was reported. However, although control mechanisms that employ eye movements have proven to be precise, they lack application from the rehabilitation point of view. In addition, the work of [14] presented a BMI that only controlled the start and maintenance of the gait of a lower-limb exoskeleton and they obtained an average accuracy of 74.4%. In our previous research [15] that also combined the MI and attention paradigms to control an exoskeleton, the percentage of epochs with correct commands issued was 56.77%. Slightly superior results were achieved with the current BMI algorithm.

5. Conclusions

The current research presents a BMI system based on MI and attention paradigms that has been tested to control a lower-limb exoskeleton. Participants performed 2–5 sessions to assess the effect of practice on the performance. Each session was divided into two parts: the training and test phases. First, participants completed trials in which they had to perform certain brain tasks and the exoskeleton was controlled remotely by the laptop with predefined commands. During half of the trials, the exoskeleton was walking, and during the other half, it was completely static. Therefore, contrary to previous works, brain tasks to discriminate happened under the same conditions. Moreover, this setup can reduce the effect of artifacts on the predictions. The average performance in the last session was $68.44 \pm 8.46\%$ for the MI paradigm and $65.45 \pm 5.53\%$ for the attention paradigm. The second part of the each session consisted of closed-loop controlled trials in which the exoskeleton was commanded by the predictions of the BMI. The BMI worked as a state machine that used different classifiers depending on whether the exoskeleton was static or moving. Training trials were used to train the classifiers corresponding to each state of the state machine. The BMI took a decision every 0.5 s and the average percentage of correct commands chosen was $64.50 \pm 10.66\%$ for the last session of both subjects.

Participants did not have any motor impairment, but since the main objective of the system is to promote neurorehabilitation and neuroplasticity, future research will focus on people with motor disabilities.

Author Contributions: Conceptualization, L.F. and M.O.; methodology, L.F., V.Q. and M.O.; software, L.F. and V.Q.; validation, M.O. and E.I.; formal analysis, L.F. and V.Q.; investigation, L.F. and V.Q.; resources, M.O., E.I. and J.M.A.; data curation, E.I.; writing—original draft preparation, L.F.; writing—review and editing, L.F. and M.O.; visualization, L.F.; supervision, M.O., E.I. and J.M.A.; project administration, J.M.A.; funding acquisition, J.M.A. All authors have read and agreed to the published version of the manuscript.

Funding: This research was funded by the Spanish Ministry of Science and Innovation, the Spanish State Agency of Research, and the European Union through the European Regional Development Fund in the framework of the project Walk—Controlling lower-limb exoskeletons by means of brain–machine interfaces to assist people with walking disabilities (RTI2018-096677-B-I00); and by the Consellería de Innovación, Universidades, Ciencia y Sociedad Digital (Generalitat Valenciana), and the European Social Fund in the framework of the project Desarrollo de nuevas interfaces cerebro–máquina para la rehabilitación de miembro inferior (GV/2019/009).

Institutional Review Board Statement: The study was conducted according to the guidelines of the Declaration of Helsinki, and approved by the Institutional Review Board of Miguel Hernandez University of Elche (DIS.JAP.03.18 and 22/01/2019).

Informed Consent Statement: Informed consent was obtained from all subjects involved in the study.

Data Availability Statement: Not applicable.


Conflicts of Interest: The authors declare no conflict of interest.

References

1. Bogue, R. Robotic exoskeletons: A review of recent progress. *Ind. Robot.* **2015**, *42*, 5–10. [[CrossRef](#)]
2. Kwak, N.S.; Müller, K.R.; Lee, S.W. A convolutional neural network for steady state visual evoked potential classification under ambulatory environment. *PLoS ONE* **2017**, *12*, e0172578. [[CrossRef](#)] [[PubMed](#)]
3. Zhang, Y.; Prasad, S.; Kilicarslan, A.; Contreras-Vidal, J.L. Multiple kernel based region importance learning for neural classification of gait states from EEG signals. *Front. Neurosci.* **2017**, *11*, 170. [[CrossRef](#)]
4. Liu, D.; Chen, W.; Pei, Z.; Wang, J. A brain-controlled lower-limb exoskeleton for human gait training. *Rev. Sci. Instrum.* **2017**, *88*, 104302. [[CrossRef](#)] [[PubMed](#)]
5. Kilicarslan, A.; Grossman, R.G.; Contreras-Vidal, J.L. A robust adaptive denoising framework for real-time artifact removal in scalp EEG measurements. *J. Neural Eng.* **2016**, *13*, 026013. [[CrossRef](#)] [[PubMed](#)]
6. Kilicarslan, A.; Prasad, S.; Grossman, R.G.; Contreras-Vidal, J.L. High accuracy decoding of user intentions using EEG to control a lower-body exoskeleton. In Proceedings of the 2013 35th Annual International Conference of the IEEE Engineering in Medicine and Biology Society (EMBC), Osaka, Japan, 3–7 July 2013; pp. 5606–5609. [[CrossRef](#)]
7. Pfurtscheller, G.; Neuper, C.; Flotzinger, D.; Pregenzer, M. EEG-based discrimination between imagination of right and left hand movement. *Electroencephalogr. Clin. Neurophysiol.* **1997**, *103*, 642–651. [[CrossRef](#)]
8. Pfurtscheller, G.; Lopes Da Silva, F.H. Event-related EEG/MEG synchronization and desynchronization: Basic principles. *Clin. Neurophysiol.* **1999**, *110*, 1842–1857. [[CrossRef](#)]
9. Seeland, A.; Manca, L.; Kirchner, F.; Kirchner, E.A. Spatio-temporal comparison between ERD/ERS and MRCP-based movement prediction. In Proceedings of the BIOSIGNALS 2015—8th International Conference on Bio-Inspired Systems and Signal Processing, Lisbon, Portugal, 12–15 January 2015; pp. 219–226. [[CrossRef](#)]
10. Rajasekaran, V.; López-Larraz, E.; Trincado-Alonso, F.; Aranda, J.; Montesano, L.; Del-Ama, A.J.; Pons, J.L. Volition-adaptive control for gait training using wearable exoskeleton: Preliminary tests with incomplete spinal cord injury individuals. *J. Neuroeng. Rehabil.* **2018**, *15*, 4. [[CrossRef](#)]
11. Stippich, C.; Ochmann, H.; Sartor, K. Somatotopic mapping of the human primary sensorimotor cortex during motor imagery and motor execution by functional magnetic resonance imaging. *Neurosci. Lett.* **2002**, *331*, 50–54. [[CrossRef](#)]
12. Bakker, M.; de Lange, F.P.; Stevens, J.A.; Toni, I.; Bloem, B.R. Motor imagery of gait: A quantitative approach. *Exp. Brain Res.* **2007**, *179*, 497–504. [[CrossRef](#)]
13. Batula, A.M.; Mark, J.A.; Kim, Y.E.; Ayaz, H. Comparison of Brain Activation during Motor Imagery and Motor Movement Using fNIRS. *Comput. Intell. Neurosci.* **2017**, *2017*, 5491296. [[CrossRef](#)]
14. Rodríguez-Ugarte, M.; Iáñez, E.; Ortiz, M.; Azorín, J.M. Improving Real-Time Lower Limb Motor Imagery Detection Using tDCS and an Exoskeleton. *Front. Neurosci.* **2018**, *12*, 757. [[CrossRef](#)] [[PubMed](#)]
15. Ortiz, M.; Iáñez, E.; Gaxiola, J.; Kilicarslan, A.; Azorín, J.M.; Member, S. Assessment of motor imagery in gamma band using a lower limb exoskeleton. In Proceedings of the 2019 IEEE International Conference on Systems, Man and Cybernetics, Bari, Italy, 6–9 October 2019; pp. 2773–2778.
16. Choi, J.W.; Huh, S.; Jo, S. Improving performance in motor imagery BCI-based control applications via virtually embodied feedback. *Comput. Biol. Med.* **2020**, *127*, 104079. [[CrossRef](#)]
17. Gharabaghi, A. What Turns Assistive into Restorative Brain-Machine Interfaces? *Front. Neurosci.* **2016**, *10*, 456. [[CrossRef](#)]
18. Torkamani-Azar, M.; Kanik, S.D.; Aydin, S.; Cetin, M. Prediction of reaction time and vigilance variability from spatio-spectral features of resting-state EEG in a long sustained attention task. *IEEE J. Biomed. Health Inform.* **2020**, *24*, 2550–2558. [[CrossRef](#)]
19. Ferrero, L.; Quiles, V.; Ortiz, M.; Iáñez, E.; Azorín, J.M. BCI Based on Lower-Limb Motor Imagery and a State Machine for Walking on a Treadmill. In Proceedings of the International IEEE EMBS Conference on Neural Engineering, Sorrento, Italy, 4–6 May 2020.
20. Costa, Á.; Iáñez, E.; Úbeda, A.; Hortal, E.; Del-Ama, A.J.; Gil-Agudo, Á.; Azorín, J.M. Decoding the Attentional Demands of Gait through EEG Gamma Band Features. *PLoS ONE* **2016**, *11*, e0154136. [[CrossRef](#)]
21. McFarland, D.J.; McCane, L.M.; David, S.V.; Wolpaw, J.R. Spatial filter selection for EEG-based communication. *Electroencephalogr. Clin. Neurophysiol.* **1997**, *103*, 386–394. [[CrossRef](#)]
22. Ramoser, H.; Muller-Gerking, J.; Pfurtscheller, G. Optimal spatial filtering of single trial EEG during imagined hand movement. *IEEE Trans. Rehabil. Eng.* **2000**, *8*, 441–446. [[CrossRef](#)]
23. Rainford, B.D.; Daniell, G.J. μ SR frequency spectra using the maximum entropy method. *Hyperfine Interact.* **1994**, *87*, 1129–1134. [[CrossRef](#)]
24. Izenman, A. Linear Discriminant Analysis. In *Modern Multivariate Statistical Techniques*; Springer Texts in Statistics; Springer: New York, NY, USA, 2006.
25. Zich, C.; De Vos, M.; Kranczoch, C.; Debener, S. Wireless EEG with individualized channel layout enables efficient motor imagery training. *Clin. Neurophysiol.* **2015**, *126*, 698–710. [[CrossRef](#)]
26. Gordileeva, S.Y.; Lukoyanov, M.V.; Mineev, S.A.; Khoruzhko, M.A.; Mironov, V.I.; Kaplan, A.Y.; Kazantsev, V.B. Exoskeleton control system based on motor-imaginary brain-computer interface. *Sovrem. Tehnol. Med.* **2017**, *9*, 31–36. [[CrossRef](#)]

Article

Brain Symmetry Analysis during the Use of a BCI Based on Motor Imagery for the Control of a Lower-Limb Exoskeleton

Laura Ferrero ^{1,*} , Mario Ortiz ¹ , Vicente Quiles ¹ , Eduardo Iáñez ¹ , José A. Flores ² and José M. Azorín ¹ 

¹ Brain–Machine Interface System Lab, Miguel Hernández University of Elche, 03202 Elche, Spain; mortiz@umh.es (M.O.); vquiles@umh.es (V.Q.); eianez@umh.es (E.I.); jm.azorin@umh.es (J.M.A.)

² Department of Engineering, Miguel Hernández University of Elche, 03202 Elche, Spain; ja.flores@umh.es

* Correspondence: lferrero@umh.es

Abstract: Brain–Computer Interfaces (BCI) are systems that allow external devices to be controlled by means of brain activity. There are different such technologies, and electroencephalography (EEG) is an example. One of the most common EEG control methods is based on detecting changes in sensorimotor rhythms (SMRs) during motor imagery (MI). The aim of this study was to assess the laterality of cortical function when performing MI of the lower limb. Brain signals from five subjects were analyzed in two conditions, during exoskeleton-assisted gait and while static. Three different EEG electrode configurations were evaluated: covering both hemispheres, covering the non-dominant hemisphere and covering the dominant hemisphere. In addition, the evolution of performance and laterality with practice was assessed. Although slightly superior results were achieved with information from all electrodes, differences between electrode configurations were not statistically significant. Regarding the evolution during the experimental sessions, the performance of the BCI generally evolved positively the higher the experience was.



Citation: Ferrero, L.; Ortiz, M.; Quiles, V.; Iáñez, E.; Flores, J.A.; Azorín, J.M. Brain Symmetry Analysis during the Use of a BCI Based on Motor Imagery for the Control of a Lower-Limb Exoskeleton. *Symmetry* **2021**, *13*, 1746. <https://doi.org/10.3390/sym13091746>

Academic Editor: Fabrizio Vecchio

Received: 30 July 2021

Accepted: 13 September 2021

Published: 19 September 2021

Publisher’s Note: MDPI stays neutral with regard to jurisdictional claims in published maps and institutional affiliations.



Copyright: © 2021 by the authors. Licensee MDPI, Basel, Switzerland. This article is an open access article distributed under the terms and conditions of the Creative Commons Attribution (CC BY) license (<https://creativecommons.org/licenses/by/4.0/>).

Keywords: brain symmetry; Brain–Computer Interfaces; electroencephalography; exoskeleton; motor imagery; laterality; hemisphere specialization

1. Introduction

Motor imagery (MI) is defined as the process of imagining or performing a mental execution of a movement without any actual muscle activation. MI, the observation of an action and the actual motor execution produce similar brain patterns [1]. There are different techniques to measure brain activity, with electroencephalography (EEG) being one of the most commonly used [2].

Sensorimotor rhythms (SMR) are brain oscillations recorded over the sensorimotor cortex. Motor processing produces changes in the ongoing SMR as event-related desynchronization (ERD) and synchronization (ERS). The phenomenon of ERD in alpha and beta band rhythms is associated with cortical areas that are ready to prepare a movement, and ERS is correlated with resting areas [3].

MI has been frequently employed in Brain–Computer Interfaces (BCI) [4]. BCIs are systems that record brain activity, for instance with EEG, and decode this information to generate commands for controlling external devices. In the case of MI, BCI must identify this brain pattern from the EEG.

Different devices have been commanded by means of BCI, including robotic orthosis and exoskeletons that can provide motor assistance for people with motor disabilities [5,6].

There are different BCI control paradigms for this kind of devices. The most commonly used are based on external stimuli such as steady-state visually evoked potentials [7] or auditory evoked potentials [8], and those related with real motion or MI such as motion-related cortical potentials [9–11] or ERD/ERS [12–16]. Controlling a BCI with MI can emulate the lost motor function by inducing mechanisms of neuroplasticity [17].

The brain's anatomical structure and function varies between left and right hemispheres. There are neural functions and cognitive processes that tend to be specialized to one hemisphere or the other, and this property is defined as brain laterality [18]. Some of them include face and body perception and motor skills [19]. Each brain hemisphere controls the contralateral side of the body, and the natural asymmetry of the brain is the cause of left/right side dominance, i.e., better performance or preference for using one hand, foot or eye [20,21]. Different models of lateralization have been proposed: homogeneous lateralization, which considers the dominance of all organs from the same side; crossed lateralization, which contemplates different dominances; and the undefined model, which has the hypothesis that the dominance cannot be determined [20].

Virtual reality has been employed to study lateralization among individuals, revealing that the performance of real motion tasks with the dominant hand is similar to the one obtained with both hands. In addition, this trend is also noticeable with the dominant body side for controlling the posture to perform certain tasks [20].

Previous studies have attempted to discern between right hand and left hand MI [12]. The effects of handedness on the SMR desynchronization have also been assessed. Zapala et al. [22] compared the performance of an upper-limb MI based BCI between left- and right-handed individuals. This BCI employed common spatial patterns (CSP) to extract features that could be used to distinguish between left and right MI classes, concluding that left-handed participants showed lower accuracy. Additionally, the power of the signal during MI was studied in different brain regions. Left-handed participants showed no differences in SMR in the right parietal brain region between right and left hand MI. However, right-handers showed higher lateralization. Shieh et al. [23] designed an algorithm that identified the best spectral and spatial patterns to discriminate between left and right hand MI. Results showed that for left MI, spatial patterns covered right hemisphere areas and the opposite way for right MI.

Regarding lower-limb, since the foot brain area is located in the interhemispheric fissure, left and right lower-limb areas are close. Therefore, it is difficult to distinguish between each limb movement or MI, since they produce similar EEG patterns. Pfurtscheller et al. [24] showed that hand MI produces a mu band (around 10 Hz) ERD, while foot MI produces an ERS in the hand cortical representation area with no laterality influence. However, a clear subject dependency was also reported. Tariq et al. [25] analyzed EEG patterns when performing right and left foot dorsiflexion MI and designed a BCI that had to discriminate between both types of MI. In mu frequency band, ERD/ERS patterns showed a lateralized distribution during left and right foot MI. Regarding beta frequency band, ERD/ERS showed a power concentration at the vertex, which is the cortical foot area representation [25]. In addition, contralateral dominance was found during right foot MI in electrode C3 for ERS patterns [26].

Crémers et al. [27] and Jahn et al. [28] observed right hemisphere specialization during MI of the gait. This brain task was found to be associated with activity in frontal and parietal areas, mainly on the right hemisphere and on the left side of the cerebellum [27].

The aim of this paper is to evaluate the performance of a BCI to control a lower-limb exoskeleton when using information from dominant, non-dominant and both brain hemispheres. We thereby assess whether there is a hemisphere specialization during MI of gait. In addition, since subjects participated in several sessions, this research studies the evolution of performance with practice as sessions go on, as well as whether and how this hemisphere specialization is affected.

2. Materials and Methods

2.1. Subjects

Five healthy subjects participated in the study (mean \pm age, 23.2 ± 1.3). They did not report any known disease and had no movement impairment. They did not have any previous experience with BCI. All participants were right-handed and right-footed, with four of them being men and one female. They were informed about the experiments

and signed an informed consent form in accordance with the Declaration of Helsinki. All procedures were approved by the Responsible Research Office of Miguel Hernández University of Elche (Spain).

2.2. Equipment

Electroencephalography (EEG) was employed to record brain activity with a set of 32 slim electrodes (Brain Products GmbH, Germany) positioned on a 64-electrode actiCap (Brain Products GmbH, Germany). Four electrodes were located next to the eyes for recording electrooculography (EOG). Ground and reference electrodes were located on the right and left ear lobes, respectively. The remaining 27 electrodes were placed over the cap following the 10-10 international system: F3, FZ, FC1, FCZ, C1, CZ, CP1, CPZ, FC5, FC3, C5, C3, CP5, CP3, P3, PZ, F4, FC2, FC4, FC6, C2, C4, CP2, CP4, C6, CP6, P4. Signals were amplified with an actiCHamp module (Brain Products GmbH, Germany) and transmitted wirelessly with MOVE (Brain Products GmbH, Germany) to pyCorder recorder software (Brain Products GmbH, Germany).

Subjects wore a H3 exoskeleton (Technaid, Madrid, Spain), which provides assistance for walking. The subjects used crutches for extra support and a member of the research staff was behind them to prevent any possible risk of falling in case of loss of balance. Control commands and exo status were sent and received via Bluetooth. Figure 1 shows the experimental setup.

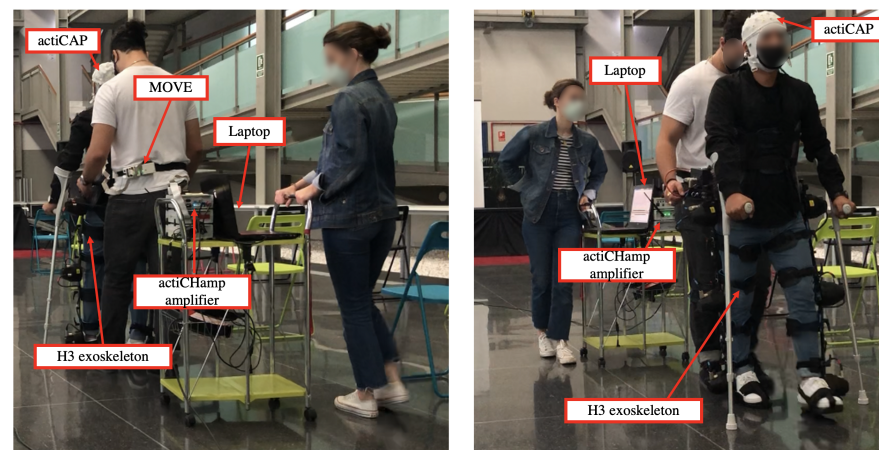


Figure 1. Experimental setup. Two operators were present during each session. One of them carried the equipment and the other one was behind each participant for safety reasons.

2.3. Experimental Design

The experimental design was the same presented in [16]. Each subject performed 5 sessions, which were divided in training and testing. During training, the exoskeleton was in opened-loop control, which means it was controlled with predefined commands sent by the laptop. Then, during the test phase, the exoskeleton was controlled by commands issued in real time from the BCI based on the EEG patterns of the subject. Only the training data were employed for this research. Figure 2 shows the schema of the protocol.

For training, each subject performed 22 trials. They had to perform a sequence of three mental tasks: MI of the gait, idle state, and a regressive count. For idle state, participants were asked to be as relaxed as possible. As in this research the attention mental task is not analyzed, only data from MI and idle states were considered.

During the use of an exoskeleton, there are two possible states that the subject can be in: standing and moving. Due to that, MI must be analyzed in both states which makes necessary the creation of two different classifier models. One is based on the traditional definition of MI, while the other one combines MI with motor execution. This way, half

of the 22 trials were performed in a full standing status (full-static) with the exoskeleton without performing any movement, 11 trials, and the other half were performed in a full motion status (full-motion) assisted by the exoskeleton, 11 trials. For both conditions, the sequence of mental tasks was identical.

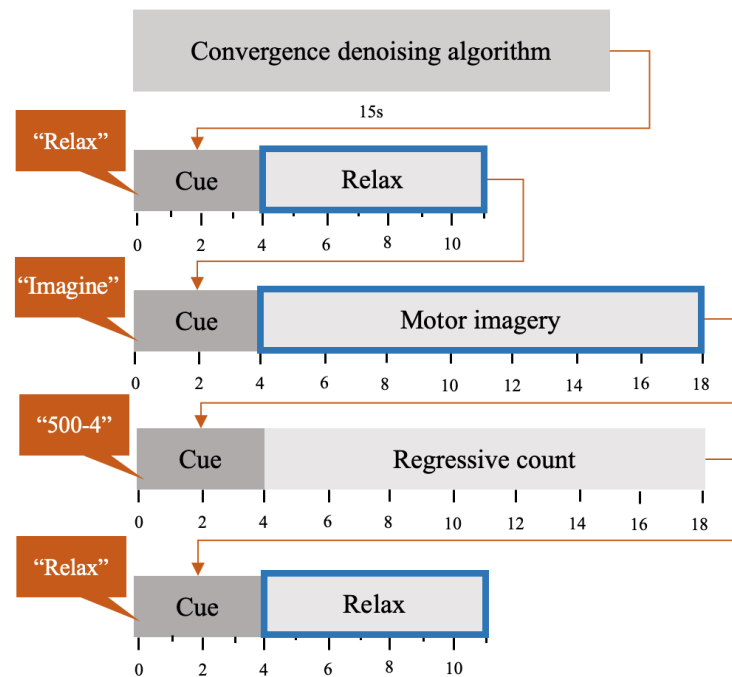


Figure 2. Schema of the protocol for each trial. This sequence was repeated 11 times while static and 11 with exoskeleton-assisted gait. Only information from events with blue border was considered for this research.

2.4. BCI

2.4.1. Acquisition

EEG signals were acquired at 200 Hz sample ratio. All the analysis were done following a pseudo online approach to simulate a real-time application. Epochs of 1.5 s were processed with 0.5 s of shifting. Therefore, the processing of each epoch must be performed in less than 0.5 s.

2.4.2. Pre-Processing

EEG signals went through two hardware filters assigned in the pyCorder app (Brain-Products, Germany): a Notch filter at 50 Hz to remove the contribution of the power line and a high-pass filter at 0.5 Hz. Afterwards, H_{∞} denoising framework was applied [11]. This algorithm employs EOG signal, estimates its contribution to each EEG channel and removes it. In addition, it also estimates and removes any signal drift.

2.4.3. Processing

Three different methodologies were employed for feature extraction: Filter Bank Common Spatial Patterns (FBCSP) [29], Stockwell Transform (ST) [30], and Welch's Power Spectral Density (PSD) estimation [31].

FBCSP

FBCSP applies Common Spatial Patterns (CSP) [32] at different frequency ranges. For this research, EEG signals went through 4 band-pass filters that included alpha and beta rhythms: 5–10 Hz, 10–15 Hz, 15–20 Hz, and 20–25 Hz. CSP transforms EEG data

to construct optimal spatial filters that aim to discriminate between two different brain patterns. In this case, it must discriminate between MI and idle state.

First, covariance matrices are computed for each class, MI and idle state, and normalized as in

$$C_1 = \frac{X_1 X_1^T}{\text{trace}(X_1 X_1^T)}, C_2 = \frac{X_2 X_2^T}{\text{trace}(X_2 X_2^T)}. \quad (1)$$

where X are EEG data from each class that have N number of channels and T number of samples, $N * T$.

These matrices are computed for each trial and then all the matrices from the same class are averaged: \overline{C}_1 and \overline{C}_2 . Afterwards, \overline{C}_1 and \overline{C}_2 are combined into the composite spatial covariance matrix, and it is factorized as

$$C = \overline{C}_1 + \overline{C}_2 = U_0 \Sigma U_0^T. \quad (2)$$

Σ is the diagonal matrix of eigenvalues, and U_0 is a matrix of eigenvectors. The results of the decomposition are combined as

$$P = \Sigma^{1/2} U_0^T, \quad (3)$$

$$S_1 = P \overline{C}_1 P^T, S_2 = P \overline{C}_2 P^T. \quad (4)$$

S_1 and S_2 have the same eigenvectors, and the sum of both matrices of eigenvalues is the identity matrix.

$$S_1 = U \Sigma_1 U^T, S_2 = U \Sigma_2 U^T \text{ and } \Sigma_1 + \Sigma_2 = I. \quad (5)$$

The matrix of spatial filters is obtained as

$$W = U^T P. \quad (6)$$

where Z is the projection of the original EEG signal S into another space. Columns of W^{-1} are the spatial patterns.

$$Z = W X. \quad (7)$$

Z has the same dimensions as the original signal X . However, first and last rows are filters that can discriminate better in terms of their variance. Consequently, as final features, only m first and last components of Z are considered, resulting in Z_p . Finally, the variances of each component are computed and normalized with the logarithm as

$$f_p = \log \frac{\text{var}(Z_p)}{\sum_{i=1}^{2m} Z_p}. \quad (8)$$

f_p is the vector of features with dimension $(fbands * 2 * m) * T$. m was set to 4 so the dimension is $32 * T$.

ST and Welch's PSD

Before applying ST and Welch's estimation, EEG signals were filtered with spatial Laplacian filter [33]. It enhances the local activity of each electrode while reducing spatial noise.

ST performs a time-frequency decomposition [30]. It performs a phase correction of the wavelet transform with a window that is a Gaussian function of the frequency. The output for each channel is the spectrum of the signal represented as the amplitude with respect to the time and frequency. Frequencies considered were alpha and beta rhythms 8–14 and 20–30 Hz, and a summatory was computed with the amplitude of all of them.

Welch's methodology is employed for estimating the power spectral density (PSD). It is implemented by dividing the signal into overlapping segments, each segment is windowed and then the periodogram is computed for each of them. Finally, PSD is calculated by

averaging the periodogram of all the segments. Following the same procedure as ST, power of frequencies in alpha and beta bands were added.

Only information from 18 electrodes—FC3, FC1, FCZ, FC2, FC4, C3, C1, CZ, C2, C4, CP3, CP1, CPZ, CP2, CP4, P3, PZ, P4—was used for ST and Welch’s method. Electrodes covered premotor area, supplementary motor area, primary motor cortex, inferior and superior parietal lobule.

The vector of features had different dimensions based on the processing method: 1×32 in FBCSP, and $1 \times$ number of electrodes in ST and Welch’s estimation.

2.4.4. Classification

Once all the features were extracted, a leave-one-out cross-validation was performed for each subject and session. Furthermore, full-motion and full-static trials were evaluated separately by two independent models. The classifier employed was a Linear Discriminant Analysis (LDA) [34]. It has been commonly used on previous investigations [16,35,36] due to its high reported precision and short computational time [37,38]. Consequently, all full-static trials for each subject and experimental session were considered for cross-validation. For each iteration of the algorithm, all trials but one were employed for training the model, testing it with the remaining one. The same process was done with full-motion trials.

2.4.5. Evaluation

For the evaluation, the percentage of epochs correctly classified was calculated. Then, this value was averaged thorough all the steps of cross-validation.

3. Results

All the subjects performed five sessions. However, the data considered for analysis of S4 included four sessions, as the first one was discarded due to the presence of glitches in the signal due to wireless communication problems.

Although all subjects performed eleven trials per session in full-motion and eleven in full-static, some of them were not considered for the analysis. Performing MI while wearing an exoskeleton is a complex task, so it is easy for users to get distracted [16]. Therefore, those trials statistically considered as outliers were removed. Consequently, 7.54 ± 1.77 trials in full-static and 7.33 ± 1.86 trials in full-motion were selected from each subject.

3.1. Methodology Influence

As indicated in Section 2.4.3 several methodologies were used for extracting the MI brain patterns. Table 1 shows the average accuracy obtained with them: FBCSP, ST and Welch’s method, during the full-motion and full-static trials.

Table 1. Performance of different methodologies over all sessions: during motor imagery (MI) events (%MI), during idle state (%Relax) and total (%Total). With three different methodologies: Filter Bank Common Spatial Patterns (FBCSP), Stockwell Transform (ST) and Welch’s Power Spectral Density estimation (Welch’sPSD).

		FBCSP	ST	Welch’s PSD
Full-static	%MI	64.7 ± 6.5	58.0 ± 6.4	62.6 ± 7.6
	% Relax	67.5 ± 8.9	62.5 ± 8.0	65.1 ± 6.1
	%Total	66.1 ± 6.6	60.2 ± 5.1	63.8 ± 4.6
Full-motion	%MI	61.0 ± 8.5	56.8 ± 8.6	60.0 ± 10.0
	% Relax	62.5 ± 8.0	55.5 ± 12.4	58.8 ± 11.0
	%Total	61.7 ± 6.2	56.1 ± 7.3	59.4 ± 8.3

A statistical analysis was performed to examine the differences among the methodologies in terms of accuracy. Prior to performing one-way repeated-measures ANOVA

test, some assumptions must be verified. This process was repeated for full-static and full-motion trials.

- Full-static: The accuracies of two trials were detected as outliers (one for Welch's PSD and one for FBCSP). They were removed as well as the same value for all methodologies to be compared. Afterwards, Shapiro–Wilk test was employed to verify if the data from each group followed a normal distribution and check if the normality null hypothesis could not be rejected (p -value > 0.01). In addition, the sphericity assumption was assessed with Mauchly's test. Results from the ANOVA test showed that the performance of FBCSP, ST and Welch's method were statistically different (p -value < 0.01). Afterwards, pair-wise t -test comparisons were conducted, detecting that all methodologies differed significantly from each other (p -value < 0.01).
- Full-motion: The accuracies of 10 trials were identified as outliers and removed (six for ST and four for FBCSP). Data from each methodology followed a normal distribution (p -value > 0.01), and the sphericity assumption was not violated. Results from ANOVA showed significant differences among methodologies (p -value < 0.01) showing the pair-wise t -test comparisons differences between CSP and ST and between ST and Welch PSD (p -value < 0.01).

As CSP showed the highest global accuracy, this approach was the one chosen for the rest of the research. Further analysis will be focused only on this methodology.

3.2. Subject Influence

Previous studies have identified differences among subjects in the usage of BCI [39], so subject differences were tested in terms of accuracy. Table 2 shows the average performance for each of the subjects. The differences were analyzed with a one-way ANOVA test. The distribution of outliers that were excluded from the statistical analysis is shown in Supplementary Material, Figure S1.

Table 2. Subject differences in performance during motor imagery (MI) events (%MI), during idle state (%Relax) and in total (%Total).

		S1	S2	S3	S4	S5
Full-static	%MI	59.5 ± 7.6	70.4 ± 6.4	63.4 ± 4.6	64.7 ± 6.6	65.4 ± 4.0
	% Relax	69.4 ± 7.1	67.7 ± 7.5	63.1 ± 3.3	69.2 ± 16.0	67.8 ± 10.5
	%Total	64.4 ± 6.2	69.0 ± 5.7	63.3 ± 1.7	67.2 ± 11.2	67.2 ± 11.2
Full-motion	%MI	62.8 ± 7.7	64.3 ± 9.0	54.9 ± 9.0	64.2 ± 11.0	59.3 ± 5.4
	% Relax	64.5 ± 3.5	62.7 ± 6.0	60.7 ± 11.5	65.1 ± 13.0	59.8 ± 6.0
	%Total	63.6 ± 3.0	63.5 ± 5.5	57.8 ± 5.4	57.8 ± 5.4	57.8 ± 5.4

- Full-static: The accuracies of 10 trials were identified as outliers (four for S1, three for S2 and three for S3) and removed. Afterwards, Shapiro–Wilk test was applied, and results showed that the data from each subject followed a normal distribution (p -value > 0.01). Finally, the last assumption to check in order to apply the one-way ANOVA was the data homoscedasticity. This assumption was fulfilled, as assessed by Bartlett test (p -value > 0.01). The ANOVA test showed significant differences among subjects (p -value < 0.01), and the pair-wise t -test indicated that S1 had a different behavior than the rest (p -value < 0.01).
- Full-motion: The accuracies of eight trials were detected as outliers (one for S2, one for S3, one for S4 and five for S5) and removed from the analysis. Data from each subject were normally distributed as assessed by Shapiro–Wilk test (p -value > 0.01). However, the homoscedasticity assumption was violated, p -value < 0.01 from the Barlett test. Therefore, a non-parametric Kruskal–Wallis test was employed. Results from this test showed no significant differences among subjects (p -value > 0.01).

3.3. Training Evolution and Differences between Hemispheres

As there was a subject dependency, this section analyzes the laterality individually per subject with FBCSP. For the laterality analysis, the performance of FBCSP was assessed using the information from all electrodes, using only the ones located on the dominant hemisphere and using the ones located on the non-dominant hemisphere. Due to the fact that all the subjects were right-footed, the left brain hemisphere was considered as dominant. In this section, the evolution of the performance with the sessions was also assessed, as can be seen in the different images of Figure 3. Furthermore, it was determined whether the best electrode configuration changed with training in terms of performance.

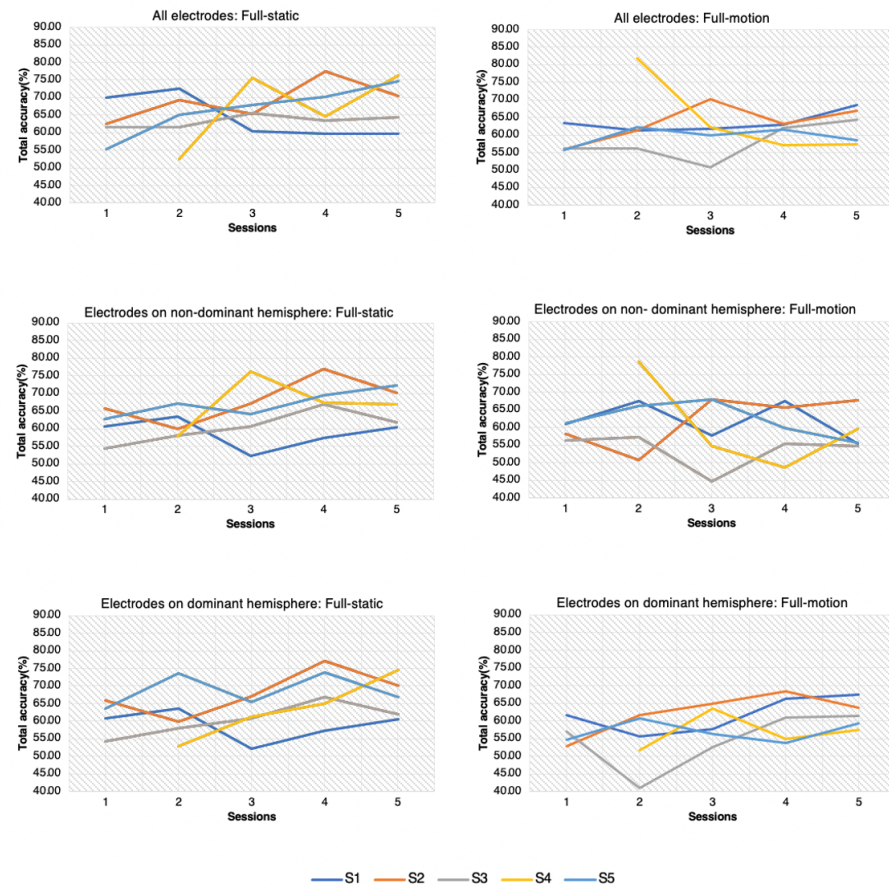


Figure 3. Training evolution for full-static and full-motion trials with different electrode configurations: all electrodes, only electrodes located on non-dominant hemisphere and electrodes on dominant hemisphere.

In sum, the statistical analysis of three hypotheses was per subject: differences among sessions, differences among electrode configurations and the interaction between both.

3.3.1. S1

- Full-static: Data of all sessions and electrode configurations did not follow a normal distribution. Therefore, instead of performing a two-way ANOVA test, three independent Kruskal–Wallis tests were employed: one assessing differences among sessions, another one with electrode configurations and the third one combining both variables as a new grouping variable. No differences were found for any group (p -value > 0.01).
- Full-motion: Initially, the ANOVA assumption for a normal distribution of the data was not fulfilled. The accuracies of 4 trials were detected as outliers and removed (one for EEG configuration with all electrodes, one for electrodes on the non-dominant

hemisphere and two for the electrodes on the dominant hemisphere). With the remaining data, all the ANOVA test assumptions were matched, and results did not show statistically relevant differences (p -value > 0.01).

3.3.2. S2

- Full-static: The ANOVA analysis of the results verified that there were not differences among the sessions and the electrode configurations. In addition, the interaction between the sessions and the configurations was not significant.
- Full-motion: ANOVA test revealed significant differences among sessions (p -value < 0.01). Sessions 1 and 2 showed worse accuracy than 3, 4, and 5, as was assessed with a pair-wise t -test.

3.3.3. S3

- Full-static: ANOVA test did not reveal statistically significant differences among sessions and electrode configurations. Furthermore, the interaction between sessions and electrode configurations was not significant (p -value > 0.01).
- Full-motion: ANOVA test only indicated differences among sessions, and pair-wise t -test indicated that the behavior of session 3 was significantly worse in comparison with 1, 4 and 5.

3.3.4. S4

- Full-static: Data of all sessions and electrode configurations did not follow a normal distribution. Four outliers were detected and discarded (three for the EEG configuration with all electrodes and one for the configuration of electrodes on dominant hemisphere). However, data of all groups still did not follow a normal distribution. Three independent Kruskal–Wallis tests were performed as in S1. Results showed that there were statistically significant differences among sessions (p -value < 0.01). Performance of session 2 differed from the one of sessions 3 and 5, as verified with Dunn’s Kruskal–Wallis Multiple Comparisons. In addition, the interaction between electrode configurations and sessions was significant (p -value < 0.01). This means that the performance of the BCI with each electrode configuration varied from session to session. The performance of session 2 was better than sessions 3 and 5 with two electrode configurations, all electrodes and electrodes on the non-dominant hemisphere. In the case of the setup on the dominant-hemisphere, the performance of session 2 was worse.
- Full-motion: The performance was statistically different among different sessions, as assessed by ANOVA test. Furthermore, the interaction between session and configuration was statistically significant (p -value < 0.01).

3.3.5. S5

- Full-static: ANOVA test revealed significant differences among sessions (p -value < 0.01), and session 1 was significantly worse than session 5, as assessed with pair-wise t -test.
- Full-motion: Results from ANOVA verified that there were no differences among sessions (p -value > 0.01).

Slightly superior results were achieved with the electrodes covering both hemispheres. However, no statistically significant differences were found among the three electrode configurations. In S4, the evolution of performance with practice was dependent on the selected configuration of electrodes.

On the other hand, the accuracy evolved positively with more training, but the growth was not completely linear. In fact, in some cases, the accuracy dropped after the fourth session. Comparing both types of trials, this positive trend was more evident in the full-static ones.

4. Discussion

4.1. Study Limitations

It should be pointed out that the present research, as any preliminary study, presents some limitations.

First, the exoskeleton was working in opened-loop control. This means that it was commanded by predefined instructions during the trials. However, as the final objective of the research is to develop a BCI taking into account the lateralization that works in closed-loop control, the findings should be tested in the future in this scenario.

Another concern is about the homogeneity of the database. All the participants were in their twenties and presented right-dominance for both hands and feet. This allows for a robust database, since they shared some common features, but further research should be done to generalize the findings to other population groups.

Another limitation lies in the fact that performing maintained gait imagery while wearing an exoskeleton can be difficult. Participants can suffer from fatigue, and it is more difficult to focus on the mental tasks, which usually makes for lower BCI accuracies [16].

4.2. Algorithm Influence

The purpose of this study was to gain a better understanding of hemisphere specialization during MI of the gait when using a BCI to control a lower-limb exoskeleton. It was studied for different subjects and across different sessions. Three processing algorithms were compared for the BCI—FBCSP, ST and Welch's PSD—and the highest results were obtained with FBCSP. This is consistent with previous investigations, which appointed FBCSP as a more robust method [40] The accuracy for full-static trials was $66.1 \pm 6.6\%$ and for full-motion trials, $61.7 \pm 6.2\%$.

4.3. BCI Performance Comparison

Only a few works in the literature have designed and evaluated a BCI based on maintained MI of the gait for controlling an exoskeleton without any other control paradigm based on external stimuli such as visual stimuli [7]. This pattern of results is consistent with the previous literature [41] and our previous research [16,42].

Whereas our previous research of a BCI based on MI of gait to control a treadmill [35] did not show differences between static and trials in motion, the present study has shown some variation. A possible explanation may be the higher complexity of walking with crutches assisted by an overground exoskeleton in comparison with walking on a treadmill.

4.4. Subject Influence

The results of this research provide supporting evidence that the performance of the BCI has significant differences among subjects [43]. Therefore, laterality of each subject was studied independently.

4.5. Hemisphere Dominance

Foot brain area is located in the interhemispheric vertex, so brain representations of each limb are very close [25]. Contrary to investigations of foot dorsiflexion MI [25], the MI of the gait was studied without considering each foot separately. Therefore, the brain lateralization of each limb was not studied, but the whole gait imagination process during two different scenarios was instead studied: full-static and full-motion.

In order to study the brain asymmetry, three electrode configurations were compared: electrodes covering both hemispheres, covering the non-dominant hemisphere (right hemisphere) and covering the dominant hemisphere (left hemisphere). There were no statistically significant differences among them in terms of performance. However, all subjects except S5 obtained the highest BCI average accuracy with information from both hemispheres when performing purely MI (full-static) and MI combined with robot-assisted gait (full-motion). S5 showed the highest results when using information from dominant hemisphere for trials in full-static MI and with information from non-dominant hemisphere

for trials in full-motion MI with the exoskeleton assistance. These variations in brain asymmetry among subjects are consistent with the findings of Nielsen et al. [44].

The results from this research showed that the performance with electrodes on the dominant side (left) was slightly superior to the non-dominant side (right) for the majority of subjects. This differs from the findings of Crémers et al. [27] and Jahn et al. [28], which observed right hemisphere specialization during MI of the gait, especially in frontal and parietal areas. However, Sabaté et al. [45] studied MI and motor execution of both hands in patients with unilateral brain damage, and they found that patients with left-side stroke decreased the velocity of movements, suggesting the left hemisphere plays a crucial role in motor planning. An fMRI investigation of gait MI identified dissimilar lateralization for brain regions involved in motor planning, as the posterior parietal cortex showed lateralization on the dominant hemisphere (left), and the activity of pre-supplementary motor was only found on non-dominant side (right) [46]. Although differences among electrode configurations were not statistically relevant, the usage of electrodes covering only the dominant hemisphere could reduce the preparation time. The reduction of the number of electrodes as well as the employment of dry or semi-dry electrodes would considerably reduce the preparation complexity and promote the usage of BCI in real-life scenarios [47,48].

4.6. Evolution of Performance with Practice

Finally, the evolution of performance with practice was assessed for the different electrode configurations. In general, the evolution was positive, and the BCI accuracy of the last session was higher than the first one. These results are consistent with previous research [49]. However, this positive trend was more significant in full-static trials. In fact, for some subjects and electrode configurations, the evolution of performance of full-motion trials was negative. This difference can be attributable to the difficulty of performing mental tasks during robotic-assisted gait. In addition, the evolution of performance with practice was not statistically different among each electrode configuration.

5. Conclusions

The current research studied the brain lateralization in terms of performance of a BCI based on MI of the gait for controlling a lower-limb exoskeleton. This analysis was carried out for five different subjects who participated in five sessions. Significant differences were found among participants, so they were studied independently. For the majority of participants, the performance improved with training. Regarding brain lateralization, three different approaches were compared: EEG recording of both brain hemispheres, the left hemisphere and the right hemisphere. Results from each EEG setup were not statistically different, but the BCI with information from both hemispheres showed the highest accuracy. Collectively, our results showed that BCI accuracy was marginally higher with EEG data from the dominant hemisphere than the non-dominant hemisphere, and since all participants were right-footed, the dominant side was the left hemisphere. Future research might extend this research with more participants to validate the conclusions drawn in this study. If so, the BCI could use only information from half of the electrodes, reducing the setup preparation time. In addition, considering that the final user of this kind of BCI are people with spinal cord injury, future research should replicate this study with them, trying to identify whether there are similarities or differences in comparison to able-bodied subjects.

Supplementary Materials: The following are available online at <https://www.mdpi.com/article/10.3390/sym13091746/s1>, Figure S1: Boxplots representing the distribution of trial accuracies grouped by method and subject.

Author Contributions: Conceptualization, L.F. and M.O.; methodology, L.F., V.Q., M.O. and J.A.F.; software, L.F. and V.Q.; validation, M.O. and E.I.; formal analysis, L.F. and V.Q.; investigation, L.F. and V.Q.; resources, M.O., E.I., J.A.F. and J.M.A.; data curation, M.O.; writing—original draft preparation,

L.F.; writing—review and editing, L.F., M.O. and J.M.A.; visualization, L.F.; supervision, M.O., E.I. and J.M.A.; project administration, J.M.A.; funding acquisition, J.M.A., J.A.F. and M.O. All authors have read and agreed to the published version of the manuscript.

Funding: This research was funded by the Spanish Ministry of Science and Innovation, the Spanish State Agency of Research and the European Union through the European Regional Development Fund in the framework of the project Walk-Controlling Lower-Limb Exoskeletons by Means of Brain–Machine Interfaces to Assist People with Walking Disabilities (RTI2018-096677-B-I00), and by the Consellería de Innovación, Universidades, Ciencia y Sociedad Digital (Generalitat Valenciana), and the European Social Fund in the framework of the project Desarrollo de Nuevas Interfaces Cerebro–Máquina Para la Rehabilitación de Miembro Inferior (GV/2019/009).

Institutional Review Board Statement: The study was conducted according to the guidelines of the Declaration of Helsinki, and approved by the Institutional Review Board of Miguel Hernandez University of Elche (DIS.JAP.03.18 and 22 January 2019).

Informed Consent Statement: Informed consent was obtained from all subjects involved in the study.

Data Availability Statement: Data not available to external researchers due to restrictions of the ethical committee.

Conflicts of Interest: The authors declare no conflict of interest. The funders had no role in the design of the study; in the collection, analyses, or interpretation of data; in the writing of the manuscript; or in the decision to publish the results.

References

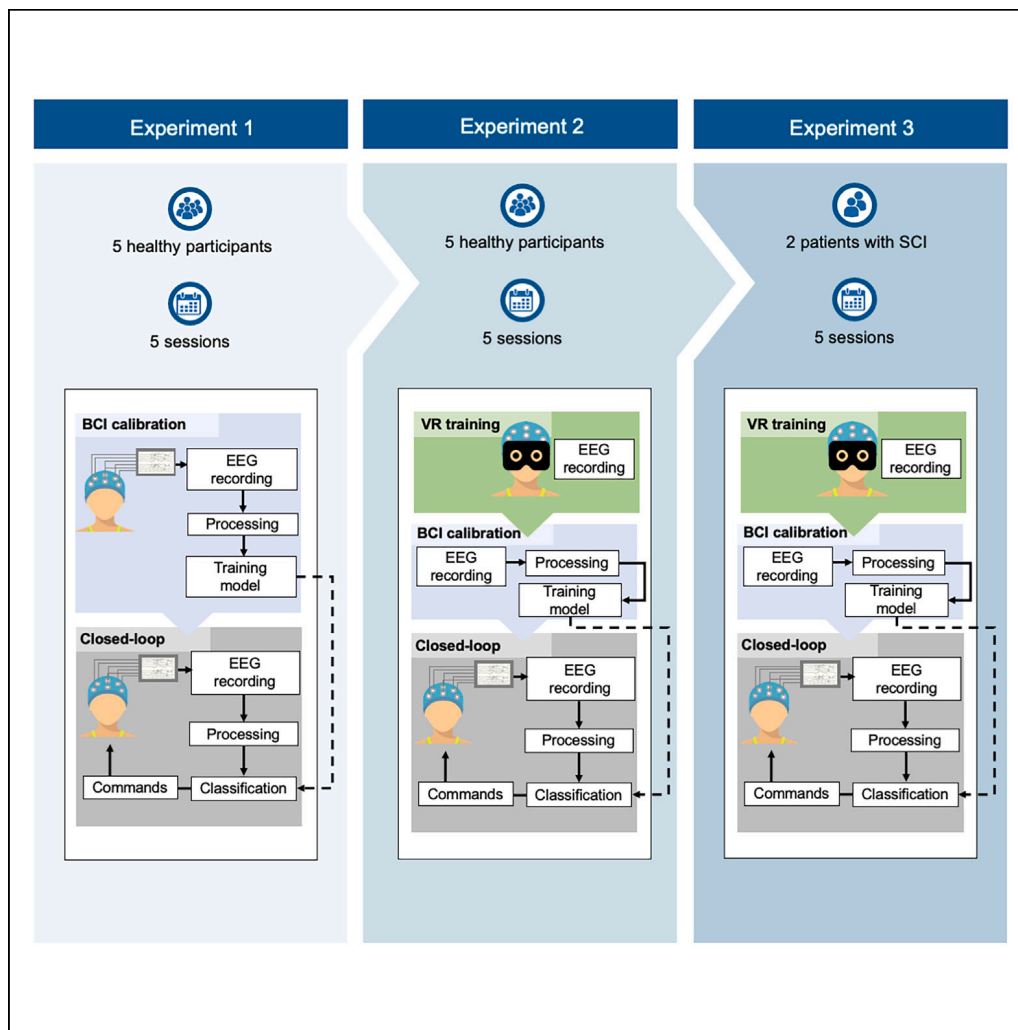
1. Mulder, T. Motor imagery and action observation: Cognitive tools for rehabilitation. *J. Neural Transm. (Vienna Austria 1996)* **2007**, *114*, 1265–1278. [[CrossRef](#)]
2. Lee, K.; Liu, D.; Perroud, L.; Chavarriaga, R.; Millán, J.d.R. A brain-controlled exoskeleton with cascaded event-related desynchronization classifiers. *Robot. Auton. Syst.* **2017**, *90*, 15–23. [[CrossRef](#)]
3. Pfurtscheller, G.; Neuper, C.; Andrew, C.; Edlinger, G. Foot and hand area mu rhythms. *Int. J. Psychophysiol.* **1997**, *26*, 121–135. [[CrossRef](#)]
4. Donati, A.R.; Shokur, S.; Morya, E.; Campos, D.S.; Muioli, R.C.; Gitti, C.M.; Augusto, P.B.; Tripodi, S.; Pires, C.G.; Pereira, G.A.; et al. Long-Term Training with a Brain-Machine Interface-Based Gait Protocol Induces Partial Neurological Recovery in Paraplegic Patients. *Sci. Rep.* **2016**, *6*, 30383. [[CrossRef](#)]
5. He, Y.; Eguren, D.; Azorín, J.M.; Grossman, R.G.; Luu, T.P.; Contreras-Vidal, J.L. Brain-machine interfaces for controlling lower-limb powered robotic systems. *J. Neural Eng.* **2018**, *15*. [[CrossRef](#)]
6. Soleimani Amiri, M.; Ramli, R.; Ibrahim, M.F.; Abd Wahab, D.; Aliman, N. Adaptive Particle Swarm Optimization of PID Gain Tuning for Lower-Limb Human Exoskeleton in Virtual Environment. *Mathematics* **2020**, *8*, 2040. [[CrossRef](#)]
7. Kwak, N.S.; Müller, K.R.; Lee, S.W. A convolutional neural network for steady state visual evoked potential classification under ambulatory environment. *PLoS ONE* **2017**, *12*, e0172578. [[CrossRef](#)]
8. Yu, Z.; Li, L.; Song, J.; Lv, H. The Study of Visual-Auditory Interactions on Lower Limb Motor Imagery. *Front. Neurosci.* **2018**, *12*, 509. [[CrossRef](#)] [[PubMed](#)]
9. Zhang, Y.; Prasad, S.; Kilicarslan, A.; Contreras-Vidal, J.L. Multiple kernel based region importance learning for neural classification of gait states from EEG signals. *Front. Neurosci.* **2017**, *11*, 170. [[CrossRef](#)] [[PubMed](#)]
10. Liu, D.; Chen, W.; Pei, Z.; Wang, J. A brain-controlled lower-limb exoskeleton for human gait training. *Rev. Sci. Instr.* **2017**, *88*, 104302. [[CrossRef](#)] [[PubMed](#)]
11. Kilicarslan, A.; Grossman, R.G.; Contreras-Vidal, J.L. A robust adaptive denoising framework for real-time artifact removal in scalp EEG measurements. *J. Neural Eng.* **2016**, *13*, 026013. [[CrossRef](#)]
12. Pfurtscheller, G.; Neuper, C.; Flotzinger, D.; Pregenzer, M. EEG-based discrimination between imagination of right and left hand movement. *Electroencephalogr. Clin. Neurophysiol.* **1997**, *103*, 642–651. [[CrossRef](#)]
13. Pfurtscheller, G.; Lopes Da Silva, F.H. Event-related EEG/MEG synchronization and desynchronization: Basic principles. *Clin. Neurophysiol.* **1999**, *110*, 1842–1857. [[CrossRef](#)]
14. Seeland, A.; Manca, L.; Kirchner, F.; Kirchner, E.A. Spatio-temporal comparison between ERD/ERS and MRCP-based movement prediction. In Proceedings of the BIOSIGNALS 2015 8th International Conference on Bio-Inspired Systems and Signal Processing, Proceedings, Part of 8th International Joint Conference on Biomedical Engineering Systems and Technologies, BIOSTEC 2015, Lisbon, Portugal, 12–15 January 2015; pp. 219–226. [[CrossRef](#)]
15. Choi, J.; Kim, K.T.; Jeong, J.H.; Kim, L.; Lee, S.J.; Kim, H. Developing a Motor Imagery-Based Real-Time Asynchronous Hybrid BCI Controller for a Lower-Limb Exoskeleton. *Sensors* **2020**, *20*, 7309. [[CrossRef](#)] [[PubMed](#)]
16. Ferrero, L.; Quiles, V.; Ortiz, M.; Iáñez, E.; Azorín, J.M. A BMI Based on Motor Imagery and Attention for Commanding a Lower-Limb Robotic Exoskeleton: A Case Study. *Appl. Sci.* **2021**, *11*, 4106. [[CrossRef](#)]

17. Gharabaghi, A. What Turns Assistive into Restorative Brain-Machine Interfaces? *Front. Neurosci.* **2016**, *10*, 456. [[CrossRef](#)] [[PubMed](#)]
18. Tomasi, D.; Volkow, N.D. Laterality patterns of brain functional connectivity: Gender effects. *Cereb. Cortex (New York NY 1991)* **2012**, *22*, 1455–1462. [[CrossRef](#)]
19. Ocklenburg, S.; Hirstein, M.; Beste, C.; Güntürkün, O. Lateralization and cognitive systems. *Front. Psychol.* **2014**, *5*, 1143. [[CrossRef](#)]
20. Sokołowska, B. A novel virtual reality approach for functional lateralization in healthy adults. *Brain Res.* **2021**, *1766*, 147537. [[CrossRef](#)]
21. Parsons, L.M.; Gabrieli, J.D.; Phelps, E.A.; Gazzaniga, M.S. Cerebrally lateralized mental representations of hand shape and movement. *J. Neurosci.* **1998**, *18*, 6539–6548. [[CrossRef](#)]
22. Zapała, D.; Zabielska-Mendyk, E.; Augustynowicz, P.; Cudo, A.; Jaśkiewicz, M.; Szewczyk, M.; Kopiś, N.; Francuz, P. The effects of handedness on sensorimotor rhythm desynchronization and motor-imagery BCI control. *Sci. Rep.* **2020**, *10*, 2087. [[CrossRef](#)]
23. Shieh, C.P.; Yang, S.H.; Liu, Y.S.; Kuo, Y.T.; Lo, Y.C.; Kuo, C.H.; Chen, Y.Y. Simultaneously Spatiospectral Pattern Learning and Contaminated Trial Pruning for Electroencephalography-Based Brain Computer Interface. *Symmetry* **2020**, *12*, 1387. [[CrossRef](#)]
24. Pfurtscheller, G.; Brunner, C.; Schlo, A.; Lopes, F.H. Mu rhythm (de) synchronization and EEG single-trial classification of different motor imagery tasks. *NeuroImage* **2006**, *31*, 153–159. [[CrossRef](#)]
25. Tariq, M.; Trivailo, P.M.; Simic, M. Mu-Beta event-related (de)synchronization and EEG classification of left-right foot dorsiflexion kinaesthetic motor imagery for BCI. *PLoS ONE* **2020**, *15*, e0230184. [[CrossRef](#)]
26. Tariq, M.; Uhlenberg, L.; Trivailo, P.; Munir, K.S.; Simic, M. Mu-beta rhythm ERD/ERS quantification for foot motor execution and imagery tasks in BCI applications. In Proceedings of the 2017 8th IEEE International Conference on Cognitive Infocommunications (CogInfoCom), Debrecen, Hungary, 11–14 September 2017; pp. 91–96. [[CrossRef](#)]
27. Crémers, J.; Dessoullières, A.; Garraux, G. Hemispheric specialization during mental imagery of brisk walking. *Hum. Brain Mapp.* **2012**, *33*, 873–882. [[CrossRef](#)]
28. Jahn, K.; Deuschländer, A.; Stephan, T.; Strupp, M.; Wiesmann, M.; Brandt, T. Brain activation patterns during imagined stance and locomotion in functional magnetic resonance imaging. *NeuroImage* **2004**, *22*, 1722–1731. [[CrossRef](#)]
29. Ang, K.K.; Chin, Z.Y.; Zhang, H.; Guan, C. Filter Bank Common Spatial Pattern (FBCSP) in brain–computer interface. In Proceedings of the International Joint Conference on Neural Networks, Hong Kong, China, 1–8 June 2008; pp. 2390–2397. [[CrossRef](#)]
30. Ortiz, M.; Rodríguez-Ugarte, M.; Iáñez, E.; Azorín, J.M. Application of the Stockwell Transform to Electroencephalographic Signal Analysis during Gait Cycle. *Front. Neurosci.* **2017**, *11*, 660. [[CrossRef](#)] [[PubMed](#)]
31. Solomon, O.M.J. *PSD Computations Using Welch's Method. [Power Spectral Density (PSD)]*; Technical Report; Sandia National Labs.: Albuquerque, NM, USA, 1991. [[CrossRef](#)]
32. Ramoser, H.; Müller-Gerking, J.; Pfurtscheller, G. Optimal Spatial Filtering of Single Trial EEG During Imagined Hand Movement. *IEEE Trans. Rehabil. Eng. A Publ. IEEE Eng. Med. Biol. Soc.* **2001**, *8*, 441–446. [[CrossRef](#)] [[PubMed](#)]
33. McFarland, D.J.; McCane, L.M.; David, S.V.; Wolpaw, J.R. Spatial filter selection for EEG-based communication. *Electroencephalogr. Clin. Neurophysiol.* **1997**, *103*, 386–394. [[CrossRef](#)]
34. Izenman, A. Linear Discriminant Analysis. In *Modern Multivariate Statistical Techniques*; Springer Texts in Statistics; Springer: New York, NY, USA, 2013.
35. Ferrero, L.; Quiles, V.; Ortiz, M.; Iáñez, E.; Azorín, J.M. BCI Based on Lower-Limb Motor Imagery and a State Machine for Walking on a Treadmill. In Proceedings of the International IEEE EMBS Conference on Neural Engineering, Virtual, Italy, 4–6 May 2021.
36. Ferrero, L.; Ortiz, M.; Quiles, V.; Iáñez, E.; Azorín, J.M. Improving Motor Imagery of Gait on a Brain–Computer Interface by Means of Virtual Reality: A Case of Study. *IEEE Access* **2021**, *9*, 49121–49130. [[CrossRef](#)]
37. Tariq, M.; Trivailo, P.M.; Simic, M. Classification of left and right foot kinaesthetic motor imagery using common spatial pattern. *Biomed. Phys. Eng. Express* **2019**, *6*, 15008. [[CrossRef](#)] [[PubMed](#)]
38. Zhang, C.; Eskandarian, A. A Computationally Efficient Multiclass Time-Frequency Common Spatial Pattern Analysis on EEG Motor Imagery. In Proceedings of the 2020 42nd Annual International Conference of the IEEE Engineering in Medicine & Biology Society (EMBC), Montreal, QC, Canada, 20–24 July 2020.
39. Leeuwis, N.; Paas, A.; Alimardani, M. Vividness of Visual Imagery and Personality Impact Motor-Imagery Brain Computer Interfaces. *Front. Hum. Neurosci.* **2021**, *15*, 634748. [[CrossRef](#)]
40. Lotte, F.; Bougrain, L.; Cichocki, A.; Clerc, M.; Congedo, M.; Rakotomamonjy, A.; Yger, F. A review of classification algorithms for EEG-based brain–Computer interfaces: A 10 year update. *J. Neural Eng.* **2018**, *15*, 031005. [[CrossRef](#)]
41. Gordleeva, S.Y.; Lukoyanov, M.V.; Mineev, S.A.; Khoruzhko, M.A.; Mironov, V.I.; Kaplan, A.Y.; Kazantsev, V.B. Exoskeleton control system based on motor-imaginary brain–computer interface. *Sovrem. Tehnol. V Med.* **2017**, *9*, 31–36. [[CrossRef](#)]
42. Ortiz, M.; Ferrero, L.; Iáñez, E.; Azorín, J.M.; Contreras-Vidal, J.L. Sensory Integration in Human Movement: A New Brain-Machine Interface Based on Gamma Band and Attention Level for Controlling a Lower-Limb Exoskeleton. *Front. Bioeng. Biotechnol.* **2020**, *8*, 735. [[CrossRef](#)]

43. Zhang, T.; Liu, T.; Li, F.; Li, M.; Liu, D.; Zhang, R.; He, H.; Li, P.; Gong, J.; Luo, C.; et al. Structural and functional correlates of motor imagery BCI performance: Insights from the patterns of fronto-parietal attention network. *NeuroImage* **2016**, *134*, 475–485. [[CrossRef](#)] [[PubMed](#)]
44. Nielsen, J.A.; Zielinski, B.A.; Ferguson, M.A.; Lainhart, J.E.; Anderson, J.S. An Evaluation of the Left-Brain vs. Right-Brain Hypothesis with Resting State Functional Connectivity Magnetic Resonance Imaging. *PLoS ONE* **2013**, *8*, e71275.
45. Sabaté, M.; Gonzalez, B.; Díaz, M. Brain lateralization of motor imagery: Motor planning asymmetry as a cause of movement lateralization. *Neuropsychologia* **2004**, *42*, 1041–1049. [[CrossRef](#)]
46. Labriffe, M.; Annweiler, C.; Amirova, L.E.; Gauquelin-Koch, G.; Ter Minassian, A.; Leiber, L.M.; Beauchet, O.; Custaud, M.A.; Dinomais, M. Brain Activity during Mental Imagery of Gait Versus Gait-Like Plantar Stimulation: A Novel Combined Functional MRI Paradigm to Better Understand Cerebral Gait Control. *Front. Hum. Neurosci.* **2017**, *11*, 106. [[CrossRef](#)]
47. Li, G.L.; Wu, J.T.; Xia, Y.H.; He, Q.G.; Jin, H.G. Review of semi-dry electrodes for EEG recording. *J. Neural Eng.* **2020**, *17*, 51004. [[CrossRef](#)]
48. Li, G.; Wang, S.; Li, M.; Duan, Y.Y. Towards real-life EEG applications: Novel superporous hydrogel-based semi-dry EEG electrodes enabling automatically ‘charge–discharge’ electrolyte. *J. Neural Eng.* **2021**, *18*, 046016. [[CrossRef](#)] [[PubMed](#)]
49. Zich, C.; De Vos, M.; Kranczioch, C.; Debener, S. Wireless EEG with individualized channel layout enables efficient motor imagery training. *Clin. Neurophysiol.* **2015**, *126*, 698–710. [[CrossRef](#)] [[PubMed](#)]

Article

Brain-computer interface enhanced by virtual reality training for controlling a lower limb exoskeleton



Laura Ferrero,
Vicente Quiles,
Mario Ortiz,
Eduardo Iáñez,
Ángel Gil-Agudo,
José M. Azorín

lferrero@umh.es

Highlights

Virtual reality training system to enhance subjects' ability to perform motor imagery

Speed up brain-computer interfaces (BCIs) training

Closed-loop experiments for controlling a lower-limb exoskeleton by means of BCI

Assessment of the BCI to control an exoskeleton with patients with spinal cord injury

Ferrero et al., iScience 26, 106675
May 19, 2023 © 2023 The Authors.
<https://doi.org/10.1016/j.isci.2023.106675>



Article

Brain-computer interface enhanced by virtual reality training for controlling a lower limb exoskeleton

Laura Ferrero,^{1,2,4,*} Vicente Quiles,^{1,2} Mario Ortiz,^{1,2,4} Eduardo Láñez,^{1,2} Ángel Gil-Agudo,⁵ and José M. Azorín^{1,2,3,4,6}

SUMMARY

This study explores the use of a brain-computer interface (BCI) based on motor imagery (MI) for the control of a lower limb exoskeleton to aid in motor recovery after a neural injury. The BCI was evaluated in ten able-bodied subjects and two patients with spinal cord injuries. Five able-bodied subjects underwent a virtual reality (VR) training session to accelerate training with the BCI. Results from this group were compared with a control group of five able-bodied subjects, and it was found that the employment of shorter training by VR did not reduce the effectiveness of the BCI and even improved it in some cases. Patients gave positive feedback about the system and were able to handle experimental sessions without reaching high levels of physical and mental exertion. These results are promising for the inclusion of BCI in rehabilitation programs, and future research should investigate the potential of the MI-based BCI system.

INTRODUCTION

Robotic orthoses and exoskeletons have emerged as wearable devices with the potential to enhance physical performance and assist locomotion.¹ Their inclusion in rehabilitation programs has shown to promote the recovery of motor function, particularly among patients who have experienced a stroke or a spinal cord injury (SCI).² These debilitating injuries can significantly impact patients' quality of life and autonomy, underscoring the importance of robotic exoskeletons in facilitating their recovery and ability to live independently.

The interfaces used to control these devices typically rely on a combination of mechanical and electrical instruments. For instance, the H3 exoskeleton (Technaid, Spain) is controlled through commands sent via a smartphone application, whereas the Rex exoskeleton (Rex Bionics, New Zealand) is operated via a joystick.³

BCIs provide a direct and intuitive mean of communication between subjects and their devices, eliminating the need for external controls.^{3,4} These systems record brain activity and translate it into control commands for an output device. Two types of BCI exist based on the control paradigm used: synchronous and asynchronous.

Synchronous BCIs rely on external cues to guide the user. Some of them are based on various external stimuli and evoked potentials. Among these, two visually evoked potentials – P300 and steady-state visual evoked potentials (SSVEP)^{5,6} – are the most commonly employed. Another type of synchronous BCI uses oscillatory EEG patterns that subjects modulate using specific mental strategies after a cue. An example of such a BCI is motor imagery (MI), where subjects simulate a given action without physically executing it.⁷ Brain activity is only analyzed during predefined time intervals, and a cue indicates the beginning and the end of each interval.

In contrast, asynchronous BCIs continuously record and analyze brain signals without any temporal constraints. Subjects internally control their brain switches to produce the desired commands for the output device. However, the primary limitation of these BCIs relies on their validation. The system either instructs subjects when to switch, or they report themselves changes in their mental procedures.⁸

¹Brain-Machine Interface System Lab, Miguel Hernández University of Elche, Elche, Spain

²Instituto de Investigación en Ingeniería de Elche-13E, Miguel Hernández University of Elche, Elche, Spain

³Valencian Graduate School and Research Network of Artificial Intelligence (valgrAI), Valencia, Spain

⁴The European University of Brain and Technology (NeurotechEU)

⁵Hospital Nacional de Paraplégicos de Toledo, Toledo, Spain

⁶Lead contact

*Correspondence: lferrero@umh.es

<https://doi.org/10.1016/j.isci.2023.106675>



Recent studies have demonstrated that the practice of motor imagery combined with movement-associated feedback may facilitate motor recovery in patients who have suffered neural injuries.⁹ This effect is believed to be mediated by the brain's neuroplasticity, which refers to the nervous system's ability to adapt and recover by reorganizing its neural pathways. The performance of mental motor imagery with motion feedback has shown to promote this property.^{10,11}

In the field of BCI, electroencephalography (EEG) is commonly used to monitor brain activity because of its high temporal resolution, non-invasive recording, and portability. EEG primarily measures the activity of pyramidal neurons that are oriented in the same direction with respect to the cortical surface, allowing one to detect their signals without cancellation. However, EEG has some limitations, as the electrical signal from these neurons is attenuated as it travels through the dura, skull, and scalp before reaching the recording electrode.^{2,12}

There are more works in the literature that have worked with EEG based on upper limb MI^{13–18} than on lower-limb MI. The main limitation of lower-limb MI is that the leg area of the motor cortex is deeply located, around 1–4 cm from the surface. Therefore, EEG cannot accurately record this activity and it can be highly influenced by activity occurring near the surface of the skull.¹⁹ There are some authors that have tried to discriminate leg MI with respect to other types of MI that can be more easily identified by EEG as left-hand, right-hand and tongue MI and results obtained were promising.²⁰ However, considering a BCI for rehabilitation, it would be interesting to have a non-intention condition in which subjects do not have to perform MI of another task to pause the system.²¹ There are previous studies that have assessed this issue having leg MI versus idle state.^{9,22–29} During idle state subjects must be relaxed. Accordingly, MI acts as the active condition and idle state as the passive one. Nevertheless, the performance metrics of these approaches are worse than the ones that employ upper-limb MI.

Although there are many studies based on MI BCI, the closed-loop control of an external device remains briefly addressed in the literature, especially in the case of lower-limb MI. Most of the previous studies performed an offline approach in which the subjects first perform certain brain patterns and once they finish the experiment, data are classified and analyzed. This means that no real-time feedback was provided to the subject during the experimentation, working the BCI in an opened-loop control of the external device. Real-time feedback is crucial for subject's rehabilitation.^{20,22–24}

Instead of working with MI tasks, some authors have designed experimental approaches for a closed-loop control based on motion intention. Motion intention is a cortical potential produced by the motor cortex just before a movement is performed. In³⁰ and³¹ a patient with spinal cord injury (SCI) walked assisted by an exoskeleton that was triggered by an external operator while their EEG was recorded. Then, motion intention was decoded and used to start/stop the exoskeleton. Moreover, in^{32,33} four patients with SCI were instructed to attempt to initiate a movement while they were standing and wearing an exoskeleton with their legs blocked. Then, for the real control, patients were asked to perform the same attempt when they wanted to initiate the gait. To ensure safety during the experiment, the participants were only allowed to have complete and unrestricted control over the exoskeleton during specific time intervals, whereas the rest of the time the exoskeleton was blocked. However, the main benefit of MI in comparison with motion intention is that it requires the subjects to mentally repeat a certain movement and they have to be cognitively involved during the duration of the task which promotes motor recovery.³⁴

Barria et al.⁹ combined an MI with visual and/or haptic feedback to enhance the performance of the model, whereas Choi et al.²⁸ included eye blinking in the control loop. Do et al.²⁹ developed a BCI based purely on MI of the legs for controlling a treadmill suspended robotic gait orthosis and it was evaluated with an able-bodied individual and a patient with SCI. Rodríguez-Ugarte et al.²⁵ presented an experimental design for controlling the start of the gait of a robotic exoskeleton based on MI of the gait during determined time intervals. They employed transcranial direct current stimulation (tDCS) for improving the practice of MI and it was evaluated with 12 able-bodied subjects. In our previous studies,^{26,27} we presented two different BCI based on MI of the gait adding the level of attention of the user in the control paradigm. Therefore, a new command was sent to the exoskeleton only if the attention level to the gait of the user was above a threshold. Whereas the inclusion of this second rule reduced the number of false positives, the sensibility of the model decreased significantly.

Table 1. Patients' details

Subject	P1	P2
Gender	Male	Male
Age	51	62
Weight	75 kg	71 kg
Injury level	T4	L3
ASIA injury assessment	C	B
Injury type	Incomplete	Incomplete

One of the primary challenges faced by a BCI is its calibration. During the calibration process, the subject performs a series of mental tasks, such as imagining movements and the BCI records the associated brain activity. These data are then used to train the BCI to recognize the patterns of brain activity associated with specific actions. However, this calibration process can be time-consuming and fatiguing for the subjects, particularly for those with impairments who may require shorter session scenarios.^{2,35}

Typically, calibration is done at the beginning of each experimental session because of the non-stationary nature of EEG data. However, researchers have been exploring calibration-free approaches using subject-independent techniques or transfer learning to reduce or eliminate the calibration process altogether.^{2,36} However, the effectiveness of these approaches can vary across individuals.^{36,37}

Another alternative to reduce the burden of calibration is to improve the quality of the mental tasks performed. In a recent study, participants performed mental imagery tasks while observing an accumulative bar displayed on a screen. The bar increased as the BCI decoded the mental tasks, and subjects were unable to start the experimental session until reaching a certain level of precision.²⁸

Another challenge in BCI applications based on MI is the variation in the way subjects perform mental tasks, resulting in high variability in success rates. In this study, we tackled both challenges using a virtual reality (VR) system. Participants were immersed in a VR environment where they practiced MI strategies for gait while receiving visual feedback. Then, they used these mental tasks to calibrate a BCI to control a robotic lower-limb exoskeleton without the VR feedback. As participants had already practiced in VR, less data was necessary for the BCI to achieve a high accuracy ratio, reducing the required training time and physical effort. To test the effectiveness of the VR system, we compared the BCI accuracies between subjects who underwent VR training and a control group that did not. The system was tested in closed-loop control with a lower-limb exoskeleton as presented in our previous research,²⁷ but this time with 12 subjects, including two patients suffering from SCI.

This study's contributions include:

- The design and proposal of a VR training system to enhance subjects' ability to perform MI tasks and speed up the BCI training process.
- A comparison of BCI accuracies between subjects that used VR for the BCI training and a control group that did not use it.
- Closed-loop experiments for controlling a lower-limb exoskeleton by means of the BCI.
- Assessment of these experiments with not only able-bodied subjects but also patients with SCI, analyzing the usability of the BCI application.

RESULTS

Ten able-bodied subjects participated in the study. They had no movement impairment and did not report any known disease. Concerning BCI, they did not have any previous experience. Five participants were randomly included in control group and the other five in the VR group. Furthermore, two patients with SCI were recruited from the National Hospital of Paraplegics in Toledo. They had no prior experience with BCI technology. Further patient's details are specified in [Table 1](#).

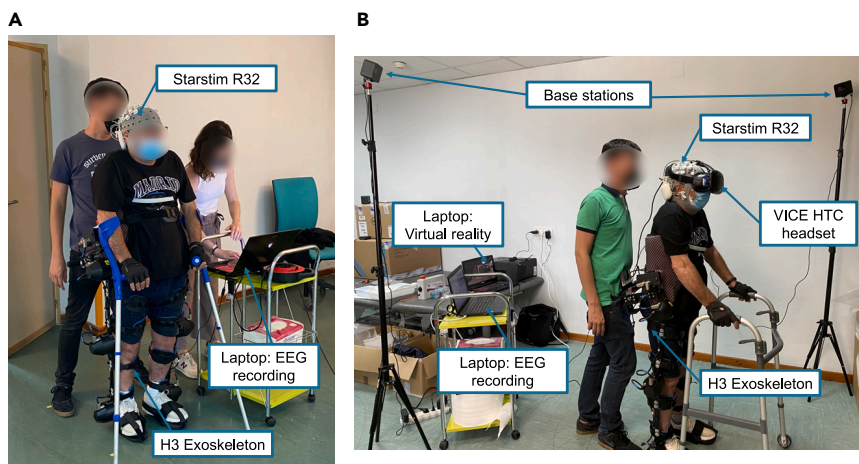


Figure 1. Experimental setup

(A) Calibration and closed-loop sessions; and (B) VR immersion.

Participants wore an EEG cap that recorded their brain-activity and wore a lower-limb robotic exoskeleton that assisted the gait. In addition, participants that were included in VR group used a VR environment. The setup of the experiment can be seen in [Figure 1](#).

Experimental design

Three distinct experiments were conducted, as illustrated in [Figure 2](#). In the first experiment, five participants underwent a conventional calibration phase with the BCI. The calibration was followed by a closed-loop evaluation, where the exoskeleton was controlled by their thoughts resulting in motion feedback. They participated in five sessions scheduled in five different days, each of which consisted of a calibration and a closed-loop phase. Experiment 2 involved the VR system, in which five subjects participated in five experimental sessions too. Each session followed a similar format to the first experiment, but included a practice of mental tasks during VR immersion with visual feedback. The calibration phase was then shortened to half of that in experiment 1 before moving onto the closed-loop phase. Finally, experiment 3 involved two patients with incomplete SCI who underwent the same experimental sessions as in experiment 2, but with a reduced duration of VR immersion. However, in this experiment, the first of the five sessions did not involve closed-loop control phase because patients needed more time to become familiar with the system.

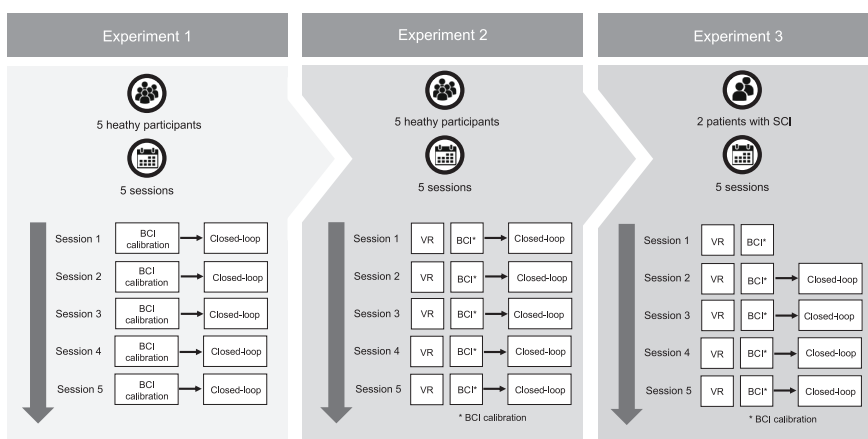


Figure 2. Schema of the three experiments that were conducted in the present study

The first two experiments involved able-bodied participants, and were conducted to evaluate the system before its implementation with patients suffering from spinal cord injury (SCI). In the third experiment, subjects only performed the closed-loop phase in sessions 2 to 5.

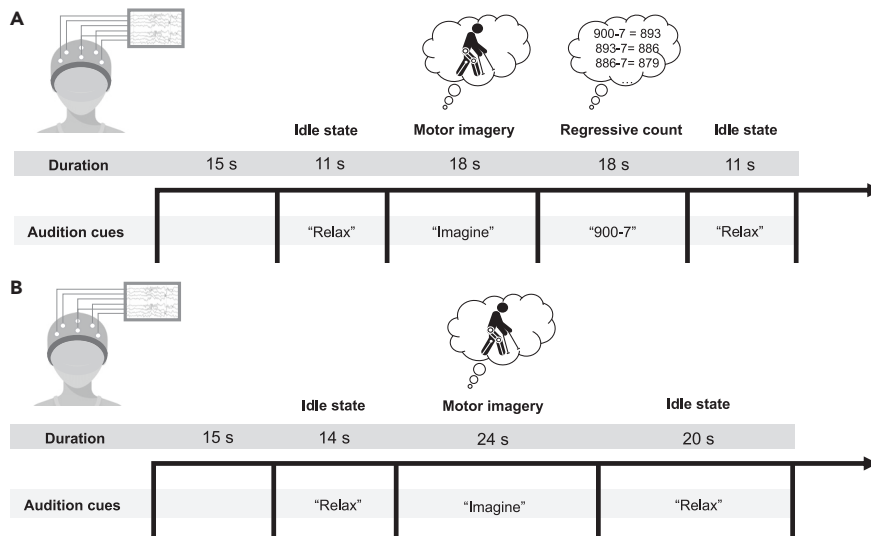


Figure 3. Sequence of mental practices to perform

(A) VR immersion and calibration trials (training); and (B) closed-loop trials. At the beginning of each task an audition cue indicated what participants had to do.

Experiment 1: Control group

In Figure 2, we can see that experiment 1 involved five able-bodied participants who took part in five experimental sessions. Each session consisted of a calibration phase, during which the participants performed 22 trials. The sequence of each trial can be seen in Figure 3A. The trial began with a 15-s period in which the participants were not required to perform any mental task. This initial data was utilized to adjust the algorithms that were used to clean the EEG signals. After this, an acoustic cue signaled the start of the first mental task, which involved the participants relaxing in an idle state. Following this, another acoustic cue indicated the start of the MI period, during which the participants were instructed to focus on imagining the movement of their legs as if they were walking (kinesthetic imagination). Then, another cue signaled the transition to the regressive count task, during which the participants had to mentally perform a series of subtractions (e.g., $900-7$, $893-7$, $886-7$, $879-7$, etc.). Finally, a cue specified the start of the second idle state period. It is important to note that the data obtained during the regressive count period was not used for this BCI and was discarded. Therefore, only two classes were considered: 'Idle state' and 'MI of the gait'.

As reported by Ferrero et al.,²⁷ in the experimental setup, participants were assigned to perform two different types of trials: standing still with the exoskeleton (11 trials) and walking with the exoskeleton (11 trials). The exoskeleton was programmed to initiate and terminate gait based on pre-established commands, depending on whether the trial was in static or motion. Notably, the sequence of tasks was identical for all trials (as depicted in Figure 3A), as this was done to facilitate the creation of a dual-state BCI (illustrated in Figure 4), which was then utilized in the closed-loop control phase.

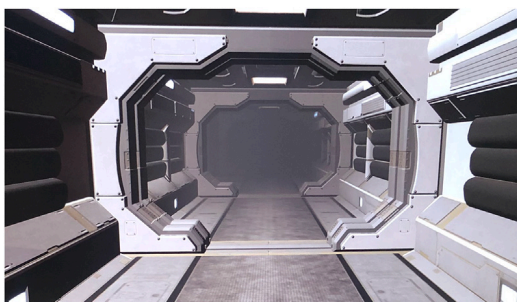


Figure 4. Operation scheme of the brain-machine interface

When subjects were standing still with the exoskeleton (static condition), Static model was the one that ruled. It decided to keep the exoskeleton static or to start the gait based on the brain patterns detected from the subject. On the other hand, when subjects were walking assisted by the exoskeleton (moving condition), Motion model oversaw the control. This model could decide to keep on the movement or to stop.

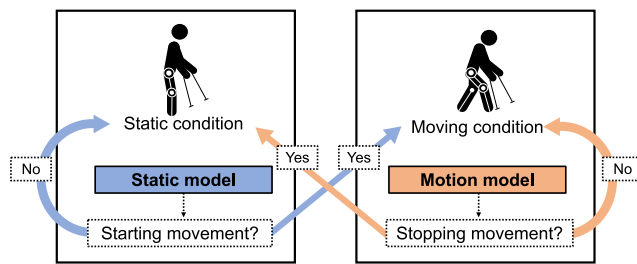


Figure 5. Virtual reality environment

It is a corridor inside a spacecraft developed in Unity engine (Unity Technologies, US).

A BCI based on motor imagery usually decodes two mental states to command the exoskeleton: 'Idle state' versus 'MI'. However, to ensure the accuracy of the BCI, the training data used to calibrate the BCI must be obtained under the same conditions as during the closed-loop phase. This means that the idle state and MI mental classes should be collected not only when the exoskeleton is static but also when it is in motion. To achieve this, four different events were collected during training trials: static idle state, idle state in motion, static MI, and MI in motion. These four classes were then used to create two different classifier models: Static ('Static idle state' versus 'Static MI of the gait') and Motion ('Idle state in motion' versus 'MI of the gait in motion').

In the closed-loop control phase, the initiation and cessation of the exoskeleton gait were controlled by the subject's mental practices and the BCI decoding system. During this phase, subjects performed five trials as described in Figure 3B which included the same mental tasks as in the calibration phase but without the regressive count event. The models trained during the calibration phase, namely Static and Motion, were utilized for the control process (see Figure 4). As a dual-state machine, the Static model was used to keep the exoskeleton standing still and to detect the starting of the gait. However, once the exoskeleton initiated the gait, the BCI control model switched to Motion model, which was used to maintain the exoskeleton in motion until the desire to stop was detected. This would prompt a change of the model to Static again. Because the classes used in the model were collected in the same noise conditions, it was ensured that the differences between the classes were solely based on the mental tasks.

Experiment 2: VR group

In experiment 2, the study included five able-bodied participants who were engaged in five experimental sessions. These sessions were similar to experiment 1. However, they also involved a prior training phase which included VR immersion. In this experiment, a shorter calibration phase with only 12 trials (six in static and six in motion) was used. During the VR immersion phase, the participants were placed in a virtual corridor inside a spacecraft in a first-person view, as depicted in Figure 5. They completed ten trials under similar conditions as the calibration phase (see Figure 3A). For five of these trials, the participant's avatar walked through the corridor, and for the other five, it stood still, providing visual feedback. It should be noted that the movement of the avatar was predefined, and did not depend on the participants' mental practices.

The closed-loop phase was identical to experiment 1.

Experiment 3: Patients with SCI

Once the experimental setup was evaluated with able-bodied subjects, it was tested with patients with SCI. Accordingly, they participated in five sessions in different days and each session included three phases: VR, calibration, and closed-loop control of an exoskeleton. The sequence of mental tasks to perform was identical to Figure 3. The only difference with respect to able-bodied participants was that VR sessions were shorter. They performed 6 trials in the VR environment: three with the avatar being static and three with the avatar walking through the corridor. Then, they performed 12 trials for the calibration. And for closed-loop control of an exoskeleton, participants did seven trials. However, only five were in real control and considered for metrics assessment of the BCI, in the other two the BCI was manually forced to work perfectly as if they did the mental practices well. This strategy was employed to prevent them from getting frustrated.

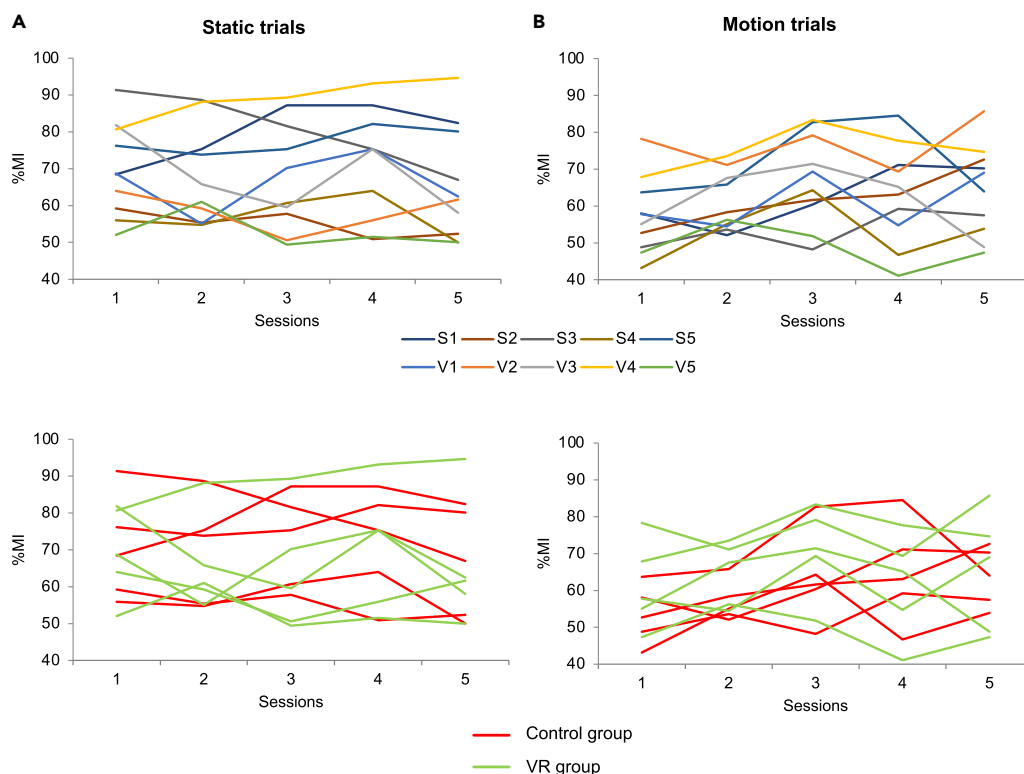


Figure 6. Results from experiment 1

(A) Results in static trials; (B) and motion trials. %MI is the accuracy of the model that goes from 0 to 100. S1–S5 are participants included in control group and V1–V5 are participants included in VR group.

During each session, we measured the level of exertion that patients perceived with the scale Borg Rating of Perceived Exertion Scale.³⁸ This range goes from 6 (“not effort at all”) to 20 (“absolute maximal effort, exhaustion”), and it was used as an indicator to terminate the experimental session if the level perceived was close to the maximum. In addition, after the last experimental session, patients filled two questionnaires: NASA Task Load Index (NASA-TLX)³⁹ that estimated the perceived mental workload; and Quebec User Evaluation of Satisfaction with Assistive Technology (QUEST 20)⁴⁰ that evaluated the satisfaction with the exoskeleton.

Calibration phase: Control versus VR group

This section compares results obtained in calibration phase between control and VR group. Figure 6 shows the average accuracy (%MI) for each session and subject. Static and trials in motion were treated independently because they were produced under different conditions. Figure 6A shows results of cross-validation leave-one-out with static trials from all ten healthy individuals. S1–S5 represent the subjects that were included in the control group from experiment 1 and V1–V5 the subjects that were included in the VR group from experiment 2. Regarding trials in motion, Figure 6B shows their results. The average %MI (avg. \pm std.) of static trials from control group for each experimental session was: $70.2 \pm 14.2\%$, $69.6 \pm 14.5\%$, $72.5 \pm 12.9\%$, $71.9 \pm 14.6\%$, $66.4 \pm 15.1\%$. For trials in movement, performances per session were: $53.3 \pm 8.0\%$, $57.0 \pm 5.4\%$, $63.5 \pm 12.4\%$, $64.9 \pm 14.1\%$, $63.6 \pm 8.0\%$. The average accuracy of VR group per session with static trials was: $69.5 \pm 12.4\%$, $65.8 \pm 13.0\%$, $63.8 \pm 16.5\%$, $70.2 \pm 16.8\%$, $65.4 \pm 17.1\%$. The average %MI of trials in movement from VR per session was: $61.3 \pm 12.0\%$, $64.6 \pm 8.7\%$, $71.0 \pm 12.2\%$, $61.6 \pm 14.1\%$, $65.1 \pm 16.7\%$.

To determine if there were any noteworthy distinctions between the VR group and the control group, a statistical analysis was conducted. However, the variability introduced by the grouping was not the only factor that could affect the results; the experimental sessions could also have an impact. Two separate analyses were conducted for static and trials in motion (further details are included in [quantification and statistical analysis](#) in STAR Methods).

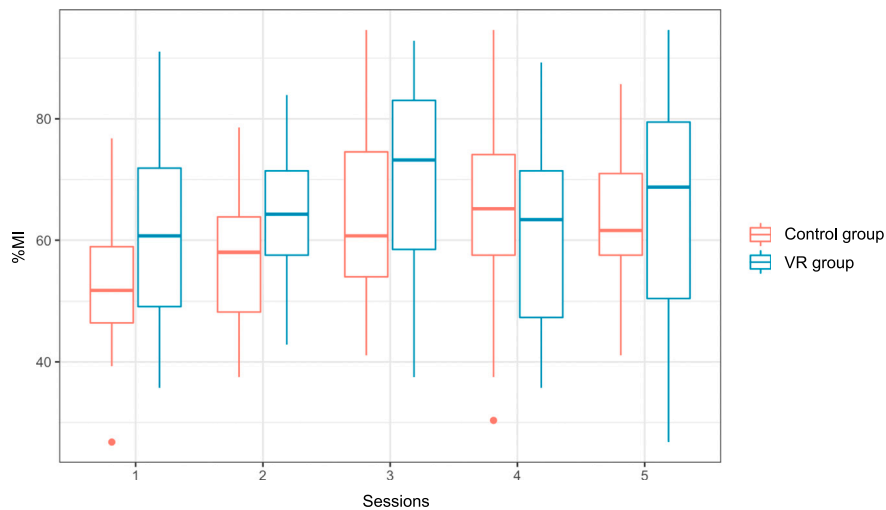


Figure 7. Boxplot of accuracies obtained in trials in movement for each session and each group

Subjects who participated in training with a VR environment and subjects who did not (control). %MI is the accuracy of the model that goes from 0 to 100.

- Static trials: No significant differences were found neither among sessions nor among groups.
- Trials in motion: The test showed that significant superior results were seen for VR group. Differences among sessions were significant. In addition, the interaction between group and sessions was significant. It means the evolution of accuracy through sessions varies from VR to control group. [Figure 7](#) shows boxplot of accuracy values for each session and group. It can be observed that VR group outperforms control group in all sessions but session 4.

[Figure 8](#) shows boxplots of accuracies obtained for all trials of each subject. It seemed that the performance of some of them was really different from the rest. Thus, a statistical test was conducted to see if these differences were relevant (further details are included in [quantification and statistical analysis in STAR Methods](#)).

- Static trials: The test showed significant differences among subjects.
- Trials in motion: The test showed significant differences among subjects too. Results could be influenced by the fact that subjects had a different training, and it was previously proven that VR group tended to have higher results. In the control group, there were three sub-groups of subjects that showed a significant different behavior: S1 and S2; S3 and S4; and S5. A similar trend was found in the VR group with three sub-groups: V1 and V3; V2 and V4; V5.

Intending to assess the evolution of performance through sessions, metrics were normalized with respect to the first session. This way, it can be studied how the accuracy evolved. New values of accuracy were computed as:

$$\% \widehat{MI}_{i,j} = \frac{\%MI_{i,j} - \%MI_1}{\%MI_1} \quad (\text{Equation 1})$$

$\%MI_{i,j}$ is the accuracy obtained for a trial j in an experimental session i , and $\%MI_1$ is the average accuracy of all trials of the first session. This value ranges from -1 to 1 .

[Figure 9](#) shows the average $\% \widehat{MI}$ that goes from -1 to 1 . Statistical analysis was repeated with this new metric for static and trials in motion (further details are included in [quantification and statistical analysis in STAR Methods](#)).

- Static trials: No differences were found among sessions or the VR and control group.
- Motion trials: Relevant differences were found among sessions and the interaction between sessions and groups was significant. Moreover, the results from control group were substantially better than the ones of the VR group.

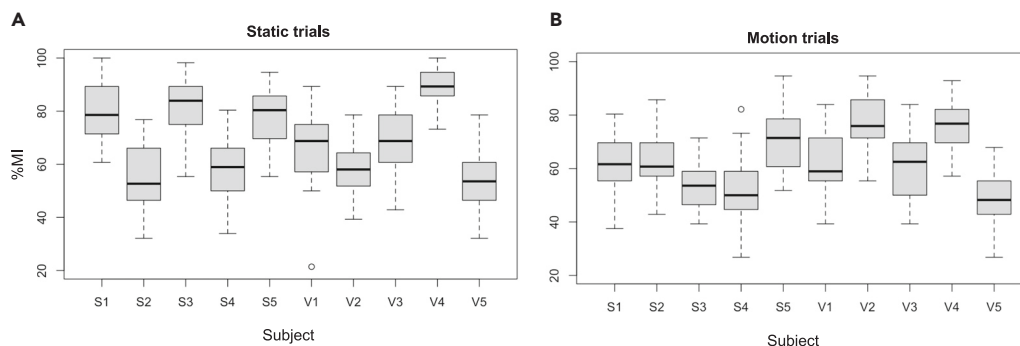


Figure 8. Boxplot of accuracies obtained

(A) Accuracies in trials in static, (B) and trials in motion for each subject. Subjects S1-S5 belong to the control group and V1-V5 to the VR group. %MI is the accuracy of the model that goes from 0 to 100.

Figure 10 shows the distribution of \widehat{MI} for each subject. Metrics were normalized with respect to the first session. However, after performing a statistical analysis, significant differences were still found in static and motion trials among subjects (further details are included in [quantification and statistical analysis in STAR Methods](#)).

To investigate potential differences in neural activity between groups and individuals, power spectral density (PSD) was computed in alpha and beta frequency ranges. These frequency ranges have been associated with motor processes in EEG literature.⁴¹ EEG signals were pre-processed according to

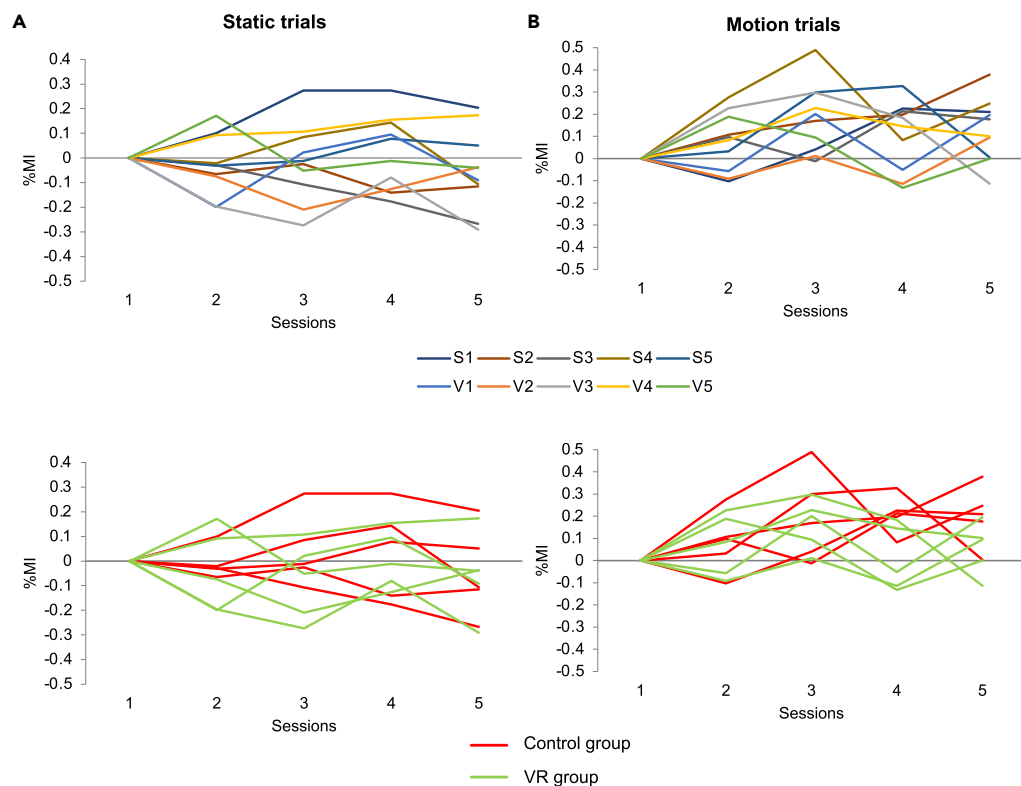


Figure 9. Results from experiment 1

(A) Results in trials in static, (B) and in motion trials. %MI is the relative accuracy of the model with respect to the first session. This value goes from -1 to 1 . S1-S5 are participants included in control group and V1-V5 are participants included in VR group.

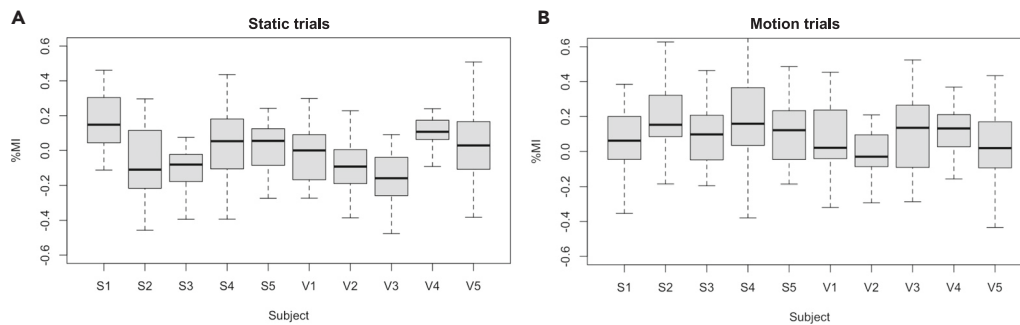


Figure 10. Boxplot of relative accuracies

(A) Relative accuracies obtained in static trials; (B) and in motion trials (B) for each subject. Subjects S1–S5 belong to the control group and V1–V5 to the VR group. %MI is the accuracy of the model that goes from 0 to 100.

method details in STAR Methods, and then subjected to independent component analysis (ICA)⁴² as a denoising technique. As ICA cannot be used in real-time, it was only used for offline analysis. The ratio of PSD during MI periods and idle state periods was computed using the formula:

$$PSD_{electrode} = \frac{PSD_{electrode}(MI) - PSD_{electrode}(idle\ state)}{PSD_{electrode}(idle\ state)} \quad (\text{Equation 2})$$

This calculation was performed for all electrodes and averaged across all trials and sessions for each subject. The resulting values were then represented as topographical maps of the scalp, providing a spatially-detailed representation of changes in neural activity. The resulting maps are displayed in Figure 11 and 12.

The spectral maps exhibited significant variation among subjects, but a common decrease in power was observed in motor areas, particularly in subjects with high accuracy such as S3, S5, and V4. These observations align with previous research in the field. During the cognitive practice of MI, there appears to be a decrease in relative power of EEG signals in frequencies related to motor function, which is then followed by an increase in power. This phenomenon is commonly referred to as event-related desynchronization/synchronization (ERD/ERS) 42.

No significant differences were observed between the groups, which is advantageous for VR group as they exhibited comparable patterns with less training.

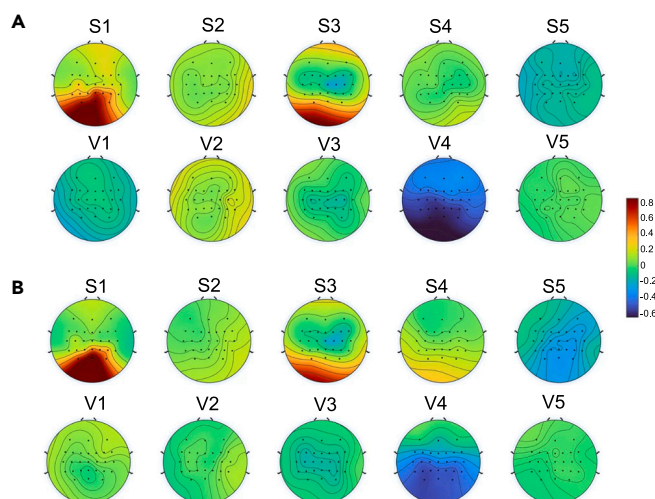


Figure 11. Spectral maps of neural activity during MI in comparison to idle state

This figure shows the activity in alpha frequency range (A) and in beta frequency range (B) only in static trials.

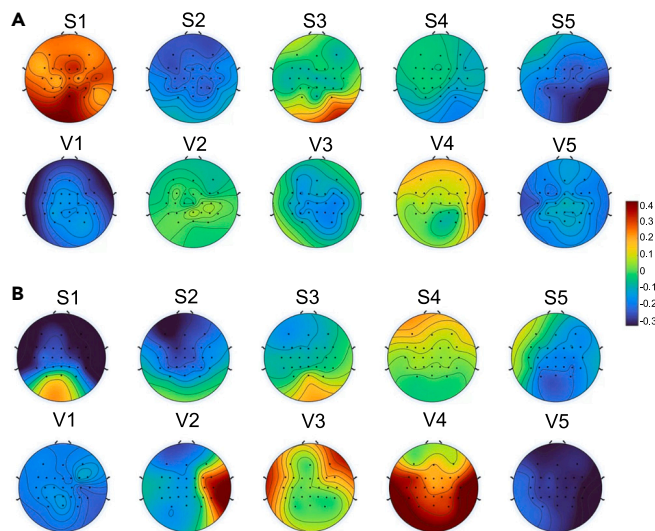


Figure 12. Spectral maps of neural activity during MI in comparison to idle state

This figure shows the activity in alpha frequency range (A) and in beta frequency range (B) only in trials in motion.

Closed-loop control phase: Control versus VR group

This section presents the findings from the closed-loop control phase of experiment 1 and 2, as observed in the five participants in the control group and the five participants in the VR group. Throughout this phase, the exoskeleton was directed by each subject's cognitive techniques. The results from the control group participants are presented in Tables 2, 3, 4, 5, and 6, whereas those from the VR group participants are detailed in Tables 7, 8, 9, 10 and 11.

Table 12 presents a detailed comparison of the average results for both groups. Metrics are further explained in Evaluation metrics in STAR Methods. In both instances, Motion model demonstrated superior performance in comparison to Static model, indicating that the model controlling continuous walking or stopping was more effective. Analyzing the outcome of the experiments conducted with %MI,

Table 2. Results from subject S1 in experiment 1

S1	Session 1	Session 2	Session 3	Session 4	Session 5	Avg.
%MI	58.97 ± 3.48	63.28 ± 4.9	64.31 ± 5.61	64.14 ± 3.14	64.83 ± 6.77	63.11 ± 63.11
%Commands	63.59 ± 8.23	63.76 ± 7.59	64.27 ± 12.91	68.03 ± 1.15	70.43 ± 9.04	66.02 ± 66.02
%Feedback EXO	65.3 ± 10.16	67.52 ± 10.81	61.71 ± 34.79	56.75 ± 31.86	60.85 ± 35.46	62.43 ± 62.43
Missing trials	0	0	0	0	0.2	0.04 ± 0.04
Static model: TPR	73.33 ± 25.28	80 ± 27.39	60 ± 22.36	50 ± 35.36	30 ± 27.39	58.67 ± 58.67
Static model: FPR	46.67 ± 38.01	36.67 ± 34.16	30 ± 27.39	20 ± 44.72	20 ± 44.72	30.67 ± 30.67
Static model: Accuracy commands	56.67 ± 27.89	66.67 ± 31.18	70 ± 27.39	80 ± 44.72	60 ± 54.77	66.67 ± 66.67
Static model: WD	0.17 ± 0.55	0.35 ± 0.6	0.36 ± 0.41	0.48 ± 0.83	0.28 ± 0.79	0.33 ± 0.33
Motion model: TPR	76.67 ± 32.49	63.33 ± 41.5	10 ± 22.36	30 ± 44.72	6.67 ± 14.91	37.33 ± 37.33
Motion model: FPR	80 ± 27.39	73.33 ± 25.28	80 ± 44.72	70 ± 44.72	60 ± 54.77	72.67 ± 72.67
Motion model: Accuracy commands	46.67 ± 7.45	36.67 ± 21.73	20 ± 44.72	30 ± 44.72	20 ± 44.72	30.67 ± 30.67
Motion model: WD	-0.21 ± 0.28	-0.26 ± 0.53	-0.64 ± 0.8	-0.4 ± 0.85	-0.45 ± 0.79	-0.39 ± -0.39

%MI refers to the accuracy of the classifier per epochs, %Commands refers to the accuracy of commands per epochs, %Feedback EXO refers to the percentage of epochs with correct feedback from the exoskeleton, TPR is true positive ratio, FPR is false positive ratio and WD is weighted discriminator.

Table 3. Results from subject S2 in experiment 1

S2	Session 1	Session 2	Session 3	Session 4	Session 5	Avg.
%MI	53.79 ± 7.28	46.72 ± 5.43	48.45 ± 7.84	50.52 ± 13.34	62.76 ± 9.8	52.45 ± 52.45
%Commands	60 ± 10.65	46.32 ± 7.39	50.6 ± 11.47	57.78 ± 19.63	57.78 ± 12.29	54.5 ± 54.5
%Feedback EXO	30.09 ± 28.38	31.79 ± 29.14	23.59 ± 32.39	44.79 ± 29.35	52.82 ± 10.07	36.62 ± 36.62
Missing trials	0	0	0	0	0	0 ± 0
Static model: TPR	90 ± 22.36	60 ± 22.36	80 ± 27.39	20 ± 44.72	100 ± 0	70 ± 70
Static model: FPR	46.67 ± 36.13	61.67 ± 16.24	73.33 ± 36.51	70 ± 27.39	16.67 ± 23.57	53.67 ± 53.67
Static model: Accuracy commands	56.67 ± 25.28	38.33 ± 11.18	46.67 ± 13.94	10 ± 22.36	80 ± 27.39	46.33 ± 46.33
Static model: WD	0.23 ± 0.5	-0.15 ± 0.24	-0.13 ± 0.29	-0.56 ± 0.49	0.71 ± 0.4	0.02 ± 0.02
Motion model: TPR	66.67 ± 31.18	66.67 ± 20.41	53.33 ± 44.72	33.33 ± 20.41	90 ± 22.36	62 ± 62
Motion model: FPR	30 ± 44.72	93.33 ± 14.91	73.33 ± 25.28	30 ± 44.72	10 ± 22.36	47.33 ± 47.33
Motion model: Accuracy commands	80 ± 27.39	46.67 ± 13.94	40 ± 22.36	70 ± 44.72	90 ± 22.36	65.33 ± 65.33
Motion model: WD	0.45 ± 0.59	-0.39 ± 0.21	-0.28 ± 0.25	0.25 ± 0.77	0.8 ± 0.45	0.17 ± 0.17

%MI refers to the accuracy of the classifier per epochs, %Commands refers to the accuracy of commands per epochs, %Feedback EXO refers to the percentage of epochs with correct feedback from the exoskeleton, TPR is true positive ratio, FPR is false positive ratio and WD is weighted discriminator.

%Feedback EXO, and %Commands per epoch, both groups exhibited a similar pattern of behavior. However, in keeping with the trend observed in the calibration trials, the performance of Motion model in the VR group far surpassed that of the control group.

Patients with SCI

Experiment 3 consisted of evaluating the proposed BCI and training approach with patients with SCI. Moreover, this research evaluated the acceptance and usability perceived from them. QUEST questionnaire evaluated their satisfaction with the lower-limb exoskeleton H3 as an assistive technology. Their responses are shown in Table 13. Patient P1 was in general more satisfied with the exoskeleton than patient P2. Both agreed that it was not very comfortable, and P2 found that the adjustment was not easy. Table 14 shows their responses to NASA-TLX questionnaire that assessed the workload perceived. They felt they had to work hard physically and mentally to reach desired results, but they were satisfied with their

Table 4. Results from subject S3 in experiment 1

S3	Session 1	Session 2	Session 3	Session 4	Session 5	Avg.
%MI	48.1 ± 6.52	62.93 ± 5.81	59.83 ± 2.9	58.79 ± 8.78	0 ± 3.25	45.93 ± 45.93
%Commands	48.03 ± 15.96	61.88 ± 8.54	58.97 ± 0	59.32 ± 7.75	0 ± 0	45.64 ± 45.64
%Feedback EXO	52.14 ± 12.78	60.34 ± 5.75	58.97 ± 0	58.12 ± 5.89	0 ± 0	45.91 ± 45.91
Missing trials	0	0.6	1	0	1	0.52 ± 0.52
Static model: TPR	60 ± 22.36	20 ± 27.39	0 ± 0	80 ± 44.72	0 ± 0	32 ± 32
Static model: FPR	80 ± 18.26	13.33 ± 18.26	0 ± 0	30 ± 44.72	0 ± 0	24.67 ± 24.67
Static model: Accuracy commands	35 ± 9.13	20 ± 27.39	0 ± 0	70 ± 44.72	0 ± 0	25 ± 25
Static model: WD	-0.35 ± 0.28	0.07 ± 0.09	0 ± 0	0.44 ± 0.88	0 ± 0	0.03 ± 0.03
Motion model: TPR	40 ± 25.28	40 ± 54.77	0 ± 0	10 ± 22.36	0 ± 0	18 ± 18
Motion model: FPR	90 ± 22.36	40 ± 54.77	0 ± 0	0 ± 0	0 ± 0	26 ± 26
Motion model: Accuracy commands	40 ± 25.28	20 ± 27.39	0 ± 0	20 ± 44.72	0 ± 0	16 ± 16
Motion model: WD	-0.5 ± 0.42	-0.12 ± 0.16	0 ± 0	0.16 ± 0.36	0 ± 0	-0.09 ± -0.09

%MI refers to the accuracy of the classifier per epochs, %Commands refers to the accuracy of commands per epochs, %Feedback EXO refers to the percentage of epochs with correct feedback from the exoskeleton, TPR is true positive ratio, FPR is false positive ratio and WD is weighted discriminator.

Table 5. Results from subject S4 in experiment 1

S4	Session 1	Session 2	Session 3	Session 4	Session 5	Avg.
%MI	55.69 ± 11.33		48.97 ± 11.59	50.34 ± 2.48	50.34 ± 10.95	51.34 ± 51.34
%Commands	55.38 ± 7.49		50.43 ± 14.13	47.01 ± 3.68	55.21 ± 6.83	52.01 ± 52.01
%Feedback EXO	56.41 ± 5.27		47.69 ± 15.26	50.09 ± 1.67	53.85 ± 6.45	52.01 ± 52.01
Missing trials	0		0	0	0	0 ± 0
Static model: TPR	50 ± 35.36		90 ± 22.36	20 ± 44.72	83.33 ± 23.57	60.83 ± 60.83
Static model: FPR	75 ± 27.64		50 ± 11.79	90 ± 22.36	61.67 ± 11.18	69.17 ± 69.17
Static model: Accuracy commands	31.67 ± 23.86		53.33 ± 7.45	10 ± 22.36	51.33 ± 15.2	36.58 ± 36.58
Static model: WD	-0.36 ± 0.54		0.18 ± 0.1	-0.76 ± 0.54	0.02 ± 0.28	-0.23 ± -0.23
Motion model: TPR	50 ± 37.27		83.33 ± 23.57	10 ± 22.36	56.67 ± 9.13	50 ± 50
Motion model: FPR	70 ± 44.72		60 ± 22.36	30 ± 44.72	70 ± 27.39	57.5 ± 57.5
Motion model: Accuracy commands	53.33 ± 38.01		63.33 ± 12.64	10 ± 22.36	50 ± 11.79	44.17 ± 44.17
Motion model: WD	-0.18 ± 0.7		0.11 ± 0.27	-0.2 ± 0.45	-0.17 ± 0.33	-0.11 ± -0.11

%MI refers to the accuracy of the classifier per epochs, %Commands refers to the accuracy of commands per epochs, %Feedback EXO refers to the percentage of epochs with correct feedback from the exoskeleton, TPR is true positive ratio, FPR is false positive ratio and WD is weighted discriminator.

performance. In addition, Borg scale was employed to measure the effort. It was measured after preparing all equipment, at the end of the VR phase, after an initial walk with the exoskeleton without the BCI, so they could get used to it, at the end of the calibration phase and at the end of the phase in which they controlled the exoskeleton with brain tasks. Results from this last scale are shown in Table 15. During each session, the level of exertion increased progressively, but patients never experienced values of exertion close to their own maximum.

The performance of the two patients during the calibration phase (see Figure 13) is within the range of able-bodied individuals (see Figure 6). Because there are significant differences among subjects, it is difficult to say if the performance of patients is in average lower or higher than able-bodied ones. Table 16 and 17 show results obtained in closed-loop trials. Contrary to able-bodied individuals, Motion model was less efficient than static one.

Table 6. Results from subject S5 in experiment 1

S5	Session 1	Session 2	Session 3	Session 4	Session 5	Avg.
%MI	51.38 ± 5.3	69.14 ± 2.95	67.76 ± 10.66	83.28 ± 3.79	55.69 ± 10.76	65.45 ± 65.45
%Commands	54.87 ± 4.5	70.43 ± 6.09	67.86 ± 11.22	85.47 ± 5.37	65.47 ± 15.03	68.82 ± 68.82
%Feedback EXO	47.35 ± 2.46	63.59 ± 7.06	59.49 ± 12.41	79.83 ± 5.88	61.88 ± 13.64	62.43 ± 62.43
Missing trials	0	0	0	0	0	0 ± 0
Static model: TPR	90 ± 22.36	80 ± 44.72	100 ± 0	60 ± 54.77	30 ± 44.72	72 ± 72
Static model: FPR	60 ± 9.13	43.33 ± 9.13	56.67 ± 14.91	30 ± 27.39	66.67 ± 20.41	51.33 ± 51.33
Static model: Accuracy commands	36.67 ± 7.45	40 ± 22.36	40 ± 9.13	50 ± 50	13.33 ± 18.26	36 ± 36
Static model: WD	-0.02 ± 0.12	0.13 ± 0.36	0.07 ± 0.2	0.24 ± 0.75	-0.47 ± 0.41	-0.01 ± -0.01
Motion model: TPR	70 ± 18.26	70 ± 27.39	70 ± 18.26	70 ± 27.39	53.33 ± 36.13	66.67 ± 66.67
Motion model: FPR	20 ± 44.72	0 ± 0	0 ± 0	0 ± 0	20 ± 44.72	8 ± 8
Motion model: Accuracy commands	93.33 ± 14.91	100 ± 0	100 ± 0	100 ± 0	66.67 ± 47.14	92 ± 92
Motion model: WD	0.64 ± 0.47	0.88 ± 0.11	0.88 ± 0.07	0.88 ± 0.11	0.41 ± 0.69	0.74 ± 0.74

%MI refers to the accuracy of the classifier per epochs, %Commands refers to the accuracy of commands per epochs, %Feedback EXO refers to the percentage of epochs with correct feedback from the exoskeleton, TPR is true positive ratio, FPR is false positive ratio and WD is weighted discriminator.

Table 7. Results from subject V1 in experiment 2

V1	Session 1	Session 2	Session 3	Session 4	Session 5	Avg.
%MI	56.9 ± 9.12	55.69 ± 2.96	56.55 ± 6.26	60 ± 10.64	58.62 ± 18.79	57.55 ± 57.55
%Commands	58.97 ± 11	57.78 ± 2.61	64.27 ± 10.68	63.08 ± 12.55	59.83 ± 26.66	60.79 ± 60.79
%Feedback EXO	58.12 ± 13.73	56.92 ± 3.45	60.68 ± 6.84	59.66 ± 12.18	60.17 ± 21.42	59.11 ± 59.11
Missing trials	0	0.2	0	0	0	0.04 ± 0.04
Static model: TPR	80 ± 44.72	70 ± 44.72	90 ± 22.36	100 ± 0	100 ± 0	88 ± 88
Static model: FPR	60 ± 25.28	36.67 ± 21.73	78.33 ± 21.73	40 ± 25.28	50 ± 37.27	53 ± 53
Static model: Accuracy commands	38.33 ± 28.63	46.67 ± 27.39	34.67 ± 10.63	70 ± 18.26	63.33 ± 21.73	50.6 ± 50.6
Static model: WD	-0.05 ± 0.43	0.19 ± 0.12	-0.22 ± 0.34	0.42 ± 0.36	0.28 ± 0.48	0.12 ± 0.12
Motion model: TPR	53.33 ± 36.13	50 ± 35.36	65 ± 25.28	73.33 ± 25.28	70 ± 29.81	62.33 ± 62.33
Motion model: FPR	60 ± 22.36	40 ± 41.83	50 ± 35.36	40 ± 22.36	33.33 ± 31.18	44.67 ± 44.67
Motion model: Accuracy commands	50 ± 28.87	50 ± 35.36	70 ± 24.01	66.67 ± 20.41	70 ± 29.81	61.33 ± 61.33
Motion model: WD	-0.09 ± 0.52	0.1 ± 0.41	0.18 ± 0.55	0.29 ± 0.41	0.37 ± 0.61	0.17 ± 0.17

%MI refers to the accuracy of the classifier per epochs, %Commands refers to the accuracy of commands per epochs, %Feedback EXO refers to the percentage of epochs with correct feedback from the exoskeleton, TPR is true positive ratio, FPR is false positive ratio and WD is weighted discriminator.

DISCUSSION

Calibration phase: Control versus VR group

In this study, the performance of two groups of subjects was compared. The control group underwent a calibration phase consisting of 11 static and 11 movement trials, whereas the VR group underwent an additional previous phase in a VR environment, followed by a calibration phase consisting of six static and six movement trials. It was observed that the VR group experienced less physical exertion because of the reduced number of walking trials with the exoskeleton.

Significant differences were observed among the subjects, with the VR group demonstrating superior performance in trials involving movement. However, no significant differences were observed in static trials. It is noteworthy that even if the performance of the two groups was similar, the VR approach could offer an alternative method of training that requires less physical effort. Furthermore, when the training was divided

Table 8. Results from subject V2 in experiment 2

V2	Session 1	Session 2	Session 3	Session 4	Session 5	Avg.
%MI	65 ± 7.8	60.52 ± 10.1	67.41 ± 6.38	55.17 ± 7.64	72.07 ± 14.11	64.03 ± 64.03
%Commands	71.11 ± 10.73	63.25 ± 16.78	62.91 ± 9.72	54.36 ± 7.75	72.14 ± 13.54	64.75 ± 64.75
%Feedback EXO	65.47 ± 11.94	62.05 ± 13.76	54.19 ± 12.89	50.26 ± 8.6	68.03 ± 11.91	60 ± 60
Missing trials	0	0	0	0.2	0	0.04 ± 0.04
Static model: TPR	70 ± 44.72	80 ± 44.72	100 ± 0	80 ± 44.72	80 ± 44.72	82 ± 82
Static model: FPR	60 ± 9.13	56.67 ± 25.28	40 ± 22.36	20 ± 44.72	43.33 ± 43.46	44 ± 44
Static model: Accuracy commands	26.67 ± 14.91	36.67 ± 21.73	53.33 ± 27.39	66.67 ± 47.14	56.67 ± 43.46	48 ± 48
Static model: WD	-0.16 ± 0.19	-0.03 ± 0.39	0.32 ± 0.38	0.52 ± 0.67	0.23 ± 0.83	0.18 ± 0.18
Motion model: TPR	70 ± 18.26	56.67 ± 25.28	80 ± 27.39	66.67 ± 47.14	63.33 ± 41.5	67.33 ± 67.33
Motion model: FPR	20 ± 44.72	30 ± 27.39	0 ± 0	10 ± 22.36	0 ± 0	12 ± 12
Motion model: Accuracy commands	93.33 ± 14.91	70 ± 27.39	100 ± 0	70 ± 44.72	80 ± 44.72	82.67 ± 82.67
Motion model: WD	0.64 ± 0.47	0.35 ± 0.51	0.92 ± 0.11	0.59 ± 0.57	0.73 ± 0.42	0.65 ± 0.65

%MI refers to the accuracy of the classifier per epochs, %Commands refers to the accuracy of commands per epochs, %Feedback EXO refers to the percentage of epochs with correct feedback from the exoskeleton, TPR is true positive ratio, FPR is false positive ratio and WD is weighted discriminator.

Table 9. Results from subject V3 in experiment 2

V3	Session 1	Session 2	Session 3	Session 4	Session 5	Avg.
%MI	54.48 ± 9.82	54.83 ± 10.53	53.97 ± 16.41	47.24 ± 5.19	47.41 ± 8.47	51.59 ± 51.59
%Commands	58.8 ± 15.5	54.87 ± 13.45	57.09 ± 20.27	49.74 ± 3.16	54.36 ± 8.56	54.97 ± 54.97
%Feedback EXO	56.58 ± 15.91	55.04 ± 8.94	57.09 ± 27.28	49.74 ± 2.04	50.6 ± 5.25	53.81 ± 53.81
Missing trials	0	0	0	0	0	0 ± 0
Static model: TPR	100 ± 0	83.33 ± 23.57	80 ± 27.39	80 ± 44.72	73.33 ± 25.28	83.33 ± 83.33
Static model: FPR	55 ± 16.24	53.33 ± 38.01	63.33 ± 24.72	86.67 ± 18.26	68.33 ± 23.86	65.33 ± 65.33
Static model: Accuracy commands	54.67 ± 11.69	56.67 ± 25.28	40 ± 9.13	28.33 ± 18.26	43 ± 16.09	44.53 ± 44.53
Static model: WD	0.18 ± 0.23	0.14 ± 0.55	-0.07 ± 0.26	-0.38 ± 0.41	-0.13 ± 0.4	-0.05 ± -0.05
Motion model: TPR	68.33 ± 20.75	66.67 ± 31.18	60 ± 25.28	43.33 ± 27.89	61.67 ± 26.09	60 ± 60
Motion model: FPR	53.33 ± 7.45	63.33 ± 41.5	60 ± 41.83	43.33 ± 25.28	80 ± 27.39	60 ± 60
Motion model: Accuracy commands	58.33 ± 11.79	53.33 ± 27.39	56.67 ± 25.28	46.67 ± 27.39	51.67 ± 19	53.33 ± 53.33
Motion model: WD	0.09 ± 0.17	-0.05 ± 0.66	-0.02 ± 0.55	0.02 ± 0.11	-0.24 ± 0.48	-0.04 ± -0.04

%MI refers to the accuracy of the classifier per epochs, %Commands refers to the accuracy of commands per epochs, %Feedback EXO refers to the percentage of epochs with correct feedback from the exoskeleton, TPR is true positive ratio, FPR is false positive ratio and WD is weighted discriminator.

into VR and calibration phases, it was perceived as less monotonous, which can be advantageous in keeping the subjects motivated and focused.

The evolution of performance through sessions was only found significant in trials in movement. Accuracy values were significantly different from last session to the first one, but accuracy growth was different among subjects. This growth was significantly different from subjects in VR and controls. The global trend was similar for the first three sessions, but in the fourth one, VR subjects got lower accuracy than in the previous session.

Closed-loop control phase: Control versus VR group

This study employed a dual-state machine for the BCI, comprising two distinct models. Static model was activated when participants were stationary, whereas Motion model was activated when participants

Table 10. Results from subject V4 in experiment 2

V4	Session 1	Session 2	Session 3	Session 4	Session 5	Avg.
%MI	51.38 ± 2.77	64.14 ± 6.64	58.45 ± 8.32	56.9 ± 5.21	50 ± 2.73	56.17 ± 56.17
%Commands	52.31 ± 3.79	63.08 ± 7.73	61.37 ± 6.38	62.22 ± 8.18	52.59 ± 5.94	58.19 ± 58.19
%Feedback EXO	47.52 ± 4.08	60.68 ± 6.54	54.7 ± 6.81	59.15 ± 7.73	0.25 ± 0.39	54.09 ± 54.09
Missing trials	0	0	0	0	0	0 ± 0
Static model: TPR	70 ± 44.72	80 ± 44.72	80 ± 44.72	100 ± 0	3.88 ± 0.79	80 ± 80
Static model: FPR	68.33 ± 20.75	36.67 ± 21.73	56.67 ± 27.89	70 ± 18.26	70 ± 44.72	62 ± 62
Static model: Accuracy commands	35 ± 22.36	53.33 ± 38.01	36.67 ± 21.73	36.67 ± 7.45	68.33 ± 20.75	38 ± 38
Static model: WD	-0.19 ± 0.51	0.27 ± 0.55	-0.03 ± 0.57	-0.08 ± 0.21	35 ± 22.36	-0.07 ± -0.07
Motion model: TPR	73.33 ± 27.89	80 ± 27.39	70 ± 29.81	56.67 ± 14.91	-0.19 ± 0.51	66.67 ± 66.67
Motion model: FPR	50 ± 35.36	23.33 ± 32.49	20 ± 27.39	30 ± 27.39	73.33 ± 27.89	30.67 ± 30.67
Motion model: Accuracy commands	76.67 ± 13.69	80 ± 29.81	83.33 ± 23.57	76.67 ± 22.36	50 ± 35.36	78 ± 78
Motion model: WD	0.25 ± 0.39	0.57 ± 0.55	0.58 ± 0.47	0.39 ± 0.42	76.67 ± 13.69	0.43 ± 0.43

%MI refers to the accuracy of the classifier per epochs, %Commands refers to the accuracy of commands per epochs, %Feedback EXO refers to the percentage of epochs with correct feedback from the exoskeleton, TPR is true positive ratio, FPR is false positive ratio and WD is weighted discriminator.

Table 11. Results from subject V5 in experiment 2

V5	Session 1	Session 2	Session 3	Session 4	Session 5	Avg.
%MI	49.66 ± 9.71	48.28 ± 8.34	45.52 ± 3.42	47.41 ± 5.24	54.66 ± 6.99	49.11 ± 49.11
%Commands	49.91 ± 10.39	47.18 ± 2.8	44.27 ± 11.02	48.03 ± 5.78	49.57 ± 9.57	47.79 ± 47.79
%Feedback EXO	43.59 ± 9.88	47.18 ± 2.8	46.67 ± 7.42	45.98 ± 6.03	54.36 ± 7.68	47.56 ± 47.56
Missing trials	0	0	0	0	0	0 ± 0
Static model: TPR	80 ± 27.39	100 ± 0	63.33 ± 41.5	90 ± 22.36	100 ± 0	86.67 ± 86.67
Static model: FPR	55 ± 11.18	73.33 ± 25.28	73.33 ± 25.28	56.67 ± 27.89	83.33 ± 23.57	68.33 ± 68.33
Static model: Accuracy commands	41.67 ± 11.79	46.67 ± 13.94	38.33 ± 26.09	46.67 ± 13.94	50 ± 0	44.67 ± 44.67
Static model: WD	0.02 ± 0.27	-0.05 ± 0.33	-0.25 ± 0.43	0.07 ± 0.35	-0.13 ± 0.24	-0.07 ± -0.07
Motion model: TPR	83.33 ± 23.57	56.67 ± 27.89	50 ± 37.27	80 ± 29.81	53.33 ± 29.81	64.67 ± 64.67
Motion model: FPR	60 ± 41.83	53.33 ± 7.45	60 ± 41.83	50 ± 35.36	63.33 ± 7.45	57.33 ± 57.33
Motion model: Accuracy commands	76.67 ± 13.69	55 ± 16.24	46.67 ± 36.13	70 ± 18.26	45 ± 18.26	58.67 ± 58.67
Motion model: WD	0.19 ± 0.46	0.02 ± 0.24	-0.12 ± 0.6	0.24 ± 0.47	-0.15 ± 0.3	0.04 ± 0.04

%MI refers to the accuracy of the classifier per epochs, %Commands refers to the accuracy of commands per epochs, %Feedback EXO refers to the percentage of epochs with correct feedback from the exoskeleton, TPR is true positive ratio, FPR is false positive ratio and WD is weighted discriminator.

walked with the assistance of an exoskeleton (as illustrated in Figure 4). The performance of the two models varied significantly, with Motion model exhibiting superior performance in both participant groups. This was primarily attributed to the higher FPR of Static model, which made it challenging for participants to remain relaxed when they had control over the exoskeleton, an experience not encountered during the calibration phase.

The %MI, %Commands, and %Feedback EXO indicators evaluated the efficiency of the BCI as a whole, independent of the performance of each model. Both groups displayed similar behavior when considering these indicators. However, focusing on the performance of each model, the weighted discriminator proved to be the most effective metric. Although the performance of Static model was similar across groups, Motion model of the VR group outperformed that of the control group. These findings align with those observed in the calibration phase (refer to section 4.1).

Table 12. Comparison between VR and control group

	Control	VR
%MI	55.83 ± 14.68	55.69 ± 6.73
%Commands	57.62 ± 15.18	57.3 ± 7.22
%Feedback EXO	51.87 ± 16.62	54.91 ± 6.43
Missing trials	0.12 ± 0.12	0.02 ± 0.02
Static model: TPR	58.61 ± 31.05	84 ± 11.79
Static model: FPR	44.93 ± 25.41	58.53 ± 16.42
Static model: Accuracy commands	42.35 ± 23.96	45.16 ± 11.91
Static model: WD	0.04 ± 0.35	0.02 ± 0.23
Motion model: TPR	46.67 ± 28.06	64.2 ± 10.8
Motion model: FPR	41.67 ± 33.49	40.93 ± 20.87
Motion model: Accuracy commands	49.86 ± 32.13	66.8 ± 14.98
Motion model: WD	0.07 ± 0.48	0.25 ± 0.3

%MI refers to the accuracy of the classifier per epochs, %Commands refers to the accuracy of commands per epochs, %Feedback EXO refers to the percentage of epochs with correct feedback from the exoskeleton, TPR is true positive ratio, FPR is false positive ratio and WD is weighted discriminator.

Table 13. Results from QUEST questionnaire

Questions	P1	P2
1. The dimensions (size, height, length, width) of the device?	4/5	3/5
2. The weight of the device?	5/5	3/5
3. The ease in adjusting (fixing, fastening) the parts of the device?	4/5	2/5
4. How safe and secure the device is?	4/5	5/5
5. The durability (endurance, resistance to wear) of the device?	4/5	4/5
6. How easy is it to use the device?	4/5	–
7. How comfortable the device is?	3/5	3/5
8. How effective the device is to solve the problem for which you are using it?	4/5	5/5
Total:	32/40	25/35

1: Not satisfied at all; 2: Not very satisfied; 3: More or less satisfied; 4: Quite satisfied; 5: Very satisfied.

As previously discussed, there were notable variations in performance across participants. Within the control group, S5 exhibited the best results, whereas S2 demonstrated the lowest performance, aligning with their respective performance in the calibration phase. In the VR group, V2 achieved the highest outcomes, whereas V5 showed the lowest. Of interest, during the calibration phase, it was V4 who demonstrated the highest performance, but the values of %MI underwent substantial changes from calibration to closed-loop phases. Various factors can influence the system's performance, such as the cognitive state and concentration level of the subject.^{43,44}

Within the control group, three subjects did not miss any trials in all sessions, whereas in the VR group, all participants except V2 did not miss any trials in all sessions. These metrics can be interpreted as 88% and 98% of trials where at least one activation command was issued during motor imagery. These results can be compared to the 84.4% accuracy reported by,³² whose approach was based on motion intention, and the exoskeleton was blocked when subjects were required to relax, giving them control over it only during specific time periods.

In the research presented by,²⁸ the average accuracy reached $84.4 \pm 5.43\%$ when starting the gait on ten able-bodied subjects. They defined a model that compared gait MI with sit MI so subjects could start the gait with the exoskeleton or could sit. This metric can be compared with our accuracy of commands in Static model. Their approach outperforms our proposed BCI. A possible explanation could be that BCI models perform best when different MI patterns are being compared.^{20,44} However, it was crucial in our design to include a non-intention condition.²⁵ reported an accuracy of 73.4% in seven participants. Because the exoskeleton was only free during periods of MI, these metrics are in accordance with our Motion model that showed an average accuracy of $49.86 \pm 32.13\%$ in control group and $66.8 \pm 14.98\%$ in VR group. In addition, our approach was completely free for the user to transition among tasks.

In our previous studies,^{26,27} MI and attention paradigms were combined to control an exoskeleton. In²⁶, % Commands was 56.77% and in²⁷ it was 64.08%. Results obtained in this paper are within the same range, but in the VR group less information was employed to train the classifier which supposes a similar performance with a lower protocol time.

Table 14. Results from NASA-TLX

Item	P1	P2
Mental demand	85/100	80/100
Physical demand	85/100	25/100
Temporal demand	70/100	10/100
Performance	95/100	100/100
Effort	85/100	90/100
Frustration level	90/100	0/100

Table 15. Results from borg rating of perceived exertion scale

Sessions	P1					P2				
	1	2	3	4	5	1	2	3	4	5
Time 1	11	11	10	11	10	8	8	7	6	6
Time 2	12	12	11	11	11	10	8	9	7	8
Time 3	13	12	11	11	11	13	10	10	11	9
Time 4	13	13	12	12	11	15	12	11	11	11
Time 5	–	13	13	12	12	–	13	15	14	15

Time 1: after preparing all equipment.

Time 2: at the end of the virtual reality phase.

Time 3: after an initial walk with the exoskeleton without the BCI.

Time 4: at the end of the calibration phase.

Time 5: and at the end of the phase in which they controlled the exoskeleton with brain tasks.

Patients with SCI

Results from calibration phase of P1 showed a positive trend throughout sessions. This trend was evident in static and trials in motion. P2 did not demonstrate the same learning effect. It is important to note that whereas both patients suffered an incomplete SCI, the injury of P2 affected motor function to a greater extent. P2 may need more practice with the system before reaching an acceptable level of performance.

The ratio of missing trials was 0 for P1 and 0.05 for P1. Therefore, P1 could activate the exoskeleton in all the trials and P2 only missed one trial in last session. Results are in line with²⁹ They evaluated their BCI with a patient with SCI and it was only focused on activation of the exoskeleton which corresponds to our Static model. On the other hand,^{30,31} defined a closed-loop scenario in which an SCI patient was asked to stop the gait. They obtained 99.31% correct stopping commands. It is difficult to compare this study with our research because in ours, subjects had to stop the exoskeleton in a fixed short period of time instead of having several attempts to do it.⁹ evaluated their approach of combining visual/haptic feedback, and MI with five post-stroke patients. They got 50.7 and 68% of successful activation attempts which could be comparable to our TPR in static. However, although patients who suffered an SCI do not have cognitive affection, patients who suffered a stroke have brain damage, which makes it difficult to do a comparison. TPR in static was 77.71% for patient P1 and 76.67% for P2. These metrics are the number of successful activations of the exoskeleton out of all the attempts.^{32,33} used motion intention to start the movement and then, the system kept it. They both were evaluated with four SCI and results from³³ were 79%, 93.10%, 87.10% and 68.81% for each patient. Again, these metrics can be confronted to our TPR in static.³² reported an average accuracy of 77.6%. However, metrics were computed with different rules as a trial was considered successful if at least an activation command was sent to the exoskeleton. In our results, P1 got a 100% of trials in which at least a command was sent to the exoskeleton (0 missing trials), and P2 got 100% in all sessions, but last one with 80%. The proposed BCI was proven to be at least as effective as previous approaches presented in the literature with more restricting assessing metrics.

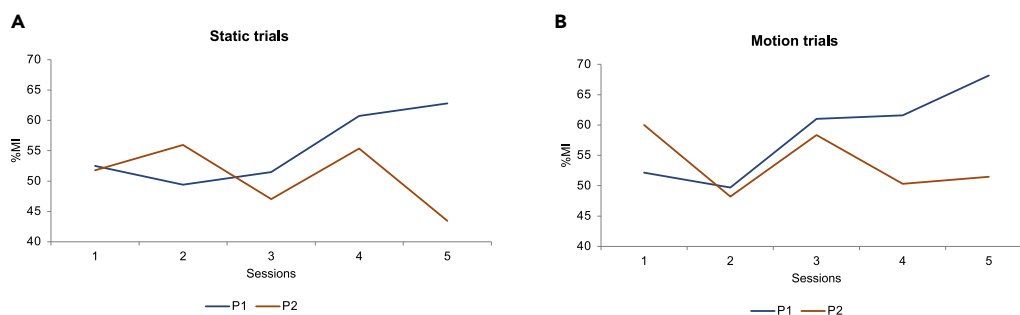


Figure 13. Results from calibration phase of experiment 3

Results (A) in static trials, (B) and trials in motion. %MI is the accuracy of the model that goes from 0 to 100.

Table 16. Results from patient P1 in closed-loop trials of experiment 3

P1	Session 2	Session 3	Session 4	Session 5	Avg.
%MI	50.52 ± 8.35	46.55 ± 13.41	53.97 ± 3.48	50 ± 6.68	50.26 ± 3.03
%Commands	54.19 ± 16.51	45.81 ± 19	59.15 ± 9.15	54.36 ± 15.33	53.38 ± 5.54
%Feedback EXO	57.61 ± 18.98	46.67 ± 16.86	55.04 ± 8.01	54.87 ± 16.24	53.55 ± 4.75
Missing trials	0	0	0	0	0 ± 0
Static model: TPR	73.33 ± 25.28	80 ± 27.39	87.5 ± 25	70 ± 27.39	77.71 ± 7.74
Static model: FPR	70 ± 27.39	40 ± 36.51	73.33 ± 25.28	43.33 ± 9.13	56.67 ± 17.43
Static model: Accuracy commands	44.67 ± 7.67	60 ± 36.51	30 ± 18.26	46.67 ± 7.45	45.33 ± 12.28
Static model: WD	-0.14 ± 0.19	0.28 ± 0.66	-0.09 ± 0.25	0.13 ± 0.13	0.04 ± 0.2
Motion model: TPR	56.67 ± 43.46	73.33 ± 25.28	66.67 ± 33.33	80 ± 27.39	69.17 ± 9.95
Motion model: FPR	86.67 ± 18.26	50 ± 50	50 ± 35.36	80 ± 27.39	66.67 ± 19.44
Motion model: Accuracy commands	40 ± 25.28	63.33 ± 34.16	71.67 ± 18.26	53.33 ± 7.45	57.08 ± 13.63
Motion model: WD	-0.4 ± 0.34	0.17 ± 0.77	0.2 ± 0.37	-0.16 ± 0.15	-0.05 ± 0.29

%MI refers to the accuracy of the classifier per epochs, %Commands refers to the accuracy of commands per epochs, %Feedback EXO refers to the percentage of epochs with correct feedback from the exoskeleton, TPR is true positive ratio, FPR is false positive ratio and WD is weighted discriminator.

Furthermore, the BCI implemented in this study provided complete and unrestricted control for patients to initiate, maintain, stop, and remain stationary during gait without any predefined time limitations imposed by the experimental protocol or periods of no control over the exoskeleton. This was achieved by designing a dual-state machine control BCI that relied on two distinct models to initiate and terminate exoskeleton movement, resulting in a more realistic and practical approach to the real-time control of an exoskeleton.

Limitations of the study

This research has some limitations, especially regarding the dataset. All able-bodied participants shared common features. They were in their 20s, presented right-dominance laterality, and did not have previous experience with a BCI. Nevertheless, there were significant differences among subjects in terms of BCI performance. Thus, it was difficult to draw conclusions regarding performance. For future studies, it would be interesting that each subject tries both experimental conditions with a random order and both spaced in

Table 17. Results from patient P2 in closed-loop trials of experiment 3

P2	Session 2	Session 3	Session 4	Session 5	Avg.
%MI	56.55 ± 12.4	47.76 ± 4.46	47.76 ± 10.74	42.07 ± 11.36	48.53 ± 5.98
%Commands	55.73 ± 21.21	48.21 ± 10.48	52.99 ± 5.2	42.91 ± 9.62	49.96 ± 5.64
%Feedback EXO	54.53 ± 24.34	49.91 ± 11.56	49.23 ± 4.7	43.42 ± 7.53	49.27 ± 4.56
Missing trials	0	0	0	0.2	0.05 ± 0.1
Static model: TPR	90 ± 22.36	70 ± 44.72	86.67 ± 18.26	60 ± 41.83	76.67 ± 14.14
Static model: FPR	56.67 ± 14.91	70 ± 18.26	73.33 ± 18.07	58.33 ± 16.67	64.58 ± 8.32
Static model: Accuracy commands	43.33 ± 9.13	33.33 ± 20.41	40 ± 12.25	35 ± 25.28	37.92 ± 4.59
Static model: WD	0.05 ± 0.18	-0.22 ± 0.31	-0.15 ± 0.27	-0.13 ± 0.29	-0.11 ± 0.12
Motion model: TPR	60 ± 36.51	63.33 ± 24.72	72 ± 15.92	66.67 ± 20.41	65.5 ± 5.12
Motion model: FPR	50 ± 35.36	73.33 ± 25.28	73.33 ± 25.28	75 ± 28.87	67.92 ± 11.97
Motion model: Accuracy commands	60 ± 36.51	56.67 ± 9.13	60 ± 13.69	63.33 ± 24.72	60 ± 2.72
Motion model: WD	0.1 ± 0.71	-0.14 ± 0.24	-0.09 ± 0.36	-0.19 ± 0.34	-0.08 ± 0.13

%MI refers to the accuracy of the classifier per epochs, %Commands refers to the accuracy of commands per epochs, %Feedback EXO refers to the percentage of epochs with correct feedback from the exoskeleton, TPR is true positive ratio, FPR is false positive ratio and WD is weighted discriminator.

time. Half of them would be first included in control group and then in VR, and the opposite for the other half. This way, differences among subjects would be mitigated.

Providing the great dependence on subjects, another limitation was the size of the dataset. Although more subjects participated in this study than for most of BCI applications,³ the database was not vastly large to represent all possible usage outcomes. Consequently, it was difficult to demonstrate which would be the average efficiency of the system. Future research should consider extending the sample size to have a better representation of the whole population.

On the other hand, for training with the VR environment, subjects wore the exoskeleton, and it was blocked in a standing straight position. It involved less physical exertion than walking with the exoskeleton, but it still required some effort, especially for patients. Looking forward, further attempts could evaluate a training phase with VR devices in which participants remain seated.

Conclusions

Overall, current research compared two training alternatives for an MI based BCI for controlling a lower-limb exoskeleton. One alternative consisted of conventional calibration training with the BCI and the exoskeleton; and the other consisted of a pre-calibration session with a VR environment combined with a shorter conventional calibration phase. Results demonstrate that the employment of a shorter calibration phase which involves less information for the model did not worsen the effectiveness of the BCI. In fact, the performance of the Motion model improved. Moreover, the BCI was evaluated for controlling a lower-limb exoskeleton in ten healthy subjects and two patients with SCI. Usability and acceptance were evaluated in patients. Results were promising for a lower-limb MI based BCI system. Consequently, future research could continue to explore the inclusion of this type of systems with robotic devices in rehabilitation programs.

STAR★METHODS

Detailed methods are provided in the online version of this paper and include the following:

- KEY RESOURCES TABLE
- RESOURCE AVAILABILITY
 - Lead contact
 - Materials availability
 - Data and code availability
- EXPERIMENTAL MODEL AND STUDY PARTICIPANT DETAILS
- METHOD DETAILS
 - Equipment
 - BCI
 - Evaluation metrics
- QUANTIFICATION AND STATISTICAL ANALYSIS

SUPPLEMENTAL INFORMATION

Supplemental information can be found online at <https://doi.org/10.1016/j.isci.2023.106675>.

ACKNOWLEDGMENTS

This research is part of grant RTI2018-096677-B-I00, funded by MCIN/AEI/10.13039/501100011033 and by ERDF A way of making Europe; and of grant PID2021-124111OB-C31, funded by MCIN/AEI/10.13039/501100011033 and by ERDF A way of making Europe. Moreover, it was funded by the Ministry of Science, Innovation and Universities through the Aid for the Training of University Teachers FPU19/03165.

AUTHOR CONTRIBUTIONS

Conceptualization, M.O., E.I., and J.M.A.; Methodology, L.F. and V.Q.; Software, L.F. and V.Q.; Validation, L.F. and V.Q.; Formal Analysis, L.F.; Investigation, L.F., V.Q., M.O., E.I., A.G.A., and J.M.A.; Resources, A.G.A., and J.M.A.; Data Curation, L.F.; Writing – Original Draft, L.F.; Writing – Review and Editing, L.F., M.O., E.I., and J.M.A.; Visualization, L.F.; Supervision, M.O., E.I., and J.M.A.; Project Administration, J.M.A.; Funding Acquisition, L.F. and J.M.A.

DECLARATION OF INTERESTS

The authors declare no competing interests.

Received: September 25, 2022

Revised: March 6, 2023

Accepted: April 11, 2023

Published: April 15, 2023

REFERENCES

- Sirlantzis, K., Larsen, L.B., Kanumuru, L.K., and Oprea, P. (2019). 11 - Robotics. In *Handbook of Electronic Assistive Technology*, L. Najafi and D. Cowan, eds. (Academic Press), pp. 311–345. <https://doi.org/10.1016/B978-0-12-812487-1.00011-9>.
- Singh, A., Hussain, A.A., Lal, S., and Guesgen, H.W. (2021). A comprehensive review on critical issues and possible solutions of motor imagery based electroencephalography brain-computer interface. *Sensors* 21, 2173. <https://doi.org/10.3390/s21062173>.
- He, Y., Eguren, D., Azorín, J.M., Grossman, R.G., Luu, T.P., and Contreras-Vidal, J.L. (2018). Brain-machine interfaces for controlling lower-limb powered robotic systems. *J. Neural. Eng.* 15, 021004. <https://doi.org/10.1088/1741-2552/aaa8c0>.
- Tariq, M., Trivailo, P.M., and Simic, M. (2018). EEG-based BCI control schemes for lower-limb assistive-robots. *Front. Hum. Neurosci.* 12, 312. <https://doi.org/10.3389/fnhum.2018.00312>.
- Kwak, N.-S., Müller, K.R., and Lee, S.-W. (2015). A lower limb exoskeleton control system based on steady state visual evoked potentials. *J. Neural. Eng.* 12, 056009. <https://doi.org/10.1088/1741-2560/12/5/056009>.
- Kwak, N.S., Müller, K.R., and Lee, S.W. (2017). A convolutional neural network for steady state visual evoked potential classification under ambulatory environment. *PLoS One* 12, 1–20. <https://doi.org/10.1371/journal.pone.0172578>.
- Jeannerod, M. (1995). Mental imagery in the motor context. *Neuropsychologia* 33, 1419–1432. [https://doi.org/10.1016/0028-3932\(95\)00073-C](https://doi.org/10.1016/0028-3932(95)00073-C).
- Leeb, R., Friedman, D., Müller-Putz, G.R., Scherer, R., Slater, M., and Pfurtscheller, G. (2007). Self-paced (asynchronous) BCI control of a wheelchair in virtual environments: a case study with a tetraplegic. *Comput. Intell. Neurosci.* 2007, 79642. <https://doi.org/10.1155/2007/79642>.
- Barria, P., Pino, A., Tovar, N., Gomez-Vargas, D., Baleta, K., Díaz, C.A.R., Múnera, M., and Cifuentes, C.A. (2021). BCI-based control for ankle exoskeleton T-FLEX: comparison of visual and haptic stimuli with stroke survivors. *Sensors* 21, 6431. <https://doi.org/10.3390/s21196431>.
- Gharabaghi, A. (2016). What turns assistive into restorative brain-machine interfaces? *Front. Neurosci.* 10, 456. <https://doi.org/10.3389/fnins.2016.00456>.
- Donati, A.R.C., Shokur, S., Morya, E., Campos, D.S.F., Muioli, R.C., Gitti, C.M., Augusto, P.B., Tripodi, S., Pires, C.G., Pereira, G.A., et al. (2016). Long-term training with a brain-machine interface-based gait protocol induces partial neurological recovery in paraplegic patients. *Sci. Rep.* 6, 30383–30416. <https://doi.org/10.1038/srep30383>.
- Shih, J.J., Krusienski, D.J., and Wolpaw, J.R. (2012). Brain-computer interfaces in medicine. *Mayo Clin. Proc.* 87, 268–279. <https://doi.org/10.1016/j.mayocp.2011.12.008>.
- Ramoser, H., Müller-Gerking, J., and Pfurtscheller, G. (2000). Optimal spatial filtering of single trial EEG during imagined hand movement. *IEEE Trans. Rehabil. Eng.* 8, 441–446. <https://doi.org/10.1109/86.895946>.
- Lee, K., Liu, D., Perroud, L., Chavarriaga, R., Millán, J.d.R., and del, R. (2017). A brain-controlled exoskeleton with cascaded event-related desynchronization classifiers. *Robot. Autonom. Syst.* 90, 15–23. <https://doi.org/10.1016/j.robot.2016.10.005>.
- Liu, D., Chen, W., Pei, Z., and Wang, J. (2017). A brain-controlled lower-limb exoskeleton for human gait training. *Rev. Sci. Instrum.* 88, 104302. <https://doi.org/10.1063/1.5006461>.
- Gordleeva, S., Lukoyanov, M.V., Mineev, S., Khoruzhko, M.A., Mironov, V., Kaplan, A., and Kazantsev, V. (2017). Exoskeleton control system based on motor-imaginary brain-computer interface. *Sovrem. Tehnol. Med.* 9, 31. <https://doi.org/10.17691/stm2017.9.3.04>.
- Mousavi, M., and de Sa, V.R. (2021). Motor imagery performance from calibration to online control in EEG-based brain-computer interfaces. In *2021 10th International IEEE/EMBS Conference on Neural Engineering (NER)*, pp. 491–494. <https://doi.org/10.1109/NER49283.2021.9441142>.
- Parashiva, P.K., and Vinod, A.P. (2021). *Online Hand Motor Imagery Direction Decoding Using Brain Computer Interface*, pp. 17–20.
- Kline, A., Gaina Ghroaga, C., Pittman, D., Goodyear, B., and Ronsky, J. (2021). EEG differentiates left and right imagined Lower Limb movement. *Gait Posture* 84, 148–154. <https://doi.org/10.1016/j.gaitpost.2020.11.014>.
- Ang, K.K., Chin, Z.Y., Zhang, H., and Guan, C. (2008). Filter Bank common spatial pattern (FBCSP) in brain-computer interface. In *Proceedings of the International Joint Conference on Neural Networks*, pp. 2390–2397. <https://doi.org/10.1109/IJCNN.2008.4634130>.
- Rupp, R. (2014). Challenges in clinical applications of brain computer interfaces in individuals with spinal cord injury. *Front. Neuroeng.* 7, 38. <https://doi.org/10.3389/fneng.2014.00038>.
- Höller, Y., Thomschewski, A., Uhl, A., Bathke, A.C., Nardone, R., Leis, S., Trinka, E., and Höller, P. (2018). HD-EEG based classification of motor-imagery related activity in patients with spinal cord injury. *Front. Neurol.* 9, 955. <https://doi.org/10.3389/fneur.2018.00955>.
- Formaggio, E., Masiero, S., Bosco, A., Izzi, F., Piccione, F., and Del Felice, A. (2017). Quantitative EEG evaluation during robot-assisted foot movement. *IEEE Trans. Neural Syst. Rehabil. Eng.* 25, 1633–1640. <https://doi.org/10.1109/TNSRE.2016.2627058>.
- Yu, Z., Li, L., Song, J., and Lv, H. (2018). The study of visual-auditory interactions on lower limb motor imagery. *Front. Neurosci.* 12, 509. <https://doi.org/10.3389/fnins.2018.00509>.
- Rodríguez-Ugarte, M., Iáñez, E., Ortiz, M., and Azorín, J.M. (2018). Improving real-time lower limb motor imagery detection using tDCS and an exoskeleton. *Front. Neurosci.* 12, 757.
- Ortiz, M., Ferrero, L., Iáñez, E., Azorín, J.M., and Contreras-Vidal, J.L. (2020). Sensory integration in human movement: a new brain-machine interface based on gamma band and attention level for controlling a lower-limb exoskeleton. *Front. Bioeng. Biotechnol.* 8, 735. <https://doi.org/10.3389/fbioe.2020.00735>.
- Ferrero, L., Quiles, V., Ortiz, M., Iáñez, E., and Azorín, J.M. (2021). A bmi based on motor imagery and attention for commanding a lower-limb robotic exoskeleton: a case study. *Appl. Sci.* 11, 4106. <https://doi.org/10.3390/app11094106>.
- Choi, J., Kim, K.T., Jeong, J.H., Kim, L., Lee, S.J., and Kim, H. (2020). Developing a motor imagery-based real-time asynchronous hybrid BCI controller for a lower-limb exoskeleton. *Sensors* 20, 7309. <https://doi.org/10.3390/s20247309>.
- Do, A.H., Wang, P.T., King, C.E., Chun, S.N., and Nenadic, Z. (2013). Brain-computer interface controlled robotic gait orthosis. *J. NeuroEng. Rehabil.* 10, 111.
- Kilicarslan, A., Prasad, S., Grossman, R.G., and Contreras-Vidal, J.L. (2013). High accuracy decoding of user intentions using

- EEG to control a lower-body exoskeleton. In Conference proceedings : Annual International Conference of the IEEE Engineering in Medicine and Biology Society, 2013Conference proceedings : Annual International Conference of the IEEE Engineering in Medicine and Biology Society (IEEE), pp. 5606–5609. <https://doi.org/10.1109/EMBC.2013.6610821>.
31. Kilicarslan, A., Grossman, R.G., and Contreras-Vidal, J.L. (2016). A robust adaptive denoising framework for real-time artifact removal in scalp EEG measurements. *J. Neural. Eng.* 13, 026013. <https://doi.org/10.1088/1741-2560/13/2/026013>.
 32. López-Larraz, E., Trincado-Alonso, F., Rajasekaran, V., Pérez-Nombela, S., del-Ama, A.J., Aranda, J., Minguez, J., Gil-Agudo, A., and Montesano, L. (2016). Control of an ambulatory exoskeleton with a brain-machine interface for spinal cord injury gait rehabilitation. *Front. Neurosci.* 10, 359.
 33. Rajasekaran, V., López-Larraz, E., Trincado-Alonso, F., Aranda, J., Montesano, L., Del-Ama, A.J., and Pons, J.L. (2018). Volition-adaptive control for gait training using wearable exoskeleton: preliminary tests with incomplete spinal cord injury individuals. *J. NeuroEng. Rehabil.* 15, 1–15. <https://doi.org/10.1186/s12984-017-0345-8>.
 34. Malouin, F., Jackson, P.L., and Richards, C.L. (2013). Towards the integration of mental practice in rehabilitation programs. A critical review. *Front. Hum. Neurosci.* 7, 576. <https://doi.org/10.3389/fnhum.2013.00576>.
 35. Zhang, X., She, Q., Chen, Y., Kong, W., and Mei, C. (2021). Sub-band target alignment common spatial pattern in brain-computer interface. *Comput. Methods Progr. Biomed.* 207, 106150. <https://doi.org/10.1016/j.cmpb.2021.106150>.
 36. Ferrero, L., Quiles, V., Ortiz, M., Juan, J.V., Iáñez, E., and Azorín, J.M. (2022). Inter-session transfer learning in MI based BCI for controlling a lower-limb exoskeleton. In *Bio-inspired Systems and Applications: from Robotics to Ambient Intelligence*, J.M. Ferrández Vicente, J.R. Álvarez-Sánchez, F. de la Paz López, and H. Adeli, eds. (Springer International Publishing), pp. 243–252.
 37. He, H., and Wu, D. (2020). Transfer learning for brain-computer interfaces: a euclidean space data alignment approach. *IEEE Trans. Biomed. Eng.* 67, 399–410. <https://doi.org/10.1109/TBME.2019.2913914>.
 38. Borg, G. (1970). Perceived exertion as an indicator of somatic stress. *Scand. J. Rehabil. Med.* 2, 92–98.
 39. Hart, S.G., and Staveland, L.E. (1988). Development of NASA-TLX (task Load Index): results of empirical and theoretical research. In *Human Mental Workload*, P.A. Hancock and P. Meshkati, eds. (North-Holland), pp. 139–183. [https://doi.org/10.1016/S0166-4115\(08\)62386-9](https://doi.org/10.1016/S0166-4115(08)62386-9).
 40. Demers, L., Weiss-Lambrou, R., and Ska, B. (2002). The Quebec user evaluation of satisfaction with assistive Technology (QUEST 20): an overview of recent progress. *Technol. Disabil.* 14, 101–105. <https://doi.org/10.13072/midss.298>.
 41. Pfurtscheller, G., Brunner, C., Schlögl, A., and Lopes da Silva, F.H. (2006). Mu rhythm (de) synchronization and EEG single-trial classification of different motor imagery tasks. *Neuroimage* 31, 153–159. <https://doi.org/10.1016/j.neuroimage.2005.12.003>.
 42. Delorme, A., and Makeig, S. (2004). EEGLAB: an open source toolbox for analysis of single-trial EEG dynamics including independent component analysis. *J. Neurosci. Methods* 134, 9–21. <https://doi.org/10.1016/j.jneumeth.2003.10.009>.
 43. Torkamani-Azar, M., Jafarifarmand, A., and Cetin, M. (2020). Prediction of motor imagery performance based on pre-trial spatio-spectral alertness features. In *Annual International Conference of the IEEE Engineering in Medicine and Biology Society. IEEE Engineering in Medicine and Biology Society. Annual International Conference, 2020*, pp. 3062–3065. <https://doi.org/10.1109/EMBC44109.2020.9175929>.
 44. Padfield, N., Zabalza, J., Zhao, H., Masero, V., and Ren, J. (2019). EEG-based brain-computer interfaces using motor-imagery: techniques and challenges. *Sensors* 19, 1423–1434. <https://doi.org/10.3390/s19061423>.
 45. Rodríguez-Ugarte, M., Iáñez, E., Ortiz, M., and Azorín, J.M. (2017). Personalized offline and pseudo-online BCI models to detect pedaling intent. *Front. Neuroinf.* 11, 45. <https://doi.org/10.3389/fninf.2017.00045>.

STAR★METHODS

KEY RESOURCES TABLE

REAGENT or RESOURCE	SOURCE	IDENTIFIER
Software and algorithms		
MATLAB 2018a	MathWorks, USA	https://es.mathworks.com/products/matlab.html
Rstudio 1.4.1106	Posit, USA	https://posit.co/downloads/
R programming language 1.0.2	R Foundation, USA	https://www.r-project.org/
NIC V2.0.5c	Neuroelectrics, Spain	https://neuroelectrics.com/resources/software
FBCSP	Ang et al. ²⁰	

RESOURCE AVAILABILITY

Lead contact

Further information and requests for resources should be directed to and will be fulfilled by the lead contact, José M. Azorín (jm.azorin@umh.es).

Materials availability

This study did not generate new unique reagents.

Data and code availability

All data reported in this paper will be shared by the [lead contact](#) upon request. This paper does not report original code. Any additional information required to reanalyze the data reported in this paper is available from the [lead contact](#) upon request.

EXPERIMENTAL MODEL AND STUDY PARTICIPANT DETAILS

Ten able-bodied subjects participated in the study (mean age, 23.5 ± 2.0). Five females and five males. They had no movement impairment and did not report any known disease. They were informed about the experiments and signed an informed consent form in accordance with the Helsinki declaration. All procedures were approved by the Responsible Research Office of Miguel Hernández, University of Elche Spain (DIS.JAP.03.18, 22/01/2019). Five participants were randomly included in Control group and the other five in the VR group.

In addition, two patients with spinal cord injury (SCI) were recruited from the National Hospital of Paraplegics in Toledo. They also signed an informed consent form in accordance with the Helsinki Declaration and had no prior experience with BCI technology. Further patient's details are specified in [Table 1](#).

METHOD DETAILS

Equipment

EEG signals were recorded with Starstim R32 (Neuroelectrics, Spain) at 500 Hz. The placement of 27 wet electrodes followed the distribution of the international 10-10 system, with electrode positions including F3, FZ, F4, FC5, FC3, FC1, FCZ, FC2, FC4, FC6, C5, C3, C1, CZ, C2, C4, C6, CP5, CP3, CP1, CPZ, CP2, CP4, CP6, P3, PZ, P4. Ground and reference electrodes were positioned on the right ear lobe. NIC v2.0.5c software (Neuroelectrics, Spain) was used to record EEG in the laptop.

All participants wore H3 exoskeleton (Technaid, Spain). It is a powered hip-knee-ankle exoskeleton that emulates the human walking. Participants were provided with crutches or a trolley to ensure standing and walking stability. To prevent any risk of falls, a technician also held the exoskeleton from the back. High-level control commands were transmitted from the computer via Bluetooth to initiate and stop the gait at a constant speed.

Virtual reality equipment, including an HTC VIVE headset (HTC, Taiwan) with a resolution of 2160 x 1200 (1080 x 1200 per eye) and a refresh rate of 90 Hz, two base stations to track the headset's location, Steam software (Valve, United States), and a self-developed environment created with Unity engine (Unity Technologies, United States) were used in the study. The equipment setup is illustrated in [Figure 1](#).

BCI

This section describes the analysis performed to decode mental tasks from EEG data. MATLAB 2018a was used to connect through TCP/IP with NIC v2.0.5c software and get EEG data, analyze it and send control commands to the exoskeleton. While the exoskeleton was controlled in closed-loop, a decision was taken every 0.5 s. This means that every 0.5 s, the BCI could decide to stay static, start walking, keep on walking, or stop the gait. The epochs of analysis were 1 s length with a shifting of 0.5s. Therefore, once 0.5 s of current data were recorded, epochs of 1s had to be pre-processed, processed, classified, and translated into a control instruction before new 0.5 s of data were available.

The analysis of trials in opened-loop control, such as VR and calibration phases, was performed simulating a real-time scenario (pseudo-online analysis). Consequently, although the analysis was performed afterward, it was done with epochs of data of 1 s and 0.5 s of overlapping. [Figure S1](#) shows the overall schema of the BCI.

Pre-processing

The first step of the BCI consisted of increasing the signal to noise ratio. Epochs of 1 s of EEG were filtered with a Notch filter at 50 Hz that mitigated the contribution of the power line, and a high-pass filter at 0.1 Hz for reducing DC offset. The Notch filter was directly applied in the NIC recording software and the high-pass filter was applied with state-variables Butterworth function in MATLAB.

Processing

The following step focused on extracting signal features that could be used to discriminate between different mental patterns. Our BCI used filter-bank common spatial patterns (FBCSP).²⁰ Firstly, signals were band-pass filtered into different frequency bands: 5–10, 10–15, 15–20, 20–25 Hz. Then, common spatial patterns (CSP) were extracted from each band. CSP estimated a spatial filter that maximized the discriminability between two classes.

$X_1 \sim N \cdot T$ and $X_2 \sim N \cdot T$ are EEG data from two different brain patterns. N is the number of channels and T is the number of samples. In CSP algorithm, their covariance matrices were computed as:

$$C_1 = \frac{X_1 X_1^T}{\text{trace}(X_1 X_1^T)}, C_2 = \frac{X_2 X_2^T}{\text{trace}(X_2 X_2^T)} \quad (\text{Equation 3})$$

Covariance matrices were calculated independently for each trial and then, averaged. Afterwards, they were combined and factorized:

$$C = \overline{C_1} + \overline{C_2} = U_0 \Sigma U_0^T \quad (\text{Equation 4})$$

Σ is the diagonal matrix of eigenvalues and U_0 is a matrix of eigenvectors. Subsequently, results from previous factorization were used to transform each averaged covariance matrix:

$$P = \Sigma^{\frac{1}{2}} U_0^T \quad (\text{Equation 5})$$

$$S_1 = P \overline{C_1} P^T, S_2 = P \overline{C_2} P^T \quad (\text{Equation 6})$$

As a result of [Equation 6](#), S_1 and S_2 had the same matrix of eigenvectors and the addition of the two matrices of eigenvalues resulted in the identity matrix.

$$S_1 = U \Sigma_1 U^T, S_2 = U \Sigma_2 U^T, \Sigma_1 + \Sigma_2 = I. \quad (\text{Equation 7})$$

U and P were employed to estimate the spatial transformation matrix, W .

$$W = U^T P. \quad (\text{Equation 8})$$



The original data was transformed with W . Resulting Z had the same dimensions as the original data, $N \cdot T$, but new channels were ordered based on their discriminative power. Top and last channels were more discriminative in terms of variance and middle ones were less discriminative.

$$Z = WX \quad (\text{Equation 9})$$

For dimensionality reduction, only $m = 3$ first and last discriminant rows of Z were selected as features, Z_p . In addition, the variance of each dimension of Z_p was calculated and log-normalized.

$$f_p = \log \frac{\text{var}(Z_p)}{\sum_{i=1}^{2m} Z_p} \quad (\text{Equation 10})$$

Classification

As explained in the previous subsection, a vector of features was obtained for each epoch of data. Then, a linear discriminant analysis (LDA) was used as the classifier. It was trained with epochs of class 'Idle state' and 'MI of gait', and it predicted these two classes. Two models were created independently for the static and motion trials.

Calibration phase. Trials from calibration phase in the three experiments were evaluated with leave-one-out cross-validation. Moreover, trials in static and trials in motion were assessed independently.

In this study, two approaches were compared, control and VR group (experiment 1 and 2). Therefore, for having a fair comparison, the classifier was trained with the same number of trials. For each subject and session.

- If the subject was in control group:
 - Leave-one-out cross-validation with last six training trials in static.
 - Leave-one-out cross-validation with last six training trials in motion.
- If the subject was in VR group:
 - Leave-one-out cross-validation leave-one-out with all six training trials in static.
 - Leave-one-out cross-validation with all six training trials in motion.

For both conditions, one trial was selected for evaluation while the remaining five trials were used for training the classifier model. This process was repeated for each of the six trials, so that each trial was used for evaluation once. The accuracy of the BCI system was then calculated as the average of the six cross-validation iterations for both the static and motion conditions.

Closed-loop control phase. Two LDA classifiers were trained using the data from the calibration phase for the static and motion conditions, respectively. These classifiers were denoted as Static and Motion. Subsequently, based on the status of the exoskeleton, either stationary or in motion, one of the classifiers was used during each epoch and it predicted either 'Idle state' or 'MI of the gait'. More information about this process is provided in section 2.3 and experiment 1. A depiction of this dual-state machine BCI can be seen in [Figure 4](#).

Output commands

There was an additional step in the BCI for the closed-loop control of an exoskeleton that consisted of translating predictions from the classifier into control instructions. The classifier provided predictions with a value of 1 for epochs labeled as 'MI of the gait' and 0 for epochs labeled as 'Idle state'. To minimize the number of false positives and false negatives, these predictions were smoothed using a moving mean of 4 s. The resulting values ranged from 0 to 1, with values above a 'activation threshold' triggering a command to initiate the gait. Additionally, during movement, values below the 'deactivation threshold' would trigger a command to stop the exoskeleton's motion.

To determine the appropriate thresholds for activation and deactivation, calibration data was utilized. Specifically, the results from a leave-one-out cross-validation with six static trials were used to determine the

'activation threshold', while the results from a leave-one-out cross-validation with six motion trials were used to determine the 'deactivation threshold'.

To optimize the 'activation threshold, predictions from six static trials were utilized. These predictions were first smoothed using a moving mean of 4 s. To identify the optimal activation threshold, three plateaus were identified from each static trial: the first idle state, MI, and second idle state periods. A plateau was defined as consecutive points with a slope near 0, ranging between -0.05 and 0.05 . [Figure S2](#) demonstrates an example of a trial and the three plateaus that were identified. In cases where more than one plateau was found for each task, the highest one was selected.

Once the plateaus were identified, the intermediate point between the plateau of the first idle state and the plateau of MI was computed and defined as the single trial 'activation threshold' as can be seen in [Figure S2](#). This process was repeated for all six static trials. Outliers were subsequently removed, and the remaining resting values were averaged to identify a reliable activation threshold that could be utilized in the closed-loop control of the exoskeleton.

Similarly, the process was repeated using results from motion trials to define the 'deactivation threshold'. In this case, the threshold was defined as the intermediate point between the plateau of MI and the plateau of the second idle state period. Once again, outliers were removed, and resting values were averaged to obtain a reliable deactivation threshold that could be utilized in the closed-loop control of the exoskeleton.

As the last step, some rules were defined to avoid overfitting and to correlate both thresholds:

- 'Activation threshold' could not be lower than the average prediction value during first idle state period (in static trials).
- 'Deactivation threshold' could not be higher than the average prediction value during MI period (in trials in motion).
- 'Activation threshold' could not be higher than the average prediction value during MI period (in trials in motion).

Evaluation metrics

Calibration phase

The accuracy was computed as the percentage of epochs with correct predictions (%MI). This value was estimated for each trial without considering the initial task employed for the convergence of the algorithms.

Closed-loop control phase

The following metrics were computed for evaluation.

- %MI: percentage of epochs with correct predictions.
- %Commands: percentage of epochs with correct commands issued.
- %Feedback EXO: percentage of epochs with correct feedback from the exoskeleton.
- Missing trials: percentage of trials in which the exoskeleton never activated during MI period.
- Static model
 - o TPR (true positive ratio): ratio of how many activation commands were issued during MI period of how many times subjects were static.
 - o FPR (false positive ratio): ratio of how many activation commands were issued during idle state period of how many times subjects were static.
 - o Accuracy commands: percentage of correct activation commands issued out of all activation commands.
 - o WD (Weighted discriminator): this metric was introduced in,⁴⁵ it ranges from -1 to 1 and it is calculated as:

$$WD = 0.4 \frac{TPR}{100} + 0.6 \frac{\text{Accuracy commands}}{100} - \frac{FPR}{100} \quad (\text{Equation 11})$$

- Motion model
 - o **TPR**: ratio of how many deactivation commands were issued during idle state period out of how many times subjects were moving.
 - o **FPR**: ratio of how many deactivation commands were issued during MI period of how many times subjects were moving.
 - o **Accuracy commands**: percentage of correct deactivation commands issued out of all deactivation commands.
 - o **WD (Weighted discriminator)**: it is calculated as detailed above but with metrics corresponding to Motion model.

QUANTIFICATION AND STATISTICAL ANALYSIS

To determine if there were any noteworthy distinctions between the VR group and the control group in calibration data, a statistical analysis was conducted with Rstudio 1.1.441 and R programming language 4.0.2. The variability introduced by the grouping was not the only factor that could affect the results; the experimental sessions could also have an impact. To account for this, a two-way ANOVA test was performed with accuracy (%MI) as the dependent variable and group and session as independent variables, $\text{accuracy} \sim \text{group} \cdot \text{session}$. In order to obtain reliable results from the ANOVA test, the dataset must satisfy three assumptions: normality, equality of variances, and independence. Two separate analyses were conducted for static and trials in motion. Saphiro test was employed to test normality with `saphiro_test()` function and data was organized by group and session variable with `group_by()`. Equality of variances was evaluated with Barlett test and `bartlett.test()` function.

- Static trials: Since data did not follow a normal distribution, Kruskal-Wallis test was employed instead of ANOVA with `kruskal.test()` function. No significant differences were found neither among sessions nor among groups ($p\text{value} > 0.05$).
- Trials in motion: All assumptions were not met, so Kruskal-Wallis test was conducted. It showed that significant superior results were seen for VR group ($p\text{value} < 0.05$). Differences among sessions were significant ($p\text{value} < 0.05$). In addition, the interaction between group and sessions was significant. It means the evolution of accuracy through sessions varies from VR to control group.

Furthermore, to determine the significance of inter-subject differences in accuracy, a separate ANOVA test was performed for each trial type using accuracy as the dependent variable and subjects as the independent variable, $\text{accuracy} \sim \text{subjects}$.

- Static trials: Data satisfied all requirements and the results of the ANOVA test showed significant differences among subjects ($p\text{value} < 0.05$). The test was performed with `aov()`.
- Trials in motion: Requirements were also met and the results from the ANOVA test showed significant differences among subjects ($p\text{value} < 0.05$) too. Results could be influenced by the fact that subjects had a different training, and it was previously proven that VR group tended to have higher results. Therefore, two independent ANOVA tests were conducted for the control and VR subjects. In the control group, there were three sub-groups of subjects that showed a significant different behavior: S1 and S2; S3 and S4; and S5. A similar trend was found in the VR group with three sub-groups: V1 and V3; V2 and V4; V5.

Intending to assess the evolution of performance through sessions, metrics were normalized with respect to the first session. This way, it can be studied how the accuracy evolved. New values of accuracy were computed as:

$$\widehat{\%MI}_{i,j} = \frac{\%MI_{i,j} - \%MI_1}{\%MI_1} \quad (\text{Equation 12})$$

$\%MI_{i,j}$ is the accuracy obtained for a trial j in an experimental session i , and $\%MI_1$ is the average accuracy of all trials of the first session. This value ranges from -1 to 1 .

Figure 9 shows the average $\widehat{\%MI}$ that goes from -1 to 1 . The two-way ANOVA accuracy ~ group · session was repeated with this new metric for static and trials in motion.

- Static trials: Data did follow a normal distribution, but the variance was not equal for all groups. Thus, Kruskal-Wallis test was conducted and no differences were found among sessions or the VR and control group (p value > 0.05).
- Motion trials: As the requisite of equal variances was violated, Kruskal-Wallis test was employed. It found relevant differences among sessions and the interaction between sessions and groups was significant. Moreover, the results from control group were substantially better than the ones of the VR group (p value < 0.05).

Lastly, an assessment was made of inter-subject differences in normalized accuracy, $\widehat{\%MI}$. As the distribution of normalized accuracy was non-normal, a Kruskal-Wallis test was utilized. Significant differences were observed among subjects in both static and motion trials (p value < 0.05).

